UNIVERSITY OF LEEDS

Multi-scale atmospheric and oceanic coupled processes influencing Maritime Continent rainfall

Ashar Ali Aslam

Submitted in accordance with the requirements for the degree of Doctor of Philosophy

The University of Leeds

School of Earth and Environment

September 2025

Declaration of authorship

The candidate confirms that the work submitted is their own, except where work which has formed a part of jointly authored publications has been included. The contribution of the candidate and other authors to each piece of work has been indicated below. The candidate confirms that appropriate credit has been given within this thesis where reference has been made to the work of others.

The publication Aslam, 2025, *Rainfall over the Maritime Continent: key processes, scale interactions, and model representation*, *Weather*, p176-185, doi: `https://doi.org/10.1002/wea.7731` is included as a component of Chapter 1 (the introduction) of this thesis. The text was solely written by the candidate. The candidate performed all data analysis, producing all figures and interpreting them.

The publication Aslam et al., 2024, *Mid-level dry air intrusions over the southern Maritime Continent*, *Quarterly Journal of the Royal Meteorological Society*, 150(759), p727-745, doi: `https://doi.org/10.1002/qj.4618`, jointly authored with Juliane Schwendike, Simon C. Peatman, Cathryn E. Birch, Massimo A. Bollasina and Paul Barrett, is included as Chapter 2 of this thesis. The text was solely written by the candidate, with comments from co-authors. The candidate performed all data analysis and produced all figures. All co-authors contributed to method refinement and interpretation of results.

The publication Aslam et al., 2025, *Atmospheric response to mesoscale ocean eddies in the Maritime Continent*, *Journal of Geophysical Research: Atmospheres*, 130(4), e2024JD042606, doi: `https://doi.org/10.1029/2024JD042606`, jointly authored with Juliane Schwendike, Simon C. Peatman, Adrian J. Matthews, Cathryn E. Birch, Massimo A. Bollasina, Paul A. Barrett and Marina V.C. Azaneu, is included as Chapter 3 of this thesis. The text was solely written by the candidate, with comments from co-authors. The candidate performed all data analysis and produced all figures. All co-authors contributed to method refinement and interpretation of results.

The fourth chapter Aslam et al., *The atmospheric dynamics associated with two Sumatra squalls over the western Maritime Continent*, jointly authored with Juliane Schwendike, Simon C. Peatman, Rajesh Kumar, Paul A. Barrett, Cathryn E. Birch, Massimo A. Bollasina, Kalli Furtado and Adrian J. Matthews, has been submitted to *Journal of Geophysical Research: Atmospheres*. The text was solely written by the candidate, with comments from co-authors. The candidate performed all data analysis and produced all figures. All co-authors contributed to method refinement and interpretation of results, and Kumar ran the SINGV model simulations.

This copy has been supplied on the understanding that it is copyright material and that no quotation from this thesis may be published without proper acknowledgement.

© 2025 The University of Leeds, Ashar Ali Aslam

Acknowledgements

I want to firstly thank my phenomenal team of supervisors: Juliane Schwendike, Simon Peatman, Cathryn Birch, Massimo Bollasina, Paul Barrett, and Adrian Matthews. You've all championed everything I've done, from core PhD work to other antics, and have most definitely helped me to become the scientist I am today. I couldn't be more grateful - hey, maybe I'll get a shot at supervising you one day.

These thanks are extended to the wider Atmospheric and Cloud Dynamics group. Special credit goes to the 'Schwendike Schwestern', from Fran, Ben, Michael, and Amethyst (the older siblings), to Alex, Yvonne, Anistia, and Yuqing (the babies), to Jonathan, James, Kilian, and Jack (adopted through means of WRF and ncl).

This PhD was funded by the NERC SENSE Earth Observation CDT (grant number NE/T00039X/1). From battling through the weeks of group projects, to the Firbush field course, to the visit to the ESA ESRIN facility in Frascati, I've loved being part of the glorious SENSE Cohort 2. Cheers to Anna for leading such an amazing programme, and to Ross, Joey, Jess, Sally, Jamie, and Eilish for riding the waves here in Leeds with me, as well as Emily, Megan, Sam, Eszter, and Jacob for providing the best guidance as the year above.

To all of the other awesome people in the UK-wide southeast Asia research community - in particular, Sam, Natasha, Dan, Jack, and Eliza - we will get 'TerraMaris

2: Field Campaign Boogaloo' one day. Thank you to the people I met at the Met Office during my CASE-funded visits, particularly the APP group who made me feel part of the family, and to all the great friends I've made through RMetS student conferences. I'd also like to thank colleagues in partner organisations, such as those at the Centre for Climate Research Singapore and Met Malaysia, and those involved in WCSSP southeast Asia, for all their incredible insight, amazing discussions, and provision of sweet treats during in-person visits.

Thanks to my wonderfully chaotic office (Live, Laugh, (E)Leven.06), and to the folks in ICAS for the weekly board games, baked goods, and all-round excitement. Katie and Joanna, thank you for being my highly-caffeinated academic moms who I look up to. Sarah, thank you for the shared music taste, and having literally the same brain as myself. Heather, Regan, Arundhati, Craig, Robin, Robert, and Liam - you all continue to inspire me, and I'm so thankful to know such powerful individuals. YD4P, thank you for continuing to rise and resist. Thank you to Will, Sop, Drew, Gina, and Alice for bringing the good fight into the department. Solidarity forever.

Matilda and Laura - you have been my rocks from the very beginning. Here's to many more years of our adventures, you absolute gems.

Thank you Mum and Dad for your unwavering support, love, and sacrifices you've made along the way. I hope my work will always make you proud, and that many more samosas and Morrisons bargains are on the horizon. To my wonderful siblings, siblings-in-law and close cousins - thank you for making your brother feel so valued and celebrated. Particular mention goes to my sister Tahmeena - you got me into Earth sciences and now I'm firmly rooted in it... good game. Thank you for also making it easier to network when people recognise me as The Baby Aslam^{TM}.

Lastly, I'd like to thank a certain AAA. You have grown so much over the years, both as a scientist and as a person. Keep on growing in confidence you amazing goofball, because you absolutely deserve it.

Abstract

The Maritime Continent (MC) archipelago in southeast Asia experiences heavy rainfall all year round, modulated by processes over a range of spatial and temporal scales. Scale interactions between these processes, combined with complex coastlines and orography, make understanding the regional meteorology more difficult. Limitations to our process knowledge mean errors persist in weather and climate models for the MC, with these errors propagating globally. In this thesis, several understudied atmospheric and oceanic coupled processes, on meso-to-synoptic scales, are analysed.

The first novel finding is that mid-level dry air intrusions, which are transient phenomena of extratropical origin, suppress convection over the southern MC, while enhancing rainfall on their eastern margin towards northern Australia, by influencing low-level wind circulations between the tropics and extratropics. Secondly, the characteristics of mesoscale ocean eddies are derived across the entire MC through usage of satellite altimetry data. Eddy-induced sea surface temperature and surface heat flux anomalies lead to minimal imprint on the atmosphere, an unexpected result given the significant eddy-associated signatures observed elsewhere. Lastly, high-resolution convective-permitting simulations show that Sumatra squalls, observed over the western MC, have dynamical structures as seen more broadly for tropical squall lines. Compared to previous studies, the diurnal cycle, vertical wind shear, density cur-

rents, moisture flux convergence and low-to-mid-tropospheric winds are shown to more directly influence Sumatra squall evolution.

Further interactions between processes investigated in this thesis, and the more extensively studied large-scale modes of variability, include how the Madden-Julian Oscillation may influence dry air intrusion occurrence, and how equatorial waves modulate Sumatra squall propagation. Improvements to our knowledge of these key processes and associated interactions which influence rainfall variability will positively impact our ability to model, forecast, and predict severe weather over the MC.

Contents

1 Introduction **1**

1.1 Key processes 8

1.1.1 Interannual variability: El Niño Southern Oscillation and Indian Ocean Dipole 8

1.1.2 Intraseasonal variability: Madden–Julian Oscillation and equatorial waves 10

1.1.3 Diurnal cycle 14

1.1.4 Synoptic circulations 16

1.2 Scale interactions 17

1.2.1 MJO–diurnal cycle interactions 18

1.2.2 ENSO–diurnal cycle interaction 20

1.2.3 Equatorial wave–diurnal cycle interactions 20

1.3 Model representation 21

1.3.1 Resolution 22

1.3.2 Parametrisation 23

1.3.3 Coupling 23

1.3.4 Future projections 24

1.4 Scope for research 26
1.4.1 Motivation 28
1.4.2 Knowledge gap 1: tropical-extratropical interactions 30
1.4.3 Knowledge gap 2: mesoscale air-sea interactions 32
1.4.4 Knowledge gap 3: diurnal land-sea interactions 33
1.4.5 Thesis aims and structure 35

2 Mid-level dry air intrusions over the southern Maritime Continent 38
2.1 Introduction 40
2.2 Methods 46
2.2.1 Data 46
2.2.2 Dry event identification 46
2.2.3 Trajectory analysis 47
2.2.4 Association with modes of variability 49
2.3 Results 51
2.3.1 Dry event characteristics and parcel trajectories 51
2.3.2 Regulatory mechanisms 56
2.3.3 Association with modes of variability 62
2.3.4 Impact on rainfall 64
2.4 Discussion 66
2.5 Conclusions 73

3 Atmospheric response to mesoscale ocean eddies in the Maritime Continent 77
3.1 Introduction 79

3.2 Methodology 85
3.2.1 Eddy detection and tracking 85
3.2.2 Eddy composite construction 88
3.2.3 Comparison to the environment 89
3.3 Results 90
3.3.1 Eddy characteristics 90
3.3.2 Eddy characteristics: regional comparison 92
3.3.3 Eddy composites 97
3.4 Discussion 107
3.5 Conclusion 112

4 The atmospheric dynamics associated with two Sumatra squalls over the western Maritime Continent 116

4.1 Introduction 118
4.2 Methodology 123
4.2.1 Case description 123
4.2.2 Data 124
4.2.3 Model simulations 125
4.3 Results 126
4.3.1 Synoptic overview: observations 126
4.3.2 Synoptic overview: model comparison to observations 129
4.3.3 Vertical profile analysis 136
4.4 Discussion 143
4.5 Conclusions 152

5 Conclusions **155**

5.1 Overview of results 157

5.1.1 Regional rainfall is influenced by extratropical synoptic-scale transients 157

5.1.2 Minimal atmospheric response to mesoscale ocean eddies beyond the near-surface 158

5.1.3 Improved understanding of multi-scale mechanisms influencing squall line dynamics 160

5.2 Contribution of research to the field 162

5.2.1 Individual research themes 163

5.2.2 Synthesis 166

5.3 Future work 169

5.3.1 Broader impacts of extratropical transients on the Tropics . . 169

5.3.2 Mesoscale air-sea interactions across the Maritime Continent . 171

5.3.3 Continued analysis of Sumatra squalls 173

5.3.4 From field campaigns to modelling studies 176

5.4 Summary and concluding remarks 178

List of Figures

1.1 Map of the Maritime Continent, with climatological means of rainfall and lower-tropospheric wind for each season. 6

1.2 Schematics showing the role of the Indian Ocean Dipole, El Niño Southern Oscillation, Madden-Julian Oscillation, equatorial waves, and diurnal cycle in influencing Maritime Continent rainfall. 9

1.3 Rainfall anomalies associated with the various phases of the El Niño Southern Oscillation, Indian Ocean Dipole and Madden-Julian Oscillation, relative to climatology. 11

1.4 Local solar hour of maximum rainfall across the Maritime Continent. 16

1.5 Schematic outlining the scale interaction between the Madden-Julian Oscillation and the diurnal cycle. 19

2.1 Map of the Maritime Continent, with climatological means of rainfall and lower-tropospheric wind for each season. 42

2.2 Variance in daily mean mid-level specific humidity, and an illustration of the method used for identification of dry events. 48

2.3 Air parcel trajectories for selected dry events. 52

2.4 Distribution of air parcels related to dry events in the boreal winter and summer. 55
2.5 Lead-lag composites of mid-level specific humidity and wind anomalies, and upper-level wind anomalies, associated with boreal winter dry events. 57
2.6 Lead-lag composites of mid-level specific humidity and wind anomalies, and upper-level wind anomalies, associated with boreal summer dry events. 58
2.7 Hovmöller plots of upper-level and mid-level geopotential height anomalies associated with boreal winter and summer dry events. 61
2.8 Precipitation anomalies, relative to mean rainfall, for boreal winter and summer dry events. 65
2.9 Schematic showing the mechanisms regulating the occurrence of dry events and their impacts on rainfall. 67

3.1 Map of the Maritime Continent. 80
3.2 Eddy characteristics across the region of analysis. 93
3.3 Histograms of eddy characteristics for each eddy hotspot. 96
3.4 Composites of anomalies associated with eddies in the Kuroshio Extension. 99
3.5 Composites of anomalies associated with eddies in the South China Sea. 101
3.6 Composites of anomalies associated with eddies in the southeast tropical Indian Ocean. 103
3.7 Composites of anomalies associated with eddies in the Sulawesi Sea. . 105

4.1 Map of the western Maritime Continent. 120

4.2 Satellite imagery of cloud top brightness temperature and rainfall associated with the Sumatra squall case studies. 128
4.3 Madden-Julian Oscillation and equatorial wave characteristics around the time of the two Sumatra squall case studies. 130
4.4 Modelled cloud and rainfall characteristics associated with the first Sumatra squall. 132
4.5 Modelled cloud and rainfall characteristics associated with the second Sumatra squall. 134
4.6 Hovmöller plot comparing observations and model outputs for the two Sumatra squall case studies. 135
4.7 Mean along-transect winds across vertical levels for the two Sumatra squall case studies. 137
4.8 Cross-sections of along-transect wind and moisture flux convergence for the first Sumatra squall. 139
4.9 Cross-sections of along-transect wind and moisture flux convergence for the second Sumatra squall. 141
4.10 Schematics outlining the evolution of two Sumatra squall case studies, alluding to their similarities and differences. 145

List of Tables

2.1 Indices used for analysing links between large-scale modes of variability and dry events. 50

2.2 Boreal winter and summer dry event frequency across different modes of variability. 63

3.1 Number of anticyclonic and cyclonic eddies within each eddy hotspot. 94

List of Acronyms

ADT Absolute dynamic topography

AVISO Archiving, Validation and Interpolating of Satellite Oceanographic (data)

BMKG Badan Meteorologi, Klimatologi, dan Geofisika

BoM Bureau of Meteorology

BSISO Boreal Summer Intraseasonal Oscillation

CCRS Centre for Climate Research Singapore

CISK Conditional instability of the second kind

CLS Collecte Localisation Satellites

CMEMS Copernicus Marine Environment Monitoring Service

CMIP Coupled Model Intercomparison Project

CNES Centre National D'Études Spatiales

CORDEX Coordinated Regional Climate Downscaling Experiment

CPM Convection-permitting model

DAI Dry air intrusion

DJF December, January, February

DMI Dipole Mode Index

DUACS Data Unification and Altimeter Combination System

ECMWF European Centre for Medium-Range Weather Forecasts

ENSO El Niño Southern Oscillation

EOF Empirical orthogonal function

ERA5 ECMWF Reanalysis Version 5

GCM Global climate model

GLOBE Global Land One-km Base Elevation

GPM Global Precipitation Measurement (mission)

IMERG Integrated Multi-satellitE Retrievals for GPM

INCOMPASS Interaction of Monsoon Precipitation and Convective Organization, Atmosphere, Surface and Sea

IOD Indian Ocean Dipole

ITCZ Intertropical Convergence Zone

ITF Indonesian Throughflow

JJA June, July, August

JULES Joint UK Land Environment Simulator

LAM Limited-area model

LHF Latent heat flux

LT Local time

MAM March, April, May

MC Maritime Continent

MCS Mesoscale convective system

MFC Moisture flux convergence

MJO Madden-Julian Oscillation

MSS Meteorological Service Singapore

NOAA National Oceanic and Atmospheric Administration

NWP Numerical weather prediction

ONI Ocean Niño Index

ORAS5 Ocean ReAnalysis System 5

PC2 Prognostic Cloud fraction and Prognostic Condensate (scheme)

PV Potential vorticity

RMM Real-time multivariate MJO

SETIO Southeast tropical Indian Ocean

SHF Sensible heat flux

SLA Sea level anomaly

SLP Sea level pressure

SON September, October, November

SSH Sea surface height

SST Sea surface temperature

S2S Seasonal-to-subseasonal

TCLW Total cloud liquid water

TCWV Total column water vapour

TOGA COARE Tropical Ocean Global Atmosphere Coupled Ocean-Atmosphere Response Experiment

UM (Met Office) Unified Model

UTC Coordinated Universal Time

WISHE Wind-induced surface heat exchange

WMO World Meteorological Organisation

WMRG Westward-moving Mixed Rossby-Gravity (waves)

WWRP World Weather Research Programme

YMC Years of the Maritime Continent

Chapter 1

Introduction

Components of this chapter were published in *Weather* (2025).

Tropical convection traditionally refers to the extensive clusters of clouds and storms which lay within the Tropics of Cancer (23.5°N) and Capricorn (23.5°S). The Tropics are characterised by weak shifts in temperature across the year, with alternative descriptions specifying this wide region as where the diurnal changes to temperature are greater than the annual variability across the seasons (Riehl, 1979). Convection here is broadly influenced by high sea surface temperatures (SSTs) and low-level humidity, which encourage moist convergence and resultant destabilisation of the lower-troposphere.

Motion within the tropical atmosphere differs fundamentally to that observed in the mid-latitudes. Balances between the pressure gradient and Coriolis forces, associated with quasi-geostrophic theory, apply to the mid-latitudes, with deviations from this approximation due to inertia. This inertia, however, is small relative to the magnitude of the Coriolis force, which strengthens poleward. In contrast, with Coriolis forces tending to zero towards the Equator, quasi-geostrophic approximations break down in the Tropics. Instead, motion is influenced primarily by convective processes and diabatic heating of the atmosphere.

A fundamental component of circulations on planetary scales is contributed to by tropical convection. Broadly following the convective-radiative (quasi-)equilibrium framework, tropical convection acts to collectively remove instabilities induced by the large-scale surface fluxes and radiative cooling (Arakawa and Schubert, 1974; Yano and Plant, 2012). Intense near-equatorial solar heating, contrasting that received towards the poles, lends itself to forming the Hadley overturning circulation, where air warms and rises at the Equator, cooling and eventually subsiding as it moves poleward. Low-level convergence of trade winds close to the Equator leads

to the development of the Intertropical Convergence Zone (ITCZ), with convection here providing the necessary source of ascending air for the Hadley circulation, concentrated in particular regions known as hot towers (Riehl and Malkus, 1958; Riehl, 1977). Changes to SST patterns through ocean currents also assist in the development of zonally-oriented Walker circulations, Monsoons, unique to the various geographic regions across the Tropics, represent seasonal shifts in circulation and precipitation patterns, relative to the ITCZ, with a strong influence held by land-sea differences in rates of heating.

However, balances pertaining to the described equilibria do not hold for smaller spatial scales, as convection actively reduces local atmospheric static stability, with a characteristic self-enforced positive feedback loop. Notably over the ocean, convection can itself lower surface pressure further due to the induced vertical motion, supplementing the large-scale convergence and instability which enabled storm initiation (termed as conditional instability of the second kind, CISK). Intensification of convection may also be due to the winds associated with convection inducing surface heat exchange (WISHE) to fuel continued storm activity (Smith, 1997).

Changes to the environment, such as induced vertical wind shear and presence of synoptic atmospheric waves, can also assist in convective intensification and its eventual organisation. Self-aggregation of convection may also take place without the need for broader environmental shifts, driven by feedbacks and heterogeneities produced by the convection itself. Such feedbacks can be due to mechanisms including the generation of cold pools from precipitation downdrafts which localise moisture convergence and ascent, and the radiative effects of cloudy versus clear sky conditions in influencing local circulations (e.g. Gray and Jacobson, 1977; Tao et al., 1996;

Holloway et al., 2017).

Therefore, a range of cloud configurations and meteorological patterns can be observed across the Tropics over a range of scales, from those associated with planetary-scale dynamical and thermodynamical balances, to transient and synoptic-scale modifications of the environment by convection. Two distinct convective modes can be derived from these broad patterns. The first, deep convection, relates to the intense ascent extending to the mid-to-upper-troposphere, associated with the previously mentioned hot towers, presenting either as just one convective cell associated with a strong updraft, to the organisation of convective cells to form larger, long-lived systems, often associated with cumulonimbus. Shallow modes of convection, on the other hand, have a more limited vertical extent constrained to the lower-troposphere, associated with cumulus and stratocumulus (e.g. Johnson et al., 1999).

Deep convection will remain the focus for the remainder of this thesis. With a key role in the vertical transport of heat, energy, momentum, and moisture within the atmosphere, as well as contributing intense amounts of rainfall on the more local-to-regional scales, understanding the processes intrinsic to deep convection, and its role in overall meteorology, in the Tropics is paramount. This thesis, however, focuses on a specific region of the Tropics known as the Maritime Continent (MC).

The MC refers to thousands of islands and many shallow seas in southeast Asia (Figure 1.1a). The MC experiences heavy rainfall and deep convection all year round (Figure 1.1b–e), which is a result of the high SSTs and variable topography characterising the region. Regional rainfall is observed to be twice that of the global mean (Yamanaka et al., 2018). Since deep convection and the associated latent heat release from intense rainfall across the entire Tropics enables the generation of Rossby

waves and the subsequent propagation of these waves towards the extratropics (Jin and Hoskins, 1995), the MC is considered a crucial region for influences on the global weather and climate system, if not the most crucial (Ramage, 1968).

On seasonal-to-annual timescales, rainfall patterns are modulated by the interplay between the South Asian and Australian monsoon circulations to the north and south, respectively (Figure 1.1b-e). These circulations, particular the South Asian monsoon, are crucial in the redistribution and transport of moisture which primes the environment for the development of deep convection. Across the MC, there tends to be more rainfall in the boreal winter (December-February, or DJF) due to the development of the northeast monsoon, and lower amounts in the boreal summer (June-August, or JJA) as moisture is redirected by the southwest monsoon towards mainland southeast Asia (e.g. As-syakur et al., 2013).

Highlighted previously for the entire Tropics, additional processes beyond the monsoon circulations, and the roles of high SSTs, influence the environmental state. However, many additional processes influence the environmental state within the MC, modulating regional patterns in convection (Yamanaka, 2016). These processes operate over a wide range of scales, from larger-scale modes of variability to more local and transient variability regulated by finer-scale processes. The geographical complexity of the MC, however, relative to other regions of the Tropics, lends itself to developing unique scale interactions, as well as geographical variability in responses to forcings, thereby making understanding the environment of the MC comparatively more difficult (Yamanaka, 2016).

The intensity of rainfall experienced over the MC causes many detrimental impacts, such as flooding and landslides which can lead to significant health crises and

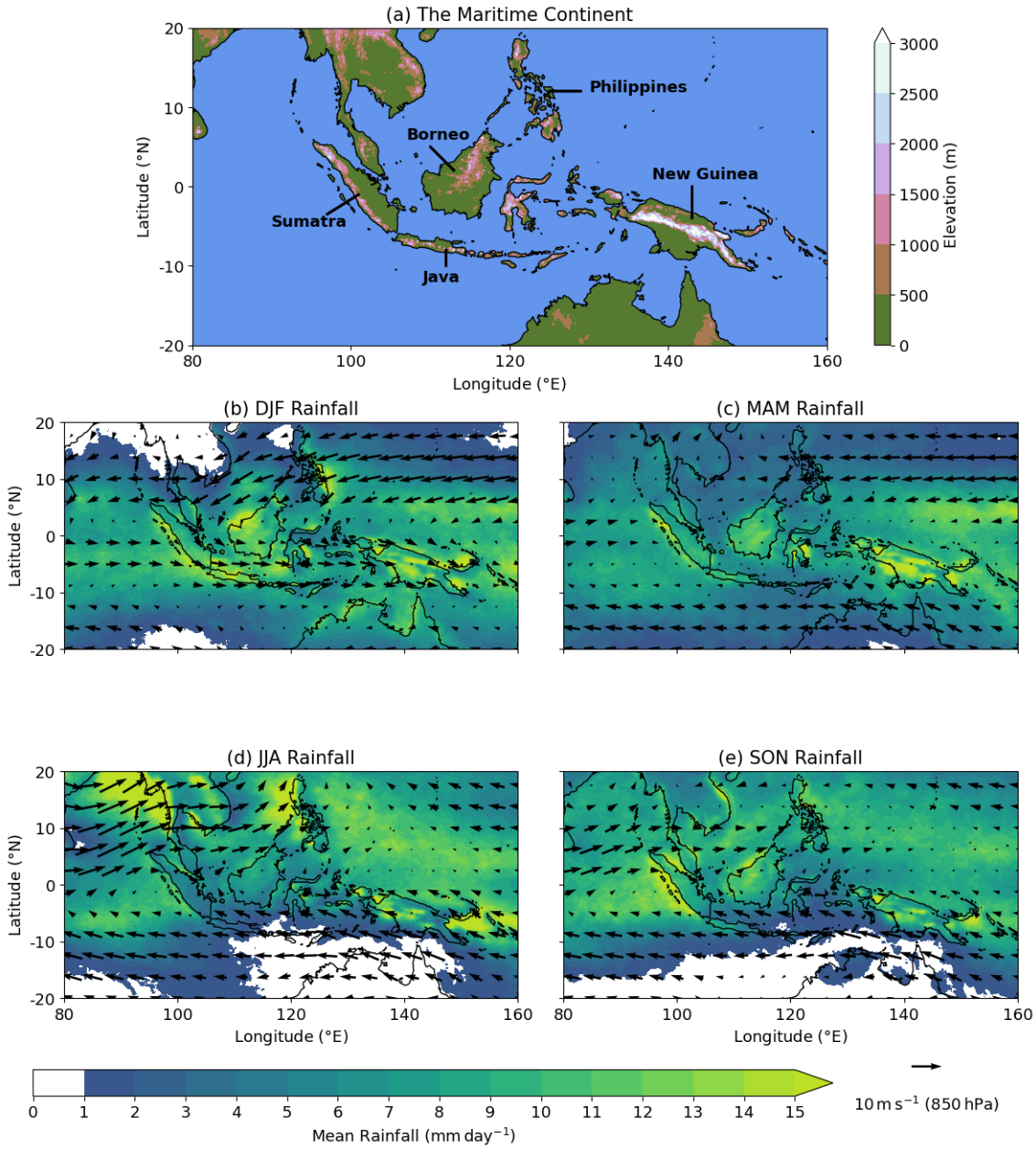

Figure 1.1: (a) Map showing the topography of the Maritime Continent, with some of the constituent islands labelled. Panels (b), (c), (d) and (e) show the climatological means of IMERG GPM (Huffman et al., 2020) precipitation rates for December–February (DJF), March–May (MAM), June–August (JJA), and September–November (SON) respectively, from 20 years of data from December 2000 to November 2020. Black arrows represent mean ERA5 (Hersbach et al., 2020) 850 hPa wind for the equivalent time period, highlighting seasonal shifts in primarily the South Asian (north), but also the Australian (south), monsoon circulations which influence Maritime Continent meteorology.

loss (Torti, 2012; Wijayanti et al., 2017). With a population of over 500 million people residing across the MC, better understanding the processes which govern the regional rainfall patterns is crucial. However, weather stations, providing key ground-based observations, are unevenly distributed across the MC (Koh and Teo, 2009), with access to the data itself difficult. Therefore, we rely on broader-scale observations such as from satellites, as well as regional-to-local-scale climate models to improve our understanding. Conducting more extensive research into the meteorology of the region will help to improve flood forecasting systems and other solutions for minimising regional vulnerability to disaster and emergency.

The introduction to this thesis provides a review of the key features related to the severe weather observed across the MC, and highlights both the growth in knowledge and remaining gaps. Firstly, processes well-understood to impact MC rainfall are outlined in Section 1.1, with an exploration of the various scale interactions that exist between some of these processes in Section 1.2. In Section 1.3, the ability of current state-of-the-art weather and climate models in representing these processes, and any deficiencies that have persisted, are addressed, including where improvements are needed, while also discussing future climate projections of MC rainfall. Section 1.4 provides an overall scope for further research in this field, outlining the core motivations, related to the impact and forecasting capabilities of severe weather over the MC, and the identified knowledge gaps. This chapter concludes with the aims and structure of this thesis.

1.1 Key processes

The MC experiences rainfall all year round and several processes regulate regional precipitation patterns. The background environmental state of the MC is modulated by large-scale modes of variability, with local and more transient variability regulated by finer-scale processes. These processes are described in schematic form in Figure 1.2, and discussed in order from the larger-scale and more predictable, to the finer-scale associated with higher orders of variability in patterns of convection.

1.1.1 Interannual variability: El Niño Southern Oscillation and Indian Ocean Dipole

The El Niño Southern Oscillation (ENSO) is one of the two modes of variability influencing the MC on interannual timescales, with notable broad influences on global climate (e.g. McPhaden et al., 2006). ENSO consists of two phases – El Niño and La Niña – which each have different broad impacts on rainfall in the MC (e.g. Haylock and McBride, 2001; Rauniyar and Walsh, 2013). The large-scale circulation associated with ENSO consists of a strengthened Walker circulation over the MC during La Niña. This circulation is weakened during El Niño. Changes to circulations are modulated by SSTs in the central-eastern tropical Pacific, with warmer SSTs linked to El Niño and colder SSTs linked to La Niña. Equatorial easterlies weaken during El Niño, shifting the preferential location of convection further east, which results in reduced large-scale rainfall (negative anomalies of up to around $3\,\mathrm{mm\,day^{-1}}$ relative to climatology) over the MC (Figure 1.3a). La Niña results in strengthening equatorial easterlies and large-scale ascent over the MC, enhancing large-scale rainfall (positive

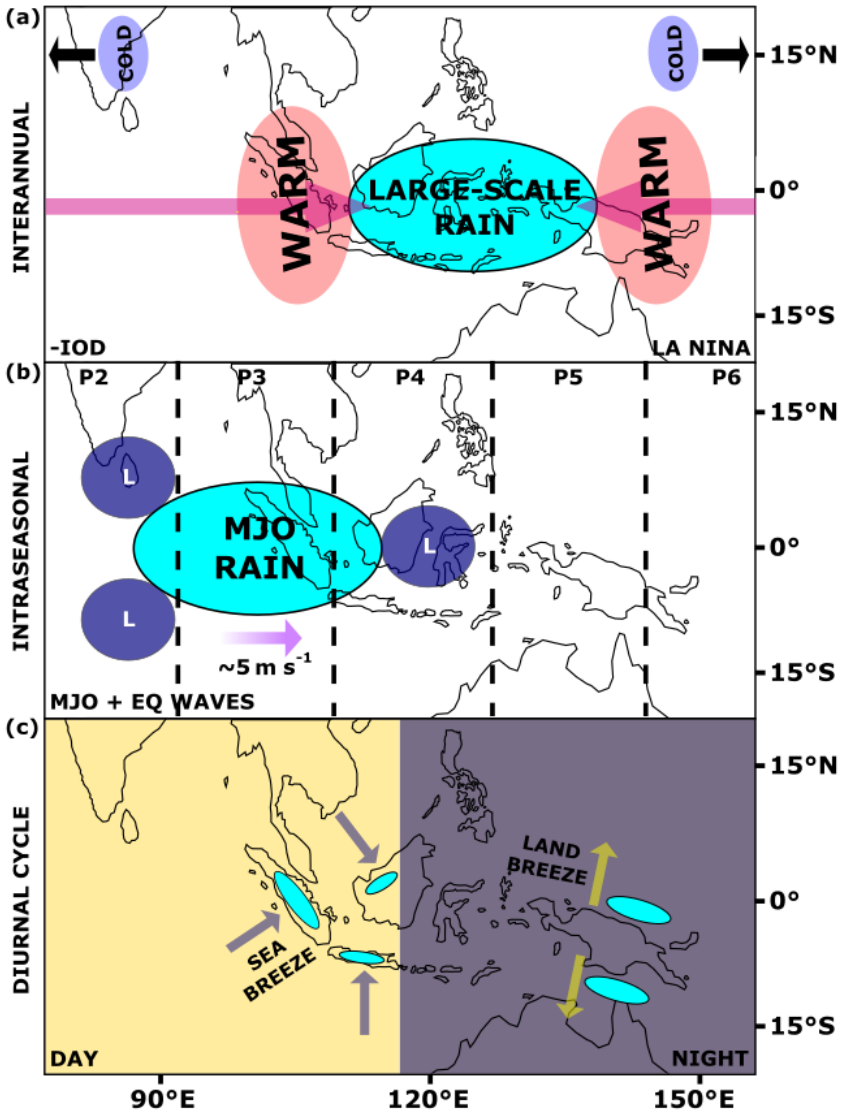

Figure 1.2: A set of schematics briefly summarising various processes which influence rainfall patterns over the Maritime Continent. These are at (a) interannual timescales, associated with the Indian Ocean Dipole (IOD) and El Niño Southern Oscillation (ENSO), shown for their respective negative phases, (b) intraseasonal timescales, associated with the Madden–Julian Oscillation (MJO) and equatorial waves and (c) diurnal timescales, associated with land-sea breeze dynamics. In (b), labels at the top of the panel highlight approximate geographical locations in which the MJO is active at each phase. In (c), cyan ovals are as in (a) and (b) but for rainfall associated with diurnal convective propagation.

anomalies of up to around 3 mm day^{-1} relative to climatology), shown in Figures 1.2a and 1.3b. These relationships are more distinct in the dry season (Hendon, 2003), though Jia et al. (2016) highlight that for strong El Niño and La Niña events in the wintertime, rainfall is reduced and enhanced, respectively, in the northern and eastern MC by up to 5 mm day^{-1}.

The Indian Ocean Dipole (IOD) is another mode of variability important on interannual timescales (e.g. Saji et al., 1999; Saji and Yamagata, 2003), and has similar phases to ENSO. During the positive IOD, high and low SSTs are observed in the western and eastern Indian Ocean, respectively. The converse applies to the negative IOD. These SSTs produce a Walker-like circulation with enhanced easterlies across the Indian Ocean during the positive IOD, leading to enhanced descent over the MC and uplift over eastern Africa. Suppression of rainfall is primarily observed over the western portion of the MC during this phase (Figure 1.3c). The negative IOD has a circulation opposite to that of the positive IOD. Therefore, the negative IOD favours an increase in rainfall over the MC, as displayed in Figure 1.2a alongside the La Niña signal originating from the Pacific, though rainfall enhancement is primarily observed from the southwestern MC to mainland southeast Asia (Figure 1.3d).

1.1.2 Intraseasonal variability: Madden–Julian Oscillation and equatorial waves

The Madden–Julian Oscillation (MJO, Figure 1.2b) is the main source of intraseasonal variability in the Tropics, with a long-period oscillation of roughly 30-90 days (e.g. Madden and Julian, 1994). Wheeler and Hendon (2004) derived eight MJO phases through empirical orthogonal function analysis of top-of-atmosphere outgoing

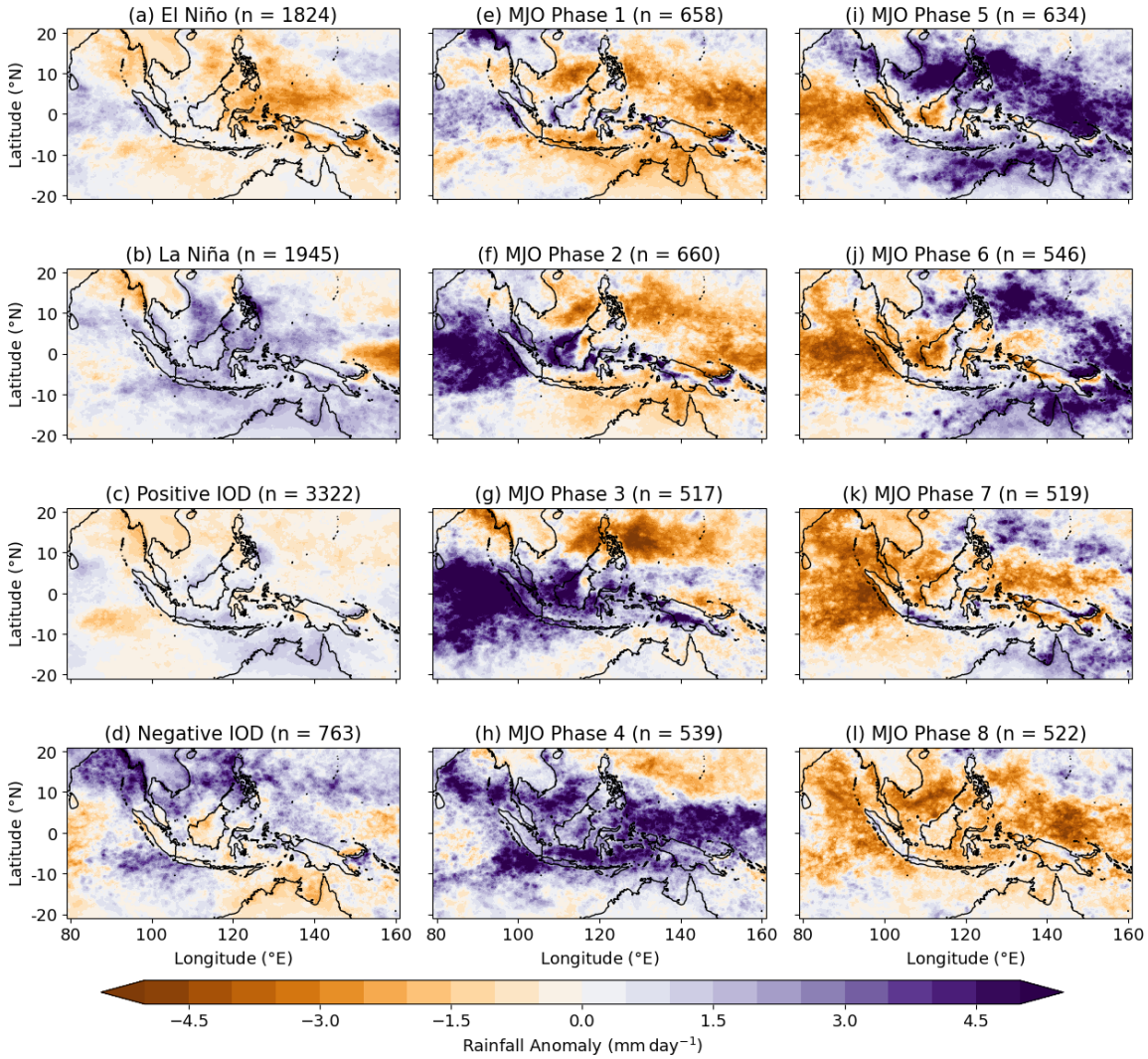

Figure 1.3: Rainfall anomalies over the Maritime Continent for (a-b) the El Niño and La Niña phases of the El Niño Southern Oscillation, (c-d) the positive and negative phases of the Indian Ocean Dipole, and (e-l) the eight phases of the Madden-Julian Oscillation, as described by Wheeler and Hendon, 2004. These anomalies are relative to the mean across 20 years of GPM rainfall from December 2000-November 2020. Values of n represent the number of days within each of the phases, over which composites are constructed. MJO RMM1 and RMM2 data (Wheeler and Hendon, 2004) are used to define the active phase of the MJO, where if the amplitude ($\sqrt{RMM1^2 + RMM2^2}$) exceeds 1, an MJO event occurs. ONI data for ENSO is derived from the average sea surface temperature anomaly of the central-eastern tropical Pacific. DMI data for IOD is derived from the anomalous sea-surface temperature gradient between the the western equatorial and southeastern equatorial Indian Ocean. Both ONI and DMI data are broadcast to daily equivalents and later smoothed with a 31-day running mean. El Niño events are defined for days where ONI is $\geq$ 0.5°C, and La Niña events are defined where ONI is $\leq$ -0.5°C. Positive IOD events are defined for days where DMI is $\geq$ 0.2°C, and negative IOD events are defined where DMI is $\leq$ -0.2°C.

longwave radiation and zonal wind at 850 and 200 hPa. These phases describe the eastward propagation of the active, or convective, phase of the MJO through the tropical warm pool from the Indian Ocean to the West Pacific. The active (suppressed) envelope can be characterised by rainfall anomalies exceeding $\pm 5\,\mathrm{mm\,day^{-1}}$ in regions, relative to climatology (Figure 1.3e–l). Applying the convention of Wheeler and Hendon (2004), the active phase of the MJO is observed over the MC during Phases 4–5. Over the MC, Liang et al. (2022) showed that the MJO can be attributed to around 60% of total rainfall, and 50% of total extreme rainfall.

The MJO propagates at a speed of around $5\,\mathrm{m\,s^{-1}}$ as SSTs and induced surface heat fluxes help to prime the atmosphere to the east for further convection, at a feedback timescale of around seven days, suppressing convection to the west (Hendon and Glick, 1997; Woolnough et al., 2000, 2001; Zhang, 2005). Several theories attempt to explain MJO propagation, as outlined in a thorough review by Zhang et al. (2020).

One key theory involves moisture modes, where MJO propagation is dictated by tropical moisture anomalies (e.g. Adames and Maloney, 2021). Instability to this mode occurs even though precipitation is a strongly increasing function of saturation in the tropical atmosphere (Raymond and Fuchs, 2009), as this instability is non-linear. Precipitation does not simply remove humidity from the environment, with the convection itself leading to increased moisture import and further excitation of convection, through latent heat release, leading to a positive feedback loop. Cloud-radiative feedbacks, such as the increased longwave warming effect of deep convection, and surface fluxes through heightened SST anomalies and enhanced wind-driven evaporation in the lower-levels, further prime the troposphere and associated convective environment. These non-linearities can in turn affect MJO propagation and the

structure of the associated moisture field (e.g. Sobel and Maloney, 2013; Adames and Wallace, 2015; Chen and Wang, 2019; Wang et al., 2020).

Synoptic-scale inertial gravity waves embedded within the MJO are also thought to enable eastward propagation (e.g. Yang and Ingersoll, 2013). The theory does not explicitly incorporate moisture, other than in enabling precipitation to occur once convective instability has developed. Convection can help to excite gravity waves to transport mass away from convection, producing a cycle of convective excitation. Other studies also suggest the active envelope consists of both mesoscale and synoptic-scale components (Majda and Stechmann, 2009), thereby challenging the canonical view of the MJO being a purely large-scale mode.

One of the other key theories relates MJO characteristics to equatorial wave dynamics (e.g. Hendon and Salby, 1994; Maloney and Hartmann, 1998; Matthews, 2000). Equatorial waves have theoretical structures described by solutions to the shallow water equations (e.g. Matsuno, 1966; Gill, 1980). Examples of equatorial waves include Kelvin (eastward-moving with no meridional velocity component), mixed Rossby-gravity (non-zero meridional velocity, with eastward- and westward-moving solutions) and equatorial Rossby waves (westward-moving). These waves are trapped near the Equator due to equatorward reductions in the magnitude of the Coriolis force towards zero values, and can be excited by processes such as diabatic heating of the tropical atmosphere.

During the active phase of the MJO, a tongue of low pressure strengthens to the east, associated with a Kelvin wave, with pressure troughs to the northwest and southwest, associated with Rossby waves (Matsuno, 1966; Gill, 1980). The opposite is observed for the suppressed phase of the MJO. Through this hypothesis, MJO physics

can be related to equatorial waves through the feedbacks between these dynamics and the moist properties of the large-scale convective field (Wang et al., 2016).

However, equatorial waves are also independently influential on meteorology across the Tropics and the MC. As shown by filtered satellite observations of outgoing long-wave radiation (Wheeler and Kiladis, 1999), equatorial waves help to organise and can couple with tropical convection on synoptic to sub-seasonal timescales, thereby affecting the probability of rainfall. Ridout and Flatau (2011), for example over the western MC, show that these waves are key in shifting regions of low-level moisture convergence. Significant increases in extreme precipitation can be observed when high amplitude waves are present over the MC. Senior et al. (2023) found extreme precipitation may be around 60% more likely when convectively coupled Kelvin waves are observed over western Sumatra. Latos et al. (2021) found extreme rainfall to be twice as likely over Sulawesi when these waves are present, and up to eight times as likely if there is additional activity from other equatorial waves. Ferrett et al. (2020) found extreme precipitation over the broader MC can be up to four times more likely in the presence of high amplitude waves. However, each wave has a spatially variable degree of influence on rainfall patterns across the MC (Yang et al., 2003; Ferrett et al., 2020; Peatman et al., 2021).

1.1.3 Diurnal cycle

The intensity of diurnal temperature fluctuations was described previously as a key descriptor of the broader tropical atmosphere. The diurnal cycle is the most fundamental process controlling variability in convection over the MC on local scales, modulated by complex land-sea interactions, making its role much more distinct than

that over other regions of the Tropics (e.g. Yang and Slingo, 2001). These interactions develop initially through daytime insolation, where increased warming of the land relative to the ocean, due to differences in heat capacity, sets up a land-sea temperature contrast. This contrast forces sea breeze convergence onto land, through the induced pressure gradient, and upslope mountain winds, forming deep convection and precipitation into the afternoon and evening inland/on mountain flanks (Qian, 2008). Overnight, the land cools more rapidly than the ocean, reversing the pressure gradient, forming land breezes and downslope mountain winds, and in some cases, resulting in offshore propagation of the convection that formed overland. These processes are depicted in Figure 1.2c.

Mechanisms associated with the propagation of convection offshore overnight remain an active area of research. Authors such as Mori et al. (2004) and Yokoi et al. (2017) provide thorough overviews of existing hypotheses. These include various interactions between the ambient wind, gravity waves, cloud structure, and thermal instability produced by diabatic processes over land (e.g. Satomura, 2000; Nesbitt and Zipser, 2003; Warner et al., 2003; Hassim et al., 2016; Peatman et al., 2023). Mori et al. (2004) and Yokoi et al. (2017) both state that offshore propagation and subsequent decay of convection over land is likely driven by a combination of these theories.

The diurnal cycle in rainfall is common to most islands in the MC, with a distinct diurnal peak in the maximum rainfall from the afternoon to the late evening over land, compared to the morning over the ocean (Figure 1.4). The impact of the diurnal cycle is variable across the region, though. For example, changes in wind regimes and circulations both day-on-day and over the MC can modulate the strength of

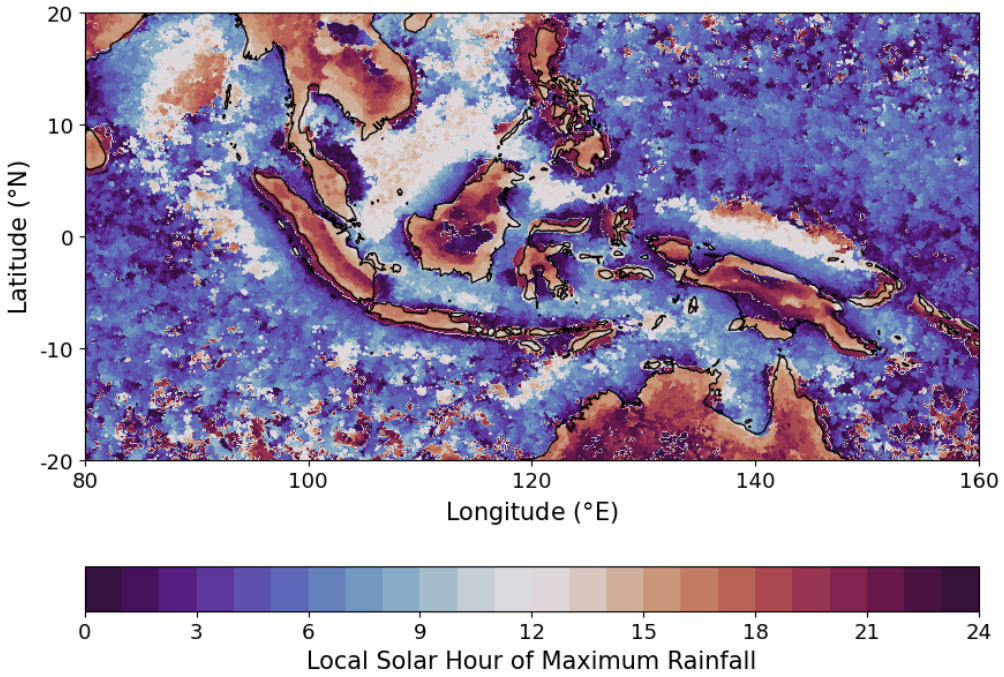

Figure 1.4: Local solar hour of maximum rainfall for each gridpoint across the entirety of the Maritime Continent, derived from the mean diurnal cycle of 20 years of GPM rainfall from December 2000-November 2020.

the diurnal cycle over land, with additional higher-order components of variability influencing diurnal characteristics further (e.g. Peatman et al., 2021; Mustafa et al., 2024). Therefore, the role of the diurnal cycle cannot be generalised for the entire region.

1.1.4 Synoptic circulations

There are other well-documented processes which influence rainfall patterns in the MC; however, they operate on more variable and synoptic spatial and temporal scales. For example, cold surges are phenomena which form due to strengthened prevailing low-level northerly-to-northeasterly winds due to cold air outbreaks originating from

the Siberian High (e.g. Koseki et al., 2013). Cold surges bring enhanced rainfall at their leading edges due to perturbing pre-existing monsoonal flow. Closely related to, and often induced by, cold surges are Borneo vortices (e.g. Hardy et al., 2023; Crook et al., 2025). These form in the later phases of the northeasterly monsoon over the South China Sea and are one of the main drivers of rainfall in regions such as Malaysia.

On top of these, tropical cyclones are also impactful in the MC. Tropical cyclones are well-known destructive weather systems with impacts felt worldwide – in the MC, compared to other processes, these systems tend to mostly detrimentally impact the northern MC, primarily in boreal summer, through induced precipitation and wind extremes (e.g. Takahashi, 2011; Li et al., 2022). Tropical cyclones in this region have the potential to reduce larger-scale rainfall over the MC through changes to the wind field, leading to anomalous region-wide subsidence and moisture divergence (e.g. Scoccimarro et al., 2020; Li et al., 2024). Latos et al. (2023) identified that environmental spin-up driven by processes such as equatorial waves and the MJO can also cause unusual near-equatorial tropical cyclones to form.

1.2 Scale interactions

While various key processes have particular direct impacts on MC rainfall, additional interactions between them exist on a range of spatial and temporal scales. These interactions make the meteorological patterns across the region more difficult to understand.

1.2.1 MJO–diurnal cycle interactions

A well-known scale interaction exists between the MJO and the diurnal cycle. Generally, it is expected that the active (suppressed) envelopes of the MJO lead to increases (reductions) in large-scale rainfall over the MC. Oh et al. (2012) noted that the strong MJO winds and their interactions with monsoonal flow can in fact disrupt convergence, and therefore convective characteristics, over islands on diurnal timescales. Their study highlighted a reduction in average land rainfall by around $0.5\,\mathrm{mm\,hr^{-1}}$ as the MJO active envelope passes over the MC from the Indian Ocean. Convergence and therefore convection may, as a result, be concentrated over the ocean, though with a smaller increase in oceanic rainfall relative to the decrease in rainfall over land.

Additionally, Peatman et al. (2014) showed that a 'vanguard of precipitation' jumps ahead of the active MJO envelope by one phase (around six days) while the MJO is in its suppressed phase over the MC (depicted schematically in Figure 1.5). This phenomenon is influenced by the strong diurnal cycle over land, where changes in the amplitude of the diurnal cycle account for 80% of the changes in daily mean rainfall during an MJO cycle. Related to equatorial wave dynamics, frictional and topographic moisture convergence is driven by the eastward pressure gradient. Clear sky conditions, which promote destabilisation of the atmosphere through incoming insolation, ahead of the main convective envelope combine with the low thermal inertia of the land, allowing a rapid response to the diurnal cycle, moistening the environment to the east and enabling convection to develop. Thus, the islands act as a precipitation barrier to the smooth MJO propagation across the MC (e.g. Qian, 2008; Birch et al., 2016; Ajayamohan et al., 2021).

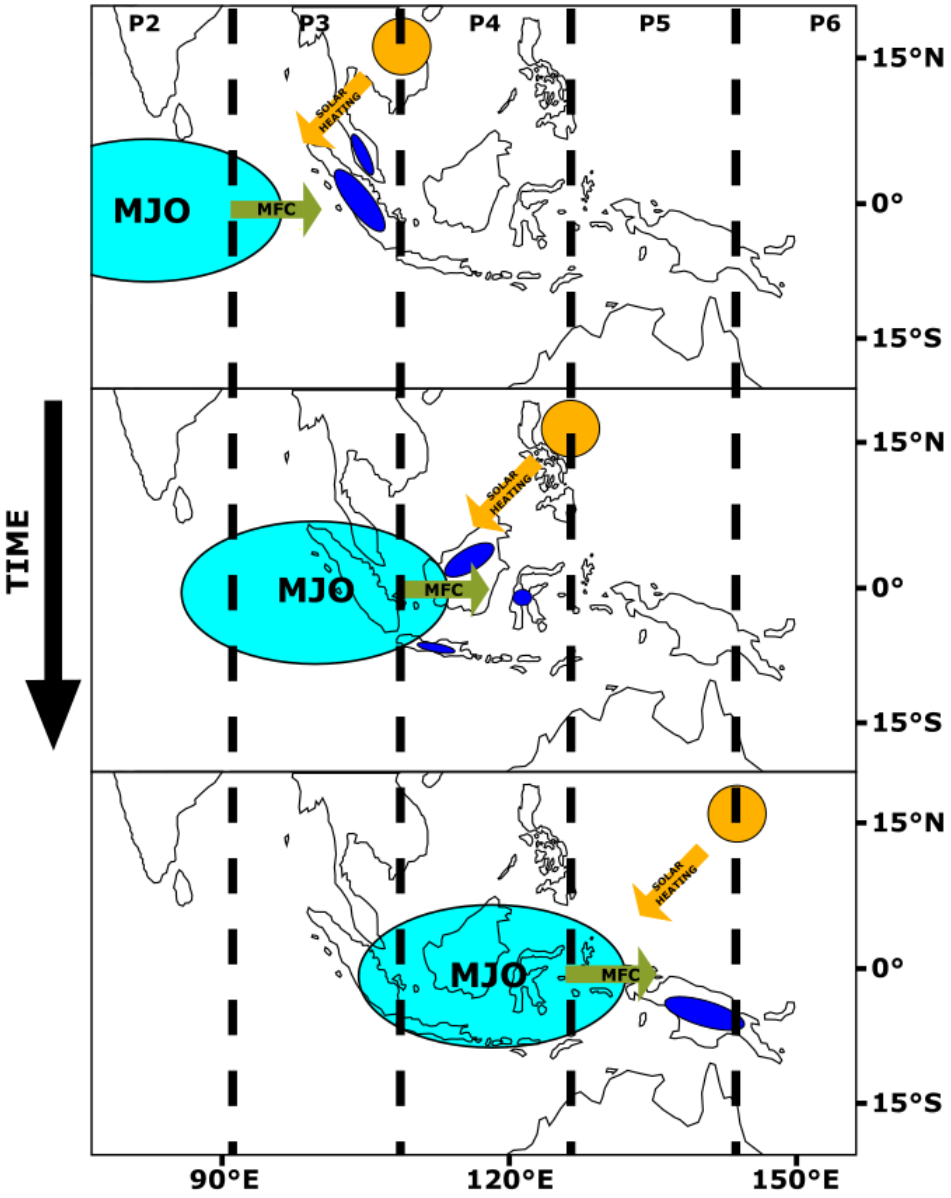

Figure 1.5: Schematic outlining a scale interaction between the Madden-Julian Oscillation and the diurnal cycle. Convergence of moisture (MFC) ahead of the active envelope, combined with diurnal heating of the land, leads to convection initiating around one phase ahead of the active envelope (dark blue ovals).

1.2.2 ENSO–diurnal cycle interaction

Similar to the MJO, ENSO interacts with the diurnal cycle. During El Niño, when there is suppressed convection over the MC, the diurnal cycle may be excited due to increased incoming solar radiation, giving precipitation anomalies of the opposite sign over the islands, relative to the ocean (Rauniyar and Walsh, 2013). Peatman et al. (2021) also deduced that, for Sumatra, on more local spatial scales, El Niño events exhibit a more offshore style of wind regime, leading to divergence in the MC lower-troposphere. The opposite is observed for La Niña, where heightened onshore flow can suppress the diurnal cycle by limiting seaward propagation of convection, reducing the contribution from diabatic effects over land.

Lu et al. (2023) observed opposite geographical relationships between modifications of the diurnal cycle amplitude between El Niño and La Niña. In their study, the amplitude is enhanced over the western MC and reduced over the east in El Niño, with the opposite findings for La Niña, attributed to shifts primarily in ENSO-regulated background moisture and convergence. However, diurnal winds were identified as being four times as important in modulating these interactions in the eastern MC, compared to the west. These findings emphasise the two-way interactions between the diurnal cycle and large-scale modes of variability.

1.2.3 Equatorial wave–diurnal cycle interactions

Equatorial waves also have the potential to interact with the diurnal cycle. Baranowski et al. (2016) showed that Kelvin waves can enhance island precipitation, as well as increase the probability of wave propagation across the MC, if they arrive in phase with the diurnal cycle. Sakaeda et al. (2020) found that Kelvin waves can

also modulate the diurnal amplitude by modifying the lower-tropospheric wind field, thereby enhancing perturbations in moisture and vertical motion over land. Geng et al. (2020) observed similar results for mixed Rossby-gravity waves.

1.3 Model representation

The observational network across the MC is constrained by both the number and distribution of meteorological stations (e.g. Koh and Teo, 2009), with the shallow bathymetry in areas also limiting the potential for intensive ocean data collection due to the highly variable environment modulated by strong currents and waves. These limitations feedback onto other datasets which depend on existing knowledge often obtained from observations. Weather and climate models enable us to fine-tune parametrisation schemes and general model set-up to both capture processes better and to also test hypotheses in more idealised scenarios.

Simulations of MC precipitation, however, show many biases within models when compared to observations. The prediction of atmospheric and oceanic variables over the MC is challenging because of the complex regional geography and influences from remote forcings. Errors that persist within the MC have the potential to propagate globally through the induced Rossby waves originating from vertical heating over the region (Neale and Slingo, 2003; Qian, 2008; Love et al., 2011). These features additionally feedback onto the way in which we accurately predict weather. Large-scale spatial variability in precipitation tends to have greater predictive skill than at more local scales (e.g. Ferrett et al., 2021). Skill is inevitably dependent on the characterisation of key processes within models.

1.3.1 Resolution

Increasing horizontal model resolution has been shown to improve model performance through better representation of MC island geography and associated land–sea breeze circulations (e.g. Schiemann et al., 2014; Rashid and Hirst, 2017). Neale and Slingo (2003) and Qian (2008) highlighted, through island-removal experiments, that under-representation of the complex geography of the MC and associated circulations/dynamics can alter simulated rainfall by around 15%. Tan et al. (2021) found that by varying which island was removed in sensitivity experiments can significantly impact the role of the lower-tropospheric zonal winds in modulating the magnitude and sign of moisture convergence and rainfall intensity over neighbouring islands.

Inclusion of the islands can help to improve interactions with larger-scale modes of variability (Holloway et al., 2013), whilst making responses of convection to island-specific processes, such as gravity wave forcing, more realistic (Love et al., 2011). Precipitation sensitivity to complex orography is reduced, thereby confining wet biases over smaller areas (Argüeso et al., 2020).

However, studies have emphasised that changes in resolution are only effective at the coarsest scales, up to a 'threshold' (e.g. Pearson et al., 2014). In GCMs, Neale and Slingo (2003) state a threefold increase in horizontal resolution is still insufficient to resolve diurnal processes. Rainfall can become too strong at higher resolution, with poor timings in the diurnal cycle over the islands (Li et al., 2017). Therefore, some processes still remain unresolved even with fining of horizontal grid spacing.

1.3.2 Parametrisation

With increases in computing power, convection-permitting models (CPMs), where convection is represented explicitly, are shown to better resolve both rainfall and the land-sea breeze circulations (e.g. Birch et al., 2016). These CPMs provide more realistic temperature and moisture tendencies compared to their parameterised counterparts (Holloway et al., 2012).

While CPMs agree with existing hypotheses such as the impacts of the diurnal cycle on rainfall and improving characteristics of spatially heterogeneous features, biases persist. In particular, these issues are often linked to diurnal rainfall characteristics, with potential for overestimation of land-based precipitation and feedbacks onto large-scale modes of variability (e.g. Birch et al., 2016; Hassim et al., 2016; Vincent and Lane, 2016; Ajayamohan et al., 2021).

These findings imply unresolved processes that require parametrisation remain. Further modification of parameterised processes can also help, such as through cloud property schemes and prescribed ocean conditions (e.g. Su et al., 2022; Okugawa et al., 2024). However, fundamental issues in employed model physical parametrisations, which represent sub-grid processes, are linked to limitations in current knowledge.

1.3.3 Coupling

Xue et al. (2020) produced a review on the role of coupling in modelling studies across the MC, highlighting that there are unresolved physical processes and inadequate representation of the ocean–atmosphere system, which can be alleviated by the introduction of coupling. Coupling is beneficial in managing atmospheric-ocean feedbacks, such as those related to SSTs, heat fluxes, wind and moisture, which can

correct deficiencies in intraseasonal variability in precipitation (Pegion and Kirtman, 2008; Klingaman and Woolnough, 2014; DeMott et al., 2019).

A more diurnal representation of SSTs when implementing coupling is increasingly preferable (e.g. Bernie et al., 2007). Diurnal rectification and air-sea feedbacks induced by sub-daily coupling can result in more accurate diurnal evolutions of convection, while also improving tropical mean state SST and precipitation distributions (Bernie et al., 2008; Li et al., 2020).

This imposed diurnal SST is sensitive to vertical resolution. By mixing the upper ocean to various depths to simulate coarsened vertical resolution, Karlowska et al. (2024) noted weakened diurnal SST variability; thereby, in their study, weakening the feedback with the MJO and reducing regional rainfall. Similarly, Ma and Jiang (2021) found increased vertical resolution warmed the surface ocean, helping to enhance moisture gradients and convergence, convective instability and vertical circulations to the east of the active envelope, strengthening MJO propagation.

Mean biases in the environmental state can affect the sensitivity to coupling (Klingaman and DeMott, 2020). Coupling may be insufficient to fully correct mean-state biases, which remain reliant on model configuration, including parametrisations and imposed sensitivities (Klingaman and Woolnough, 2014; DeMott et al., 2019; Li et al., 2020).

1.3.4 Future projections

Our modelling capabilities of the present climate inform our projections for the future. As the MC already experiences extreme rainfall regulated by processes operating over a wide range of spatial and temporal scales, it is important to assess how these

patterns may change with global warming. Models can help extend inferences gained from observational analysis of rainfall trends over recent decades, both spatially and temporally, given these may tend to be very location-specific (e.g. Li et al., 2018).

Various studies as part of the Coordinated Regional Climate Downscaling Experiment (CORDEX) aimed to provide climate information at finer spatial resolutions, using dynamical downscaling to capture more regional and synoptic variability (e.g. Supari et al., 2020; Tangang et al., 2020; Ngai et al., 2022). By analysing various indices reflective of both wet and dry extremes, these studies find reductions in mean future rainfall of up to 30% in boreal summer, primarily across Indonesia. In boreal winter, equivalent increases are observed over the northern MC and mainland Indochina. These results were noted to be due to changes to the monsoonal circulation and the associated moisture convergence in the future climate.

Kang et al. (2019), through application of CMIP5 scenarios to regional climate model projections, found a significant decrease in intermonsoon rainfall, linked to shifts in the regional meridional circulation. Hsu et al. (2025) observed an amplification of wet and dry extremes with global warming, driven by solely dynamic processes, and combined moist thermodynamic and dynamic processes, respectively.

Studies have also highlighted (extreme) rainfall may be modulated by shifts in larger-scale forcing (Liang et al., 2022). Chen et al. (2023) found an eastward shift in the ENSO-related rainfall dipole across the MC in the dry season, with additional amplifications of the drying (wetting) commonly associated with El Niño (La Niña). Ghosh and Shepherd (2023) found, using CMIP6 scenarios, similarly strong changes in dry season rainfall driven by shifts in the forcings associated with both basin-wide warming and the equatorial SST gradient across the Pacific Ocean, tied to ENSO.

However, studies have noted that climate models struggle to reproduce the correct SST patterns and trends across the Pacific, which will feedback onto the Walker circulation and related large-scale flows, thereby potentially affecting projections for the MC (e.g. Dhame et al., 2025).

While Chen et al. (2023) reported that even historically biased models do not have significantly different future projections, uncertainty across ensemble members will persist. Each member, in isolation, will have varying ability to successfully capture key processes highlighted, or alluded to, in the 'Resolution', 'Parametrisation', and 'Coupling' sections, such as evolution of the mean state, processes intrinsic to natural climate variability or local-scale effects (Xiao et al., 2022; Ghosh and Shepherd, 2023). As a result, projections may offer too broad a range of potential outcomes, which could reduce their overall reliability.

1.4 Scope for research

Through this literature review, an insight into various components associated with the literature around the meteorology observed across the MC has been provided. Active research in this scientific area is crucial given the risks posed to communities in the region due to extreme rainfall. There are several key processes influencing rainfall patterns over the MC, including the diurnal cycle and larger-scale modes of variability, such as the MJO, ENSO, IOD and equatorial waves. These processes interact with one another, leading to complex regional precipitation patterns, further impacted by additional synoptic-scale and transient processes. These interactions cannot be generalised for the entirety of the region, with studies requiring to focus

on particular constituent islands within the archipelago.

The resultant limitations in our knowledge of meteorological processes in the MC, as well as the inherent difficulty in predicting convection, mean that systematic biases exist in the simulation of precipitation. These biases have been addressed through significant efforts in improving the way in which we model convection, a function of the increase in computational power overtime. Increasing the horizontal resolution within simulations allows us to better visualise island-specific processes, which are sensitive to the representation of complex topography in the region. Removing the requirement for parametrisation of various processes also gives a more realistic representation of convection. The unique geographical configuration of the MC means that coupling to the ocean helps to correct air-sea interactions, such as surface heat flux exchange, which affect convective processes.

Even with these developments in modelling capabilities, the representation of precipitation and convection continues to deviate away from observations. The requirement for better representation of key processes will also be crucial for future projections of MC rainfall, given the potential for significant shifts in the nature of convection across the region. We remain dependent on newer observations to help inform us on the finer-scale, complex interactions that significantly influence the environmental state of the MC. In turn, these observations would provide insight into the components within existing models that need readdressing, particularly sub-grid processes that often remain parameterised. The advent of sub-kilometre modelling approaches across the Tropics will inevitably prove beneficial for better representation of convection, which may be coupled with more intensive statistical and machine learning approaches. These approaches may help with analysing features previously

difficult to pick out from non-linear, higher-order variability and complex relationships between a range of environmental parameters in the region.

1.4.1 Motivation

The primary driver for research into rainfall patterns over the MC, as stated throughout, comes through the impact and detriment that the region experiences due to severe weather. Primary impacts include flooding, landslides, damage to infrastructure and loss, with regards to both health and economy (e.g. Torti, 2012; Wijayanti et al., 2017; Narulita and Ningrum, 2018). Impacts are a function of factors such as event severity, duration and probability, demographic, socioeconomic status, displacement and healthcare access (e.g. Hashim and Hashim, 2014; Jang et al., 2021). Risk has been further exacerbated through rapid urbanisation, ecosystem changes and generally slow developments towards more resilient infrastructure (Emam et al., 2016). With particular emphasis on the latter, developments for mitigating disaster may show disparities between wealthier urban, and poorer rural, areas, thereby modifying risk levels (Hamel and Tan, 2022). Therefore, accurate forecasting of rainfall over the MC is crucial.

However, our ability to accurately predict weather across the MC is highly variable in both space and time (Zhang et al., 2016; Ferrett et al., 2023). On seasonal-to-subseasonal (S2S) scales, larger-scale variability is easier to predict - for example, skill in MJO prediction, particularly in the wet season, is up to around four weeks ahead (Wang et al., 2019; Abhik et al., 2023). Local-scale variability is harder to predict even with convective-permitting forecasts, due to the importance of the representation of the diurnal cycle, associated with the complex geography of the region (Ferrett et al.,

2021), and (sub-)cloud-scale processes remain parametrised. For limited-area models (LAMs), as an example, there is additional influence of errors in process representation at the boundaries, driven by global models (Wolf et al., 2024).

Wang and Li (2020) note that increases in ensemble members, which each have better, and diverse, process characterisation, may provide one route for improved forecasting. Sharma et al. (2023) add that being selective of ensemble members which, together, maximise skill can help to improve the spread and reduce error in forecasts, while increasing the temporal scales in which skill is maintained up to. Other studies have developed pattern-conditioned and hybrid forecasts which incorporate knowledge related to broader planetary to synoptic-scale circulations, and statistical relationships between key processes and rainfall, which improve skill (e.g. Ferrett et al., 2023; Gonzalez et al., 2023). Newer developments are now shifting towards using machine learning methods which can benefit near-real time forecasting (nowcasting) of regional meteorology (Smith et al., 2024).

Fundamentally, process knowledge is most important for better forecasting, with research into rainfall patterns across the MC, using observations, models, and other datasets, feeding into the diagnostics used in numerical weather prediction (NWP). However, it should be emphasised that better prediction of these hazards will not solely improve the prediction of impacts or early warning. Outlined in the World Weather Research Programme (WWRP) High Impact Weather project of the World Meteorological Organisation (WMO), value chain frameworks (Golding et al., 2019) are increasingly becoming fundamental in providing a bridge from the observations to effective warnings and action. These frameworks implement informational needs of the end users, combining physical understanding and forecasting of hazards with

the decision and communication aspects of warnings (e.g. perception of, and the relationship of hazard with, risk and impact).

The work conducted as part of this thesis is therefore done with the aim to contribute to the pipeline from process understanding - the focus of the conducted research - going towards better warnings, training of forecasters, decision-making and disaster preparedness. Within this chapter, extensive work has been outlined related to process knowledge, from large-scale modes of variability to the diurnal cycle to scale interactions between various phenomena. Several knowledge gaps have been identified, and are outlined in the three following subsections. These gaps relate primarily to transient and/or synoptic-scale to mesoscale processes across the MC, which remain understudied.

1.4.2 Knowledge gap 1: tropical-extratropical interactions

As highlighted earlier in this chapter, the latent heat originating from the intense rainfall and convection over the MC interacts with atmospheric processes elsewhere. This interaction comes through the generation and propagation of Rossby waves, and associated transferral of energy, towards the extratropics (Jin and Hoskins, 1995). Ramage (1968) coined the region to be an 'atmospheric boiler box' as the MC is important in influencing global atmospheric circulation. Therefore, the region represents a source of broader tropical-extratropical interactions.

A primary source of the influence of the extratropics on the MC are cold surges (e.g. Koseki et al., 2013), as described in Section 1.1.4, which originate from Northern Hemisphere cold air outbreaks. These surges perturb the monsoonal flow, leading to anomalies of enhanced rainfall on synoptic spatial and temporal scales. From

the Southern Hemisphere, similar interactions have been proposed, linked to dry air intrusions (DAIs), researched briefly in a few studies specific to regions within the MC (e.g. Murata et al., 2006; Seto et al., 2006; Feng et al., 2021).

Disturbances forming along extratropical wave trains promote the descent of DAIs from the upper-troposphere/lower-stratosphere (e.g. Browning, 1997; Funatsu and Waugh, 2008; Casey et al., 2009). These transient intrusions perturb tropical humidity, impacting regional meteorology (e.g. Brown and Zhang, 1997; Knippertz, 2007; Ryoo et al., 2008). Breaks in tropical precipitation and convective suppression are observed through modification of the convective profile and associated energetics (e.g. Mapes and Zuidema, 1996; Yoneyama and Parsons, 1999; Parker et al., 2016; Fletcher et al., 2020). DAIs themselves can also modify the lower-level wind and moisture field, with low-level convergence at their leading edge lifting nearby warm, moist air, thereby organising deep convection and increasing rainfall downstream (e.g. Allen et al., 2009; Berry and Reeder, 2016; Ward et al., 2021).

DAIs have been observed over the southern MC with potential links to changes to the convective environment, and associated wind and moisture fields (Murata et al., 2006; Seto et al., 2006; Feng et al., 2021). However, studies have not extensively analysed these processes beyond individual events. Given regional rainfall can be influenced by synoptic-scale and transient variability, DAIs warrant further investigation. Additionally, as regional models for the MC are prescribed with particular lateral boundary conditions, transients such as these intrusions may not be fully captured. Understanding the key regulatory mechanisms and resultant impacts on rainfall will help better understand the perturbations they induce on the environment, building to how they are represented along model boundaries.

1.4.3 Knowledge gap 2: mesoscale air-sea interactions

Ocean-atmosphere processes are known to be important in the MC - primary research that has been conducted revolves around heat fluxes that emerge from the warm pool in which the MC sits. When integrated over the MC, these fluxes can modify local-to-large-scale circulations in the atmosphere. These studies tend to compare the broader role of ocean-atmosphere coupling in models in modifying atmosphere processes, as highlighted in Section 1.3.3 (e.g. Xue et al., 2020).

On finer spatial scales, little work has been conducted with relation to the role of air-sea interactions in modifying rainfall patterns in the MC. Elsewhere, in the world, air-sea interactions at these scales have been analysed by using mesoscale ocean eddies (spatial and temporal scales on the order of 100 km and 10-100 days respectively; e.g. Chelton et al., 2011) as a representation of fine-scale variations in SSTs. These anomalies are key in facilitating the aforementioned air-sea interactions (e.g. Frenger et al., 2013; Bôas et al., 2015; Seo et al., 2023). Induced surface heat fluxes can modify the lower-tropospheric wind field and atmospheric boundary stability which can then lead to changes in cloud and rainfall.

Mesoscale ocean eddies represent a key component of the mixing associated with the MC, generated particularly along narrow passages or straits, and through interaction between currents (e.g. Ffield and Gordon, 1996; Sprintall et al., 2014; Wang et al., 2021). No studies have assessed the air-sea interactions attributed to mesoscale ocean eddies across the MC - limited studies exist for these interactions across the Tropics more broadly (e.g. Liu, Li, Chen, Fang and Li, 2018; Roman-Stork et al., 2021; Aguedjou et al., 2023). These studies found potential roles of the SST anomalies attributed with mesoscale ocean eddies to influence atmospheric properties. As the MC

operates as a broad heat and energy source for the development of convection, testing whether anomalies at finer-scales have an influence may help inform the running of coupled ocean-atmosphere models for NWP, and how complex they need to be, in representing these mesoscale features.

1.4.4 Knowledge gap 3: diurnal land-sea interactions

Across the MC, the diurnal cycle is well-known for influencing land-sea breeze circulations, helping in the development of convection over the islands (e.g. Qian, 2008). As outlined in Section 1.1.4, a unique phenomenon, where convection is generated in the afternoon over the land and then propagates offshore overnight, is observed over the entirety of the region. This convection may manifest as lines of storms represented by mesoscale convective systems (MCSs; e.g. Peatman et al., 2021).

Numerous studies have explored the propagation of convection offshore from islands across the MC, and the specific storm-scale dynamics associated with them. Of particular focus has been the island of Sumatra in the western MC. Research has identified the role of processes such as the background wind field, density currents, gravity waves and local-scale thermodynamics in modulating the convection propagation offshore towards the Indian Ocean (e.g. Peatman et al., 2023, 2025).

Minimal work has focused on convection propagating eastwards from western Sumatra. Studies have highlighted regional variability in the propagation of rainfall, from north to south Sumatra, dependent on seasonal shifts in monsoon circulation (e.g. As-syakur et al., 2019). Compared to westward-propagating systems, eastward-propagating convection must travel further across Sumatra to reach the coast, and associated extreme rainfall is not as pronounced or frequent, driven by reduced in-

teractions with wind-induced convergence (e.g. Marzuki et al., 2021). Hence, this direction of convection propagation may not receive as much attention.

There is limited knowledge of the specific details of the storm-scale dynamics associated with eastward-propagation convection. A Sumatra squall is an MCS that forms over Sumatra and propagates roughly eastward, observed primarily in the intermonsoon seasons and southwest monsoon, impactful in the nighttime to early morning over Singapore and Peninsular Malaysia (Lo and Orton, 2016). Initial work by Chan et al. (2019) showed Sumatra squalls have features akin to classical squall structure gained from knowledge elsewhere in the world (e.g. Houze, 2018). Sumatra squall initiation is thought to be formed due to low-level convergence over either the Barisan mountains of Sumatra, or over the Malacca Strait. Propagation and intensification, similar to studies such as Peatman et al. (2023), were shown by Chan et al. (2019) to be linked to interactions with the wind field and density currents. Recently, Nguyen et al. (2025) found interactions between Sumatra squalls and modes of variability such as the MJO and equatorial waves, which influence MCS characteristics region-wide (e.g. Crook et al., 2024).

Understanding both large-scale and storm-scale drivers of the convection propagating eastward over Sumatra is beneficial for applications in NWP across the western MC. With more knowledge of these processes, modelling and forecasting capabilities can be enhanced for the region by informing key diagnostic variables that are crucial for convective characteristics to form.

1.4.5 Thesis aims and structure

This PhD thesis broadly aims to contribute to improving our understanding of the variability in MC rainfall, by analysing a variety of key processes and scale interactions through usage of a combination of observational, reanalysis and model data. Several identified knowledge gaps were outlined in the previous subsection, and are explored in Chapters 2-4.

The main objectives of this PhD are to:

- Investigate the role of mid-level dry air intrusions on meteorology over the Maritime Continent.
  - Where are dry air intrusions sourced from?
  - What causes dry air intrusion development and propagation towards the Maritime Continent?
  - How do these transients influence regional rainfall patterns?
- Investigate the atmospheric response to mesoscale ocean eddies across various Maritime Continent seas.
  - What are the characteristics of mesoscale ocean eddies in the Maritime Continent?
  - Can the SST signatures of these eddies significantly influence atmospheric properties such as wind, cloud and rainfall?
  - Are the eddy characteristics and influences on the atmosphere different to those observed elsewhere in the globe?

- Investigate the dynamics associated with Sumatra squalls.
  - What processes influence the evolution of Sumatra squalls?
  - How similar are Sumatra squalls to squall lines observed across the Maritime Continent, and elsewhere?
  - What phenomena or environmental characteristics explain any differences associated with these weather systems?

Chapter 2 investigates the processes associated with mid-level dry air intrusions over the southern MC, just one form of tropical-extratropical interaction. This study uses reanalysis data to identify dry events through analysis of anomalies in mid-tropospheric humidity near to the MC, coupled with parcel trajectory analysis to determine attribution to dry air intrusions. From here, key regulatory mechanisms are analysed, and impacts on rainfall are determined. Such work provides further knowledge on this understudied process and the importance of interactions at the boundaries of the region.

Ocean-atmosphere interactions related to the SST anomalies associated with mesoscale ocean eddies are analysed in Chapter 3. Satellite altimetry data is used to track and gain insight into the characteristics of these eddies, for which reanalysis data is collocated upon to determine atmospheric responses to the eddies across the MC. With the increased focus in ocean-atmosphere coupled modelling studies for the region, this work will help to provide a bridge between solely oceanic and atmospheric studies with key information into the importance of the spatial and temporal scales for which air-sea interactions are significant in influencing MC meteorology.

In Chapter 4, analysis of convective-permitting simulations of Sumatra squalls is

conducted, to gain insight into the associated storm-scale dynamics of these systems over the western Maritime Continent. This work gives deeper knowledge into their initiation, propagation, intensification and dissipation mechanisms, and was conducted in partial collaboration with scientists at the Centre for Climate Research Singapore (CCRS). The research will enable the exploration and identification of diagnostic variables that could be useful for forecasting and modelling these squalls further.

Chapter 5 summarises the results in Chapters 2-4, synthesising them to construct overall conclusions, while determining the impact of the work and any recommendations for future research.

Chapter 2

Mid-level dry air intrusions over the southern Maritime Continent

Published in *Quarterly Journal of the Royal Meteorological Society* (2024).

Abstract

Patterns in extreme precipitation across the Maritime Continent in southeast Asia are known to be modulated by many processes, from large-scale modes of variability such as the Madden–Julian Oscillation, to finer-scale mechanisms such as the diurnal cycle. Transient mid-level dry air intrusions are an example of a feature not extensively studied over the Maritime Continent, which has the potential to influence rainfall patterns. Here, we show that these dry air intrusions originate from upper level disturbances along the subtropical jet. Mid-level cyclonic circulation anomalies northwest of Australia from December to February (DJF) intensify westerlies in the southern Maritime Continent, advecting dry air eastward. In contrast, mid-level anticyclonic circulation anomalies northwest of Australia from June to August (JJA) intensify southern Maritime Continent easterlies, advecting dry air westward. The resultant transport direction of associated air parcels is also dependent on the seasonal low-level monsoon circulation. Dry air intrusions are important in influencing low-level wind and rainfall patterns, suppressing rainfall over seas near the southern Maritime Continent in both seasons, as well as over southern Maritime Continent islands in DJF and the Indian Ocean in JJA. In both seasons there is enhanced rainfall to the east of the intrusion, where there is moist return flow to the extratropics. This study highlights the importance of synoptic-scale extratropical features in influencing meteorological patterns in the Tropics.

2.1 Introduction

The Maritime Continent (MC) in southeast Asia consists of an archipelago of thousands of islands and several shallow seas (Figure 2.1a). High sea-surface temperatures and variable topography make the region conducive to the formation of deep convection all year round. Rainfall over the MC (Figure 2.1b-c) is twice the global mean (Yamanaka et al., 2018), with mean precipitation rates exceeding $10\,\mathrm{mm\,day^{-1}}$ (Ichikawa and Yasunari, 2006). The associated latent heat release influences the global atmospheric circulation and climate through Rossby wave generation and subsequent propagation towards the extratropics (Jin and Hoskins, 1995). The MC has therefore been termed an 'atmospheric boiler box' (Ramage, 1968).

Deep convection over the MC encompasses multiple spatial and temporal scales, and several mechanisms modulate precipitation patterns. These processes include the diurnal cycle of solar heating (e.g. Mori et al., 2004; Qian, 2008; Yokoi et al., 2017), large-scale modes of variability such as the Madden–Julian Oscillation (MJO; e.g. Madden and Julian, 1971, 1972, 1994), El Niño–Southern Oscillation (ENSO; e.g. Haylock and McBride, 2001), the Indian Ocean Dipole (IOD; e.g. Saji et al., 1999; Saji and Yamagata, 2003), and equatorial waves (e.g. Wheeler and Kiladis, 1999; Yang et al., 2003; Ferrett et al., 2020). Scale interactions also exist between processes, adding further variability, and therefore complexity, to our understanding of convective organisation, water vapour profiles, and cloud structure over the MC (e.g. Rauniyar and Walsh, 2013; Peatman et al., 2014, 2021). Limitations in our knowledge of these mechanisms lead to errors in model-simulated precipitation patterns over the MC, primarily due to issues in resolving finer scale features, or because of the parametrisation design (e.g. Yang and Slingo, 2001; Neale and Slingo, 2003;

Qian, 2008; Birch et al., 2016; Vincent and Lane, 2016).

Another feature with the potential to influence regional precipitation patterns is a dry air intrusion (DAI), which is a descending tongue of low specific, and relative, humidity and high potential vorticity (PV), hundreds of kilometres in width, injected from the upper troposphere/lower stratosphere (Danielsen, 1968; Appenzeller and Davies, 1992; Brown and Zhang, 1997). Extratropical wave trains act as a source of DAIs, as shown by back trajectory analysis (e.g. Cau et al., 2005, 2007; Casey et al., 2009) and neural networks (Silverman et al., 2021). Amplification of disturbances along the upper level subtropical jet leads to isentropic folding of the tropopause and anticyclonic Rossby wave breaking, forcing descent of upper level dry air (Numaguti, 1995; Bithell et al., 1999; Funatsu and Waugh, 2008)). The resultant direction that dry air is transported depends on factors such as the jet position and the background wind field (Homeyer and Bowman, 2013).

The frequency of DAI events has large spatial variability. Waugh and Polvani (2000), Stohl (2001), Casey et al. (2009), and Raveh-Rubin (2017) produced climatologies of DAI occurrence (the latter two offering global coverage). DAIs are most prevalent over the Pacific and Indian oceans, occurring more often in the winter season for each hemisphere. However, they contribute to anomalously dry air all year round.

Atmospheric soundings show DAIs sit atop sharp stable layers, produced by anomalous long-wave cooling of the top of the underlying moist air (Mapes and Zuidema, 1996; Zhang and Chou, 1999; Johnson et al., 2001). The radiative and convective profile in the Tropics can therefore be perturbed by humidity fluctuations attributed to DAIs coming from the extratropics (Brown and Zhang, 1997; Ryoo

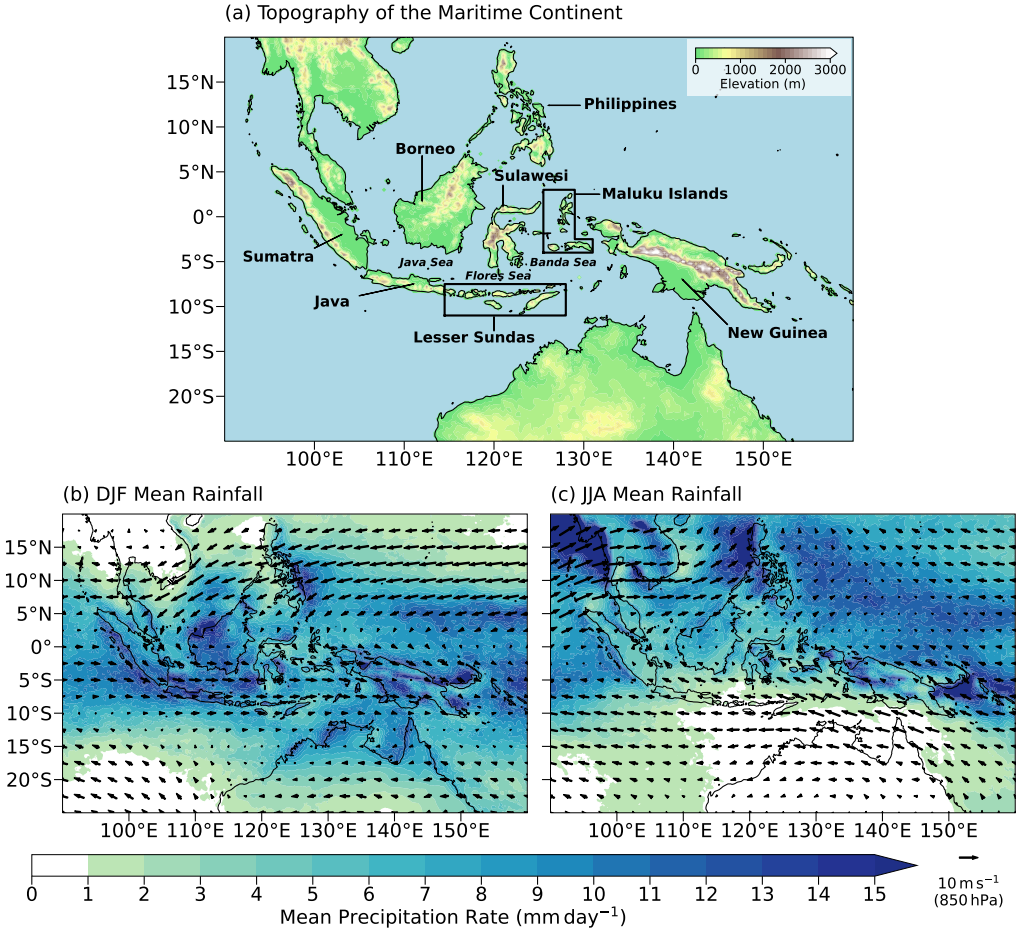

Figure 2.1: (a) Map showing the topography/elevation of the Maritime Continent, with some of its constituent islands and seas labelled. (b-c) The climatological means of Global Precipitation Measurement precipitation rates for (b) December 2000–February 2001 to December 2019–February 2020 (DJF) and (c) June–August 2001 to June–August 2020 (JJA). Black arrows represent 850 hPa wind.

et al., 2008). Such disturbances can affect the moisture field and the low-latitude circulation, thereby impacting regional meteorology and environmental conditions (e.g. Rodwell, 1997; Knippertz, 2007).

Localised, transient breaks in tropical precipitation on daily-to-weekly time-scales can be associated with DAIs. This link has been observed in regions such as the tropical West Pacific during the Tropical Ocean Global Atmosphere Coupled Ocean–Atmosphere Response Experiment (TOGA COARE; e.g. Mapes and Zuidema, 1996; Yoneyama and Parsons, 1999; Lucas and Zipser, 2000; Lucas et al., 2000; Parsons et al., 2000) and the Indian subcontinent, such as through the Interaction of Monsoon Precipitation and Convective Organisation, Atmosphere, Surface and Sea project (INCOMPASS; e.g. Parker et al., 2016; Fletcher et al., 2020; Volonté et al., 2020).

Mid-level DAIs cap the moist boundary layer, decreasing boundary-layer parcel buoyancy and increasing convective inhibition. Gradual increases in boundary-layer equivalent potential temperature and potential instability lead to convective available potential energy build-up (Brown and Zhang, 1997; Yang et al., 2009; Parker et al., 2016). Increases in convective available potential energy allow convection to erode the dry air layer, primarily through convective cloud detrainment. Convective recovery is, however, non-steady, being influenced by both local factors (e.g. the diurnal cycle, orography, convective structure, and surface feedbacks) and remote factors (including synoptic circulations and dynamics originating from the extratropics) (Mapes and Zuidema, 1996; Brown and Zhang, 1997; Redelsperger et al., 2002; Fletcher et al., 2018; Volonté et al., 2020).

DAIs can also result in low-level convergence, vertical motion, and increased convection when encountering warm, moist air masses on eastward margins and leading

edges, through isentropic displacement and reductions in potential stability ahead of upper-level troughs (e.g. Funatsu and Waugh, 2008; Vaughan et al., 2017). Disturbances along the jet stream and their resultant DAIs can therefore steer and organise deep convection, through which increases in rainfall may be observed (Allen et al., 2009; Berry and Reeder, 2016). However, the environment near to the intrusion must be moist enough to be conducive to the formation of deep convection (de Vries et al., 2016, 2018; Kumar et al., 2019). As DAIs themselves modify the lower-level wind field, they can therefore enhance the moisture flux enabling convection downstream (Rodwell, 1997; Knippertz, 2007; Ward et al., 2021).

Despite insights gained from previous studies across the Tropics, DAIs have not been extensively studied in relation to MC precipitation. Murata et al. (2006) and Seto et al. (2006) used rawinsonde, radar, and surface meteorological data and identified DAIs over Sumatra. Murata et al. (2006) noted events where there is convective suppression behind eastward-propagating squall lines. Seto et al. (2006) found this suppression to be associated with intensification of westerly winds. More recently, Feng et al. (2021) used the Sumatran Global Positioning System array to investigate summer intraseasonal variability in precipitable water vapour, a property that influences the propagation of the satellite signal. DAIs over Sumatra were associated with interactions linked to Rossby waves propagating in the Southern Hemisphere midlatitudes. However, these studies use a small number of events in their analysis and do not explicitly analyse impacts on rainfall in the region.

Rodwell (1997) highlighted that limits to the accuracy of seasonal forecasts and predictability of rainfall can be influenced by synoptic-scale/transient events such as DAIs, particularly if a single event provides significant contributions to the seasonal

anomaly. Anomalies associated with DAIs could represent a significant challenge for accurate seasonal forecasts as the slowly varying lower boundary conditions, evolving from initial conditions, cannot anticipate transient events such as DAIs. Further research into processes regulating regional precipitation will benefit society in the MC, as communities experience serious floods and landslides as a result of extreme weather. Better meteorological understanding will improve forecasting potential and ensure socioeconomic security for the 500 million people living in the MC, alleviating current vulnerability to disaster and loss (Wijayanti et al., 2017; Narulita and Ningrum, 2018).

In this study, we aim to identify mechanisms that enable the occurrence of DAIs and their impact on rainfall over the southern MC and to establish any seasonal differences. We use 42 years of European Centre for Medium-Range Weather Forecasts Reanalysis v5 (ERA5) data to identify dry events near the MC through analysis of variance and anomalies in humidity. Section 2.2 outlines the methods used, including the data utilised, the choice of study location, the workflow in identifying dry events, and computation of air parcel trajectories to determine attribution to DAIs. We present the results in Section 2.3, including parcel trajectories, regulatory mechanisms of mid-level dry events, and impacts on regional rainfall patterns. Section 2.4 synthesises these results to see whether there are similarities between this work and past studies, or whether processes and impacts related to dry events are unique for this region. Conclusions are provided in Section 2.5.

2.2 Methods

2.2.1 Data

ERA5 data of global climate and weather (Hersbach et al., 2020) are used to investigate DAIs. Instantaneous hourly ERA5 data (at a horizontal grid spacing of $0.25° \times 0.25°$, equivalent to 26 km) from 1979 to 2021 (42 years) were used. Data were used for 20 levels from 50 hPa to 1000 hPa at 50 hPa vertical resolution, for the domain of 20°N–60°S, 60°–160°E. The hourly data were then used to determine daily means for each variable across the domain. Daily mean rainfall data from the Global Precipitation Measurement (GPM) mission, preprocessed using the Integrated Multi-Satellite Retrievals for GPM (IMERG) Version 06 algorithm (Huffman et al., 2020), were also used. The IMERG algorithm inter-calibrates gauge data with precipitation estimates from satellite infrared and microwave sensors. GPM data were available at horizontal grid spacing, for 20 years from December 2000 to November 2020.

Daily means were averaged over all years for each variable to produce a climatological mean daily annual cycle, which was later smoothed using a 30-day mean.

2.2.2 Dry event identification

The analysis of the variance in daily mean specific humidity at 700 hPa was conducted for each season, in order to identify regions exhibiting fluctuations in mid-level humidity. A box was selected based on the spatial pattern of the variance. As shown in Figure 2.2a, the highest variance in mid-level specific humidity is observed either side of the MC. Prominent locations of high variance include the eastern Indian Ocean southwest of Sumatra and Java, and the southwestern tropical Pacific Ocean

near New Guinea and Australia. A box was selected covering the region of 9°–20°S, 95°–115°E, near to Sumatra and Java. This box encloses the eastern periphery of the first high-variance region identified, located between 10°–20°S and 80°–100°E.

The method of identifying dry events presented is illustrated schematically in Figure 2.2b. Anomalies in 700 hPa daily mean specific humidity were first calculated relative to the associated days and months within the smoothed mean annual cycle, averaged over the identifier box. These anomalies were then normalised by dividing by that same day within the smoothed mean annual cycle. Dry days were defined as days where normalised specific humidity anomalies are below the fifth percentile, computed for each season from 1979–80 to 2020–21. If a dry day has a normalised specific humidity anomaly more negative than the 10 days preceding and following it, the dry day represents the middle, or 'day 0', of a dry event, which is a local humidity minimum. This method is chosen so that events associated with an individual DAI are isolated, ensuring they are not accounted for more than once. Effects of DAIs are noted up to 8–15 days after an intrusion (in TOGA COARE; e.g. Yoneyama and Fujitani, 1995; Parsons et al., 2000), so defining events with a 10-day window either side of a minimum in normalised specific humidity anomalies can be justified.

2.2.3 Trajectory analysis

A Lagrangian trajectory analysis is used to track air parcels associated with dry events, as used in previous studies (e.g. Casey et al., 2009). Advection of each parcel only requires details of the three-dimensional wind field, used to track the location and physical properties of these particular parcels for time periods of interest. Trajectories were calculated by determining a first guess (denoted with a prime symbol) position

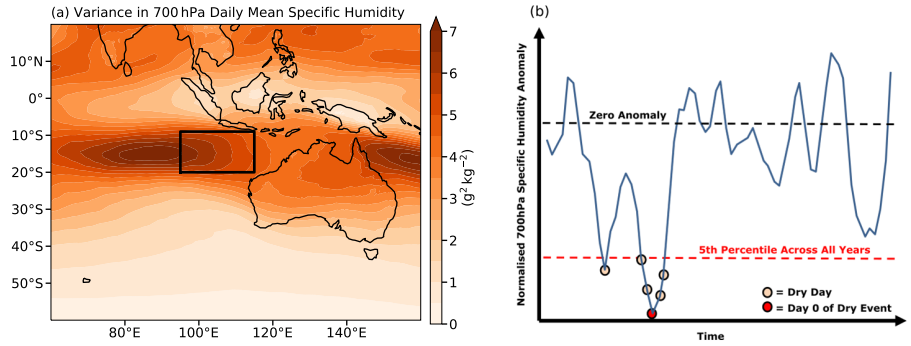

Figure 2.2: (a) Variance in daily mean specific humidity at 700 hPa for the entire time period of analysis from December 1979 to November 2021. The black box (9°–20°S, 95°–115°E) represents the selected region in this study for identification of mid-level dry events. (b) An illustration of the method described for identifying dry events. The soild line is a time series of normalised 700 hPa specific humidity anomalies for a particular season and year. The top dashed line represents zero anomaly, and the bottom dashed line represents the fifth percentile of normalised 700 hPa specific humidity anomalies as calculated across all 42 years for a particular season. Paler dots represent dry days, and darker dots represent day 0 of dry events, where the anomaly is at its most negative relative to neighbouring days.

of a parcel at time $t + \Delta t$, given by

$$\mathbf{r}'_{t+\Delta t} = \mathbf{r}_t + \mathbf{v}_t(\mathbf{r}_t) \cdot \Delta t \,, \tag{2.1}$$

where $\mathbf{r}$ is the three-dimensional spatial coordinate of the air parcel, and $\mathbf{v}$ is the three-dimensional wind velocity field at position $\mathbf{r}$ (e.g. Wernli and Davies, 1997; Draxler et al., 1998). Δt represents the time step, which is 1 day for forward trajectory analysis and -1 day for back trajectory analysis. An adjusted mean wind is determined from

$$\bar{\mathbf{v}} = 0.5[\mathbf{v}_t(\mathbf{r}_t) + \mathbf{v}_{t+\Delta t}(\mathbf{r}'_{t+\Delta t})] \,, \tag{2.2}$$

to give the final position of the air parcel

$$\mathbf{r}_{t+\Delta t} = \mathbf{r}_t + \bar{\mathbf{v}} \cdot \Delta t \,. \tag{2.3}$$

Trajectories were computed for each grid point within the identifier box (9°–20°S, 95°–115°E) at day 0, where both latitude and longitude co-ordinates are integers (12 × 21 points). As ERA5 data is at 0.25° horizontal resolution, and data is downloaded at 50 hPa vertical resolution, when a guess position is not located on these defined grid points or levels, tri-linear interpolation is applied to determine the values of $\mathbf{v}$ associated with their position $\mathbf{r}$. If $\mathbf{r}$ exists outside the domain (20°N–60°S, 60°–160°E, for vertical pressure levels between 50 and 1000 hPa), the trajectory is terminated. We find that using a daily-mean wind input does not fundamentally change the mean trajectory path compared with using an hourly input (not shown).

2.2.4 Association with modes of variability

Dry events were grouped into associations with the phases of ENSO, IOD, and MJO to determine associations between dry events and larger scale controls. Details on the data representing these modes of variability can be found in Table 2.1. Ratios were calculated from the frequencies of these events by dividing the fraction of events in each phase relative to the total number of events per season by the fraction of days in each phase relative to the total number of days in each season across the 42 years. This calculation provides a ratio between event frequency and day frequency with respect to each phase. If this ratio equals 1, the phase is as likely to occur during dry events as it is all days. If the ratio is 2, then the phase is twice as likely to occur

during dry events.

Table 2.1: The indices used in analysing links between the states of selected modes of variability and the occurrence of dry events. Details on their derivation and the definition of events related to the various modes are also provided.

Mode	**Index and Derivation**	**Event Definition**
ENSO	Monthly Ocean Niño Index (ONI, NOAA, 2019) - derived from the average temperature anomaly in the surface waters of the central-eastern tropical Pacific.	El Niño events are defined where ONI $\geqslant$ 0.5°C for 5 successive months, and La Niña events are defined where ONI $\leqslant$ -0.5°C for 5 successive months.
IOD	Monthly IOD Dipole Mode Index (DMI, Saji and Yamagata, 2003) - derived from the anomalous sea-surface temperature gradient between the the western equatorial and southeastern equatorial Indian Ocean.	Positive IOD events are defined where DMI $\geqslant$ 0.4°C for 3 successive months. Negative IOD events are defined where DMI $\leqslant$ -0.4°C for 3 successive months.
MJO	Daily real-time Multivariate MJO series 1 and 2 (RMM1 and RMM2) - the principal components of the two leading empirical orthogonal functions (EOFs), defined by EOF analysis of the combined field of outgoing longwave radiation and wind, which define the phase of the MJO (Wheeler and Hendon, 2004). The amplitude is defined as $\sqrt{RMM1^2 + RMM2^2}$.	MJO events occur when the amplitude for a specific day exceeds or is equal to 1. Where the MJO amplitude is below 1, we label an event as being under 'Phase 0'.

Statistical significance of links between dry event occurrence and large-scale modes of variability was tested through bootstrapping. For each season, we randomly subset a set of days of equivalent length to the number of events identified per season, where the state of each mode for each day is determined. We perform the calculations of

ratios as described previously for these sets of days, relative to the distribution of days in the whole season across the phases of each mode. This process is repeated 1000 times to produce a distribution of ratios for the state of each mode for each season. Percentiles for the original ratios relative to the bootstrapped distribution are then calculated. These percentiles allow the determination of the significance of association with modes of variability relative to a selected confidence interval.

2.3 Results

This section outlines the results obtained from this study. Section 2.3.1 provides details on the number of dry events identified, outcomes from parcel trajectory analysis for case studies, and for all dry events. Section 2.3.2 seeks to provide reasoning for such trajectories through understanding mechanisms regulating the occurrence of dry events. Statistical links between dry event occurrence and phases of various modes of variability are provided in Section 2.3.3. Lastly, Section 2.3.4 shows the results in analysing changes to rainfall patterns during dry events.

2.3.1 Dry event characteristics and parcel trajectories

Employing the chosen method described in Section 2.2.2, we identify 201 dry events over the 42-year period of analysis. Focusing on December–February (DJF) and June–August (JJA), we find 47 and 56 dry events respectively, equivalent to just over one event per season per year.

We first analyse where air parcels associated with identified dry events originate from and are advected to, using the parcel trajectory equations provided in Section

2.2.3. Initial analysis is performed on select events, and Figure 2.3 shows results for events that had normalised specific humidity anomalies equivalent to the event-average per season. These are the January 9, 2020 (Figure 2.3a–c), and July 26, 2020 (Figure 2.3d–f), dry events for DJF and JJA respectively.

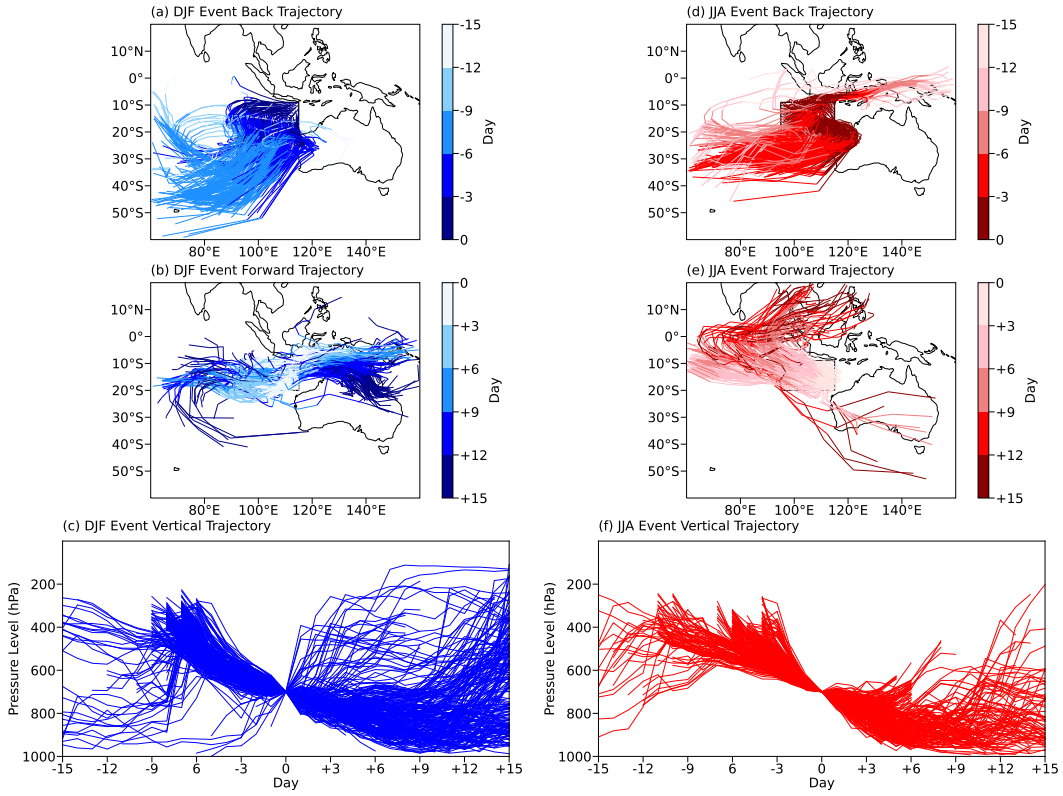

Figure 2.3: Air parcel trajectories for the (a–c) January 9, 2020, December–February (DJF) and (d–f) July 26, 2020, June–August (JJA) dry events: (a,d) back, (b,e) forward, and (c,f) vertical trajectories.

Back trajectory analysis shows that air parcels associated with the selected DJF dry event originate largely from the extratropics in the southeast Indian Ocean (30°–50°S), 6–9 days prior to the peak of the dry event (Figure 2.3a), descending from 200 to 500 hPa (Figure 2.3c). Forward trajectories show that, on average, air parcels remain confined within near-equatorial latitudes from 5° to 20°S (Figure 2.3b),

descending further to the near surface for up to 10 days after the peak of the dry event before reascending to upper levels (Figure 2.3c). Some parcels, however, ascend rapidly just after day 0. Most air parcels are advected eastward towards New Guinea and northern Australia in the southeast, with a slightly smaller portion westward towards the Indian Ocean. Some trajectories recurve back towards the Southern Hemisphere extratropics.

For the selected JJA dry event, air parcels largely originate from the extratropics as well, though slightly further north than in DJF, between 20°and 40°S, in the southeastern Indian Ocean 3–6 days prior to the peak of the dry event (Figure 2.3d), descending from the upper levels between 300 and 500 hPa (Figure 2.3f). An additional (albeit much smaller) source of air parcels is located over the Tropics around New Guinea and the western Pacific, up to 12 days prior to the peak. Forward trajectories show that most air parcels are advected towards the eastern Indian Ocean, within 6 days of the peak (Figure 2.3e). After this, up to 15 days after the peak of the dry event, many trajectories are directed northeastward towards mainland southeast Asia and the northern MC. Few trajectories return to the extratropics to the south of Australia. On average, air parcels continue descending in some cases beyond 10 days after the peak of the dry event (Figure 2.3f).

Figure 2.4 shows the distribution of air parcels associated with all dry events in DJF and JJA, to corroborate the aforementioned analysis based on individual events. Solid contours represent the limits of the trajectory to the number of days listed above the figure panels for DJF and JJA. Filled contours represent the difference between these distributions, where positive (negative) values represent where more DJF (JJA) air parcels are located. The JJA distribution is rescaled to have the same number of

parcel trajectories as DJF, by multiplying the distribution in JJA by the number of events in DJF (47), divided by the number in JJA (56).

At 10–15 days before the event, JJA parcels are located further to the north of the MC between 0° and 15° S and 80°–160°E, whereas DJF parcels are located further south over the Indian Ocean between 15°–35°S and 60°–130°E. (Figure 2.4a). Going forward in time, average trajectories suggest parcels most commonly enter the domain from the upper troposphere between 200 and 500 hPa (Figure 2.4g) and extratropics over the southern Indian Ocean to the west (Figure 2.4b). This is observed most strongly during DJF 5–10 days before the peak of the dry event, but also in JJA. Just before the peak of the dry event, most DJF parcels are close to the identifier box where trajectories began (Figure 2.4c). However, the JJA distribution suggests parcels can come from the extratropics during the 5 days before the event peak, with some advected southwestward from the Tropics. The extratropical source to the southwest is, however, common to both DJF and JJA regardless of how far back in time one goes, though JJA has an additional (yet smaller) source coming from the Tropics east of New Guinea.

Up to 5 days after the dry event peak, DJF parcels are mostly advected eastward across the MC towards New Guinea, with some also advected westward (Figure 2.4d). Up to 10 days after the event, the eastward propagation noted in DJF persists (Figure 2.4e). Compared with DJF, JJA parcels are, on average, advected northwest towards India, but some are also advected northeastward over Sumatra and Malaysia towards mainland southeast Asia (Figure 2.4d–f).

Air parcels associated with the trajectories linked to dry events have a characteristic descent from 10 days before the event peak to 10 days after (Figure 2.4g).

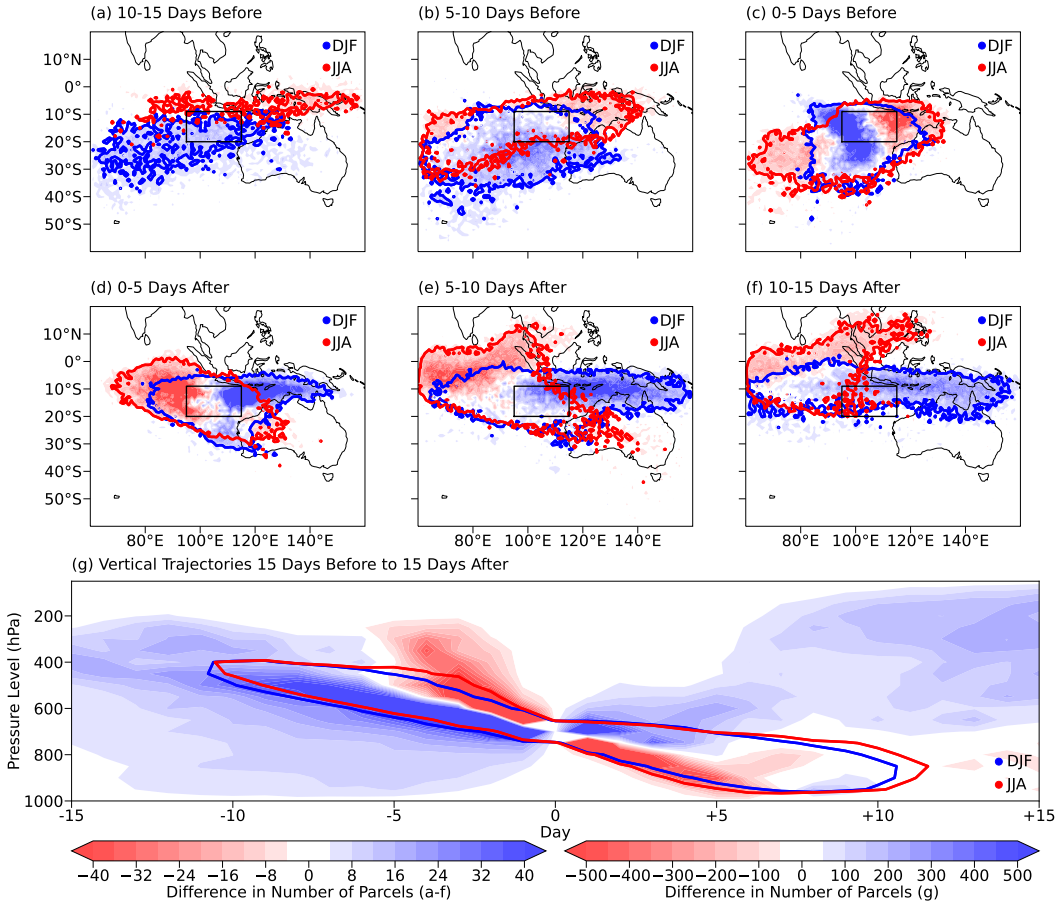

Figure 2.4: The distribution in dry-event-related air parcels as calculated through (a–c) back and (d–f) forward trajectory analysis. Solid contours represent the limits of the trajectory to the number of days listed above the figure panels for December–February (DJF) and June–August (JJA). This is indicated by contours where the sum of parcels across the days, labelled above the figure panels, is 10 parcels. Filled contours represent differences between the distribution in each season, where the difference is the JJA distribution subtracted from the DJF distribution, where the JJA distribution is rescaled to have the same number of parcel trajectories as DJF, done by multiplying the distribution in JJA by the number of events in DJF (47), divided by the number in JJA (56). This rescaling allows a difference between JJA and DJF to be calculated (otherwise there will be a tendency for differences to shift towards the negative with more parcels present in the domain in JJA than DJF, by virtue of the difference in number of events). (g) The distributions for each season as a function of time and vertical pressure level, summed over all longitudes and latitudes. Solid contours represent the limits of the vertical trajectory to the day labelled on the x-axis for DJF and JJA. These limits are indicated by contours, where the sum of parcels is 1000 parcels.

However, DJF parcels, compared with JJA, originate from the upper levels further back in time, taking longer to descend to the mid-levels. After the event, JJA parcels have a stronger descent signal than DJF parcels do, which has a broader vertical distribution, linked to an increase in the number of parcels that end up reascending to the upper levels.

2.3.2 Regulatory mechanisms

Here, we provide insight into mechanisms regulating dry event occurrence for events identified in DJF and JJA. Figures 2.5 and 2.6 show lead–lag composites of specific humidity anomalies for DJF and JJA events.

During DJF, up to 7 days before the peak of the dry event, a moist anomaly develops over northern Australia (Figure 2.5a). Mid-level westerly anomalies form over the southern MC, with a mid-level cyclonic circulation anomaly developing northwest of Australia. Between days -4 and -2, a dry anomaly south of the MC evolves, driven by southerly advection from the extratropics (Figure 2.5b). At upper levels, this advection is linked to disturbances along the subtropical jet, where a cyclonic circulation anomaly develops southwest of Australia, bounded by anticyclonic circulation anomalies either side. Mid-level circulation anomalies almost parallel those at the upper levels, extending further northward towards the MC. Westerlies over the southern MC are enhanced, and the intensified return flow to the extratropics east of the mid-level cyclonic anomaly increases the moist anomaly over Australia.

Around day 0, while the dry anomaly intensifies, upper level disturbances in the extratropics dissipate (Figure 2.5c). However, the anticyclonic circulation anomaly over Australia persists, resulting in a preserved moist anomaly there. The mid-

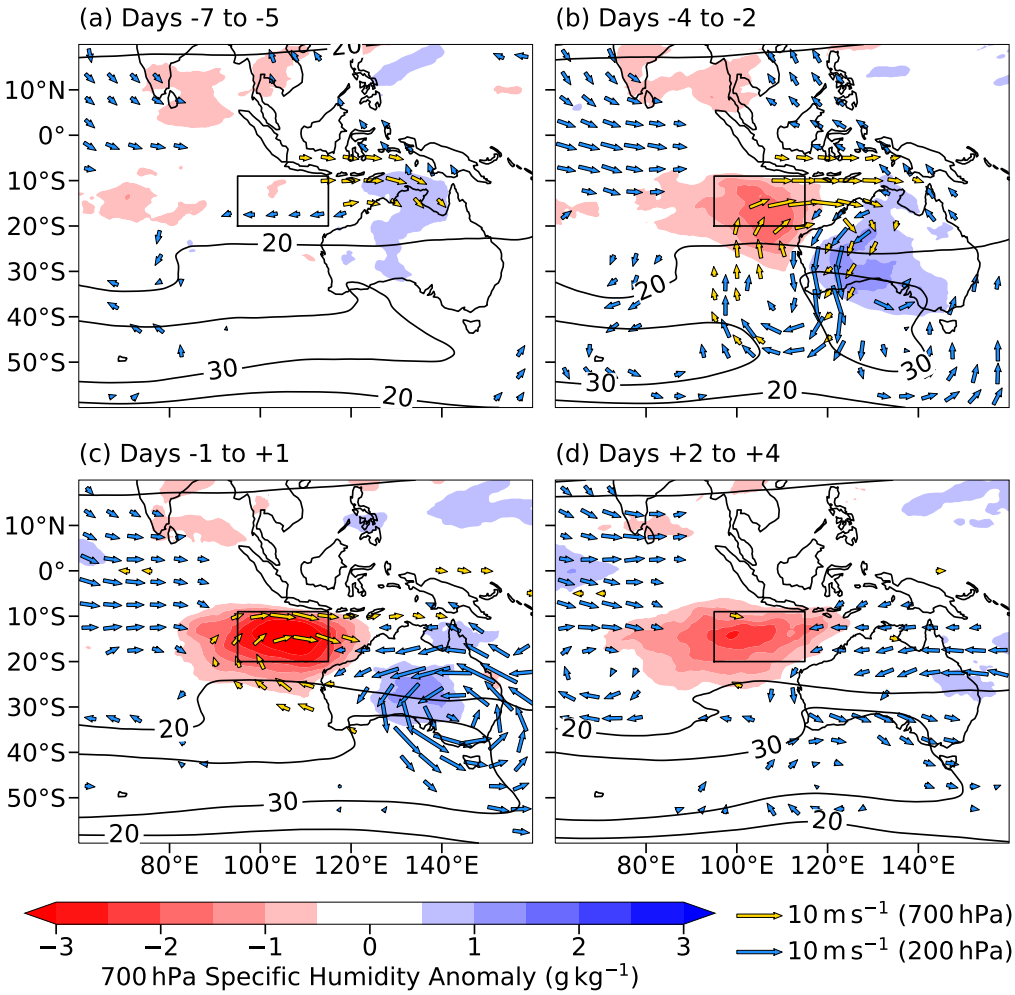

Figure 2.5: Lead–lag composites for 700 hPa specific humidity anomalies for the 47 dry events identified in December–February (DJF) from 1979–80 to 2020–21 for (a) days -7 to -5, (b) days -4 to -2, (c) days -1 to +1, and (d) days +2 to +4. Paler and darker arrows represent composite 700 hPa and 200 hPa anomalous wind respectively, calculated as the average of wind anomalies for each event relative to the DJF mean annual cycle. Anomalous wind at each level less than 2 m s^{-1} is not shown. Solid contours represent 200 hPa wind speed at 20 m s^{-1} and 30 m s^{-1}, indicating the position of the DJF subtropical upper level jet. The black box represents the domain used for identifying dry events as in Figure 2.2.

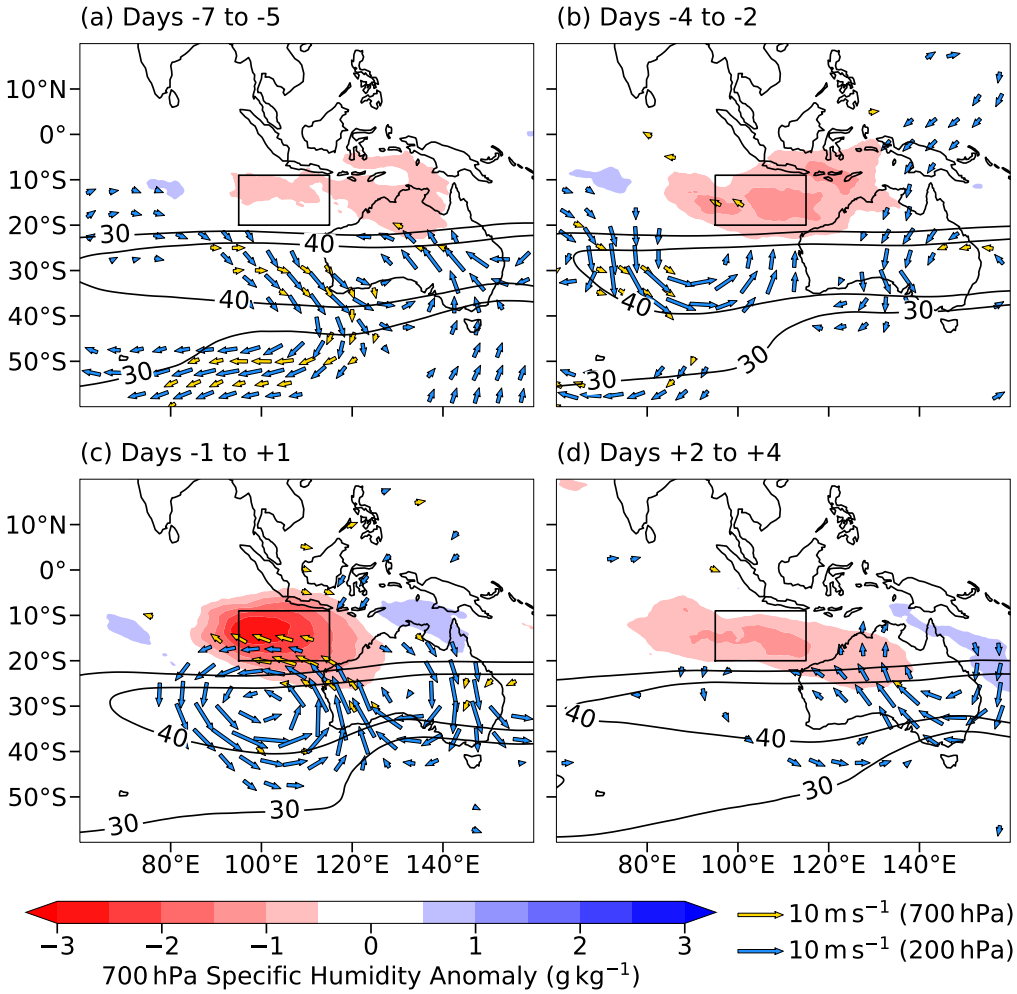

Figure 2.6: As in Figure 2.5, but for the 56 dry events identified in June–August.

level cyclonic circulation anomaly near the MC develops a northwest–southeast tilt, centred just off northwestern Australia, and the previously enhanced westerlies begin to weaken. Between days +2 and +4, the dry anomaly begins to dissipate and spreads out longitudinally, with the moist anomaly over Australia also reduced (Figure 2.5d). Anomalous mid-level westerlies in the southern MC are weaker than prior to the dry event peak, linked to the weakened mid-level cyclonic anomaly.

For JJA, between days -7 and -5, a dry anomaly forms to the east over northern Australia and seas adjacent to MC islands (Figure 2.6a). This anomaly stems from upper level disturbances further east over eastern Australia, with southeasterly advection towards the MC. However, composite mid-level wind anomalies here are weak. The pre-existing dry air migrates westward over Java, the Lesser Sundas, South Sulawesi, the Maluku Islands, and neighbouring seas (Java and Flores; Figure 2.1a) between days -4 and -2 (Figure 2.6b). A new upper level disturbance develops to the southwest of the selected box over the southeastern Indian Ocean, leading to southerly-to-southeasterly advection at the upper levels. This advection is linked to an anticyclonic circulation anomaly, intensifying easterlies at mid-levels to the west of the MC, as well as dry air advection into the Tropics.

Around day 0, strong upper level anticyclonic and cyclonic circulation anomalies are observed to the west and over Australia respectively (Figure 2.6c). A mid-level anticyclonic circulation anomaly extends into the Tropics, increasing the intensity of the dry anomaly. The dry anomaly is centred to the south of the MC, though is spread over Java and adjacent seas, due to pre-existing dry air advected from the east. The mid-level circulation anomaly is tilted northwest–southeast, with moist anomalies either side of the dry anomaly of similar tilt. The days following day

0 are associated with dissipation of upper level anomalies near the Tropics, with propagation of anomalies further to the east (Figure 2.6d). These anomalies lead to a new stream of anomalous dry air passing over Australia. Dry air originally near to the MC spreads out longitudinally, and the moist anomaly has propagated further east.

In both DJF and JJA, circulation anomalies at both upper levels and mid-levels are observed. Figure 2.7 shows time–longitude cross-sections of geopotential height for days -7 to 0, for both the upper level extratropics and mid-level near-Tropics (identifier box region) for both seasons. The choice of these boxes at these levels are in line with the geographical positions of upper and mid-level circulation anomalies noted in Figures 2.5 and 2.6. In DJF, cyclonic anomalies prior to the peak of the dry event are associated with an upper level trough in the extratropics, which is strongest at day -3 (Figure 2.7a). Descent accompanies the southerly advection of dry air to the west of the trough. Anomalies at the mid-levels can also be linked to a persistent mid-level ridge and trough (Figure 2.7b). Though the ridge does not significantly intensify over time, the trough deepens around day -3. On the other hand, the prevalent extratropical anticyclonic anomaly in JJA is attributed to an upper level ridge (Figure 2.7c). In contrast to DJF, the mid-level trough is not observed to be more intense than the ridge to the west (Figure 2.7d). Anomalies of descent accompany the southeasterly advection to the east of the ridge.

The results here show that upper level disturbances within the subtropical jet, developing around 5 days prior to the dry event peak, are a key precursor to dry event occurrence in both seasons. These disturbances drive descent of dry air towards the Tropics. In addition, enhancement in mid-level cyclonic circulation centred over

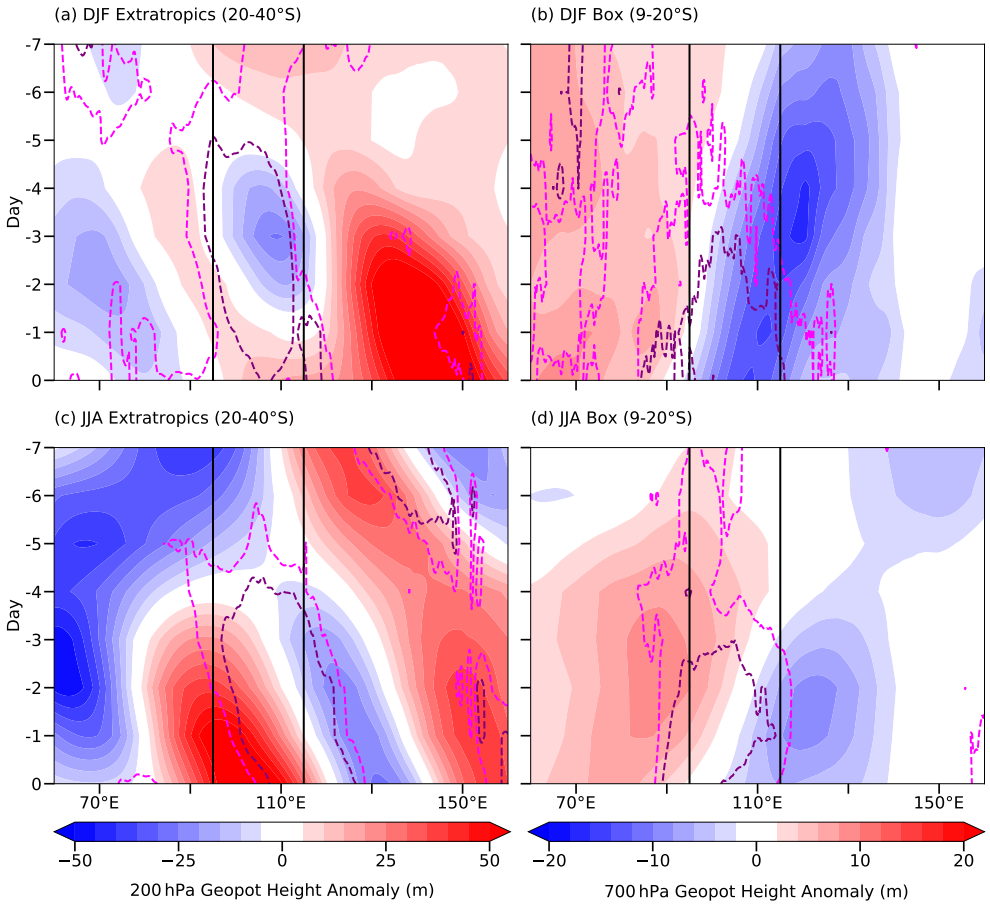

Figure 2.7: (a-b) Hovmöller plots of 200 hPa and 700 hPa geopotential height anomalies from days -7 to 0 for the 47 dry events identified in December–February (DJF) from 1979–80 to 2020–21. Anomalies at 200 hPa are averaged over 20°–40°S, and anomalies at 700 hPa are averaged over 9°–20°S. (c-d) As in (a-b), except for the 56 dry events identified in June–August (JJA). Solid lines represent the longitudinal limits of the identifier box as in Figure 2.2. For panels (a) and (c), paler and darker dashed contours represent 0.005 $\mathrm{Pa\,s^{-1}}$ and 0.010 $\mathrm{Pa\,s^{-1}}$ vertical velocity anomalies respectively, indicating regions of descent. The dashed contours in panels (b) and (d) represent 0.010 $\mathrm{Pa\,s^{-1}}$ and 0.020 $\mathrm{Pa\,s^{-1}}$ vertical velocity anomalies respectively.

northwestern Australia strengthens mid-level southerlies in DJF, enabling advection of dry air towards the MC. This circulation also produces anomalous southern MC westerlies that advect dry air eastward. On the other hand, in JJA, an enhancement in mid-level anticyclonic circulation just to the west of Australia strengthens mid-level southerlies, though directing dry air to the same region as in DJF. This circulation, too, enhances easterlies south of the MC, which advects dry air westward towards the Indian Ocean. For both seasons, these dry events can therefore be associated with DAIs. Gradual weakening of enhanced wind circulations in DJF and JJA lead to eventual dissipation of the dry anomalies. In both seasons, moist anomalies are observed to the east of the intrusion, tilted in a direction paralleling the trajectory of dry air. Additionally, for both DJF and JJA, it is apparent that the upper-level wind circulation anomalies propagate eastward while the mid-level wind and specific humidity anomalies propagate westward. From Figure 2.7, these propagation rates can be estimated from the geopotential height anomaly field as roughly $6\,\mathrm{m\,s^{-1}}$ eastward and $4\,\mathrm{m\,s^{-1}}$ westward, respectively.

2.3.3 Association with modes of variability

The previous section established anomalous circulations unique to DJF and JJA that acted as key regulatory mechanisms to the onset of a dry event. These circulations could be due to the state of the large-scale environment as modulated by modes of variability.

To investigate this possible link, the dry events in DJF and JJA were grouped into their associations with the state of ENSO, IOD, and MJO, as shown in Table 2.2 under columns labelled 'Frequency'. These values were converted to ratios as

described in Section 2.2.4, with results shown in columns labelled 'Ratio'.

Table 2.2: Dry event frequency ('Frequency') for both DJF and JJA across the states of each mode of variability analysed. Provided are ratios indicating event frequencies compared to the number of days within each season associated with each state of each mode ('Ratio') as described in Section 2.2.4. Percentiles of these ratios are obtained by comparison to the distribution of 1000 bootstrapped samples, also described in Section 2.2.4. Where these percentiles are below the 5th percentile or above the 95th percentile, ratios are highlighted in bold and are italicised. MJO phases are associated with geographical locations as follows: Phases 2 and 3 (Indian Ocean), Phases 4 and 5 (Maritime Continent), Phases 6 and 7 (West Pacific), Phases 8 and 1 (Western Hemisphere and Africa), as per Wheeler and Hendon (2004). Phase 0 represents times when the MJO amplitude is below 1 and therefore weak.

Mode	**State**	**DJF (Frequency)**	**DJF (Ratio)**	**JJA (Frequency)**	**JJA (Ratio)**
ENSO	El Niño	16	1.04	12	1.08
	Neutral	15	0.94	31	0.94
	La Niña	16	1.02	13	1.08
IOD	Positive	2	1.79	10	1.25
	Neutral	45	1.01	43	0.98
	Negative	0	0.00	3	0.75
MJO	Phase 0	14	0.87	24	0.99
	P2 and P3	2	***0.27***	12	***1.41***
	P4 and P5	7	0.90	8	***1.25***
	P6 and P7	13	1.29	7	1.04
	P8 and P1	11	***1.98***	5	***0.50***

No statistically significant associations between dry events and the state of ENSO or IOD in either season are found. The MJO, on the other hand, shows statistically significant links with dry events in each season. In DJF, the MJO is significantly more (nearly twice as) likely to be in phases 8 and 1, and significantly (nearly four times) less likely to be in phases 2 and 3 when there is a dry event. In JJA, the MJO is significantly more likely to be in phases 2 and 3 and phases 4 and 5, and signficantly (two times) less likely to be in phases 8 and 1 when a dry event occurs. Following

the associations between geographical location and MJO phase as in Wheeler and Hendon (2004), the MJO active envelope is more likely to be away from (near to) the MC when a dry event occurs in DJF (JJA), and vice versa. Therefore, there appears to be seasonal differences in associations between phase of the MJO and dry event occurrence.

2.3.4 Impact on rainfall

In this section, we analyse the impact of decreased mid-level humidity on regional rainfall patterns. We use the dry events that take place in the available GPM data record from 2000–01 to 2019–20 as GPM does not go as far back as ERA5. This subset provides 25 and 27 dry events for DJF and JJA respectively. Precipitation anomalies associated with each event are composited by lag time and then normalised with respect to the mean rainfall rate at that grid point per season (Figure 2.1b-c).

During DJF dry events, negative rainfall anomalies develop over the northwest of Australia, up to 6–10 days before the peak of the dry event (Figure 2.8a). The rainfall anomalies become larger and more widespread, aligning with the negative specific humidity anomalies between days -5 to -2 (Figure 2.8b). Positive anomalies in normalised precipitation rate are observed to the east over and offshore of the northwest Australian coastline. Around day 0, positive rainfall anomalies dissipate, but continued northward propagation of dry air coincides with decreases in rainfall, with strongest reductions at the core of the dry anomaly, south of Java (Figure 2.8c). Anomalies south of the MC dissipate and disperse after the dry event peak. These are now more prevalent further west towards the Indian Ocean (Figure 2.8d). Slight negative rainfall anomalies are observed over the Lesser Sundas and the neighbouring

Flores and Banda seas to the northeast (Figure 2.1a). Between days +6 and +10, most of the negative rainfall and humidity anomalies have dissipated, though more localised dry air and reduced rainfall signatures persist (Figure 2.8e).

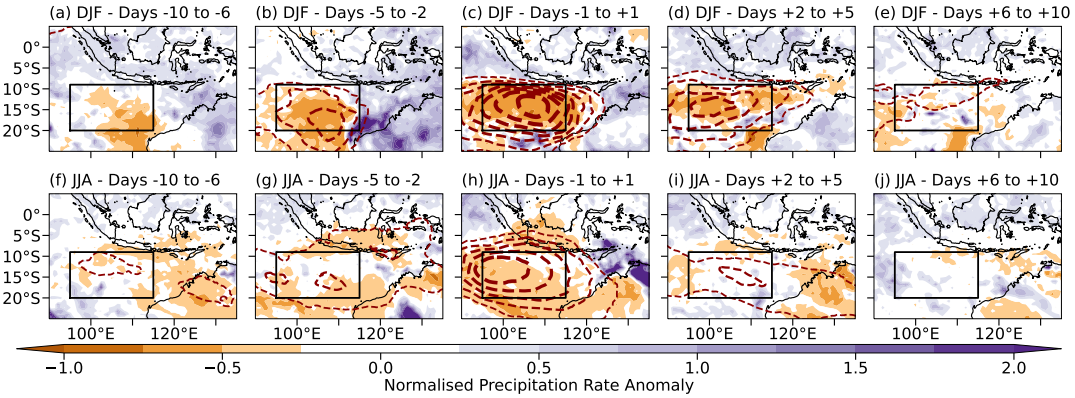

Figure 2.8: Normalised precipitation rate anomalies with respect to the mean rainfall per grid point for dry events in (a–e) December–February (DJF) and (f-j) June–August (JJA) within the available GPM record from 2000–01 to 2019–20 (25 for DJF and 27 for JJA), for days -10 to +10. Anomalies have been binned into sets of days, with smaller bins closer to day 0, which each set of data is averaged over. Dashed contours represent negative specific humidity anomalies averaged over these events, where increases in contour thickness reflect decreases (becoming more negative) in the mean specific humidity anomaly by 0.5 g kg^{-1}, starting at -0.5 g kg^{-1}. The black box represents the domain used for identifying dry events as in Figure 2.2.

For JJA dry events, there are pre-existing anomalies of reduced rainfall across the region up to prior to the dry event peak (Figure 2.8f-g). Rainfall reductions are noted over Java, the Lesser Sundas, south Sulawesi, and the Java and Flores seas (Figure 2.1a). Only 2–5 days prior to the dry event peak are anomalies originating from the south observed, along with negative specific humidity anomalies, just to the northwest of Australia. Increases in rainfall are noted to the east over Australia. Widespread reductions in rainfall, coinciding with the humidity anomalies, are observed around day 0 (Figure 2.8h). The pre-existing anomaly from the east leads to reductions over

the southern MC. The rainfall anomaly from the south shifts northwest towards the Indian Ocean with the reductions in humidity. Positive rainfall anomalies develop to the east of the dry anomaly over the Lesser Sundas and northern Australia, with a northwest–southeast tilt. Both negative and positive rainfall anomalies dissipate over the region up to 5 days after the dry event peak (Figure 2.8i). Some anomalies shift westward and southeast towards Australia, where there are further reductions in rainfall, matching the trajectory of the humidity anomalies. After day +6, observed anomalies dissipate (Figure 2.8j).

2.4 Discussion

Using the results obtained in Sections 2.3.1 to 2.3.4, we present the mechanisms controlling dry event occurrence and their impacts on rainfall in the southern MC schematically in Figure 2.9a-b for DJF and JJA.

Analysis of parcel trajectories and precursor anomalies showed that air parcels associated with dry events can be attributed to DAIs, originating from upper level disturbances along the subtropical jet. The approximate geographic location of the DAI origins - to the southwest of Australia over the southern Indian Ocean - and eventual destination to the south of the Maritime Continent aligns with that in the Lagrangian trajectory analysis of Cau et al. (2007). These processes are likely to be related to Rossby wave breaking, as indicated by similar upper level wind anomaly patterns shown in past studies (e.g. Numaguti, 1995). Parallels can also be drawn in terms of dry air sourcing and pathways leading up to a dry event, as seen in Feng et al. (2021). This work extends Feng et al. (2021)'s observations across a longer time

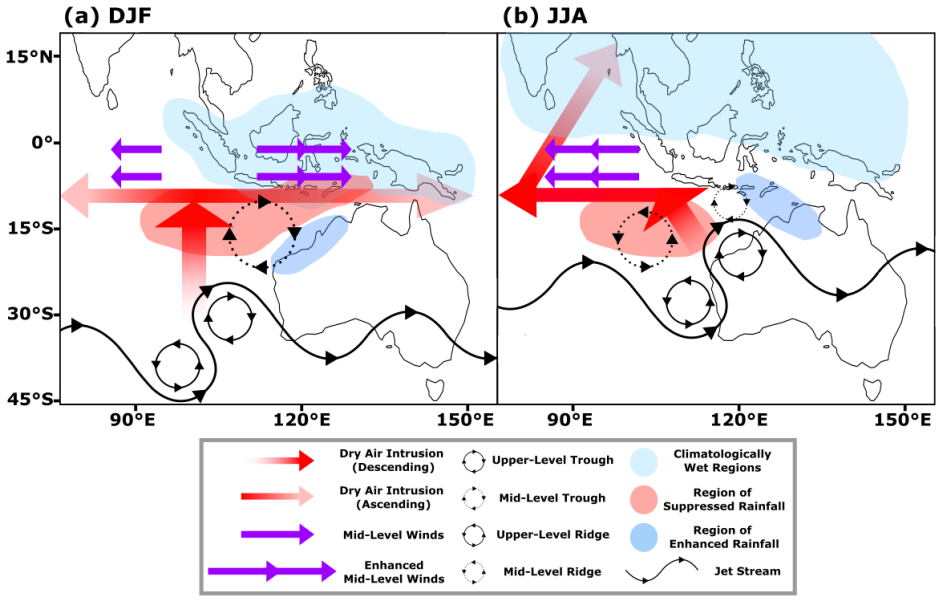

Figure 2.9: Schematic showing the mechanisms regulating the occurrence of dry events, due to extratropical mid-level dry air intrusions, to the south of the Maritime Continent, and their impacts on Maritime Continent rainfall, for (a) December–February (DJF) and (b) June–August (JJA). Arrow size is not representative of intrusion characteristics, merely representing direction and vertical motion.

period of analysis for more events. Sole and direct attribution of the dry anomalies to disturbances along the upper-level jet (around 200 hPa) should be treated with some caution, as mean trajectories suggest the dry air is sourced between 300-400 hPa (e.g. Figure 2.2g), though these disturbances aloft may still assist in transport to lower-levels.

Negative humidity anomalies observed coming from the east in JJA up to 7 days prior to the peak of the dry event may be attributed to the greater frequency of austral wintertime DAIs (e.g. Casey et al., 2009). Figure 2.2a highlighted a high-variance region in mid-level specific humidity between New Guinea and Australia. This region may be where the pre-existing dry air originates from, which reaches the

MC prior to the intrusions analysed originating from the south over the Indian Ocean in JJA.

There are visible differences, however, in terms of the mechanisms regulating the occurrence of dry events in each season. First, air parcels associated with DAIs take less time to arrive into the Tropics in JJA compared with DJF, and those found in the domain up to 15 days prior to the dry event peak are located within more equatorial latitudes in JJA than in DJF. This observation is likely to be a product of the northward migration of the subtropical jet and intertropical convergence zone ('climatologically wet region') during the austral winter (as depicted in Figure 2.9b compared with Figure 2.9a), as well as strengthening of the jet stream, leading to faster advection of air parcels. Indeed, a study by Ndarana and Waugh (2011) note primarily latitudinal, compared to longitudinal, shift in the location of Rossby wave breaking events between boreal winter and summer in a climatology for the Southern Hemisphere. However, not all points within the box are dry even when a dry event occurs. Therefore, trajectories starting in the Tropics tend to be those not associated with the dry event itself.

Second, shifting of the jet northward in JJA is likely to be altering the direction of dry air trajectories into the MC from southerly to southeasterly, with changes to geopotential height anomalies noted. Past studies have found links between jet characteristics and resultant trajectories of DAIs (e.g. Homeyer and Bowman, 2013). However, the observed trough in DJF and ridge in JJA (dotted circles in Figure 2.9) may be a result of the events that have been composited. The eventual north-west–southeast tilt attributed to the mid-level trough anomalies in the region of the dry anomaly around day 0 is expected due to refraction of midlatitude wave trains

towards the Tropics (e.g. van der Wiel et al., 2015).

Third, the most pronounced differences between DJF and JJA are in forward trajectories associated with dry events themselves. DJF air parcels have greater re-ascent after the dry event peak (shown as fading arrows in Figure 2.9a), compared with that in JJA. In addition, JJA air parcels are advected towards the Indian Ocean, with some further northeast from this position up to mainland southeast Asia, compared with DJF, where there is dominantly eastward advection towards New Guinea and some advection westward towards the Indian Ocean. The first association is that the lower level (850 hPa) climatological wind field, provided in Figure 2.1b, characteristic of the monsoon circulation in each season, suggests mean westerly motion in the lower levels in DJF across the southern-central MC, with easterlies slightly further south, while still within the box latitudes (up to 20°S). The lower level monsoon circulation explains the largely eastward propagation of air parcels in DJF after continued descent below 700 hPa. Figure 2.1c, on the other hand, shows the opposing monsoon circulation for JJA, where there are strong low-level mean easterlies across the southern MC, which would explain the largely westward advection of parcels. To the northwest of the MC into the Indian Ocean near to the Bay of Bengal and mainland southeast Asia, the low-level monsoon circulation reverses from northeasterly (as in DJF) to southwesterly, providing reasoning for eventual advection of air parcels towards the mainland. Therefore, parcels that continue descent after the peak of the dry event will likely be entrained in the mean monsoon low-level circulation, influencing their eventual trajectory.

Impacts on rainfall generally follow the trajectories presented in Figures 2.3 and 2.4. In both seasons, dry air coming from the extratropics suppresses rainfall over the

sea in the identifier box, in agreement with results from campaigns such as TOGA COARE over the tropical west Pacific (e.g. Parsons et al., 2000). In DJF, dry air propagates eastward, resulting in a suppressed rainfall signal over the Lesser Sundas of Indonesia, and neighbouring seas after the dry event. In JJA, rainfall reductions over the islands of the MC are linked to the pre-existing dry air originating from the east. As JJA trajectories are largely (north)westward, no further reductions over the MC can be attributed to the dry events studied, though rainfall suppression is apparent going into the eastern Indian Ocean.

An increase in rainfall to the east of the dry anomalies, which have a tilt paralleling that of the dry air trajectory itself, was also observed. When analysing key mechanisms regulating dry events, there was flow to the extratropics at both mid-levels and upper levels to the east of troughs, resulting in increases in mid-level specific humidity. Such moist anomalies are found in similar positions to observed positive rainfall anomalies over northwestern and northern Australia, as well as the Lesser Sundas, implying that roughly around day 0 it is possible to get increases in rainfall just to the east. Berry and Reeder (2016) observed similar positive rainfall anomalies, where Australian summertime monsoon bursts took place to the east of an upper level trough. Allen et al. (2009) note similar increases in tropical convection in this region and were able to attribute it more directly to the leading edge of a descending dry air mass from the extratropics. Several researchers have associated amplification of upper level troughs with enhanced convection at the edges and to the east of descending dry air masses elsewhere, thereby steering convection (e.g. Tompkins, 2001; Pohl et al., 2009; de Vries et al., 2016). DAIs and the associated disturbances themselves are driving the flow of moist air necessary to form convection, observed

in past studies such as Knippertz (2007) and Ward et al. (2021) over Africa.

Our investigation into associations between dry events and large-scale modes of variability (Table 2.2) found no significant link between dry event occurrence and both the phases of ENSO and the IOD. Berry and Reeder (2016), for example, also found no significant link between upper level troughs (which regulate Australian summertime monsoon bursts) near to the study region and ENSO. Pohl et al. (2009) found the opposite results for southern Africa, suggestive of global variability in associations between upper level disturbances and the large-scale modes of variability.

In contrast with ENSO and IOD, significant links with the MJO have been noted. For DJF, it was observed that the MJO active phase is significantly more likely to be in phases 8 and 1 and less likely to be in phases 2 and 3 when a dry event occurs. For JJA, when a dry event occurs, the active phase is significantly more likely to be in phases 2 to 5 and less likely during phases 8 and 1. In more condensed terms, when a dry event occurs, the MJO active phase is significantly more likely to be in the vicinity of the MC during JJA and less likely during DJF. The opposite is noted when the MJO active phase is away from the region. Therefore, we find similar results to Berry and Reeder (2016) for DJF (JJA was not examined in their work).

We hypothesise that the link between MJO phase and dry event occurrence is due to circulation anomalies that are driven by the large-scale tropical environment, most dominantly regulated by the MJO on intraseasonal time-scales (Madden and Julian, 1971, 1972, 1994), which may be a product of equatorial wave theory associated with MJO dynamics (e.g. Hendon and Salby, 1994; Maloney and Hartmann, 1998; Matthews, 2000). During the active phase, a tongue of low pressure strengthens to the east, associated with a Kelvin wave, with pressure troughs to the northwest and

southwest, associated with Rossby waves (Matsuno, 1966; Gill, 1980). The opposite is observed for the suppressed phase of the MJO. The potential for DAI trajectories to be modified by Rossby waves has in the past been researched over the Indian Ocean in the Dynamics of the MJO field campaign (Kerns and Chen, 2014; Chen et al., 2016). Their observations included a strong MJO event and DAIs over the Indian Ocean. A noted interaction linked DAIs to westward-propagating synoptic Rossby gyres in the active envelope. These gyres induced low-level wind circulations drawing the dry air eastward into the equatorial region west of the envelope, contributing to a 1- to 2-day break in the rainfall during the MJO active phase, favouring a transition to the suppressed phase. This interaction was validated in various simulations (Wang et al., 2015; Kuznetsova et al., 2019).

Mid-level westerly anomalies persist over the southern MC in DJF (double arrows in Figure 2.9a), linked to the enhanced negative geopotential height anomaly and cyclonic circulation over northwestern Australia. With the strengthened mid-level trough in DJF enhancing both descent of dry air from upper levels and equatorward and eastward advection, a similar interaction to that in Kerns and Chen (2014) may be taking place. When the active phase of the MJO is away from the MC, westward-propagating cyclonic circulations, originating from the active envelope, may enhance westerly flow near to the region of study. In the opposite phases, with reversals of anomalous vortices associated with the MJO, there may be easterly intensification, which is the reason for such air parcels propagating westward (Figure 2.9a). In JJA, opposite anomalies are noted (Figure 2.9b), though mid-level easterlies are not as persistent as the westerlies observed in DJF, likely linked to the anomalous geopotential signature being weaker. With dry events more likely when the active phase

of the MJO is to the west or over the MC, mid-level ridges (or anticyclonic circulations) are to have greater prevalence near to the region linked with the suppressed phase of the MJO being further to the east. There may be easterly intensification towards the Indian Ocean due to the anticyclonic circulation characteristic of these ridges. Therefore, MJO phase may exert a control on both mid-level circulation and geopotential characteristics noted in each season, potentially interacting with DAIs, particularly with the apparent westward shift in the mid-level geopotential height anomalies (Figure 2.7) which could be characteristics of the aforementioned equatorial Rossby waves. Deeper exploration of such associations, however, are beyond the scope of this study and would require further research.

2.5 Conclusions

We have investigated the occurrence of dry events south of the MC and underlying mechanisms in observations for DJF and JJA. Air parcels associated with dry events in both seasons originate from the extratropics in the southern Indian Ocean, as shown by back trajectory analysis, 5–10 days prior to the peak of the dry event. These air parcels are associated with synoptic mid-level DAIs regulated by amplification of upper level disturbances along the subtropical jet up to 5 days before the dry event peak. Descent of dry air takes place to the west of the upper level trough and east of the ridge. DJF intrusions are dominated by southerly mid-level advection and a mid-level cyclonic circulation anomaly (trough) northwest of Australia, whereas JJA intrusions have slight southeasterly flow of dry air from the extratropics due to a mid-level anticyclonic circulation anomaly (ridge) northwest of Australia. The

circulation anomaly in DJF enhances westerlies in the southern MC, allowing advection further east. In contrast, the anomaly in JJA enhances easterlies to the west, enabling westward advection. There are interactions between the low-level monsoon circulation in JJA, where northeasterly flow in DJF near mainland southeast Asia and the Bay of Bengal reverses to southwesterly, directing air parcels further northward. Opposing tropical–extratropical flow to the east of intrusions in both seasons transports moisture over Australia and the Lesser Sundas. Though, in both seasons, DAIs descend from around 10 days before the peak of the event to 10 days after, there is eventual re-ascent of air parcels in DJF, with more prolonged low-level flow in JJA. Transport mechanisms, influenced by circulation and geopotential anomalies, attributable to DAI occurrence may be linked to the MJO.

Dry air originating from the extratropics suppresses rainfall, supporting work from other studies analysing convective suppression in the Tropics linked to DAIs. Rainfall suppression signatures largely follow intrusion trajectories, where reduced rainfall may be found in DJF in the southern MC over the Lesser Sundas and neighbouring seas, following the eastward propagation. JJA, on the other hand, has limited rainfall reductions over the southern MC linked to the intrusions analysed. Instead, DAIs originating from further east lead to reductions over Java, Sumatra, southern Borneo, and neighbouring seas. Anomalies linked to the intrusion propagate to the Indian Ocean. In both cases, reduced rainfall can be seen developing around 5 days prior to up to 5 days after the dry event peak. In addition, signatures of positive rainfall anomalies are found to the east of the dry anomalies, indicative of enhanced convection linked to convergence of moist air coming from the Tropics to the extratropics encountering the eastward propagation of upper level disturbances and the

negative humidity anomalies. These have been observed elsewhere in the Tropics.

This work has extended past work, through usage of 42 years of data compared with select days to weeks in other studies, which were limited by the constraints of observations. However, our approach requires further validation from case study analysis of events linked to DAIs. Such validation is necessary particularly because of the limitations of sample size in terms of number of dry events per season, identified using the method employed. More events are required to provide confirmation of statistically significant links between dry events and the precursor mechanisms, processes that modulate their trajectories, and also their impacts on rainfall. All three of these links are potentially more visible on finer time-scales, so will need further analysis beyond what has been achieved here. Case study analysis will reveal the finer details on what controls dry event occurrence and impacts on convection and rainfall over the MC. Future work may also involve repeating the analysis presented, but for other regions of the MC.

Impacts originating from both the abrupt pauses in convection, enabling recharge in boundary-layer moisture, and also enhanced rainfall/steering of convection on margins through dynamical uplift and low-level interactions, are critical to understand. Future work should involve incorporation of both reanalysis and model data, as this will allow testing of the representation of synoptic processes such as DAIs in global and regional simulations, while increasing our understanding of the associated mechanisms particularly over the MC. These include interactions with the climatological mean circulation, as well as potentially large-scale modes of variability. Precise details on the influence of the MJO and whether it influences circulation and geopotential anomalies regulating DAIs were not covered in this research and would require fil-

tering of the MJO signal in relation to these events. Interactions between DAIs and background modes of variability, however, may vary across the MC, as the modes exert different controls on meteorology based on geographical location. Therefore, more generalised assumptions on their interactions over the whole of the MC cannot be made based on what was learnt from studying the southern portion of the region.

Regardless, our work has provided insight into key processes and impacts linked to DAIs (in terms of both rainfall suppression and enhancement), supporting and expanding on past studies. Improving our general understanding of MC precipitation patterns will provide benefits for forecasting and issuing severe weather warnings, as well as validation of numerical weather prediction models. Any improvements to regional systematic biases and our understanding of more complex processes will also ultimately contribute to improved situational awareness for local agencies, decision-makers, and communities.

Chapter 3

Atmospheric response to mesoscale ocean eddies in the Maritime Continent

Published in *Journal of Geophysical Research: Atmospheres* (2025).

Abstract

Mesoscale ocean eddies contribute to the mixing and transport of water properties throughout the global ocean. Sea surface temperature anomalies associated with these eddies can influence atmospheric boundary layer stability, and thus the formation of clouds. The Maritime Continent experiences the modulation of convection and precipitation by processes operating over multiple spatial and temporal scales. However, mesoscale air-sea interactions, such as those associated with the eddies the region generates, remain understudied. Applying a sea surface height-based eddy detection and tracking algorithm, we show that lower latitude eddies, such as those in the Maritime Continent, are generally fewer in number, weaker, and shorter-lived, but larger and faster-propagating, compared to those at higher latitudes. Crucially, we highlight that eddies in the Maritime Continent can significantly modify air-sea heat exchange and the near-surface wind field. However, changes to column water vapor, cloud, and rainfall are less distinct. Compared to the Kuroshio Extension, a representative case study for the extratropics, atmospheric anomalies associated with eddies in the Maritime Continent are weaker, and decreasing in magnitude toward the lower latitudes. We hypothesise that weaker sea surface temperature anomalies associated with eddies in the Maritime Continent, coupled with their faster propagation and intraseasonal variability in convection over the region, reduce the likelihood and intensity of the instantaneous atmospheric imprint. This study therefore emphasises the importance of the spatial and temporal scales with regard to air-sea interactions and their influence on cloud and rainfall across the Maritime Continent.

3.1 Introduction

The Maritime Continent in Southeast Asia, consisting of thousands of islands and many shallow seas (Figure 3.1), represents a 'low-latitude chokepoint' of the global oceans (Lee et al., 2019). This region is the only connection between different ocean basins in the tropics, where the Indonesian Throughflow (ITF) flows from the West Pacific Ocean to the southeast tropical Indian Ocean (Gordon, 2005; Sprintall et al., 2014). The resultant exchange and transformation of water masses in this region holds importance to the coupled ocean-atmosphere climate system (e.g. Godfrey, 1996; Makarim et al., 2019).

Tidal mixing and upwelling are dominant contributors to changes in water properties in the Maritime Continent, with vertical diffusivity in the constituent marginal seas being an order of magnitude greater than in the open ocean (Ffield and Gordon, 1996; Jochum and Potemra, 2008; Koch-Larrouy et al., 2010; Nagai et al., 2021). Mixing, primarily occurring along narrow passages or straits, is affected by the wind field, which can be modulated, for example, by the monsoon circulation and larger-scale modes of variability (e.g. Wirasatriya et al., 2021; Susanto and Ray, 2022). A key component of mixing is represented by mesoscale ocean eddies.

Mesoscale ocean eddies are ubiquitous in the global ocean, with spatial and temporal scales on the order of 100 km and 10–100 days, respectively (Chelton et al., 2011; Kurian et al., 2011). Mesoscale ocean eddies dominate the kinetic energy signature of the ocean (e.g. Storer et al., 2022), and are generated through both barotropic and baroclinic instabilities, produced by interactions between wind, currents, and bathymetry. These eddies are dominantly nonlinear as they rotate faster than their lateral propagation, and are in approximate geostrophic and hydrostatic

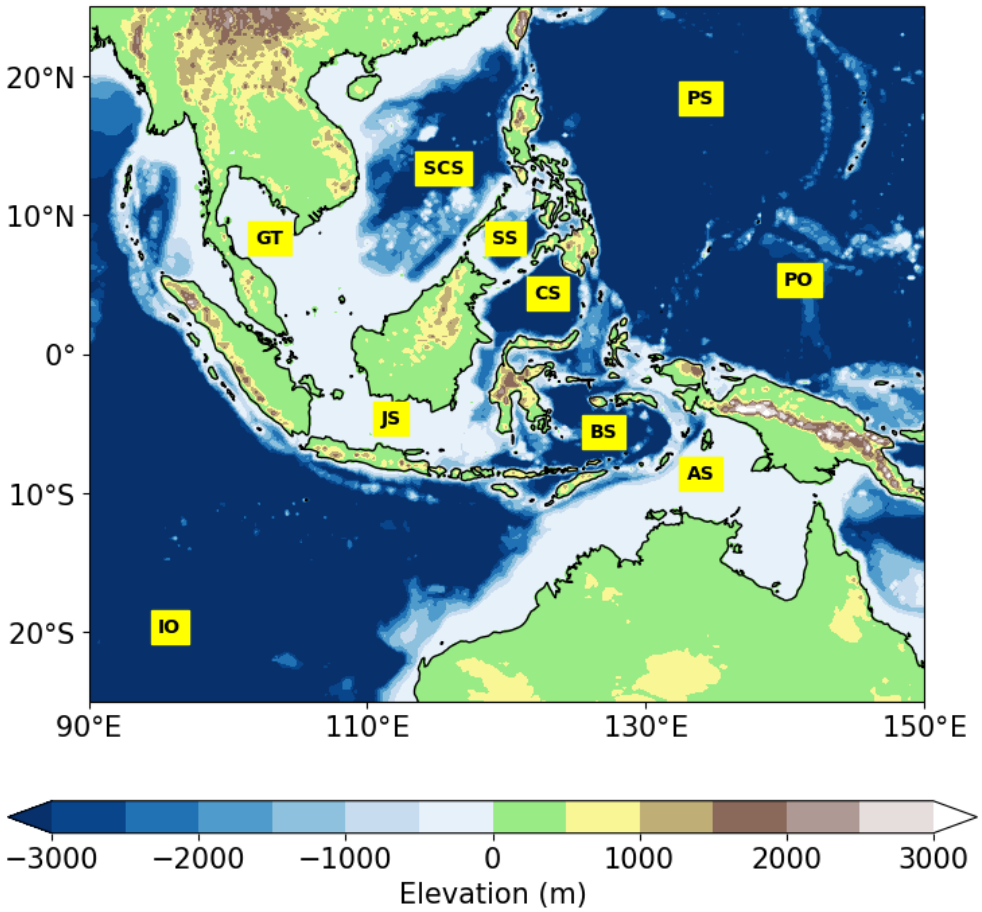

Figure 3.1: Map of the Maritime Continent located in Southeast Asia with several of the constituent seas and neighboring oceans labelled: Arafura Sea (AS), Banda Sea (BS), Celebes or Sulawesi Sea (CS), Gulf of Thailand (GT), Java Sea (JS), Indian Ocean (IO), Pacific Ocean (PO), Philippine Sea (PS), South China Sea (SCS), and Sulu Sea (SS).

balance in the horizontal and vertical dimensions, respectively (e.g. Chelton et al., 2011). Important in the transport of heat, salt, nutrients, and biogeochemical tracers (e.g. Hausmann and Czaja, 2012; McGillicuddy, 2016; Melnichenko et al., 2017), eddies exhibit regional and seasonal variability in their propagation pathways, lifetimes, amplitudes, and mechanism of genesis (e.g. Halo et al., 2014; Mason et al., 2017; Zu et al., 2022).

The various deep basins and narrow tidal straits within the Maritime Continent, and their interactions with wind and currents, are crucial in generating mesoscale ocean eddies (e.g. Chen et al., 2020; Wang et al., 2021; Pang et al., 2022). Mesoscale ocean eddies also contribute to changes in transport along the ITF (e.g. Ismail et al., 2021; Hao et al., 2022). Eddy characteristics across the Maritime Continent vary based on basin size, sea surface temperature (SST), ocean currents, coastline distance, and bathymetry (Ffield and Gordon, 1996). Eddies in the seas of the Maritime Continent are mostly short-lived, with lifespans less than 30 days (Hao et al., 2021), and are more prevalent in the northern seas forming the inflow of the ITF (Purba et al., 2020). As a result, studies have found intraseasonal variability in surface ocean characteristics is more strongly linked to mesoscale ocean eddies, as opposed to larger-scale forcing, in the northern seas (Napitu et al., 2015).

Mesoscale ocean eddies consist of two polarities - anticyclonic and cyclonic (e.g. McGillicuddy, 2016). These eddies, if located sufficiently far away from the Equator, are close to being in hydrostatic and geostrophic balance. Therefore, thermal wind relationships can explain links between their induced respective positive and negative sea surface height (SSH) anomalies, low and high sea level pressure (SLP) anomalies, and development of characteristic SST signatures.

Signatures in SST associated with mesoscale ocean eddies act as the facilitator for interactions between these ocean features and the atmosphere (e.g. Frenger et al., 2013; Bôas et al., 2015; Liu et al., 2021; Gulakaram et al., 2023; Seo et al., 2023). Warm-core eddies release heat to the atmosphere through induced surface heat fluxes, which can strengthen winds and produce anomalous wind convergence. These changes can lead to enhanced instability in the atmospheric boundary layer, thereby enhancing vertical mixing, potentially leading to more cloud and rainfall. In contrast, cold-core eddies draw in heat from the atmosphere, which can weaken winds and result in anomalous wind divergence. The boundary layer is therefore more stable, with less cloud and rainfall. Both anticyclonic and cyclonic eddies can have warm and cold cores dependent on processes governing eddy vertical thermohaline structure (e.g. Liu et al., 2020; Sun, An, Liu, Liu, Yang, Tan, Dong and Liu, 2022).

The relationship between the SST anomalies associated with eddies and influence on the atmosphere additionally results from the balance between advection and vertical mixing. When advection is weak, winds converge over the warm flank of an SST front due to the pressure gradient force (the pressure adjustment mechanism; e.g. Lindzen and Nigam, 1987; Small et al., 2008). In contrast, when advection is strong, due to enhancement of wind speed over a warm anomaly in the surface ocean, winds converge downstream (the vertical mixing mechanism; e.g. Wallace et al., 1989; Chelton et al., 2004; Park et al., 2006). These mechanisms can have competing influences on the atmospheric boundary layer (Jiang et al., 2019).

It is important to acknowledge that the background environmental state can modify the characteristics of eddies and their imprint on the atmosphere. For example, interactions with more transient processes, such as synoptic weather systems, can

add additional ocean-atmosphere feedbacks (Souza et al., 2021; Gulakaram et al., 2023). Studies have also suggested seasonality in the response to, and characteristics of, eddies in regions such as the northwest Pacific, with more intense anomalies in the wintertime due to enhanced SST anomalies (Liu, Chang, Kurian, Saravanan and Lin, 2018; Sun, Li, Yan, Zhou and Zhou, 2022). In addition, interactions between eddies and large-scale modes of variability, which regulate the environmental wind and SST field, have been observed (Roman-Stork et al., 2021).

The Maritime Continent is a region known for the modulation of atmospheric stability, convection, and rainfall by a variety of processes operating over multiple spatial and temporal scales. Processes include large-scale modes of variability, such as the Madden-Julian Oscillation (MJO, e. g. Madden and Julian, 1994), and finer-scale and more local phenomena such as the diurnal cycle of solar heating (e.g. Mori et al., 2004). Studies have also investigated the role of air-sea interactions in the Maritime Continent (see Xue et al., 2020, for a comprehensive review, primarily focusing on modelling capabilities).

Though the characteristics of eddies within the Maritime Continent are well understood, their relationship with air-sea interactions has not been studied. In fact, minimal research has been conducted into this relationship across the tropics. By using observational data to track eddies in the tropical Atlantic Ocean and analyse the associated mean atmospheric responses across the domain, Aguedjou et al. (2023) found a minimal imprint of mesoscale ocean eddies on the atmospheric boundary layer, such as in surface heat fluxes and precipitation. Toward the subtropics, such as in the South China Sea, responses in surface heat fluxes, wind, and other atmospheric properties, obtained from satellite observations, are noted in studies such as Liu, Li,

Chen, Fang and Li (2018). As the waters of the Maritime Continent act as an abundant heat source favoring the formation of convection, it is important to investigate if surface ocean anomalies even at the mesoscale can leave an imprint on the tropical atmosphere. Such analysis would, for example, help to inform decisions related to running coupled ocean-atmosphere models for numerical weather prediction and the complexity and/or resolution they require, by better understanding the role of the ocean, in the Maritime Continent.

In this study, we aim to identify the general properties of mesoscale ocean eddies in the Maritime Continent, and to determine if there is an atmospheric response to these eddies, which has not been analysed in the existing literature. We use 20 years of satellite altimetry data to detect and track eddies, which are collocated in ECMWF (European Centre for Medium-Range Weather Forecasts) Reanalysis v5 (ERA5) data (Hersbach et al., 2020) to produce composites. These composites are used to analyse whether SST anomalies at the mesoscale can interact with the atmosphere significantly enough in the Maritime Continent to affect cloud and rainfall properties, as seen in other regions. Section 3.2 presents the methodology used for eddy detection and tracking, construction of eddy composites for analysis of the corresponding atmospheric response, and statistical testing of the significance of these responses. We show results in Section 3.3, which cover the characteristics of eddies, and eddy composites in various surface and atmospheric variables. Section 3.4 compares these results to those obtained in previous studies, to establish hypotheses for the extent, or lack, of atmospheric responses to eddies in the Maritime Continent. Conclusions are given in Section 3.5.

3.2 Methodology

3.2.1 Eddy detection and tracking

Eddy detection is crucial for understanding eddy-induced ocean dynamics, and several methods have been developed primarily utilising satellite altimetry data. These methods include the Okubo-Weiss parameter method (e.g. Frenger et al., 2013), where eddies are classified based on vorticity determined from the geostrophic components of velocity, and the flow and vector geometry methods (e.g. Nencioli et al., 2010), which utilise closed contours of the stream function field. The most popular method is the SSH anomaly method. This method is parameter-free, as defined eddy edges, which depend only on a single extremum, and compared to other methods, performance is better, for example, in terms of signal-to-noise ratios and avoidance of excess eddy detection (e.g. Chelton et al., 2011).

Here, we use and adapt the eddy detection and tracking algorithm, py-eddy-tracker, of Mason et al. (2014). This open-source algorithm requires SSH data input, either using sea level anomalies (SLA; deviations of the sea surface from the mean sea surface) or absolute dynamic topography (ADT; the difference between the instantaneous SSH and the marine geoid, equivalent to the sum of SLA and the mean dynamic topography). While SLA and ADT are both effective in the identification of eddies, Pegliasco et al. (2021, 2022) suggest the usage of ADT as it is more sensitive to regions with strong SSH gradients and where recurrent mesoscale features exist, or for coastal regions, and both closed and semiclosed basins, such as in the Maritime Continent. ADT is also more sensitive to tracking smaller eddies and longer trajectories, and less sensitive to detecting meanders in currents as eddies (Halo et al.,

2014).

We obtained data for ADT (from here referred to just as SSH anomaly) through the Data Unification and Altimeter Combination System (DUACS; Taburet et al., 2019). DUACS is the operational multimission production system of altimeter data developed by Centre National D'Études Spatiales (CNES)/Collecte Localisation Satellites (CLS). Data products are estimated by merging along-track measurements from different altimeter missions from GEOSAT to Jason-3. These data are provided by Archiving, Validation and Interpolating of Satellite Oceanographic data (AVISO), available through the Copernicus Marine Environment Monitoring Service (CMEMS). SSH anomalies, relative to a 20-year mean, were predetermined by the data provider and available at $0.25° \times 0.25°$ horizontal grid spacing. We use 20 years of continuous daily data from December 2000 to November 2020.

The eddy detection algorithm removes a large-scale smoothed field, obtained from a Gaussian filter with a zonal (meridional) major (minor) radius of 10° (5°), from the SSH anomaly data, which accounts for their lateral propagation, visible in SSH data (Mason et al., 2014). Eddies are then identified using interpolated contours of this high-pass filtered data, calculated at intervals of 1 cm from -100 to 100 cm. Each 1 cm SSH interval is analysed in turn, searching downward from the previously mentioned limits to 0 cm, until a closed contour is detected. From this closed contour, the algorithm employs a set number of criteria for labelling a feature as an eddy, as described in Mason et al. (2014). These criteria include constraints to the number of pixels within the final closed contour, a maximum shape error relative to an ideal fit circle, and the requirement for only one local maxima or minima within the closed contour. Once an eddy is identified, it is relabelled as the effective perimeter, with an

associated effective radius, which represents the radius of a circle with the same area as that enclosed by the effective perimeter. The effective radius, hereon referred to as R, therefore equals $\sqrt{\frac{a}{\pi}}$, where a is the eddy area. Various properties are computed for each eddy, such as centroid, radius, amplitude, and area. Estimates of the along-track propagation rate were determined for each eddy using the centroids determined using the algorithm.

Pixels for SSH anomaly data, which correspond to the eddy are masked, representing regions unavailable for further eddy identification. Separation distances between centroids at times t and $t+1$ are computed for eddy pairs of the same polarity. $t+1$ candidates for eddies continuing the track at time t are chosen using the ellipse method as in Chelton et al. (2011). This method restricts cross-track jumping, using bounds of an ellipse with a zonally oriented major axis, 150 km radius east-west and 75 km radius north-south from the local extremum of the eddy. If multiple candidate eddies fall within an ellipse, the candidate eddy, which is a continuation of the track, is identified according to the minimum of a set of dimensionless similarity parameters (Penven et al., 2005):

$$S_{t,t+1} = \sqrt{\left(\frac{\Delta d}{d_0}\right)^2 + \left(\frac{\Delta a}{a_0}\right)^2 + \left(\frac{\Delta A}{A_0}\right)^2} \tag{3.1}$$

where Δd is the separation distance, Δa the difference in eddy area, and ΔA the difference in amplitude, between eddies at times t and $t+1$. Denominators represent characteristic values, here using those in Hao et al. (2021). A smaller value of S implies higher similarity of an eddy pair and therefore likely continued propagation of the eddy at time t. Any unused candidate eddies are labelled as new eddies. Eddy tracking continues by iteration over the time period of analysis.

3.2.2 Eddy composite construction

We use ERA5 reanalysis data (Hersbach et al., 2020) from December 2000 to November 2020 for constructing eddy composites. ERA5 is consistent with its ocean counterpart, ORAS5 (Ocean ReAnalysis System 5; Zuo et al., 2018), using both HadISST2 SST and the OSTIA sea-ice concentration to constrain surface boundary conditions. ORAS5 operates at an eddy-permitting resolution ($0.25° \times 0.25°$) and is noted to provide an appropriate representation of the SST and sea level variability, which can be attributed, for example, to eddies in the ocean. Therefore, there is comfort in using the ERA5 data to represent the atmospheric response to these eddies, modulated by their SST anomalies. Hourly, instantaneous, and single-level ERA5 data are available at a horizontal grid spacing of $0.25° \times 0.25°$. For time-dependent data such as surface heat fluxes, we calculate daily means as an average of the variables over the 24 hr. Accumulated data such as precipitation and water vapor are presented as daily totals.

For each variable, a high-pass spatial filter, using a $6° \times 6°$ Hann window, is applied, which has been used in previous studies (e.g. Bôas et al., 2015; Delcroix et al., 2019; Aguedjou et al., 2023). Application of high-pass spatial filters help to isolate signals with wavelengths larger than the extent of the window functions used, representing a larger-scale reference level. This reference can be removed from a particular variable field to produce a spatially filtered anomaly, which captures solely mesoscale variations, for example, here, in the surface and atmospheric properties analysed. We also remove the smoothed mean annual cycle of the filtered data set derived from the first three harmonics, to produce anomalies that are both spatially and temporally filtered. To construct fitted circular composites, the eddy centroid

and the radius at the mature phase, where eddy amplitude is a maximum, are taken. A two-dimensional high-resolution Cartesian grid is created for each eddy, where the eddy is normalised by its radius R up to $3R$. Filtered values are then interpolated to this uniform grid representing the normalised eddy. Eddies are further separated into their relevant warm-core and cold-core subgroups. To define warm-core (cold-core) eddies, the mean SST anomalies within $\frac{2}{3}$ of the eddy radius (Delcroix et al., 2019) must be greater than 0.1°C (less than 0.1°C). The eddies were also rotated so that the mean environmental surface wind vector is westerly (e.g. Liu et al., 2021; Frenger et al., 2013). Anomalies to the right of the composite centers can then be described as 'downstream'.

Other studies employ additional thresholds in eddy amplitude, radius at maximum amplitude, and duration, to improve the quality and robustness of results. For example, these thresholds would allow attribution of results to the strongest, largest, or longest-lasting eddies, respectively. Employing a threshold on the radius does not significantly reduce the number of eddies we analyse, compared to amplitude and duration. Using an amplitude and/or duration threshold had little impact on the spatial structure and magnitude of the anomalies we analyse (not shown), as well as reducing the number of eddies composited significantly. Therefore, we choose not to employ additional thresholds to the SST threshold when grouping and compositing eddies.

3.2.3 Comparison to the environment

To determine if composite signals in anomalies associated with the identified eddies are distinguishable from the background environment, we randomly sample selected

regions within our domain of analysis a number of times, roughly equivalent to the number of eddies within each labelled category of eddies for that region. See Section 3.3.2 for further details on the selected regions. An equivalent number of longitudes and latitudes are generated within the constraints of the region to represent eddy centroids. These random samples are composited in a similar way to the real eddies, using the mean values of eddy radii within each region, and performed for each spatiotemporally filtered variable. A t-test is applied for each composited set of eddies, where we chose a significance level of 5% to highlight whether a particular grid point within an eddy composite is significantly different, and therefore, distinguishable from the background environment. It should be noted that this method is sensitive to the number of eddies examined in each region, with background anomalies closer to zero, less 'patchy', and more distinguishable from eddy-associated anomalies where there are more eddies (not shown).

3.3 Results

3.3.1 Eddy characteristics

Figure 3.2 shows the geographical variability in eddy characteristics across the analysed domain. There is a distinct eddy-poor belt across the equator, with approximately 150 eddies crossing a particular grid point (Figure 3.2a). Several regional hotspots within the tropics, particularly in the Maritime Continent, can be observed, including the Sulawesi and Sulu Seas (Figure 3.1), near to the inflow of the ITF, where the number of eddies per grid point is 200–300. This value is what appears to be typically observed at higher latitudes. Hotspots away from the tropics have

more than 400 eddies per grid point. These areas include seas near Japan, extending eastward into the northwest Pacific Ocean, within the Kuroshio Extension.

Eddies across the tropics have smaller mean peak amplitudes in their SSH anomalies (approximately 2 cm), reaching up to 4 cm in the previously mentioned hotspots within the Maritime Continent (Figure 3.2b). These peaks are much lower than in subtropical eddy-rich regions such as the Bay of Bengal and South China Sea, where amplitudes can be up to and above 10 cm. Even more striking is the mean amplitude exceeding 10 cm in most of the northwest Pacific, primarily east of Japan toward the central northern Pacific, as well as toward Kamchatka and the South China Sea.

There is a distinct latitudinal gradient in the mean radius of eddies (Figure 3.2c). Across the open ocean, mean radii in the tropics are between 110 and 130 km, going down to around 50–70 km toward the extratropics. Within the seas of the Maritime Continent, mean radii of eddies are smaller than in the tropical open ocean, up to 80 km in the internal seas, and much lower near the coastlines.

Mean eddy duration largely follows the distribution of the number of eddies, where eddies in the tropics are short-lived with maxima of 10 days (Figure 3.2d). Regional eddy hotspots have slightly longer lifetimes, up to 15 days in the northeastern seas of the Maritime Continent, and up to 20 days toward the southeast tropical Indian Ocean. These values are smaller than values of up to 40–50 days in regions such as the Bay of Bengal. These eddies are also much more short-lived than those in the extratropics where lifetimes reach above 50 days in the open ocean. In the northwestern Pacific, bands of shorter lifetimes, one located around 35°N and another extending from Kamchatka southward past Japan toward Taiwan, are observed. Here, eddies have lifetimes of maximum 20 days.

Eddies in the tropics, particularly in the open ocean, have greater mean propagation rates, up to around 25 km (Figure 3.2e). Within the internal seas of the Maritime Continent, propagation rates reduce to around 15–20 km day^{-1}. Tending toward higher latitudes, mean propagation rates are much lower, around 5–10 km day^{-1}

3.3.2 Eddy characteristics: regional comparison

We focus our study on three regions in the Maritime Continent. These regions are shown as the southern three polygons in Figure 3.2f, with their spatial extents chosen for consistency with existing literature. From south to north, these are the southeast tropical Indian Ocean (e.g. Yang et al., 2015; Ismail et al., 2021; Wang et al., 2021; Zu et al., 2022), hereon referred to as the SETIO, the Sulawesi Sea (e.g. Hao et al., 2021, 2022), and the South China Sea (e.g. He et al., 2018; Liu, Li, Chen, Fang and Li, 2018; Liu et al., 2020). Eddies were associated with a particular region if they reach peak amplitude when their centroid is within the respective spatial bounds of each region. All three regions are known for the generation of mesoscale ocean eddies, primarily through the interaction of ocean currents and resultant changes to water properties.

However, the South China Sea is the only region in the Maritime Continent, which has been studied, with regards to air-sea interactions associated with eddies. Therefore, we also choose a well-known extratropical region, the Kuroshio Extension, within the northwest Pacific, to facilitate a comparison with existing studies. The Kuroshio Extension is an environment rich in high amplitude eddies, produced by ocean currents, which interact to form a strong meridional SST gradient (e.g. Chelton et al., 2011; Cheng et al., 2014). Studies within the Kuroshio Extension have investigated

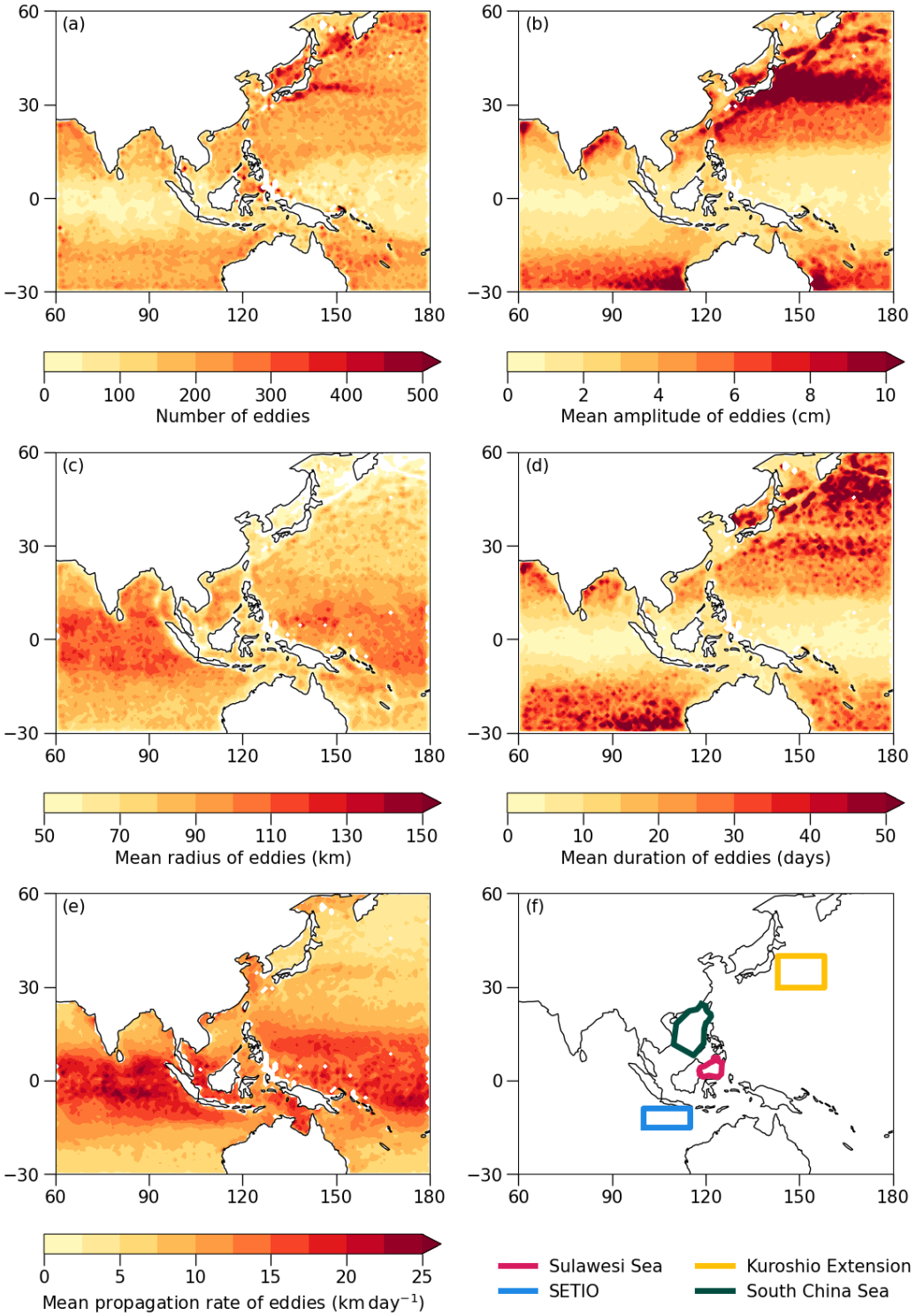

Figure 3.2: (a) Distribution of the number of eddies identified from December 2000 to November 2020, where sums are calculated within bins of 1° × 1°. The other four panels represent the mean amplitude (b), radius (c), duration (d), and propagation rate (e) of all eddies. Values in panels (b)-(d) are calculated from sums of eddy properties when each eddy is at peak amplitude, whereas the propagation rate (e) is calculated along track and plotted where eddy is at peak amplitude. Panel (f) highlights the Kuroshio Extension (yellow), South China Sea (green), Sulawesi Sea (pink), and southeast tropical Indian Ocean (SETIO; blue) from north to south respectively, which are the regions used in later analysis.

Table 3.1: The number of anticyclonic and cyclonic eddies identified in each region. Values in brackets represent the number of eddies used for later composites after imposing an absolute threshold of 0.1°C on the core of the eddy. This value is also presented as a percentage of the total number of eddies for each polarity.

	Anticyclonic eddies	**Cyclonic eddies**
Kuroshio Extension	16456 (14137 = 85.9%)	16192 (13653 = 84.3%)
South China Sea	10476 (5934 = 56.6%)	10335 (5832 = 56.4%)
Southeast Tropical Indian Ocean	8638 (3716 = 43.0%)	8261 (3605 = 43.6%)
Sulawesi Sea	4382 (2121 = 48.4%)	3224 (1621 = 50.3%)

the signatures of eddies at the surface and depth (Sun, An, Liu, Liu, Yang, Tan, Dong and Liu, 2022), in addition to surface heat flux anomalies and impacts on the atmospheric boundary layer (Ma et al., 2015, 2016). A comparison of this region with those in the Maritime Continent allows testing and validation of the existing methodology, and provides reassurance that the approach taken is suitable.

Table 3.1 shows the number of eddies identified in each of the four regions. A sharp reduction in the number of eddies is noted, as observed in Figure 3.2a, from the extratropics in the Kuroshio Extension (a total of 32648), to near-equatorial regions such as the Sulawesi (a total of 7,606). Histograms showing the distribution of mean amplitudes, radii, duration, and propagation rates of tracked eddies in the selected regions are provided in Figure 3.3. Here, we separate eddies into anticyclonic and cyclonic eddies.

The mean amplitude of eddies in the Sulawesi Sea and SETIO are similar, around 2.5 cm for anticyclonic eddies (Figure 3.3a) and 3 cm for cyclonic eddies (Figure 3.3b). Eddies in the South China Sea are around 1–1.5 cm stronger than those in the other two Maritime Continent regions. Kuroshio Extension eddies are much stronger, over 5 times that of eddies in the Sulawesi Sea and SETIO. In all three regions other than

the South China Sea, cyclonic eddies have greater amplitude than anticyclonic eddies.

The mean radius associated with eddies in the Sulawesi Sea and Kuroshio Extension is similar (70–80 km) for both anticyclonic eddies (Figure 3.3c) and cyclonic eddies (Figure 3.3d). South China Sea eddies are greater in size, around 83 km in radius, though SETIO eddies are the largest out of the four regions, with radii above 90 km. Cyclonic eddies are greater in size than anticyclonic eddies in the Sulawesi Sea and SETIO, whereas the two eddy types are similar in size in the South China Sea and Kuroshio Extension.

Sulawesi Sea eddies are the most short-lived, lasting around 9–10 days (Figures 3.3e and 3.3f). South China Sea anticyclonic eddies (cyclonic eddies) last for 4 days longer (2 days less) than those in the SETIO, but both sets of eddies last for twice as long as Sulawesi Sea eddies. In contrast, Kuroshio Extension eddies can last for between 3 and 4 weeks. South China Sea and Sulawesi anticyclonic eddies last longer than their respective cyclonic eddies, and the opposite is observed for the other two regions.

There is similarity between the mean propagation rates of anticyclonic eddies (Figure 3.3g) and cyclonic eddies (Figure 3.3h) in each region, with differences of only up to around $1\,\mathrm{km\,day^{-1}}$. SETIO eddies propagate the fastest, with means up to around $15\,\mathrm{km\,day^{-1}}$. These rates are up to $4\,\mathrm{km\,day^{-1}}$ greater than those in the Sulawesi Sea, but almost double the propagation rates observed in the South China Sea and Kuroshio Extension.

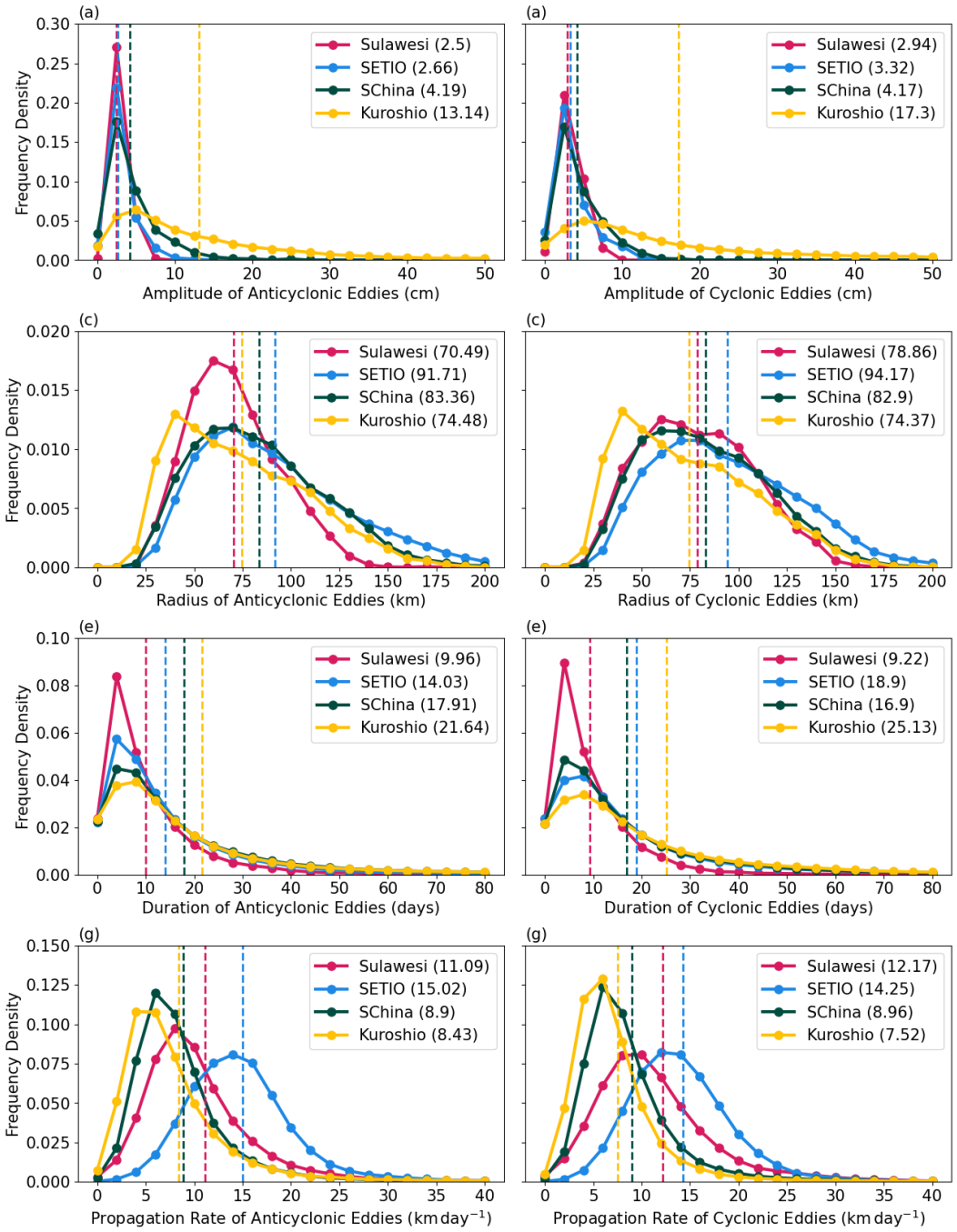

Figure 3.3: Histograms of the amplitude (a–b), radius (c–d), duration (e–f), and propagation rate (g–h) of anticyclonic and cyclonic eddies, respectively, identified in the studied eddy hotspots. The Sulawesi Sea, southeast tropical Indian Ocean (SETIO), South China Sea, and Kuroshio Extension are marked by pink, blue, green, and yellow colours, respectively. Dashed vertical lines mark the mean of each variable for the eddies in each region, as indicated in the legend. Upper limits for each variable on the x-axis are chosen to aid visual clarity.

3.3.3 Eddy composites

Here, we present composites of the property anomalies associated with mesoscale ocean eddies in each of the hotspot regions (Figures 3.4 to 3.7) in order to identify possible spatial patterns. We analyse interactions at the air-sea interface associated with eddies using sensible and latent heat fluxes (SHF and LHF, respectively, defined as positive for fluxes upwards into the atmosphere) and wind divergence at 10 m. Total column water vapor (TCWV), cloud liquid water (TCLW), and rainfall are also plotted for understanding changes to atmospheric moisture and cloud presence, which may be linked to the induced air-sea interactions. Note that colour scales for the three Maritime Continent regions (Figures 3.5 to 3.7) differ for some variables compared to the Kuroshio Extension (Figure 3.4) to better visualise results and to account for geographical variability in the responses. Any eddies with absolute SST anomalies below 0.1°C, as outlined in the methodology, were discarded. The total number of eddies therefore used in these composites is shown in brackets in Table 3.1.

Region 1: Kuroshio Extension (the extratropics)

Absolute eddy-averaged SST anomalies in the Kuroshio Extension region are around 0.6°C across the four eddy types analysed, with anomalies extending to beyond $2R$ (Figure 3.4). There is strong correspondence between SST and SHF anomalies in the Kuroshio Extension, where absolute eddy-averaged anomalies can reach values around 10 $\mathrm{W\,m^{-2}}$ (Figures 3.4a-d). These anomalies are significantly different from the background environment. Similar correspondence can be observed between SST and LHF anomalies (Figures 3.4e–h). Eddy-averaged LHF anomalies are nearly double the SHF anomalies and are similarly significant compared to the background

environment. The sign of both surface heat flux anomalies extend over $2R$, with fluxes out of (into) the ocean for warm-core (cold-core) eddies.

There is also a degree of correspondence between SST anomalies and centers of wind divergence anomalies (Figures 3.4i–l). Anomalous convergence (divergence) is observed over warm (cold) eddies, with these anomalies also noted downstream. Absolute eddy-averaged anomalies are around $10^{-6}\,\mathrm{s}^{-1}$, and are also significantly different from the background environment.

Changes to TCWV anomalies have similar spatial structure to the wind divergence anomalies, aside from warm cyclonic eddies (Figures 3.4m–p). Generally, warm-core (cold-core) eddies have increases (decreases) in TCWV near to centers of surface convergence (divergence), which are off-center relative to the SST anomaly. Absolute eddy-averaged anomalies are up to around $1\,\mathrm{kg\,m}^{-2}$, while values corresponding to regions with pronounced wind divergence anomalies approach $2\,\mathrm{kg\,m}^{-2}$. TCWV anomalies are significant relative to the background environment. TCLW anomalies tend to follow the spatial distribution as seen with TCWV, where increases (decreases) in TCLW by up to $0.05\,\mathrm{kg\,m}^{-2}$ occur relative to warm-core (cold-core) eddies (Figures 3.4q–t). The signal of these anomalies relative to TCWV, however, is slightly weaker.

Rain anomalies over Kuroshio Extension eddies have absolute eddy-averaged values around $0.05\,\mathrm{mm\,day}^{-1}$, reaching up to $0.1\,\mathrm{mm\,day}^{-1}$ within the center of the composites (Figures 3.4u–x). There is strong spatial coherence between the SST anomalies associated with the eddies and the rain anomalies, with increases (reductions) in rain over warm (cold) eddies. These anomalies are significant relative to the background environment.

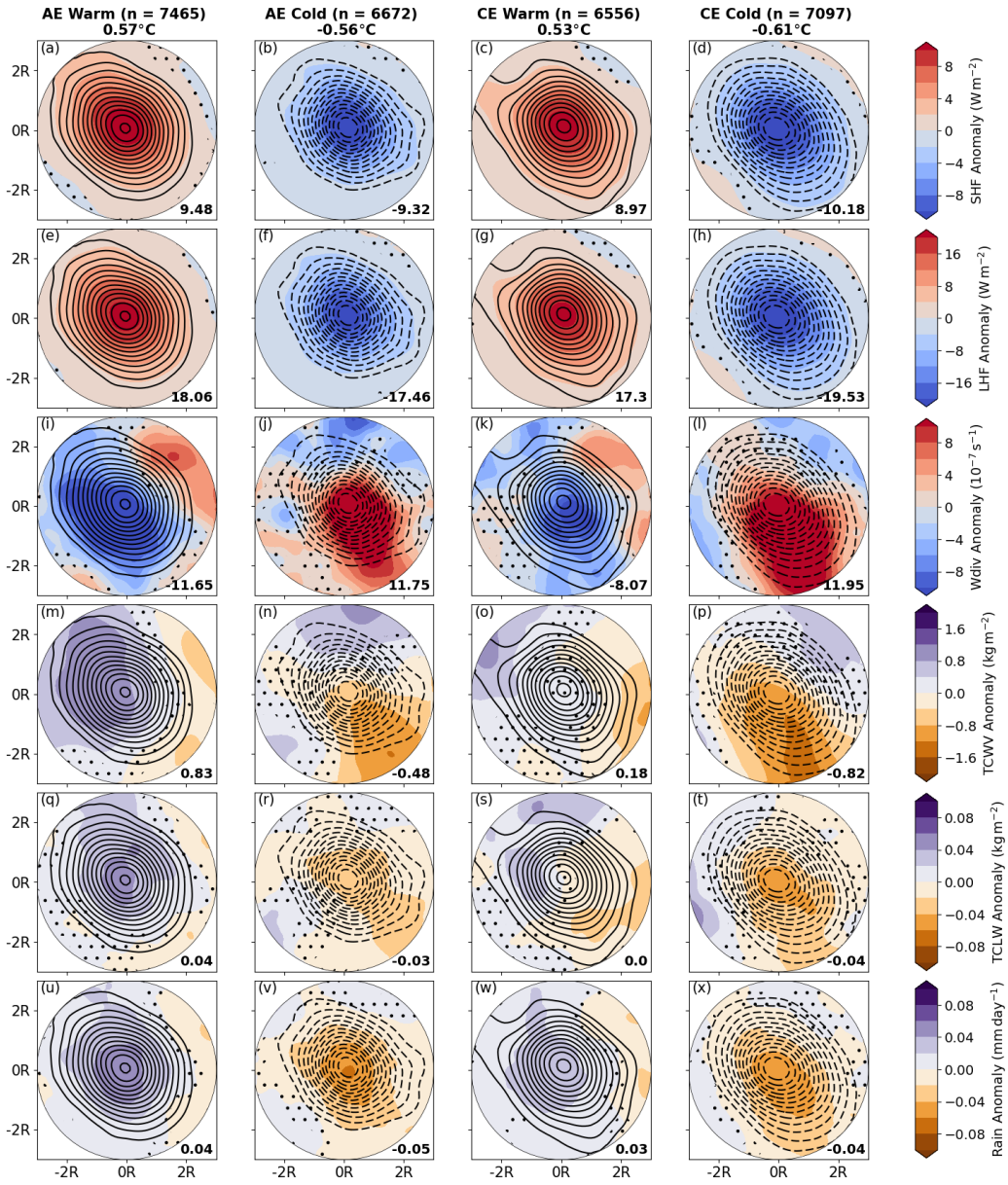

Figure 3.4: (a–d) Eddy composites of surface sensible heat flux anomalies, shown in filled contours, for the four categories of eddies (anticyclonic warm, anticyclonic cold, cyclonic warm, and cyclonic cold, respectively) in the Kuroshio Extension, plotted up to $3R$ from the centroid. Contours represent sea surface temperature anomalies in increments (reductions) of 0.05°C, starting from 0.1°C (-0.1°C) for warm (cold) eddies. Values of indicate the number of eddies composited within each panel. 'Eddy-averaged' (averaged up to $1R$) anomalies in sea surface temperature are provided next to these. (e–h), (i–l), (m–p), (q–t), and (u–x) are the same as (a–d), except filled contours now represent surface latent heat flux, 10 m wind divergence, total column water vapor, total cloud liquid water, and rain anomalies, respectively. The values in the bottom right of each panel represent 'eddy-averaged' values for each property. Dots represent regions where there is no significant difference between the eddy composites and the background environment, using a t-test at the 5% significance level, as described in Section 3.2.3.

Region 2: South China Sea (northern Maritime Continent)

SST anomalies associated with eddies in the South China Sea are between 0.2 and 0.25°C, and extend to 1.5–2R (Figure 3.5). Eddy-averaged SHF anomalies within the South China Sea are not as strong as those in the Kuroshio Extension - around $2\,\mathrm{W\,m^{-2}}$ - but are spatially coherent with the SST anomalies and significantly different from the background environment (Figures 3.5a–d). Spatial coherence and significance is also the case for LHF anomalies, where absolute eddy-averaged values are up to around $10\,\mathrm{W\,m^{-2}}$ (Figures 3.5e–h). Heat fluxes out of (into) the ocean are associated with warm-core (cold-core) eddies.

In this region, wind divergence anomaly centers are located downstream of eddies (Figures 3.5i–l). Downstream convergence (divergence) is associated with warm (cold) eddies in the rotated composites. Absolute anomalies are slightly weaker than in the Kuroshio Extension, being just shy of $10^{-6}\,\mathrm{s^{-1}}$. Nonetheless, these anomalies are statistically significant relative to the background environment.

The distribution of TCWV anomalies (Figures 3.5m–p) roughly follow that of wind divergence. Enhancements (reductions) in TCWV of just over $1\,\mathrm{kg\,m^{-2}}$, related to centers of surface convergence (divergence), are associated with warm-core (cold-core) eddies. It must be noted that these anomalies are not as spatially coherent with respect to the SST anomaly itself, though the anomalies are significant. The robustness of the signal in TCLW is of similar strength (Figures 3.5q–t). Peaks in absolute TCLW anomalies are around $0.05\,\mathrm{kg\,m^{-2}}$ at the center, though are not as robust for warm anticyclonic eddies (Figure 3.5q).

Rain anomalies are generally not statistically significant relative to the background environment (Figures 3.5u–x). Eddies in the South China Sea have near-zero eddy-

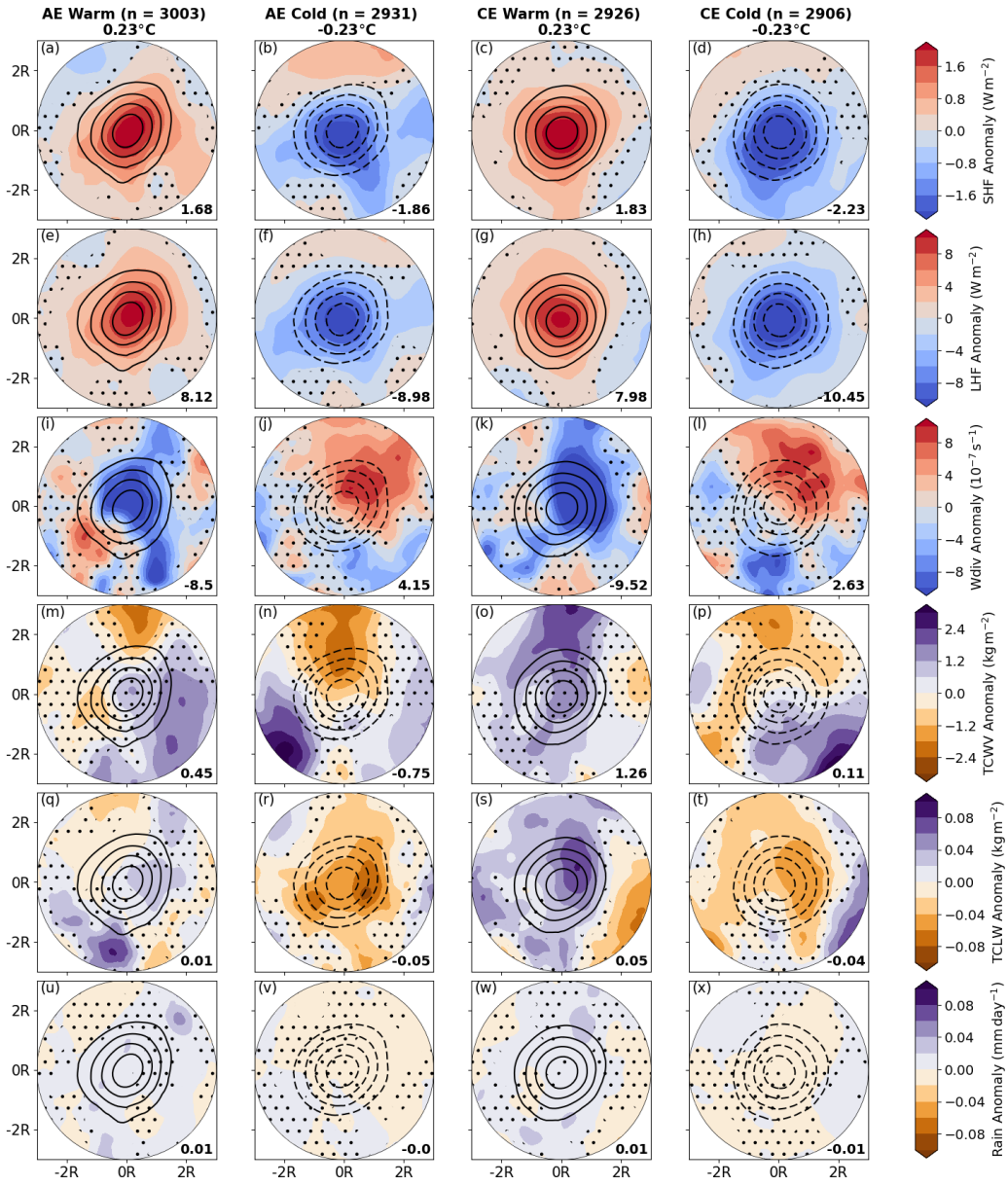

Figure 3.5: (a–d) Eddy composites of surface sensible heat flux anomalies, shown in filled contours, for the four categories of eddies (anticyclonic warm, anticyclonic cold, cyclonic warm, and cyclonic cold, respectively) in the South China Sea, plotted up to $3R$ from the centroid. Contours represent sea surface temperature anomalies in increments (reductions) of 0.05°C, starting from 0.1°C (-0.1°C) for warm (cold) eddies. Values of indicate the number of eddies composited within each panel. 'Eddy-averaged' (averaged up to $1R$) anomalies in sea surface temperature are provided next to these. (e–h), (i–l), (m–p), (q–t), and (u–x) are the same as (a–d), except filled contours now represent surface latent heat flux, 10 m wind divergence, total column water vapor, total cloud liquid water, and rain anomalies, respectively. The values in the bottom right of each panel represent 'eddy-averaged' values for each property. Dots represent regions where there is no significant difference between the eddy composites and the background environment, using a t-test at the 5% significance level, as described in Section 3.2.3. Note that, compared to Figure 3.4, the colour scales for surface heat flux and total cloud liquid water anomalies have been changed for better visualisation of results between the three regions of the Maritime Continent.

averaged rain values, with no observable signal related to the eddy. However, they do get the correct sign in cases where warm-core and cold-core eddies have anomalies of 0.1 mm day^{-1} and -0.1 mm day^{-1}, respectively.

Region 3: southeast tropical Indian Ocean (southern Maritime Continent)

Eddy-related SST anomalies in the SETIO are just over 0.15°C, with spatial extents confined to around $1R$ (Figure 3.6). Absolute eddy-averaged SHF anomalies are weaker than in the South China Sea, between 0.6 and 0.9 W m^{-2} (Figures 3.6a–d). However, there remains spatial correspondence with SST anomalies, and SHF anomalies are significant relative to the background environment. Absolute eddy-averaged LHF anomalies are around 5 times greater than that the SHF anomalies (Figures 3.6e–h). Anomalies in LHF are also significant from the background environment. As in the previous two regions, heat fluxes are observed coming out of (into) the ocean for warm-core (cold-core) eddies.

Anomalous convergence (divergence) is associated with the warm-core (cold-core) eddies in the SETIO (Figures 3.6i–l). The magnitude of these anomalies are similar to those in the South China Sea, though there remains spatial coherence with the SST anomalies, particularly for the cyclonic eddies (Figures 3.6k and 3.6l). In comparison, the anticyclonic eddies have responses both over the eddy center and downstream (Figures 3.6i and 3.6j). Wind divergence anomalies in all eddy categories are significant relative to the background environment.

Despite the anomalies seen in SHF, LHF, and wind divergence, TCWV anomalies do not appear to have a coherent spatial structure relative to the SST anomalies (Figures 3.6m–p). Absolute TCWV anomalies around the composite exceed 3 kg m^{-2}, and

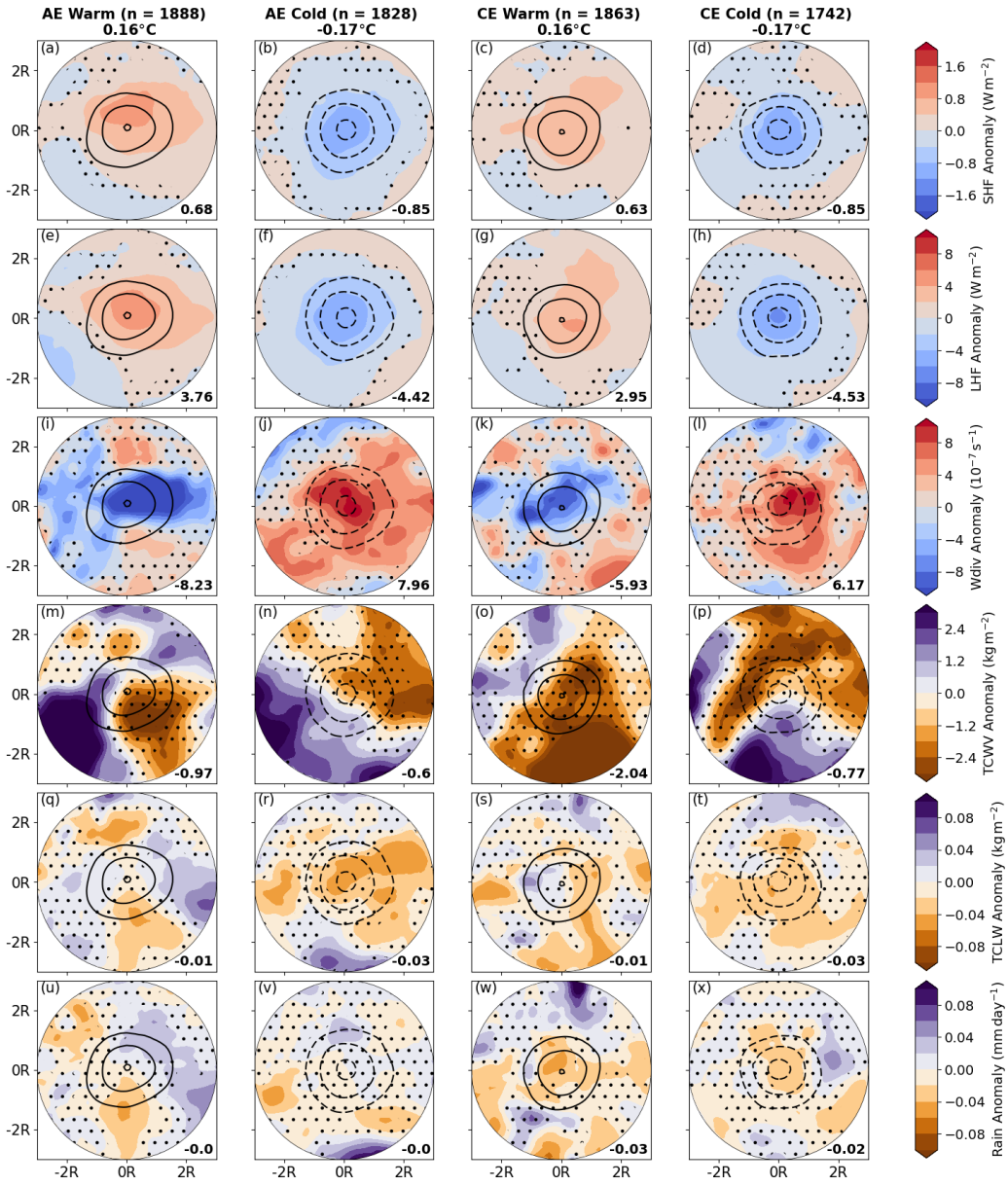

Figure 3.6: (a–d) Eddy composites of surface sensible heat flux anomalies, shown in filled contours, for the four categories of eddies (anticyclonic warm, anticyclonic cold, cyclonic warm, and cyclonic cold, respectively) in the southeast tropical Indian Ocean, plotted up to $3R$ from the centroid. Contours represent sea surface temperature anomalies in increments (reductions) of 0.05°C, starting from 0.1°C (-0.1°C) for warm (cold) eddies. Values of indicate the number of eddies composited within each panel. 'Eddy-averaged' (averaged up to $1R$) anomalies in sea surface temperature are provided next to these. (e–h), (i–l), (m–p), (q–t), and (u–x) are the same as (a–d), except filled contours now represent surface latent heat flux, 10 m wind divergence, total column water vapor, total cloud liquid water, and rain anomalies, respectively. The values in the bottom right of each panel represent 'eddy-averaged' values for each property. Dots represent regions where there is no significant difference between the eddy composites and the background environment, using a t-test at the 5% significance level, as described in Section 3.2.3. Note that, compared to Figure 3.4, the colour scales for surface heat flux and total cloud liquid water anomalies have been changed for better visualisation of results between the three regions of the Maritime Continent.

are only significant relative to the background environment where anomalies reach these magnitudes. Similar spatial incoherence is attributed to the TCLW anomalies (Figures 3.6q–t). While negative TCLW anomalies (eddy-averaged means of -0.03 $\mathrm{kg\,m^{-2}}$) are associated with cold eddies (Figures 3.6r and 3.6t), which show coherence with the wind divergence anomalies (Figures 3.6j and 3.6l), there is not as strong an association as that seen for example, in the Kuroshio Extension and the South China Sea.

While eddy-averaged rain anomalies are greater than those in the South China Sea, responses in the SETIO show little direct association with the SST anomaly, contrasting the other variables (Figures 3.6u–x). Centers of positive and negative sign, significant from the background environment, are dotted around the composites. Only cold cyclonic eddies have a slightly similar response to that observed in the Kuroshio Extension (Figure 3.4).

Region 4: Sulawesi Sea (near-equatorial Maritime Continent)

Absolute SST anomalies associated with eddies in the Sulawesi Sea are similar to those in the SETIO, extending to 1–1.5R (Figure 3.7). Mean eddy-averaged SHF anomalies are weak, with absolute eddy-averaged values ranging between 0.5 and 0.8 $\mathrm{W\,m^{-2}}$ (Figures 3.7a–d). LHF anomalies are around 2–3 times the magnitude of the SHF anomalies (Figures 3.7e–h). While both anomalies are statistically significant, the responses are not as centered over the SST anomaly as in the SETIO, aside from the anticyclonic eddies (Figures 3.7a–b and 3.7e–f). Nevertheless, the eddy-averaged signal is suggestive of heat fluxes coming out of (into) the ocean for warm-core (cold-core) eddies.

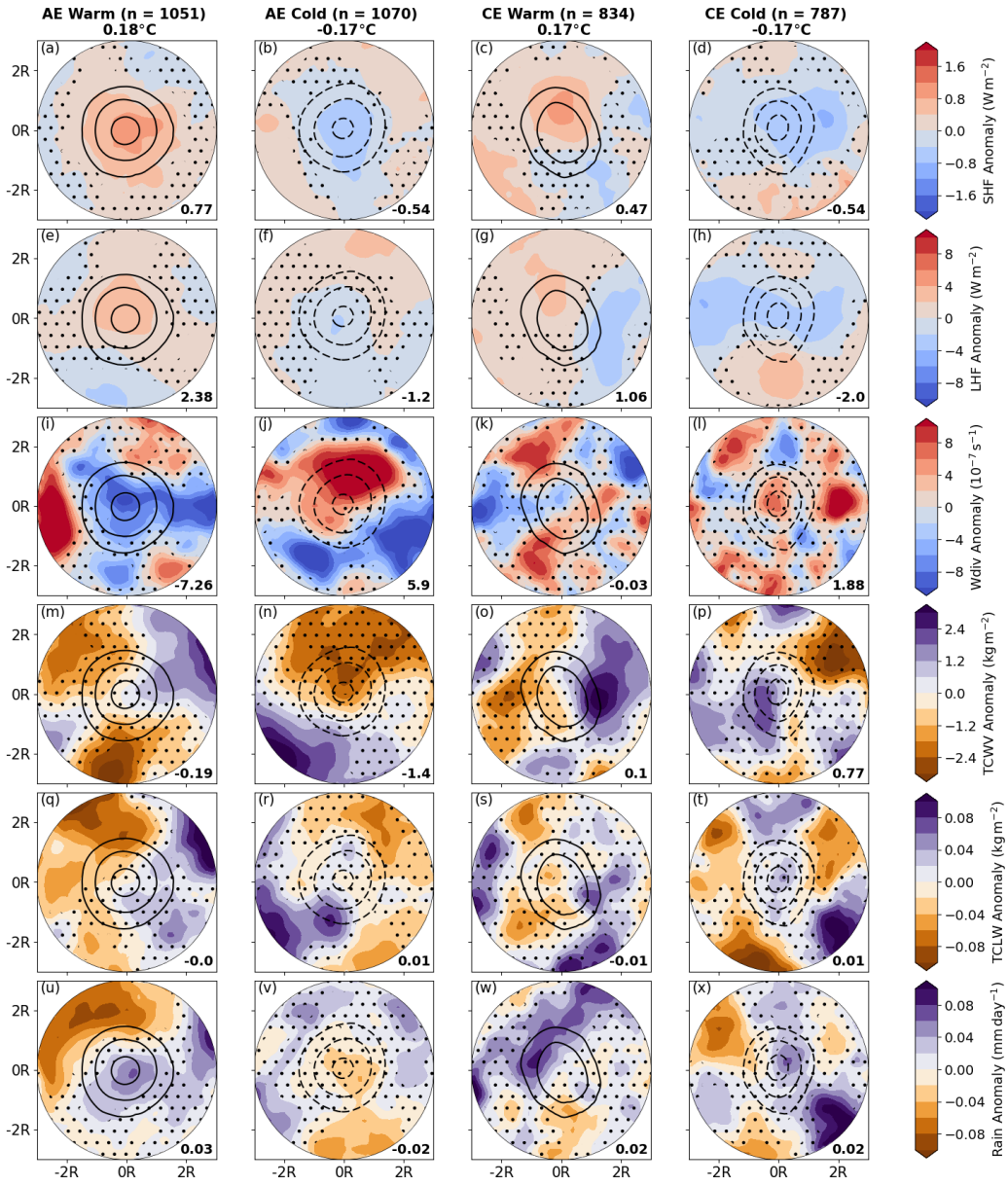

Figure 3.7: (a–d) Eddy composites of surface sensible heat flux anomalies, shown in filled contours, for the four categories of eddies (anticyclonic warm, anticyclonic cold, cyclonic warm, and cyclonic cold, respectively) in the Sulawesi Sea, plotted up to $3R$ from the centroid. Contours represent sea surface temperature anomalies in increments (reductions) of 0.05°C, starting from 0.1°C (-0.1°C) for warm (cold) eddies. Values of indicate the number of eddies composited within each panel. 'Eddy-averaged' (averaged up to $1R$) anomalies in sea surface temperature are provided next to these. (e–h), (i–l), (m–p), (q–t), and (u–x) are the same as (a–d), except filled contours now represent surface latent heat flux, 10 m wind divergence, total column water vapor, total cloud liquid water, and rain anomalies, respectively. The values in the bottom right of each panel represent 'eddy-averaged' values for each property. Dots represent regions where there is no significant difference between the eddy composites and the background environment, using a t-test at the 5% significance level, as described in Section 3.2.3. Note that, compared to Figure 3.4, the colour scales for surface heat flux and total cloud liquid water anomalies have been changed for better visualisation of results between the three regions of the Maritime Continent.

Anomalies in wind divergence show less spatial coherence with the SST anomalies, as in the SETIO (Figures 3.7i–l). Anticyclonic eddies have divergence (convergence) centered slightly over the warm-core (cold-core) eddies, but this is not the case for the cyclonic eddies where the signal is weaker and patchier. Therefore, the association between the eddies, their SST anomalies, and wind divergence is fairly weak, even if individual anomaly centers are significant from the background environment.

As in the SETIO, there is no visible coherence between eddy SST anomalies and anomalies in TCWV (Figures 3.7m–p). There is generally a random distribution of centers of either strongly negative and positive TCWV anomalies of absolute values up to $3\,\mathrm{kg\,m^{-2}}$. Only cold anticyclonic eddies show coherence with existing observations, where anomalies of surface divergence (Figure 3.7j) appear to correspond to negative TCWV anomalies at the center of the eddy (Figure 3.7n). The anomalies vary in statistical significance, and these results are similar to what is observed for TCLW (Figures 3.7q–t), where the signal, while largely paralleling that of TCWV, appears to be patchier.

Rain anomalies also have little correspondence with the eddy SST anomalies (Figures 3.7u–x). While the absolute eddy-averaged values are stronger than the SETIO and South China Sea, at a maximum of $0.03\,\mathrm{mm\,day^{-1}}$, the signal is also patchy, where anomaly centers dotted around the composites remain significant from the background environment. These anomalies can exceed absolute values of $0.1\,\mathrm{mm\,day^{-1}}$. An exception would be the anticyclonic eddies, where slightly positive and negative anomalies are located over the centers of the warm-core and cold-core eddies, respectively (Figures 3.7u and 3.7v). This response, however, remains less robust than that in the Kuroshio Extension (Figure 3.4).

3.4 Discussion

In Section 3.3.1, we identified a belt of short-lived, and low in number, eddies across the equator, while eddies were more prevalent and longer-lived at higher latitudes (Figure 3.2). Eddies are much smaller at higher latitudes as expected from the Rossby radius of deformation. However, eddies in the internal seas of the Maritime Continent are also smaller than other near-equatorial regions. The duration and distribution of these eddies had spatial similarity to the peak amplitude of identified eddies. The speed of eddy propagation also showed latitudinal dependency. These results were even more apparent when analysing the eddy characteristics through regional distributions and means (Figure 3.3).

The properties and distribution patterns of eddies we show here agree with previous studies, including those for the Kuroshio Extension and extratropics (e.g. Chelton et al., 2011; Cheng et al., 2014) and across the Maritime Continent (e.g. Hao et al., 2021; Ismail et al., 2021; Wang et al., 2021). Propagation speed has been noted to decrease with latitude, with speeds similar to those of Rossby waves closer to the tropics (Ni et al., 2020; Chen et al., 2022). Geostrophic balance and associated steady-state assumptions break down towards the Equator, meaning tendencies in near-surface currents are no-longer negligible, leading to more transient and faster-propagating eddies. Such faster propagation speed at lower latitudes may make it harder to detect eddies, leading to a visibly eddy-poor tropics (Fu et al., 2010). Chelton et al. (2007), on the other hand, suggest that most of the energy propagation in the tropics is presented as Rossby waves instead of mesoscale ocean eddies. In the Maritime Continent, however, the fewer number of eddies in many of the internal basins is largely due to shallow bathymetry, preventing the existence of mesoscale ocean eddies in the

first instance.

It is important to highlight that data resolution may be a barrier in fully characterising eddies within the internal seas of the Maritime Continent, due to complex regional geography, which may not be fully resolved with the employed data set. Nonetheless, the employed SSH data set, widely used in studies at the mesoscale, remains the highest horizontal resolution data available for such an extensive time period of analysis.

The Kuroshio Extension is shown to have eddy-averaged absolute SST anomalies of around 0.6°C (Figure 3.4). These SST anomalies have strong spatial correspondence with surface heat fluxes (absolute values of around $10\,\mathrm{W\,m^{-2}}$ and $20\,\mathrm{W\,m^{-2}}$ for SHF and LHF, respectively) and wind divergence. These results are statistically significant relative to the background environment. Patterns in wind divergence anomalies in the Kuroshio Extension could favor either the pressure adjustment mechanism (Lindzen and Nigam, 1987) or the vertical mixing mechanism (Wallace et al., 1989), as anomalies in divergence are centered dominantly over the eddy or just downstream.

We also observe significant TCWV and TCLW anomalies, which correspond roughly to the spatial signature in wind divergence. Spatially coherent rain anomalies averaging to absolute values of around $0.05\,\mathrm{mm\,day^{-1}}$ are of similar magnitude to that observed in previously cited literature (e.g. Ma et al., 2015, 2016). Given our results for the Kuroshio Extension are consistent with the literature, there is confidence in applying this methodology to the remaining areas.

The statistical significance and magnitude of anomalies vary in the Maritime Continent, however. Eddies in the South China Sea exhibit absolute eddy-averaged SST anomalies of nearly 0.25°C, and anomalies of around $2\,\mathrm{W\,m^{-2}}$ and $10\,\mathrm{W\,m^{-2}}$ for SHF

and LHF, respectively, statistically significant relative to the background environment (Figure 3.5). Similarly, significant wind divergence anomalies just downstream of the eddies were observed. Eddy-averaged anomalies in TCWV and TCLW are similar to the Kuroshio Extension. Rain anomalies, while being of the correct sign over the eddy itself, are near-zero. These results are consistent with that of Liu, Li, Chen, Fang and Li (2018), where a potential response in column water vapor is observed, but not so strongly in precipitation.

The other two regions of the Maritime Continent - the SETIO (Figure 3.6) and Sulawesi Sea (Figure 3.7) - show weaker SST anomalies (just over 0.15°C), along with weaker absolute eddy-averaged SHF (0.5–1 $\mathrm{W\,m^{-2}}$) and LHF anomalies (3–4.5 $\mathrm{W\,m^{-2}}$ and 1–2.5 $\mathrm{W\,m^{-2}}$ for the two regions, respectively). Wind divergence anomalies differ between the SETIO and Sulawesi Sea eddies, with a signal over and downstream of the eddies in the SETIO, but a slightly less robust response in the Sulawesi Sea. All anomalies remain statistically significant relative to the background environment. However, TCWV, TCLW, and rain anomalies are also fairly patchy in each region. No coherent signal can be directly attributed to the eddies, even though the anomaly centers themselves are of great magnitude, which could potentially be due to the lower number of eddies within the composites. The observed anomalies are, largely, statistically insignificant relative to the background environment.

These results suggest a potential weakening of the spatial coherence between the eddy-associated SST anomalies and relevant analysed variables as one tends toward the lower latitudes. This weakened response, particularly in the cloud and rain field, supports the work of Aguedjou et al. (2023), who found similarly weak anomalies in precipitation associated with mesoscale ocean eddies in the tropical Atlantic Ocean.

We could attribute our results to the background SST characteristics of each region. As ocean currents at higher latitudes produce more pronounced SST gradients, the mesoscale ocean eddies formed have greater associated SST anomalies. In addition, as the Coriolis parameter tends to zero towards the Equator, thermal wind balance explains reductions in SSH amplitude and the intensity of SST anomalies. These greater SST anomalies at higher-latitudes may induce a more robust, and statistically significant, response in the analysed variables in the extratropics compared to regions such as the Maritime Continent (Liu, Li, Chen, Fang and Li, 2018).

Even though we identify a robust signal in the SST and surface heat flux anomalies in the Maritime Continent, these anomalies may be too weak to affect the atmosphere instantaneously or on shorter timescales in a similar vein as seen for the extratropics. In a numerical modelling study, Skyllingstad et al. (2019) had to artificially input a 3 K SST anomaly 500 km in width, relative to an ocean of homogeneous background SST, for there to be a response in the formation of tropical convection. These anomalies are much greater than the SST anomalies and sizes associated with eddies in the Maritime Continent. We also observed faster propagation rates of eddies within the Maritime Continent (Figures 3.3g and 3.3h), which may additionally reduce the likelihood of an instantaneous atmospheric response. However, preliminary analysis conducted through recategorisation of eddies in the Maritime Continent by the propagation rate did not show sufficient evidence to support this hypothesis (not shown).

Several studies within and near the Kuroshio Extension identified that impacts of eddies on the atmospheric boundary layer, such as through vertical velocity and wind, may only reach 800–900 hPa (e.g. Ma et al., 2016; Sun, Li, Yan, Zhou and Zhou, 2022). Our results suggest moistening (drying) of the column over warm-core

(cold-core) eddies in the Kuroshio Extension and South China Sea, with potential increases (reductions) in cloud primarily in the Kuroshio Extension. The magnitude of the anomalies however suggest a relationship with shallow convection, compared to deeper convection. Rainfall anomalies associated with extratropical eddies have been observed to exceed $0.2\,\mathrm{mm\,day^{-1}}$ which, in regions such as the Southern Ocean, explain only a small portion of the variance (Frenger et al., 2013).

Initial analysis (not shown) found minimal vertical response in the atmosphere to eddies in the Maritime Continent, beyond the surface anomalies as shown in Figures 3.5 to 3.7. While it is therefore unlikely for eddies to affect rainfall patterns significantly in tropical regions such as the Maritime Continent, which experience much more rainfall all-year round, the magnitude of anomalies in rain and moisture even in the extratropics are still very small, as shown here. Therefore, it should be acknowledged that though anomalies appear more significant toward the extratropics, there remains a generally weak instantaneous response beyond the lowermost portion of the atmosphere.

While Aguedjou et al. (2023) find a generally minimal atmospheric response to mesoscale ocean eddies across the tropical Atlantic and Roman-Stork et al. (2021) note a weak response in the Bay of Bengal, Gulakaram et al. (2018) find a potential lag between eddies at peak amplitude and anomalies in the Bay of Bengal. However, in follow-up work (Gulakaram et al., 2023), relationships are suggested to be blurred by feedbacks on intraseasonal timescales. Souza et al. (2021) conducted case study analyses in the Brazil-Malvinas Confluence, identifying a clear response to eddies only when transient atmospheric systems were stable, removing potential intraseasonal variability. The importance of intraseasonal variability in modulating the atmospheric

response to eddies was also highlighted by Roman-Stork et al. (2021). The signal we observe in the Maritime Continent may also be weaker than in the extratropics as the precipitation is more convective, sporadic, and variable in nature, which may not be well resolved in the data used. Therefore, a coherent and statistically significant response, especially one that is instantaneous, in the Maritime Continent, is unlikely being a region with such high amplitude atmospheric variability, influenced by many processes particularly at intraseasonal scales.

3.5 Conclusion

In this study, we have used satellite altimetry data to detect and track eddies over a large domain including the Maritime Continent. We observe reductions in the number, mean peak amplitude, and duration of eddies, and increases in the propagation rate, at lower latitudes compared to higher latitudes, consistent with other studies. Eddy hotspots, compared to the surrounding environment, were observed particularly where prominent currents interact, such as in the Kuroshio Extension and at the inflow of the Indonesian Throughflow.

By constructing normalised eddy composites, we identify the strongest eddy-associated sea surface temperature anomalies in the Kuroshio Extension, used as an extratropical case study. Surface heat flux and wind divergence anomalies in the Kuroshio Extension are also the greatest in magnitude, and significantly different from the background environment. Column water vapor, cloud liquid water, and rain anomalies associated with the eddies are spatially coherent with sea surface temperature anomalies, and statistically significant relative to the background environment,

though are small in value.

However, anomalies associated with eddies in the Maritime Continent weaken closer to the equator. In the South China Sea, southeast tropical Indian Ocean, and Sulawesi Sea, eddies still show significant surface heat flux and wind divergence anomalies, spatially coherent with the sea surface temperature anomaly. For the South China Sea, there are also observable responses in column water vapor and cloud liquid water, but no detectable rain anomaly. Neither the southeast tropical Indian Ocean or Sulawesi Sea show distinct or coherent responses in these three anomalies. All three regions, in general, show atmospheric response, which lean toward statistical insignificance when compared to the background environmental variability.

These results suggest that latitudinal changes to the eddy-averaged sea surface temperature anomaly, dependent on the background sea surface temperature, are driving the responses noted. With the resultant enhanced heat flux and wind divergence anomalies associated with eddies in the extratropics, eddies are more likely to influence instability in the extratropical atmospheric boundary layer through modifications of column moisture, compared to tropical regions such as the Maritime Continent. These instabilities could alter the likelihood of cloud formation and rainfall. However, it should be noted that while the signal within the Maritime Continent may not be as strongly captured due to the nature of convection in terms of spatiotemporal variability, the faster propagation rates of eddies likely restrict an instantaneous response in the atmosphere from being as visible, which remains an open hypothesis to explore.

While the usage of a longer time period of analysis than existing studies allows compositing of a larger number of eddies, this analysis is limited to the instantaneous

atmospheric response. In reality, part of the response may be associated with spatial variability and potential lead-lag relationships. To better realise the finer details regarding air-sea interactions associated with mesoscale ocean eddies, case studies using observational data and analysis of high-resolution model simulations would be required.

Future studies could consider the influence that other processes, which contribute to atmospheric variability in the Maritime Continent, have on the observed response to the eddies. The extent to which, for example, transient weather systems, larger-scale modes of variability, and the background environment in general affect composited responses, as shown in studies focusing on other regions, could then be highlighted and better understood. Evaluating the influence of these eddies on particular levels in the lower troposphere would give insight into the vertical structure of the atmospheric response, beyond the surface level. Such analysis would need data sets of higher vertical resolution, constrained in particular to the lowermost levels. Additionally, it would be worth assessing whether responses exist at finer scales, using high-resolution atmospheric simulations imposed with a background ocean containing eddies.

Nevertheless, our work has filled a gap in the literature related to the atmospheric response to eddies in the Maritime Continent. This study has highlighted a distinct difference between the Maritime Continent and the extratropics in both the characteristics of mesoscale ocean eddies and their associated interactions with the atmosphere. Our results will contribute to better understanding the role of the ocean in influencing the stability of the atmosphere in the Maritime Continent, particularly at the mesoscale, while also informing the degree of importance that representing and

resolving ocean eddies in existing weather and climate models holds.

Chapter 4

The atmospheric dynamics associated with two Sumatra squalls over the western Maritime Continent

Submitted to *Journal of Geophysical Research: Atmospheres*.

Abstract

A Sumatra squall is a squall line which propagates roughly eastward towards Peninsular Malaysia and Singapore. These storms are characterised by intense rainfall and wind gusts, causing infrastructural damage, flooding, and economic losses, though limited knowledge exists of Sumatra squall dynamics. We use high-resolution convective-permitting model simulations to analyse mechanisms specific to the initiation, propagation, intensification, and dissipation of two Sumatra squalls. Convection initiation over the mountains of Sumatra is driven by diurnal forcing, a feature associated with convection development over islands across the Maritime Continent. Other characteristics associated with these Sumatra squalls share similarities with squall lines observed elsewhere. Interactions between large-scale environmental vertical wind shear, lower-tropospheric wind shear ahead of the leading edge, density currents and low-to-mid-tropospheric southwesterlies - associated with an equatorial Kelvin wave - assist in Sumatra squall propagation and intensification. These processes modify moisture flux convergence at the leading edge which, when reduced, due to weakened interaction between lower-tropospheric shear and density currents, leads to Sumatra squall dissipation. Strengthened southwesterlies throughout the life cycle of the second Sumatra squall advect convection and associated moisture perturbations over the Indian Ocean towards Sumatra, enhancing convective development initially driven by the diurnal cycle. The equatorial Kelvin wave preconditions the environment by inducing convergence, and enhances storm propagation by strengthening the southwesterlies. This work emphasises how mesoscale dynamics, such as through diurnal variability, interact with planetary-scale processes such as equatorial waves, which can then influence squall line evolution, going towards better predictability, mod-

elling, and forecasting of these high-impact weather systems.

4.1 Introduction

Mesoscale convective systems (MCSs) consist of aggregated deep convective clouds, and grow up to 100s of kilometres in horizontal scale, with the deepest centres of convection up to 100 km in width (Houze, 2004). While precipitation is concentrated in these convective cores, rainfall is also associated with a stratiform cloud, attributed with lighter precipitation, 100s of kilometres in length (Houze, 2018). Studies have shown that the heavy rainfall from MCSs can influence upper-level and global circulation, and therefore the overall energy, radiative and hydrological system (e.g. Schumacher and Houze, 2003; Houze, 2004, 2018).

Across the mid-latitudes and subtropics, such as in North America and Northern Africa respectively, MCSs rely on the interaction between cold and dry, and warm and moist, air masses along fronts, with low-level jets supporting the development of convergence and lift at the mesoscale through advection of heat and moisture (e.g. Maddox, 1983; Bluestein and Jain, 1985; Rowell and Milford, 1993). However, in tropical environments such as over West and Central Africa, where environments are warmer and moister, synoptic-scale waves hold more importance in modulating the low-level convergence for MCS generation (e.g. Fink and Reiner, 2003).

More than 50% of the total annual tropical rainfall is attributed to MCSs (e.g. Nesbitt et al., 2006; Feng et al., 2021). Longer-lasting MCSs (duration of >12 hours) account for a greater proportion (around 75%) of this rainfall (Roca et al., 2014). Over the Maritime Continent in Southeast Asia, Crook et al. (2024) showed that longer-lived

MCSs, as defined in Roca et al. (2014) and Roca and Fiolleau (2020), are responsible for a large amount (40-75%) of the precipitation from November to April, and contribute strongly to extreme rainfall days. MCS characteristics over the Maritime Continent are also influenced by processes such as the Madden-Julian Oscillation (MJO) and equatorial waves (Yuan and Houze, 2013; Crook et al., 2024).

One type of MCS observed over the western Maritime Continent (Figure 4.1) is a Sumatra squall, an example of a tropical squall line. This technical term was developed by Singaporean and Malaysian weather forecasters for squall lines which propagate roughly eastward from Sumatra towards Singapore and Peninsular Malaysia, across the Malacca Strait. Sumatra squalls are particularly impactful during the early morning, primarily in the intermonsoon months (boreal spring and autumn) and during the southwest monsoon in boreal summer (Lo and Orton, 2016). These squall lines are characterised by intense precipitation and extreme winds, leading to flooding, damage to infrastructure, disruption to both road-based and maritime traffic, and storm surges.

Chan et al. (2019) showed that characteristics of a Sumatra squall case study resembled that of 'classical' squall line structure (e.g. Redelsperger and Lafore, 1988; Rotunno et al., 1988; Weisman et al., 1988; Houze, 2004; Alfaro, 2017; Houze, 2018). For example, they are characterised by convective cell generation at the leading edge, with the development of an ascending front-to-rear flow and a rear inflow jet, embedded within a larger-scale sheared environment.

Various mechanisms have been proposed and identified to explain the initiation of Sumatra squalls. The first, and most common, hypothesis involves the diurnal cycle, one of the fundamental modes of variability across the region, as well as the entire

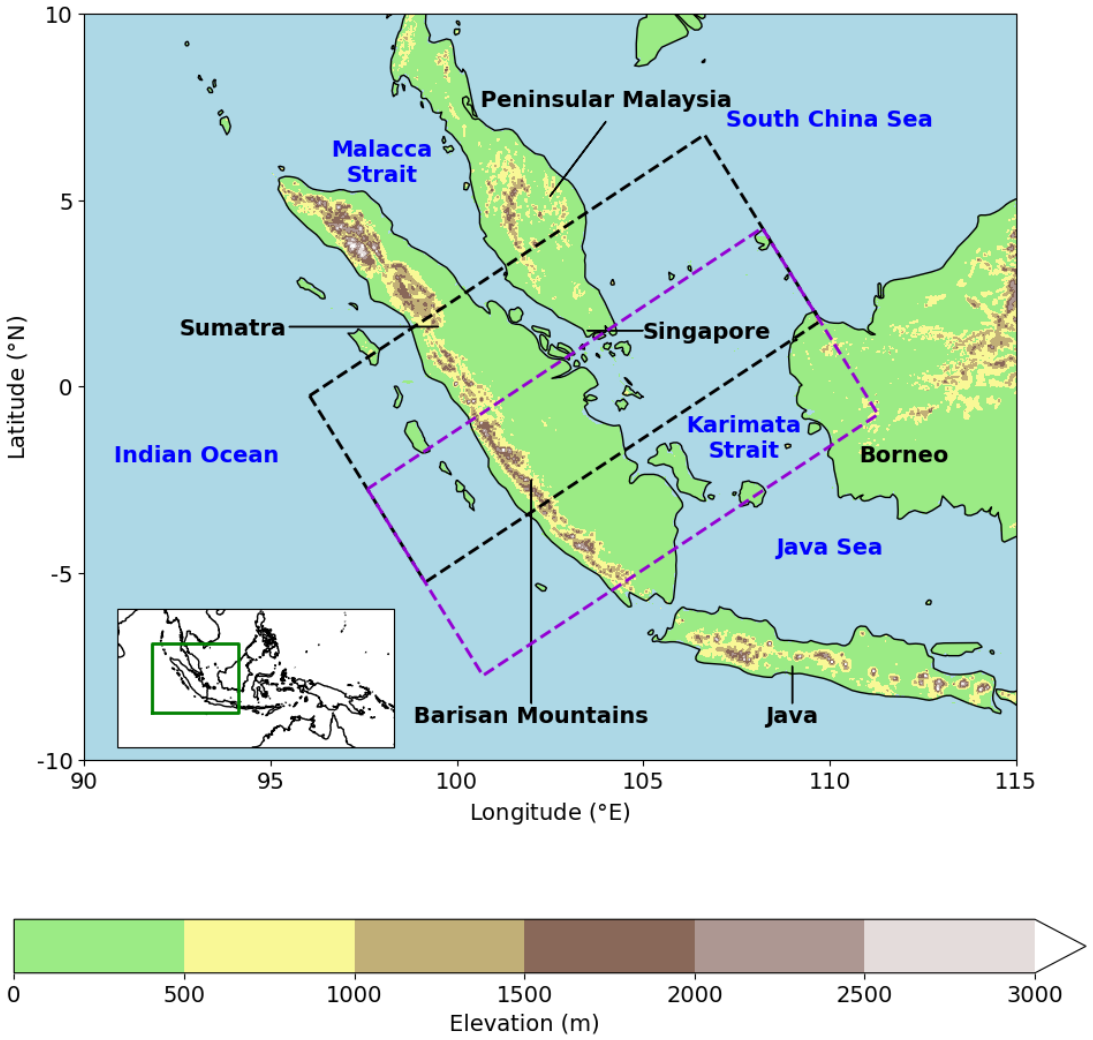

Figure 4.1: A map of the study region (as zoomed in from the green box within the figure inset showing the entirety of Southeast Asia). The black dashed box represents the region which is averaged over in the southwest-northeast direction (parallel to the Sumatran coastline), for analysis of the first Sumatra squall case study in the SINGV model data, described in Section 4.2.3. The purple dashed box represents the box over which a transect is derived for the second Sumatra squall case study. Filled contours represent elevation from GLOBE (Hastings and Dunbar, 1999).

Tropics (e.g. Yang and Slingo, 2001; Qian, 2008). Daytime insolation sets up a land-sea temperature contrast, as the land has a lower heat capacity. A pressure gradient is produced, causing sea breeze convergence onto the land. Coupled with upslope mountain winds, deep convection and precipitation form inland into the afternoon and evening. These processes have been well-studied for MCSs which propagate in the opposite direction towards the Indian Ocean, as well as convection propagating offshore from other islands across the Maritime Continent (e.g. Hassim et al., 2016; Peatman et al., 2021; Natoli and Maloney, 2023; Peatman et al., 2023).

Other hypotheses suggest that cloud formation late at night over the Malacca Strait may be important for Sumatra squall initiation (Yi and Lim, 2007). This process is driven by boundary layer convergence between the katabatic winds and land breezes from eastern Sumatra and Peninsular Malaysia. Convergence, driven by nocturnal cooling of the land, can lead to the sustaining and intensification of convection (Galvin, 2009; Fujita et al., 2010). These processes cause enhanced convection over Peninsular Malaysia (Hai et al., 2017; Nor et al., 2020).

For the same analysed case study, Chan et al. (2019) showed that propagation of a Sumatra squall is facilitated predominantly by westerly winds in the low-to-mid-troposphere. Ambient wind is a known feature in steering convection which develops initially over islands of the Maritime Continent (e.g. Sakurai et al., 2005; Yanase et al., 2017; Natoli and Maloney, 2023). Linked to the diurnal cycle, further propagation can be favoured by the formation of land breezes and downslope mountain winds overnight. Development of density currents, in addition to cold pools originating from the convection itself, may also be important (e.g. Yulihastin et al., 2021; Peatman et al., 2023). These processes, coupled with the local wind and variations in low-

level humidity, can modulate lower-tropospheric moist convergence, key for convective intensification (e.g. Fakaruddin et al., 2022; Peatman et al., 2025).

A recent composite analysis study by Nguyen et al. (2025), using a radar-derived database of Sumatra squalls, found results supporting the hypothesis of these squall lines originating from both the Barisan mountains of Sumatra and the Malacca Strait. Noting a greater occurrence of these MCSs under La Niña conditions, as well as MJO conditions that set up westerly winds and eastward storm propagation, Nguyen et al. (2025) also highlighted the importance of convectively coupled equatorial waves. Interactions with equatorial waves have been shown to intensify rainfall and potentially influence convection propagation across the region in previous studies (e.g. Ferrett et al., 2020; Peatman et al., 2021; Senior et al., 2023).

Though regional models capture the broad rainfall patterns associated with Sumatra squalls (Dipankar et al., 2020; Sun et al., 2020), and aforementioned studies provide insight into some of the characteristics associated with these squall lines, knowledge of key processes over a variety of scales is limited. While current understanding shows parallels to similar MCSs propagating away from Sumatra towards the Indian Ocean (e.g. Mori et al., 2004; Yanase et al., 2017; Yokoi et al., 2017; Bai et al., 2021; Peatman et al., 2023), further outlining of mechanisms influencing the initiation and propagation, as well as dissipation, of Sumatra squalls is needed. Lo and Orton (2016) and Chan et al. (2019) both suggest that better understanding is needed of the role of factors such as the background vertical wind shear, thermodynamic profile, and synoptic circulations on Sumatra squalls themselves.

Process understanding related to the drivers of Sumatra squalls ultimately feeds back onto our modelling, forecasting and numerical weather prediction (NWP) capa-

bilities across the Maritime Continent, which are greater for larger-scale variability on seasonal-to-subseasonal timescales, and lower for finer-scale and more transient phenomena (e.g. Ferrett et al., 2021). This addition to our knowledge is therefore necessary to meet the needs of both local communities and stakeholders, due to infrastructural damage and financial losses which are a result of extreme rainfall and winds associated with Sumatra squalls.

In this study, we provide further insight into the multi-scale dynamics associated with Sumatra squalls, by conducting case study analysis using high-resolution convective-permitting simulations. The ability of these simulations in representing Sumatra squalls, compared to satellite observations, is first analysed. We then identify the role of the vertical wind and moisture fields, shear, and density currents in modifying Sumatra squall properties across the various stages of the MCS life cycle. Interactions between the large and synoptic scales in influencing Sumatra squall characteristics are explored, which have not been investigated so far on a case study basis. Through this, we can also determine any similarities or differences relative to the knowledge gained from other studies across the Maritime Continent, and elsewhere across the globe.

4.2 Methodology

4.2.1 Case description

Our analysis focuses on two Sumatra squall case studies. The first of these propagated over Singapore in the late morning on 26 April 2019. The Meteorological Service Singapore (MSS) stated in a report that a daily total rainfall of 118.7 mm at Changi

Airport was recorded, the highest amount in a day in April 2019 (MSS, 2019). The following day, a second Sumatra squall developed, propagating towards the Karimata Strait and Borneo. Reports from Badan Meteorologi, Klimatologi, dan Geofisika (BMKG) in Indonesia reported torrential rains, flooding, and landslides in Bengkulu, Sumatra, with daily rainfall up to over 200 mm on 27 April 2019 (Paski et al., 2021).

4.2.2 Data

Rainfall data was derived from Integrated Multi-Satellite Retrievals for Global Precipitation Measurement (IMERG) Version 06 (Huffman et al., 2020). IMERG intercalibrates data from rain gauges with estimates obtained from satellite infrared and microwave sensors. IMERG data is available at half-hourly temporal resolution, and at a horizontal grid spacing of $0.1° \times 0.1°$.

Cloud top brightness temperature from the Himawari-8/9 satellites is used for evaluating convective intensity (Bessho et al., 2016). Here, we use band 13 which detects infrared radiation with a wavelength of $10.4\,\mu$m and spatial resolution of 2 km. Both observational datasets are used for the dates of the case studies analysed.

To determine the state of the MJO at the time of the case study, we use daily real-time multivariate MJO series 1 and 2 (RMM1 amd RMM2 respectively) data (Wheeler and Hendon, 2004). Outlined in Ferrett et al. (2020) and Crook et al. (2024) and fully described in Yang et al. (2023), a dataset of equatorial waves identified using the methodology in Yang et al. (2003) was also used. This method uses European Centre for Medium-Range Weather Forecasts (ECMWF) Reanalysis v5 (ERA5) data Hersbach et al. (2020), available at a horizontal grid spacing of $0.25° \times 0.25°$. ERA5 wind anomaly data is regridded to $1° \times 1°$ horizontal spacing, and filtered for variability

within the period of 2-30 days and zonal wavenumbers of 2-40. Data is then spatially projected onto parabolic cylinder functions, representing theoretical horizontal wave-mode structures, and associated wind fields, for equatorial Kelvin, Rossby (n=1 and n=2) and Westward-moving Mixed Rossby-Gravity (WMRG) waves (Gill, 1980; Yang et al., 2003).

4.2.3 Model simulations

We use the Singapore NWP model known as SINGV (e.g. Huang et al., 2019; Dipankar et al., 2020), a high-resolution convective-permitting model, which has been used previously for applications in data assimilation, ensemble prediction, and urban modelling. SINGV has a horizontal grid spacing of 1.5 km $\times$ 1.5 km, with the atmosphere represented using the Met Office Unified Model (MetUM) with Regional Atmosphere 2 (RA2T) physics (Bush et al., 2023), a fully non-hydrostatic model, forced with initial and lateral boundary conditions from ERA5 every 3 hours. SINGV operates over 80 terrain-following vertical levels up to a model top of 38.5 km, with output used in this work provided on 16 pressure levels between 100-1000 hPa.

The model employs a Prognostic Cloud fraction and Prognostic Condensate (PC2) scheme Wilson et al. (2008) to reduce the occurrence of spurious convection with high rainfall rates. The boundary layer parameterisation follows that of Boutle et al. (2014), combining the one-dimensional scheme of Lock et al. (2000) and the three-dimensional Smagorinsky-Lilly scheme (Lilly, 1962). Cloud microphysics and radiative processes are represented in the schemes of Wilson and Ballard (1999) and Edwards and Slingo (1996) respectively. SINGV also integrates the Joint UK Land Environment Simulator (JULES) for land surface modelling (Best et al., 2011).

Uncoupled (atmosphere-only) versions of the SINGV simulations were run. Two simulations were initialised on 24 and 25 April 2019 (0000 UTC) and run until 26 April and 27 April 2019 (2300 UTC) respectively, to cover the life cycles of each Sumatra squall. Modelled cloud top brightness temperature was calculated from modelled top-of-atmopshere outgoing longwave fluxes using the empirical conversions of Yang and Slingo (2001). Additional simulations for each case study were run at different initialisation times, though no significant differences were noted between the results of the original and additional squall line simulations (not shown).

4.3 Results

4.3.1 Synoptic overview: observations

On 25 April 2019 at 1600 LT (UTC+7, representing Sumatran local time), convection and rainfall associated with the first Sumatra squall begin to develop along the Barisan mountains over Sumatra (Figure 4.2a). Convection continues to intensify and organise into the evening and nighttime, primarily over southern and central Sumatra, as it propagates eastwards (Figures 4.2b-c). By the early morning, convection has strengthened and merged to form a distinct, continuous line of convection oriented parallel to the coastline (Figures 4.2d-e). This Sumatra squall is aligned along the Malacca Strait in the morning, briefly intensifying as it approaches and propagates over Singapore and southern Peninsular Malaysia (Figures 4.2f-g). After the Sumatra squall passes over the land, a period of reintensification begins over the South China Sea (Figures 4.2h-i), and by 1900-2200 LT, the first Sumatra squall has dissipated (Figures 4.2j-k).

At 0400 LT on 26 April, extensive convection is observed to the southwest of Sumatra (Figure 4.2e). This northwest-southeast oriented band of rainfall persists through the late morning and early afternoon, while propagating towards the western coast of Sumatra (Figure 4.2f-h). By 1600 LT, convection leading to development of the second Sumatra squall has aligned itself along the entirety of the Barisan mountains (Figure 4.2i). Convection then propagates eastward, reaching eastern Sumatra by nighttime, at which time the entirety of Sumatra is covered in extensive cloud and scattered, intense rainfall (Figure 4.2j-k). This Sumatra squall intensifies briefly as it enters the Karimata Strait to the east of Sumatra, and persists through the nighttime, to the morning of 27 April (Figures 4.2l-n). The second Sumatra squall then continues to propagate outside of the domain of analysis towards Borneo (Figures 4.2o-p).

The Sumatra squalls in this case study took place during Phase 3 of the MJO (Figure 4.3a). During this phase, the convectively active envelope of the MJO is located between the central Indian Ocean and the western Maritime Continent. The two Sumatra squalls are represented by the precipitation in the Hovmöllers in Figures 4.3b-e. Both Sumatra squalls are aligned with and therefore roughly propagate at the speed of the convergent phase of a Kelvin wave (Figure 4.3b). Positive relative vorticity is induced by a passing WMRG wave at the time of the events (Figure 4.3c). As each Sumatra squall intensifies and propagates eastward, a Rossby (n=1) wave is in its convergent phase while also inducing positive relative vorticity (Figure 4.3d). Minimal Rossby (n=2) wave activity is observed - very weak convergence and relative vorticity is induced by this wave during the initial stages of Sumatra squall development (Figure 4.3e).

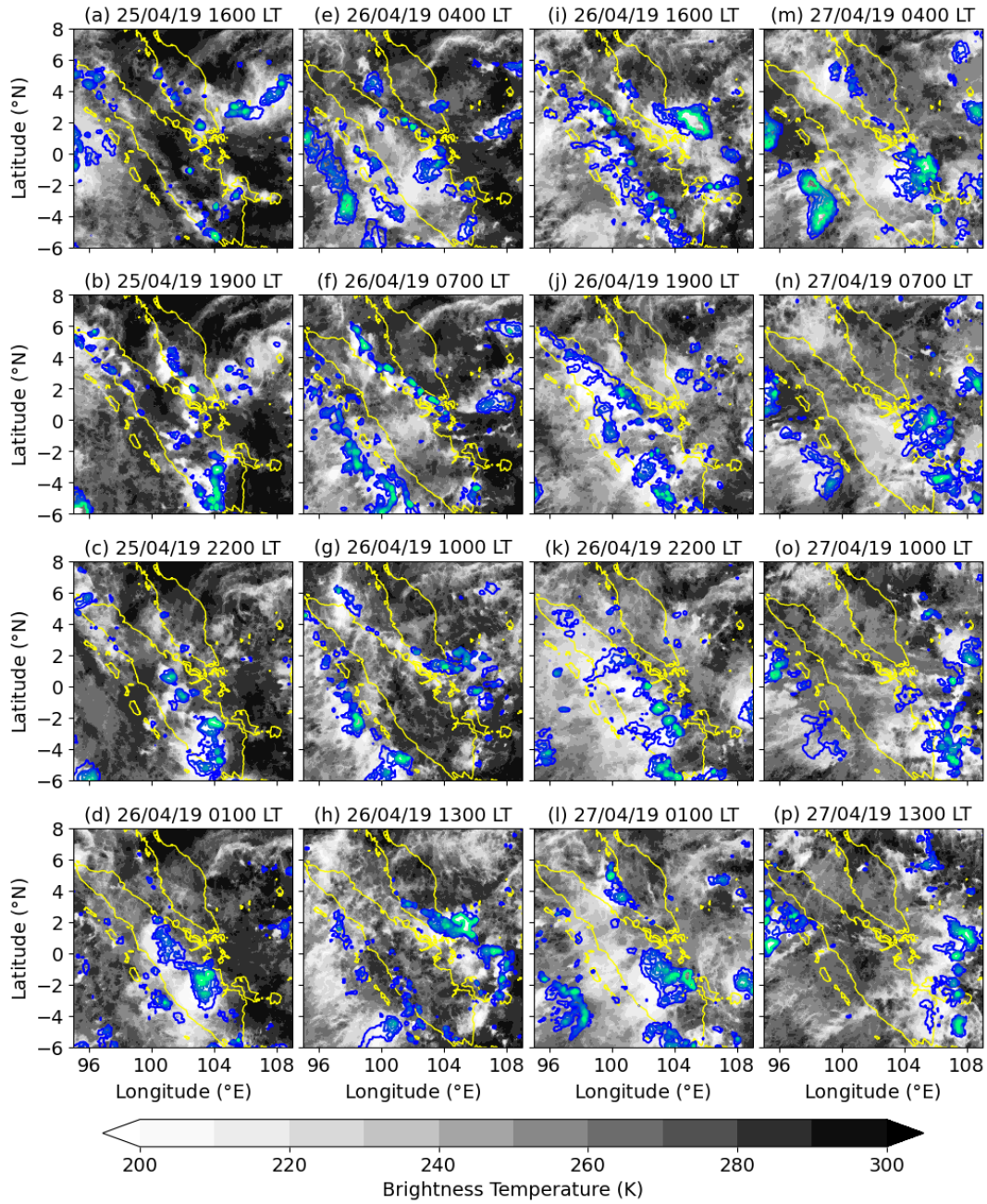

Figure 4.2: Himawari brightness temperature (shaded contours) and IMERG rainfall (contours, shown in increments of 2.5 mm hr^{-1}, from 2.5-20 mm hr^{-1}, from blues to bright greens) for the analysed pair of case studies between 25 April 2019 at 1600 LT, to 27 April 2019 at 1300 LT. Panels are plotted in intervals of 3 hours. Coastlines are shown in yellow.

For the duration of these case studies, Kelvin waves are most important in modulating the lower-tropospheric convergence, while WMRG waves induce positive relative vorticity. The Rossby waves induce convergence and positive relative vorticity at different stages of the Sumatra squall lifetimes, rather than the entire duration.

4.3.2 Synoptic overview: model comparison to observations

The next step of this study is to assess how the SINGV model performs in representing these Sumatra squalls. Modelled rainfall and cloud cover associated with the environment at the time of two Sumatra squall studies are shown in Figures 4.4 and 4.5 respectively. Comparisons to observations are shown in Hovmöller plots in Figure 4.6.

We focus firstly on the simulation initialised on 24 April 2019 run for the first Sumatra squall. At 1600 LT on 25 April, convection and rainfall forms along the Barisan mountains in the model (Figure 4.4a). Convection located over the central-southern portion of the Barisan mountains merges and propagates eastward over central and eastern Sumatra overnight and into the early morning of 26 April (Figures 4.4b-c). The most intense rainfall is concentrated at the leading edge of the region of developed deep convection. Convection then aligns itself along the Malacca Strait and eastern coast of Sumatra at 1000 LT (Figures 4.4d). The Sumatra squall then spans more broadly across Peninsular Malaysia, Singapore, and eastern Sumatra in the afternoon, with extensive cloud cover trailing the band of deepest convection and rainfall (Figure 4.4e). The system dissipates in the nighttime over the South China Sea (Figure 4.4f).

Within both observations of the first Sumatra squall (Figure 4.6a) and its model

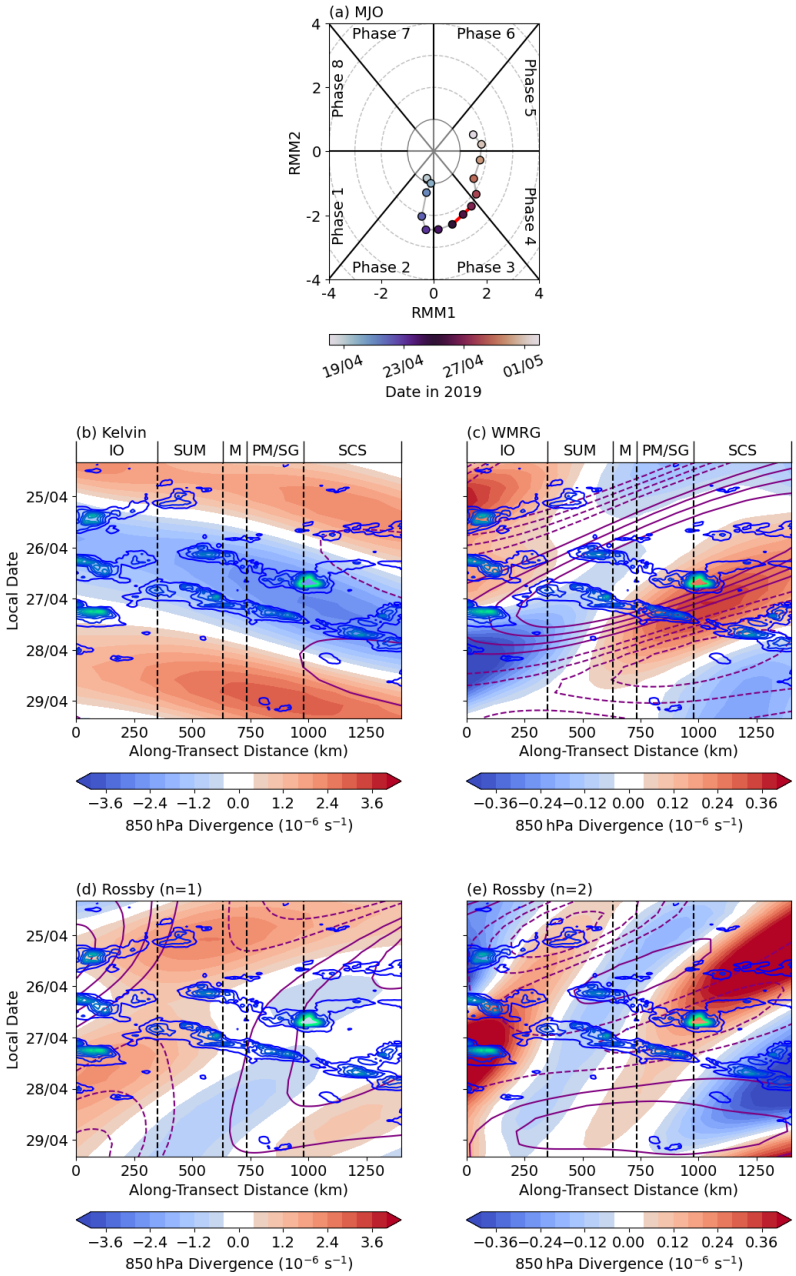

Figure 4.3: (a) Real-time Multivariate MJO (RMM) plot for 18 April-2 May 2019 (filled scatter points, moving in an anticlockwise direction). The red line represents 25-27 April 2019 when the two case study Sumatra squalls were observed. (b) Kelvin wave-attributed 850 hPa divergence, shown in filled contours, from 24 April 2019 0700 to 29 April 2019 0600 LT. Solid purple contours represent positive relative vorticity, and dashed contours negative relative vorticity, associated with the wave, plotted in increments of 0.5 s^{-1}, from -2 s^{-1} to 2 s^{-1}, apart from the zero value. IMERG rainfall is provided in blue to green contours for values from 1-10 mm hr^{-1} in increments of 1 mm hr^{-1}. Variables have been interpolated to and averaged over the transect shown as a dashed black box in Figure 4.1. Key locations are indicated above panels: Indian Ocean (IO), Sumatra (SUM), Malacca Strait (M), Peninsular Malaysia/Singapore (PM/SG), and South China Sea (SCS). (c-e) are as in (b) but for WMRG, Rossby (n=1), and Rossby (n=2) waves. Note that the colour scaling for (b) and (d) are different from (c) and (e) for visual clarity.

simulation (Figure 4.6b), convection initiates in the late afternoon to early evening over the Barisan mountains (approximately 400-450 km along-transect). While intensification over eastern Sumatra occurs at similar times, rainfall is much more intense in SINGV - for example, increases of 2-4 $\mathrm{mm\,hr^{-1}}$ in the model relative to observations are noted for convection initiating over and then propagating from the Barisan mountains, earlier in the afternoon. The cold cloud shield trailing the MCS too appears to be deeper and more extensive. The brief convective reintensification period after propagating over Peninsular Malaysia and Singapore, in observations, is not captured in the model. Though there is a roughly 3 h delay in the lifecycle of the squall line from intensification to dissipation, both Sumatra squall propagation trajectory and rate (approximately 7 $\mathrm{m\,s^{-1}}$) remain fairly consistent between observations and the model.

In the simulation for the second Sumatra squall, a band of convection is oriented northwest-southeast to the west of Sumatra over the Indian Ocean in the morning of 26 April (Figure 4.5a). This convection propagates eastwards towards the Sumatran coastline in the afternoon (Figure 4.5b) through to the evening. At this time, intense rainfall and convection also develops over central to southern Sumatra. Convection intensifies and merges primarily over southern Sumatra, while propagating eastward overnight towards eastern Sumatra (Figure 4.5c). The Sumatra squall forms a distinct line almost parallel to the eastern Sumatra coast as it reaches the Karimata Strait in the early morning on 27 April, where intense rainfall is concentrated at the leading edge of the associated deep convection (Figure 4.5d). At 1000 LT, the Sumatra squall propagates over the Karimata Strait, with a greater extent of convection oriented in the north-south direction (Figure 4.5e). This Sumatra squall maintains intensity

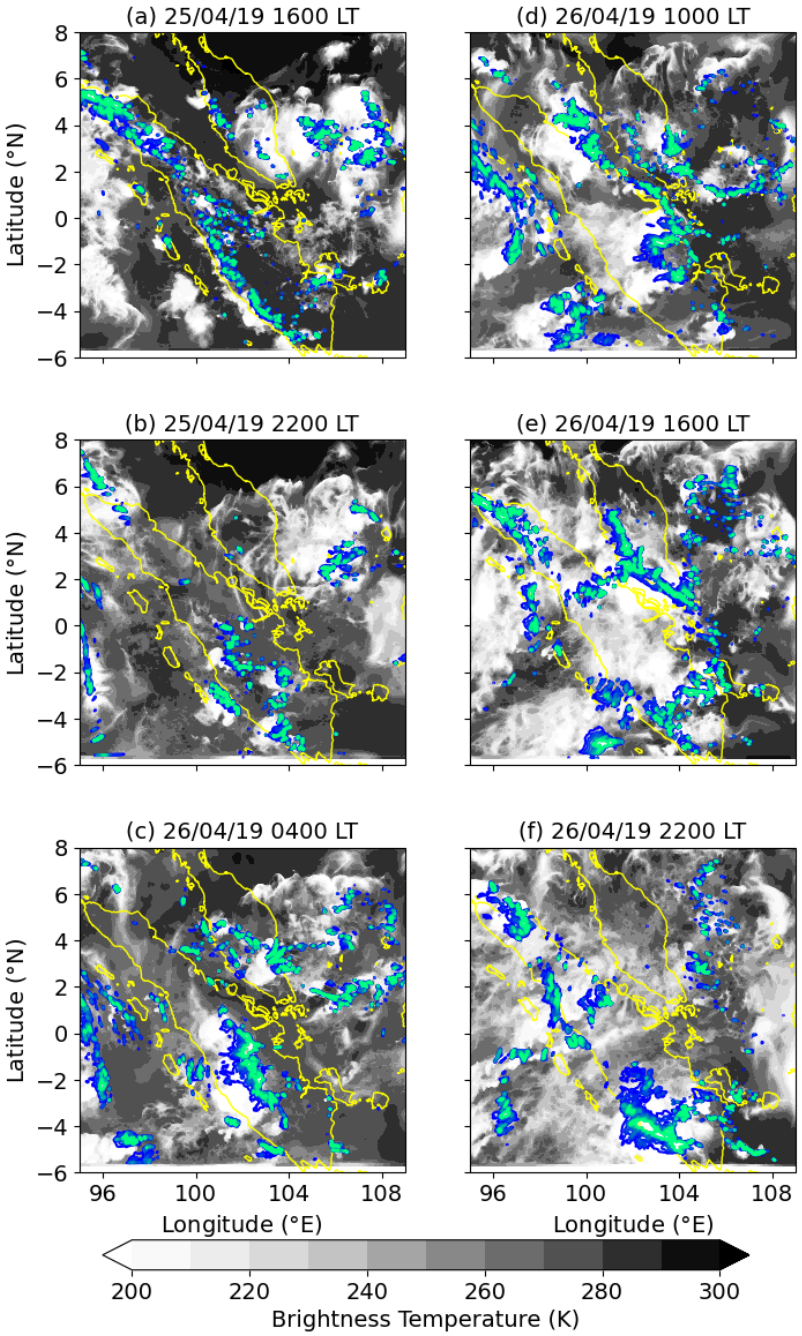

Figure 4.4: Cloud top brightness temperature (filled contours) and precipitation (contours, shown in increments of 2.5 mm hr^{-1}, from 2.5-20 mm hr^{-1}, from blues to bright greens) for the first SINGV simulation initialised on 24 April 2019 0000 UTC, or 0700 LT. Panels are plotted in intervals of 6 hours, from 25 April 2019 1600 LT to 26 April 2019 2200 LT. Coastlines are shown in yellow.

as the region of deepest convection and heavy rainfall propagates eastwards towards Borneo, outside of the domain, in the afternoon, with extensive trailing cloud (Figure 4.5f).

Convection over the Barisan mountains associated with the second Sumatra squall in the early evening is weaker in observations (Figure 4.6c) than in the model (Figure 4.6d), as exhibited by the differences in rainfall intensity. Rainfall is more intense in the model throughout the lifetime of this Sumatra squall, primarily during the initial development phase over the Barisan mountains where rain is at least $2\,\mathrm{mm\,hr^{-1}}$ greater over the transect. Similar to the first case study, the modelled trailing cloud shield is more extensive relative to the region of most intense convection. The model also captures more continuous propagation of convection from the Eastern Indian Ocean towards Sumatra, which precedes further intensification over the mountains. Propagation rates are, however, consistent between both datasets (approximately $9\,\mathrm{m\,s^{-1}}$), with less of a delay in evolutionary stages compared to the first case study.

Overall, the SINGV simulations capture both Sumatra squalls well, justifying their use in the following analysis. Both systems are characterised by eastward propagation of convection from the Barisan mountains in Sumatra overnight. However, initiation of the first Sumatra squall appears to be solely over the mountains, whereas propagation of convection from the Eastern Indian Ocean may assist in the development of the second Sumatra squall. Rainfall over the mountains is more intense as a result. The second Sumatra squall, compared to the first, also propagates further eastward, and with a greater propagation rate.

However, the model has some discrepancies in the convection simulated, such as greater rainfall intensities, morphology of the cold cloud shield, and the broader geo-

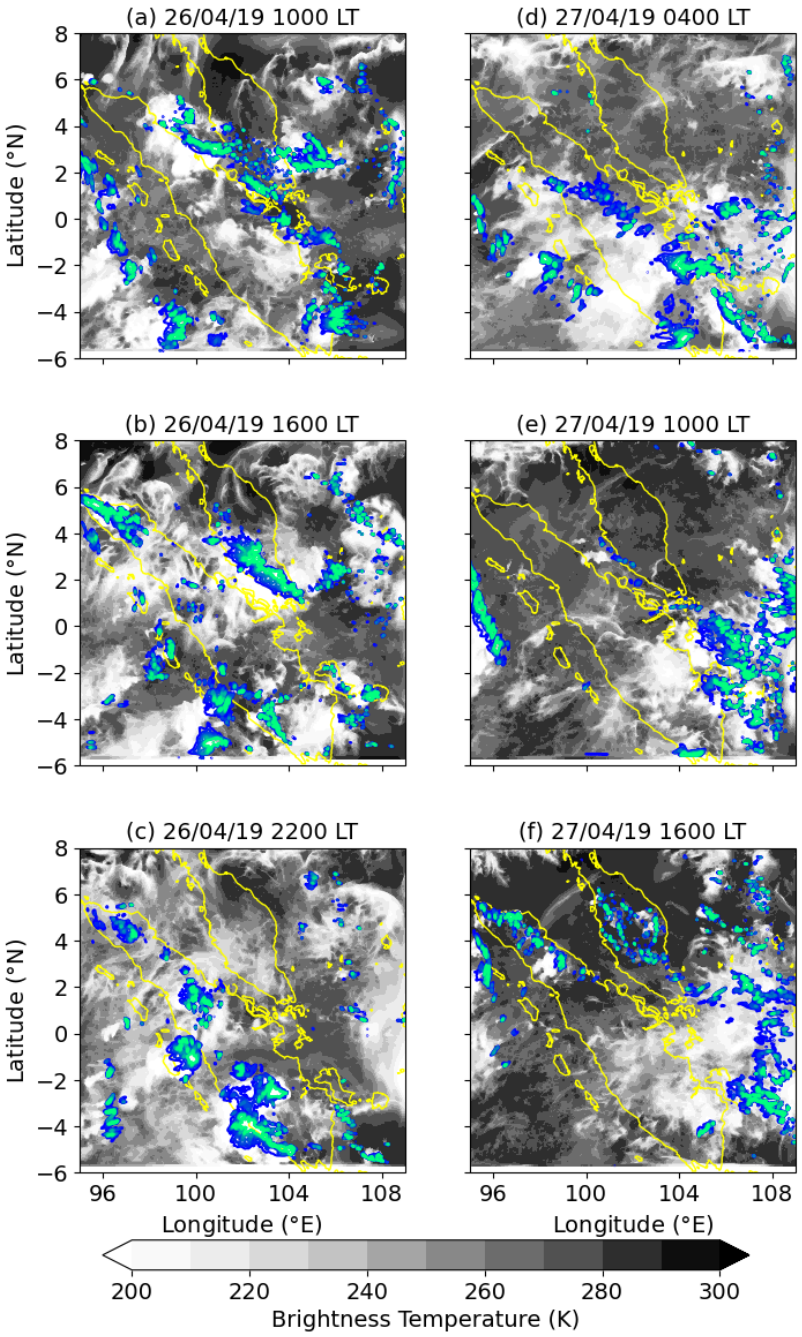

Figure 4.5: As in Figure 4.4, but for the second SINGV simulation initialised on 25 April 2019 0000 UTC, or 0700 LT. Panels are plotted in intervals of 6 hours, from 26 April 2019 1000 LT to 27 April 2019 1600 LT.

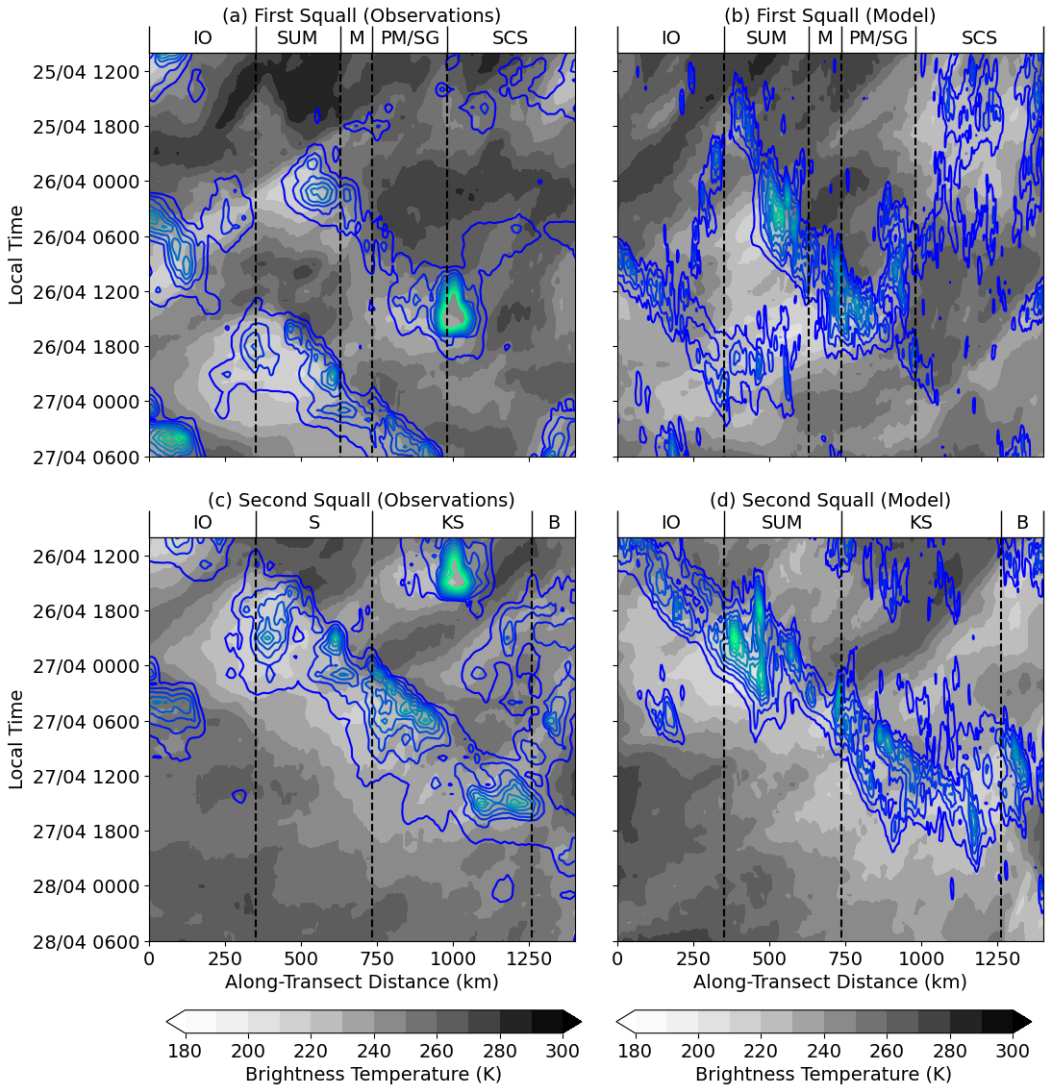

Figure 4.6: (a) Hovmöller plot of Himawari brightness temperature (filled contours) and IMERG rainfall (contours) for the first Sumatra squall analysed. Rainfall is plotted from $1\,\mathrm{mm\,hr^{-1}}$ to $10\,\mathrm{mm\,hr^{-1}}$ in increments of $1\,\mathrm{mm\,hr^{-1}}$. Variables have been interpolated to the grid shown in dashed black lines in Figure 4.1 and then averaged to create a roughly southwest-northeast oriented transect. (b) is as in (a), but cloud top brightness temperature (filled contours) and rainfall (contours) derived from the first SINGV simulation. (c) and (d) are as in (a) and (b) for the second Sumatra squall, where data is now interpolated to the dashed purple box in Figure 4.1. (d), compared to (b), represents data from the second SINGV simulation. Key locations are indicated above the panels: Indian Ocean (IO), Sumatra (SUM), Malacca Strait (M), Peninsular Malaysia/Singapore (PM/SG), South China Sea (SCS), Karimata Strait (KS) and Borneo (B).

graphical distribution of convective clusters. Errors largely stem from the enhanced convective intensity during the initiation phase. Differences in timings of the squall line evolution are identified primarily for the first case study. Despite these issues, the model simulates squall lines which resemble those which would be described as Sumatra squalls.

4.3.3 Vertical profile analysis

Both Sumatra squalls occurred within a sheared large-scale environment, relative to the climatological profile (Figure 4.7). Southwesterlies during the first Sumatra squall intensify between 600-900 hPa to around $5\,\mathrm{m\,s^{-1}}$, and northeasterlies in the upper-levels to values down to -10 $\mathrm{m\,s^{-1}}$ (Figure 4.7a). This vertical wind shear is much more intense during the second Sumatra squall, with southwesterlies extending up to 500 hPa, peaking at $10\,\mathrm{m\,s^{-1}}$ at 750 hPa (Figure 4.7b). Upper-level northeasterlies, as with the first Sumatra squall, reach values of -10 $\mathrm{m\,s^{-1}}$.

Figure 4.8 shows vertical cross-sections of the along-transect wind and moisture flux convergence (MFC, as described in Banacos and Schultz, 2005), derived through rotation of the zonal and meridional components of the wind field to the direction shown in Figure 4.1, for the first Sumatra squall. At 1600 LT, southwesterlies are present between 700-850 hPa with northeasterlies intensifying with height from around 600 hPa upwards (Figure 4.8a). Winds in the lowermost troposphere converge over the Barisan mountains, with development of updrafts characteristic of diurnally-driven convection. MFC peaks over the Barisan mountains up to around 600 hPa (Figure 4.8b). Convection propagates away from the mountains in both directions during the nighttime, though southwesterlies and downslope mountain winds

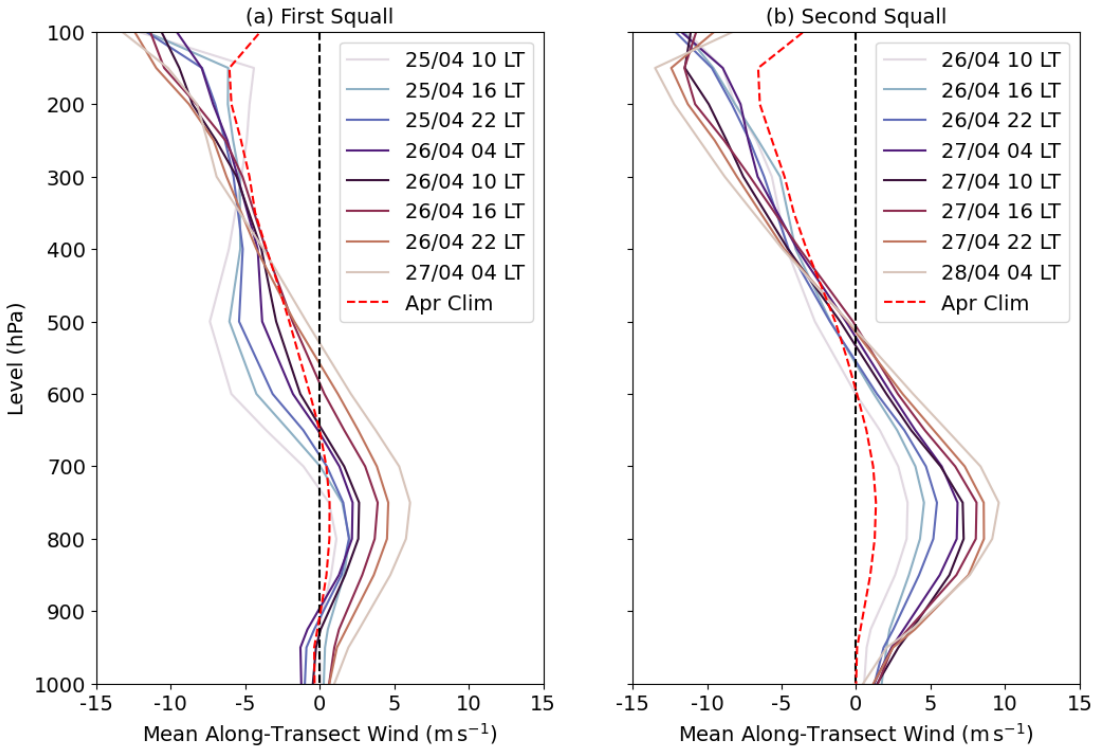

Figure 4.7: Mean along-transect wind across vertical levels during the time periods of analysis for (a) the first and (b) the second Sumatra squall analysed in the case studies. Along-transect winds are derived from the zonal and meridional components of the wind field rotated relative to the grids shown in Figure 4.1. Winds are then calculated as averages over the respective boxes used for the analysis of each Sumatra squall for 6 hourly time steps. Positive values are approximately southwesterlies. Red dashed lines represent the April climatological ERA5 along-transect wind over the vertical levels, determined for each box over 20 years from 2001-2020.

aid predominantly eastward propagation and MFC (Figures 4.8c-d). Low-level northeasterlies develop from the South China Sea towards Sumatra, which when combined with lower-tropospheric southwesterlies over Sumatra lead to convergence, and both strengthened updrafts and MFC up to around 500 hPa in the early morning of 26 April (Figures 4.8e-f). Near-surface reductions in virtual potential temperature also develop, indicating the presence of density currents. Downdrafts develop to the rear of the Sumatra squall (roughly 400 km along-transect, Figures 4.8e-f), tied to intensification of low-to-mid-tropospheric southwesterlies. To the west of Sumatra, density currents also form, with a shift from near-surface southwesterlies to northeasterlies, indicative of the land breeze.

In the later hours of the morning, convection propagates towards Peninsular Malaysia (Figure 4.8g). Southwesterlies and updrafts over the Eastern Indian Ocean, as well as downdrafts to the rear of the Sumatra squall, strengthen. Southwesterlies are noted in the lowermost levels, though low-level (moist) convergence at the leading edge of the Sumatra squall weakens (Figure 4.8h). By 1600 LT, while mid-level southwesterlies propagate further eastward, strengthening over the Eastern Indian Ocean, both the low-level northeasterlies ahead of the Sumatra squall and the density current dissipate, as the Sumatra squall passes over Peninsular Malaysia (Figure 4.8i). Downdrafts to the rear of the Sumatra squall, core convective updrafts and the associated MFC (Figure 4.8j) also weaken, and from here on, the Sumatra squall dissipates (Figures 4.8k-l).

Figure 4.9 shows similar cross-sections but for the second Sumatra squall. Intense updrafts are observed at the leading edge of enhanced mid-tropospheric southwesterlies over the Eastern Indian Ocean in the morning of 26 April (Figure 4.9a). In

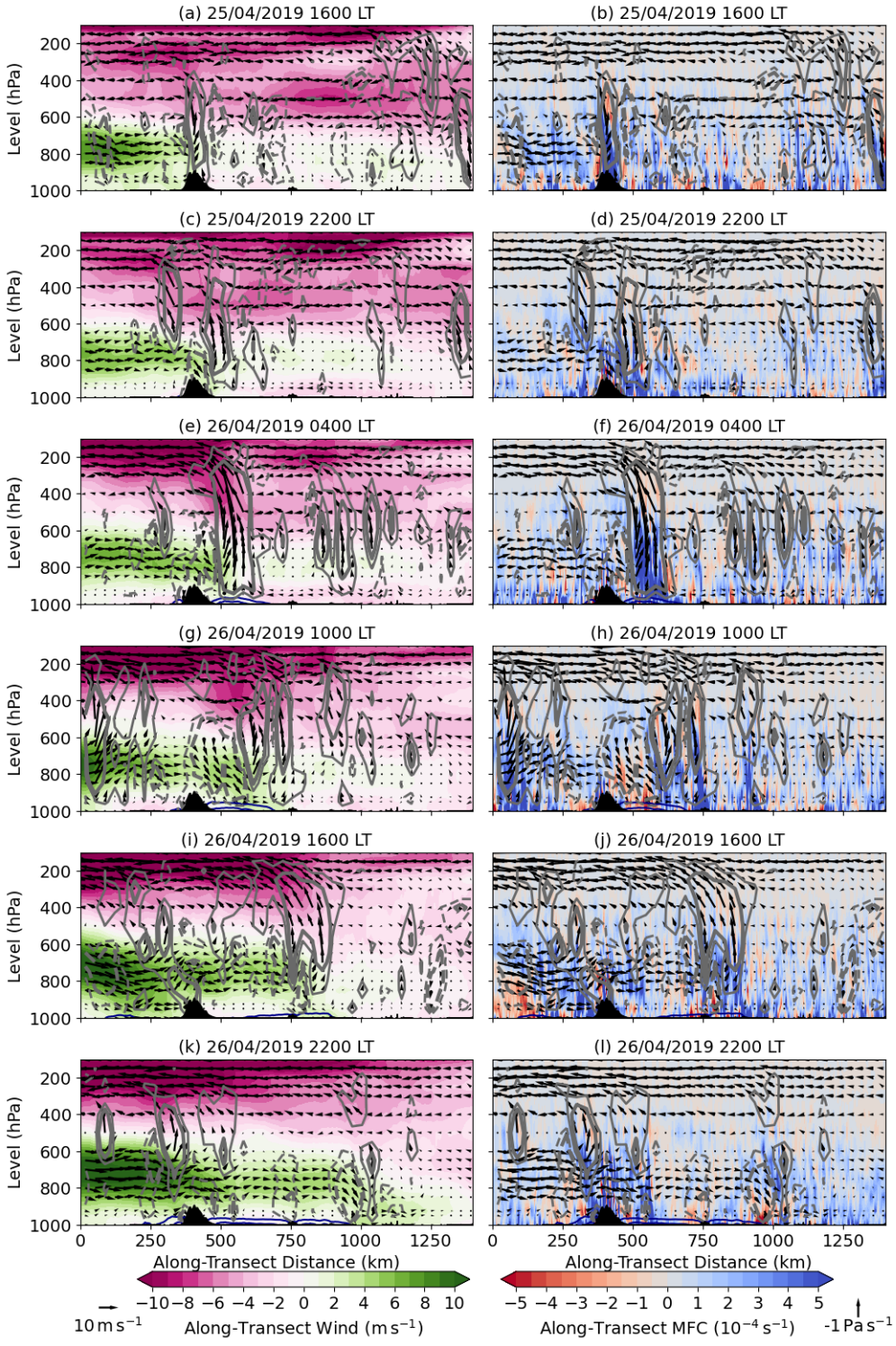

Figure 4.8: Cross-sections of along-transect wind (left) and moisture flux convergence (right), both shown in filled contours, interpolated to, and then averaged over, the dashed black grid in Figure 4.1 in the northwest-southeast direction for the first Sumatra squall, from 25 April 2019 1600 LT to 26 April 2019 2200 LT at 6 hourly time steps. Vector arrows represent along-transect and vertical winds. Grey solid (dashed) contours represent vertical velocities at -0.5 and -0.25 (0.125 and 0.25) Pa s^{-1}, where the larger magnitude values are drawn in thicker contours. Negative vertical velocities represent ascent. Blue contours represents virtual potential temperature from 302-304 K in increments of 1 K to represent the density current. Regions filled in black represent where topography is present.

this region, strong MFC is noted up to around 600 hPa (Figure 4.9b). Low-level winds directed towards the Barisan mountains from either side help in intensifiying the updrafts over land, while the convection over the ocean propagates further eastward (Figure 4.9c), thereby broadening the region of intense MFC (Figure 4.9d). Overnight, merging between diurnally-forced convection, and that advected onshore by the enhanced southwesterlies, leads to intensification of the Sumatra squall (Figure 4.9e). Increases in low-level northeasterlies ahead of the Sumatra squall, as well as development of a density current, enhance MFC and lift at the leading edge (Figure 4.9f).

In the early morning of the following day, the second Sumatra squall has propagated further eastward from Sumatra towards the Karimata Strait, with strengthened of southwesterlies to the rear, which descend downslope to lower-levels east of the mountains (Figure 4.9g). The leading edge of the Sumatra squall is aligned with the front of the developed density current. Low-level northeasterlies ahead of the Sumatra squall have dissipated, with progressive weakening of the broad region of MFC associated with convective activity (Figure 4.9h). Offshore flow is also observed towards the Eastern Indian Ocean from Sumatra, with an associated density current. Continued Sumatra squall propagation in the morning to afternoon is modulated by the intensified southwesterlies in the lower-troposphere (Figure 4.9i). With continued propagation, MFC weakens slightly (Figure 4.9j), though unlike the first Sumatra squall, the second Sumatra squall continues to propagate eastward outside of the domain of analysis (Figures 4.9k-l).

In summary, the two Sumatra squalls analysed have several similarities. Diurnal forcing is important in modulating low-level winds and MFC onto the Barisan moun-

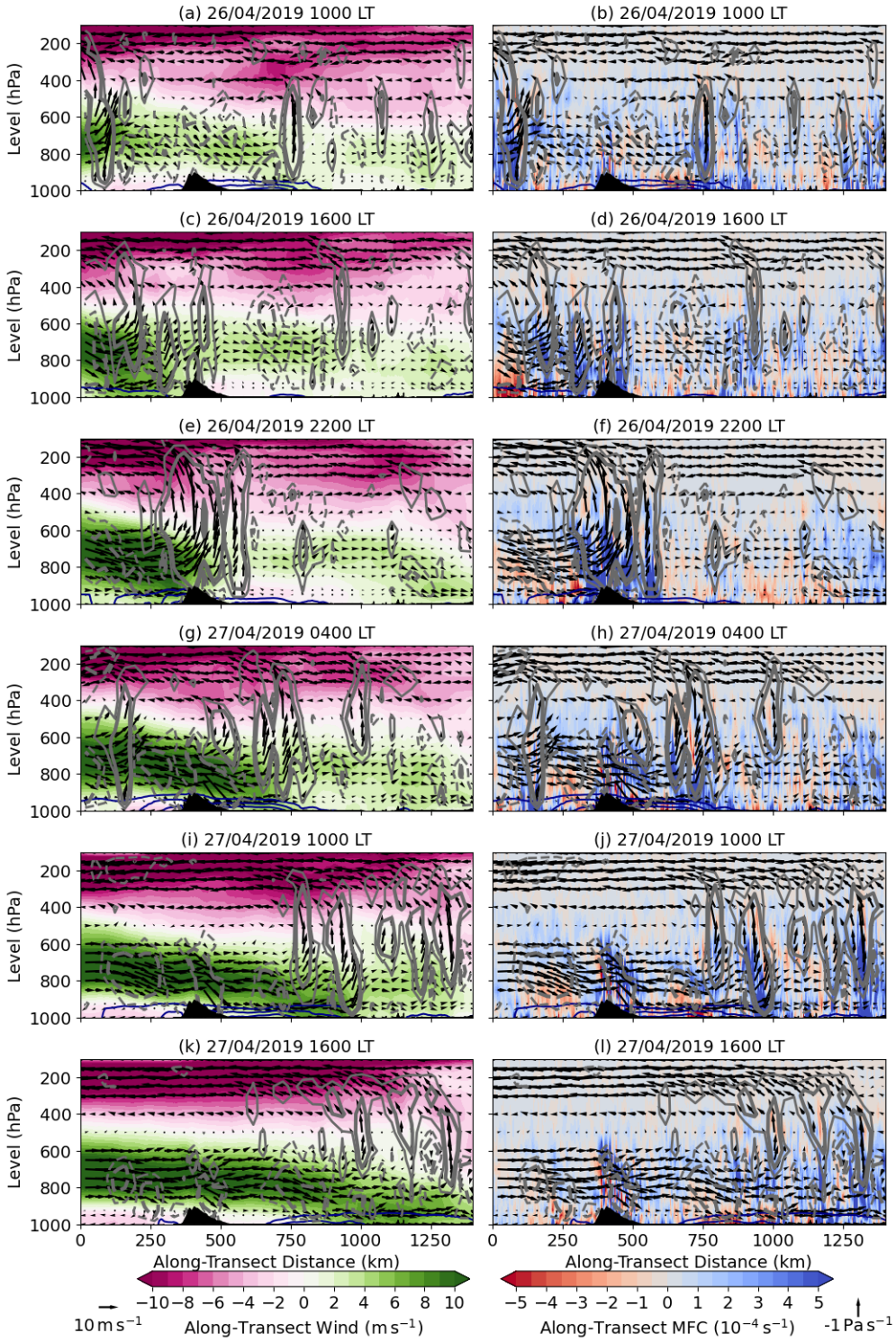

Figure 4.9: As in Figure 4.8, but for the second Sumatra squall, from 26 April 2019 1000 LT to 28 April 2019 0400 LT at 6 hourly time steps, where data is interpolated to, and averaged over (northwest-southeast), the dashed purple grid in Figure 4.1.

tains in the late afternoon, key for Sumatra squall initiation. As the systems intensify, they form characteristic ascending front-to-rear flows associated with Sumatra squall dynamics, assisted by lower-tropospheric shear induced by the low-level northeasterlies ahead of the Sumatra squall. Enhanced MFC and lift at the leading edge is influenced further by the development of density currents extending eastward over Sumatra from the mountains overnight and into the morning. Extensive southwesterlies in the low-to-mid-troposphere are noted to the rear of the Sumatra squalls, helping in storm propagation and the formation of a rear inflow jet. Reductions in the MFC, influenced by the loss of the low-level northeasterlies and density current, lead to dissipation of the first Sumatra squall. This mechanism is likely to be the case for the second Sumatra squall, further into its lifetime, when there may be reductions in MFC as it propagates further eastward, though this is not directly determinable from this analysis as the squall line moves outsides of the domain.

A few differences can also be noted. The second Sumatra squall is characterised by much stronger southwesterlies to the rear, and upper-level northeasterlies, throughout its lifetime. Slightly weaker low-level northeasterlies ahead of the second Sumatra squall are also present, but are not as distinct as the difference associated with the southwesterlies. Additionally, convection is advected onshore from the Indian Ocean by these southwesterlies prior to development of this Sumatra squall over the mountains, leading to a broader region of MFC up to the mid-troposphere.

4.4 Discussion

In this study, two Sumatra squalls observed in late April 2019 were analysed (Figure 4.2). In observations, the first Sumatra squall formed as individual convective cells over the Barisan mountains in the afternoon on 25 April 2019, propagating eastward and merging into an intense Sumatra squall overnight. This Sumatra squall propagated over Peninsular Malaysia and Singapore in the following morning, before the system dissipated over the South China Sea, after a brief period of reintensification. The second Sumatra squall was generated in the afternoon on 26 April 2019. Convective cells similarly developed over the Barisan mountains, with onshore (eastward) propagation of convection from the Eastern Indian Ocean assisting in Sumatra squall development and increases in rainfall over Sumatra. Convective cells merged as the system propagated eastward during the nighttime. This Sumatra squall continued to propagate over the Karimata Strait, towards Borneo, throughout the following day, while maintaining intensity.

Analysis of the dynamics of these Sumatra squalls was conducted using SINGV convective-permitting high-resolution simulations (Figures 4.4 to 4.6). While the SINGV model generally produces more rainfall associated with both Sumatra squalls, holds some spatial and temporal mismatches in convective characteristics, and does not capture the period of reintensification associated with the first Sumatra squall, other elements of the Sumatra squall life cycles are represented well. These include generation of convection, primarily over the mountains, geographical locations of enhanced convective activity, and propagation in terms of both speed and direction.

Both Sumatra squalls occurred within a large-scale sheared environment (Figure 4.7), and shared several similarities in their dynamics (Figures 4.8 to 4.9), as high-

lighted in the schematic in Figure 4.10. Initiation of the Sumatra squalls is tied to the diurnal cycle, with low-level onshore flow and MFC over the Barisan mountains peaking in the afternoon (Figure 4.10a). Intensification of convection relies on the MFC at the leading edge of the Sumatra squall, modulated by lower-tropospheric shear which affects the horizontal gradient in moisture fluxes particularly in the lower-levels (Figure 4.10b). Here, low-level northeasterlies ahead of the Sumatra squall interact with southwesterlies to the rear, as well as downslope winds and density currents originating from western Sumatra, thereby enhancing lift and transport of moisture to upper-levels. Updrafts tilt at the upper-levels in line with the presence of strong northeasterlies, producing a distinct ascending front-to-rear flow. Sumatra squall propagation through the night is mediated by low-to-mid-tropospheric southwesterlies, assisting in the development of a rear inflow jet. Dissipation of the Sumatra squalls, shown primarily in the first case study, is influenced by the loss of the low-level convergence driven by the interaction between near-surface northeasterlies and southwesterlies, thereby reducing the amount of moisture supplied for sustaining convection (Figure 4.10c).

Sumatra squalls are therefore similar to 'classical' MCSs deduced from global observations and modelling studies with regards to mechanisms of initiation, propagation and intensification (e.g. Houze, 2018), including studies focused more specifically on the Maritime Continent (e.g. Qian, 2008; Hassim et al., 2016; Peatman et al., 2021, 2023, 2025). Diurnally-varying land-sea breeze circulations influence MFC over land, which then enables development of deep convection. Vertical wind shear, between the lower-to-mid-levels and upper-levels, for example comparing the 300 hPa and 700 hPa levels, in the large-scale environment is important for maintaining squall line struc-

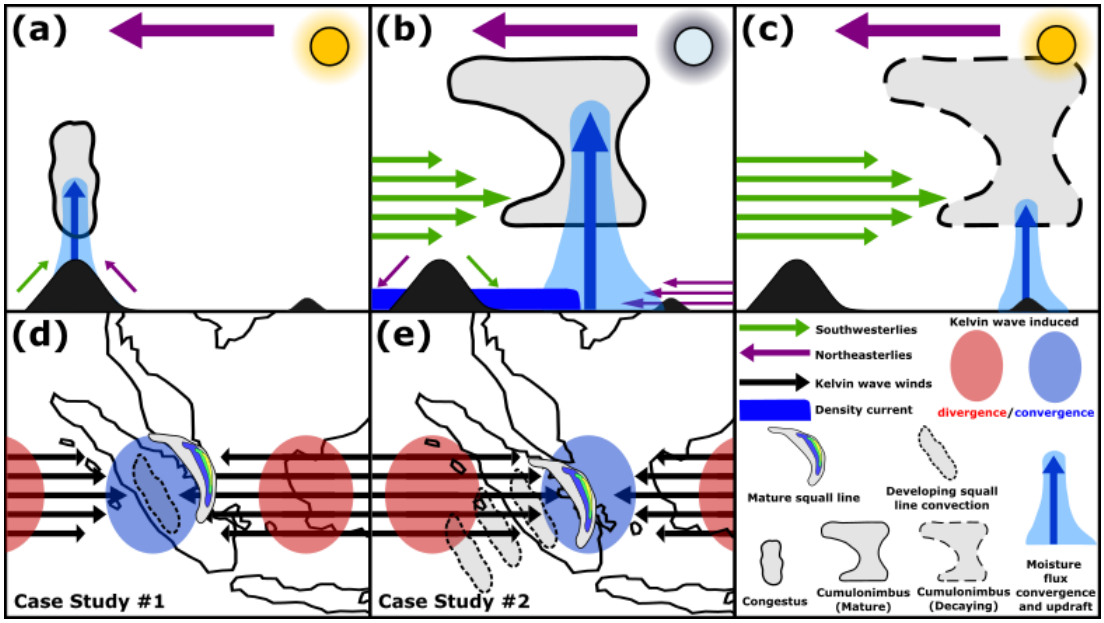

Figure 4.10: (a-c) Schematics of cross-sections of Sumatra squalls showing mechanisms of (a) initiation in the afternoon, (b) propagation and intensification during the nighttime, and (c) dissipation the following day, based on the two case study Sumatra squalls. The black 'hills' represent the locations of the Barisan mountains and Sumatra (left), and Peninsular Malaysia and Singapore (right). (d) and (e) show the interactions across the region linked to equatorial waves and synoptic-scale variability during the two analysed Sumatra squalls respectively, which are hypothesised to explain differences in their characteristics. In all panels, the length of arrows reflects the intensity of the winds for that specific feature.

ture (e.g. Rotunno et al., 1988), and lower-level vertical wind shear is key here for squall line organisation.

This low-level shear, here influenced by northeasterlies ahead of the squall line, is key in modulating moist convergence and lift within the leading edge through interactions with descending flow to the rear, known to increase updraft intensity and minimise susceptibility to entrainment (Rotunno et al., 1988; Alfaro, 2017; Mulholland et al., 2021; Baidu et al., 2022; Abramian et al., 2023). The southwesterlies also act to bolster the role of the rear inflow jet (e.g. Raymond, 1984; Redelsperger and Lafore, 1988), in mediating propagation and further displacement of boundary layer air. Deeper analysis would be required to determine precisely how much of the enhancements in wind to the rear of the MCS is due to changes in broader environmental wind, or modification of the local dynamics by the MCS itself.

The presence of density currents, which could be due to a combined effect of mountain winds, land breezes and cold pools, too acts to influence the overall inflow of moist air and modulate convective instability. These density currents help in developing localised regions of convergence at their leading edges, and can then interact with the low-level shear ahead of the squall line which balances the circulation and vorticity induced by the density current, thereby enhancing tropospheric moistening and lifting crucial for maintenance of deep convection (e.g. Rotunno et al., 1988; Weisman et al., 1988).

These results build on the findings of Chan et al. (2019) from their case study analysis, as well as the study of Nguyen et al. (2025). Compared to the aforementioned studies which focus primarily on the more mature phases of the MCS life cycle, we have provided additional understanding more specifically of the initiation

of Sumatra squalls and the processes that modulate their propagation and intensification, in terms of the observed patterns of MFC and wind. Similar interactions were also documented in Peatman et al. (2023) and Peatman et al. (2025) in their work on convection propagation towards the Indian Ocean, Nor et al. (2020) who identify the importance of orography and associated land-sea breeze circulations in modifying convective characteristics around peninsular Malaysia, as well as Hassim et al. (2016) in studies over New Guinea. Weakening of MFC and the coincident interactions associated with the wind field and density currents inevitably will minimise intensification, resulting in a dissipating Sumatra squall. Therefore, knowledge of MCS activity from elsewhere in the MC can be extended to these systems.

Comparing the two Sumatra squalls, the second Sumatra squall exhibits much stronger southwesterlies to the rear, leading to a faster propagation rate. These southwesterlies are centred within the mid-troposphere (around 750 hPa) prior to its descent, similar to Warner et al. (2003), contrasting the low-level jet observed at mid-latitudes and the subtropics (e.g. Maddox, 1983; Rowell and Milford, 1993; Salio et al., 2007). In addition to diurnal forcing of Sumatra squall intiation, convection is advected onshore from the Eastern Indian Ocean to Sumatra by these southwesterlies, where convection aligns with the leading edge of the strongest winds. These processes precede late afternoon Sumatra squall development, supplying a greater flux of moisture within the low-to-mid-troposphere and enhancing the overall strength of convection.

Both Sumatra squalls occurred during an active MJO (Figure 4.3a), but were more distinctly embedded in the convergent phase of an equatorial Kelvin wave (Figure 4.3b). The presence of this wave enhances larger-scale convergence, which helps

Sumatra squall intensification, particularly with relation to the environment of the first Sumatra squall, as it arrives in phase with the diurnal cycle (Figure 4.10d). Large-scale convergence is known for modulating the potential for convection generation (e.g.Crook and Moncrieff, 1988) - elsewhere in the Tropics, synoptic waves help to organise convection (e.g. Fink and Reiner, 2003). Various studies have indicated the role of Kelvin waves specific to the region of study in conditioning low-level flow and moisture, helping to organise and develop convection further and intensify rainfall (Kiladis et al., 2009; Ridout and Flatau, 2011; Latos et al., 2021; Nakamura and Takayabu, 2022*a*,*b*; Senior et al., 2023; Nguyen et al., 2025).

For the second Sumatra squall, convection may be advected by the intensified low-to-mid-tropospheric southwesterlies, modulated by the Kelvin wave (Figure 4.10e), as the MCS propagates roughly at the along-transect component of the speed of this equatorial wave (approximately 9-10 $\mathrm{m\,s^{-1}}$, Figure 4.3b). The presence of the Kelvin wave is also indicated further by enhanced northeasterlies at upper-levels which develop with time, thereby influencing the large-scale shear in the environment. The convection that propagates from the Indian Ocean may be tied to the outer rainbands of tropical cyclone Lorna, located southwest of Sumatra during this period of analysis as highlighted in Paski et al. (2021), which may be brought onshore by winds induced by the Kelvin wave. The earlier onset of convection for the second Sumatra squall may be explained by the maximum Kelvin wave-induced wind arriving in phase with the peak in the diurnal cycle. The resultant intensified southwesterlies will also aid in propagation of the second Sumatra squall both faster and further, relative to the first Sumatra squall.

Baranowski et al. (2016) and Senior et al. (2023) both note extreme rainfall in-

tensification particularly when Kelvin waves arrive in phase with the diurnal cycle. Therefore, the phasing between the diurnal cycle and Kelvin waves may determine the predictability of Sumatra squalls, though greater in-depth analysis into the probability of Sumatra squall occurrence for days where these phenomena operate in phase with one another will be required. We have, however, provided deeper mechanistic understanding of the interactions between the planetary-scale and mesoscale in relation to Sumatra squall characteristics, building on from the composite analysis of Nguyen et al. (2025). While the Kelvin wave speed, and the associated coupling with squall line characteristics, is less trivial to determine from the simulations, it can be inferred that a similar Kelvin wave exists in the model as the lateral boundaries are forced by ERA5, used to determine equatorial wave characteristics in Figure 4.3.

In addition to the Kelvin wave, however, positive relative vorticity was induced by a WMRG wave, during the Sumatra squalls analysed (Figure 4.3c). Equatorial Rossby waves also induced varying degrees of lower-tropospheric convergence and positive relative vorticity (Figures 4.3d-e). Nguyen et al. (2025) highlighted that equatorial Rossby waves (particularly n=1) and WMRG waves may be more crucial for the direction of propagation of Sumatra squalls. Conditions related to heightened equatorial wave activity, particularly when waves are superimposed on one another, are known to increase the probability of extreme rainfall and intensity of convection (e.g. Ferrett et al., 2020). High-resolution global models, which can represent equatorial wave activity well, should be analysed, or squall lines could be treated on a case-by-case basis as in this study through insertion of equatorial wave combinations in convective-permitting simulations, to better determine the role of equatorial waves.

A key limitation of this study is the usage of a small number of case studies,

constrained primarily by the availability of simulation data. Sumatra squalls, as with any phenomenon studied through event-based analysis, are expected to vary in characteristics. Shifts in direction of propagation, moisture transport, origins and orientation of Sumatra squalls may also vary with season (Pratiwi, 2023; Nguyen et al., 2025). The more precise role, for example, of diurnal forcing for convection initiation over the Barisan mountains, compared with nocturnal land breeze convergence for development over the Malacca Strait, another process known to be key for Sumatra squall initiation, could be determined by further case study analysis.

Analysis of more Sumatra squalls will additionally assist in understanding the specific roles of, and balance between, lower-tropospheric shear and density currents in MFC leading to convective intensification. Peatman et al. (2023) noted difficulties in analysing the importance of density currents in depth, given origins may stem from both land-sea breeze circulations, as well as cold pools resulting from rainfall evaporation. Studies such as Grant et al. (2018) have successfully employed tracers for examining the role of cold pools in idealised simulations of MCSs. Cellular formation at the leading edge, dissipation to the rear, and merging of convective cells were also not explicitly captured in this work, as well as interactions with other processes known for potential links with MCS dynamics and propagation, such as gravity waves (e.g. Redelsperger and Lafore, 1988; Mapes et al., 2003; Tulich and Kiladis, 2012; Peatman et al., 2023).

Detailed thermodynamical processes intrinsic to the Sumatra squalls, such as the extent of diabatic heating associated with updrafts (e.g. Raymond, 1984; Alfaro, 2017), are also crucial to understand. Bickle et al. (2021) highlight that over Africa, thermodynamical processes may be more important in modulating squall line char-

acteristics compared to shear. Peatman et al. (2025) captured variability in local thermodynamics in modulating the storm-relative inflow, which influence convective instability associated with offshore-propagating systems over Sumatra.

The simulation of the squall lines and overall model configuration should also be evaluated further. It was noted that the SINGV model, while producing Sumatra squalls, does not produce perfectly accurate simulations of their evolution as captured in observations. Dipankar et al. (2020), while stating that modelled rainfall associated with Sumatra squalls is more similar to observations than coarser global models, note temporal mismatches in onset and overall persistence of rainfall, in addition to remaining wet biases, common in convective-permitting models more broadly. Errors may originate through, for example, the lateral boundary conditions employed, sub-grid processes represented by microphysics and dynamics schemes, and running uncoupled simulations. Therefore, future work would require altering model configurations, such as introducing ocean-atmosphere coupling which may modulate the land-sea breeze dynamics and associated convergence, incorporating nested domains to provide potentially more reliable lateral boundary conditions, and assessing sensitivity to the various parameterisation schemes in ensemble approaches, which was explored to a degree in Dipankar et al. (2020). These avenues would provide a more rigorous and statistical assessment of model performance in simulating Sumatra squalls, which would prove useful for future research related to this topic.

4.5 Conclusions

This study analysed two Sumatra squall case studies in late April 2019. In observations, these squall lines formed over the Barisan mountains of Sumatra during the afternoon, before intensifying overnight as they propagated roughly eastward towards Peninsular Malaysia, Singapore, and neighbouring seas. High-resolution convective-permitting simulations were used to understand the dynamics of these Sumatra squalls. These simulations captured key features of the evolution of the Sumatra squalls, such as in their initiation and propagation.

The two Sumatra squalls were shown to fit the 'classical' picture of tropical squall lines with reference to the key mechanisms of initiation, propagation and intensification. Sumatra squall initiation in the afternoon was modulated by diurnally-induced onshore flow and MFC. Convection organised and intensified through enhancements of this (moist) convergence, influenced by interactions between density currents and downslope winds to the rear, and lower-tropospheric wind shear mediated by low-level northeasterlies ahead, of the leading edge. Large-scale environmental shear maintained characteristic ascending front-to-rear flow, while low-to-mid-tropospheric southwesterlies assisted in developing a rear inflow jet, enhancing squall line propagation. Sumatra squall dissipation occurred at times of reductions in low-level MFC, with corresponding weakening of the interaction between the aforementioned southwesterlies and northeasterlies, either side of the leading edge.

Equatorial waves were active during the period of analysis - in particular, both Sumatra squalls occurred while an equatorial Kelvin wave propagated over the region. This wave likely assists in development and intensification of the first squall line through modulation of large-scale lower-tropospheric convergence. In contrast,

the Kelvin wave is more crucial for propagation of the second Sumatra squall, through strengthening of low-to-mid-tropospheric southwesterlies to the rear. These enhanced winds additionally advect convection onshore from the Eastern Indian Ocean to Sumatra, preceding diurnally-induced convection development over the Barisan mountains leading to squall line initiation. Crucially, the arrival of the equatorial Kelvin wave in phase with the diurnal cycle highlights the potential for predictability of these events.

This study has provided greater understanding of the variety of processes which are important for dynamics associated with these Sumatra squalls. Crucially, stages of the entire life cycle of these squall lines, compared to the mature phase which was the focus of previous studies, have been analysed. Similar to studies of squall lines across the Maritime Continent, diurnal forcing is a key feature in initiating these Sumatra squalls over the Barisan mountains through the induced sea breezes, upslope winds and MFC. Both large-scale, and mesoscale low-level, shear, in addition to density currents, influence squall line structure, as well as the convergence and lift which are important for intensification of convection. Broader tropical MCS theory can thereby be applied to these specific local weather systems.

Several differences have also been highlighted in the characteristics of these Sumatra squalls, both by comparison to one another, and to 'theory', where interactions with synoptic variability and equatorial wave dynamics influence the mechanisms of initiation, propagation and intensification of the Sumatra squalls. This study has therefore emphasised the importance of phenomena operating over various scales, from large-scale modes of variability to mesoscale shifts in dynamical processes, in modifying Sumatra squall characteristics, and thereby extending knowledge of these particular MCSs.

Future work should analyse large-scale phenomena and determine their association with Sumatra squall occurrence, and key mechanisms (e.g. the wind and moisture field) as a means of generalising Sumatra squall dynamics. Additional interactions between these dynamics and equatorial waves will need further exploration to determine their influence on the development and propagation of Sumatra squalls. Further case study analysis using high-resolution coupled convective-permitting climate simulations will provide deeper insight into the specific dynamics and thermodynamics underlying the key mechanisms associated with the evolution of Sumatra squalls.

Overall, this addition to our knowledge of Sumatra squall dynamics will prove valuable for regional weather forecasters and modelers, through informing the environmental and storm properties that may need to be considered for improved forecasts of these high-impact weather systems, and other extremes. Ultimately, these improvements will benefit work towards better practices related to disaster awareness and management.

Chapter 5

Conclusions

This thesis aimed to improve our understanding of a range of key atmospheric and oceanic coupled processes which influence rainfall patterns across the MC in Southeast Asia. This region experiences extreme rainfall all year round, which causes extensive flooding and landslides, leading to health crises and economic losses. Process knowledge is fundamental to understanding where and when models fail, and the reasons for their biases, in addition to improving the ability to forecast and predict weather patterns associated with this rainfall, which ultimately feeds into early warning and disaster mitigation practices.

Rainfall across the MC is modulated by large-scale modes of variability, such as the MJO, ENSO, IOD and equatorial waves, to synoptic-scale processes such as cold surges and tropical cyclones. The diurnal cycle acts as another key mechanism, primarily influencing local variability in convection through effects on mesoscale processes such as land-sea breeze circulations and gravity waves. All of these processes have unique scale interactions which make understanding the regional meteorology

more difficult, impacting both model representation of convective processes and the predictive skill for the MC. Model biases, such as in the timing of diurnal cycle have overtime been corrected through increasing model spatial resolution, explicitly representing convection within CPMs, and incorporating atmosphere-ocean coupling. However, some biases persist due to the limitations in our process knowledge.

As highlighted in Chapter 1, several knowledge gaps in the literature were identified. These gaps were primarily associated with transient and/or synoptic-scale to mesoscale processes, which tend to be more difficult to accurately capture in NWP for the region, compared to larger-scale variability. Tropical-extratropical interactions were investigated in Chapter 2 by considering the role of mid-level dry air intrusions in influencing rainfall characteristics over the southern MC. In Chapter 3, the characteristics of mesoscale ocean eddies were derived more extensively across the MC, compared to previous studies, and their impact on the atmosphere through induced air-sea interactions was examined. Finally, the dynamics of Sumatra squalls, which are high-impact weather systems observed over the western MC, were analysed in high-resolution convective-permitting simulations in Chapter 4 to build upon the understanding gained from the limited existing literature on this topic. The key results associated with these research avenues are summarised in the following section.

5.1 Overview of results

5.1.1 Regional rainfall is influenced by extratropical synoptic-scale transients

There is limited knowledge as to how the Tropics and extratropics interact in modulating rainfall over the MC, particularly on synoptic spatial and temporal scales. Previous studies have mainly focused on cold surges which originate from disturbances associated with the Siberian High in the Northern Hemisphere (e.g. Koseki et al., 2013). Cold surges lead to increased rainfall and strengthened winds particularly over Peninsular Malaysia, Borneo and Java.

Another form of tropical-extratropical interactions are mid-level dry air intrusions (DAIs), which originate from upper-level disturbances along the jet stream. DAIs can lead to suppresion of convection (e.g. Mapes and Zuidema, 1996; Parker et al., 2016), while there is convective enhancement at the margins, due to differences in their characteristics compared to the surrounding environment (e.g. Allen et al., 2009). Over the MC, several studies have identified dry air coming from the Southern Hemisphere extratropics towards Sumatra and Java, leading to the shifting of locations of convection in specific case studies (Murata et al., 2006; Seto et al., 2006; Feng et al., 2021). However, no general ties between these upper-level disturbances, DAIs, and modulation of convection over the region had been made in existing research.

In Chapter 2, by identifying dry events over the southern MC using 42 years of reanalysis data, intense dry anomalies at mid-levels were shown to originate from the subtropical jet in the Southern Hemisphere. Here, upper-level disturbances, likely to be attributed to Rossby wave breaking, act as a key source of dry air. Particular

circulation anomalies at the mid-levels help to regulate the direction of DAI propagation in different seasons, additionally influenced by the seasonally-varying low-level monsoon circulation. Beneath DAIs, there is suppression of rainfall.

These intrusions additionally influence low-level wind circulations. Transport of dry air from the extratropics to the Tropics leads to an induced return flow of moist air to the extratropics to the east of these intrusions. In these regions, rainfall is enhanced, due to the contrast between DAIs and surrounding environmental characteristics. Additional interactions with the MJO were statistically derived, where the MJO active envelope is more likely to be remote from the MC during a dry event in boreal winter, but near to the MC for events occurring in the boreal summer. The MJO, and associated equatorial wave dynamics, may exert a control on the circulation anomalies influencing DAI propagation, and therefore the resultant influences in rainfall.

5.1.2 Minimal atmospheric response to mesoscale ocean eddies beyond the near-surface

Chapter 3 shifted focus towards interactions between the atmosphere and ocean. Atmosphere-ocean interactions within the MC have primarily been studied in relation to large-scale modes of variability such as the MJO, where coupling between the ocean and atmosphere are intrinsic to the development and sustenance of this mode, particularly as the active envelope crosses the MC. Further, the importance of air-sea coupling for the representation of key meteorological processes in regional models, through modification of surface heat fluxes, wind and moist convergence, has been emphasised in the literature, as outlined in an extensive review by Xue et al. (2020).

On finer spatial and temporal scales, atmosphere-ocean interactions remain understudied for the MC. One way of better understanding these interactions is through studying mesoscale ocean eddies.

Mesoscale ocean eddies are generated by barotropic and baroclinic instabilities throughout the global ocean, and contribute to the modulation of water properties such as through the transport of heat and salt (e.g. McGillicuddy, 2016). These eddies may also have particular SST signatures, facilitating ocean-atmosphere interactions through induced surface heat fluxes. Atmospheric boundary layer stability and vertical mixing are modulated by these interactions, which can influence the development of cloud and rainfall (e.g. Bôas et al., 2015; Seo et al., 2023).

These eddies are known to be generated in the MC due to the presence of deep basins and narrow tidal straits, and are key in modulating transport associated with some of the major currents in the region (e.g. Ismail et al., 2021; Hao et al., 2022). Studies within the MC have primarily focused on eddy characteristics such as life spans and regions of genesis. Research into the relationship between mesoscale ocean eddies here and air-sea interactions, on the other hand, remains limited.

By using an eddy detection and tracking algorithm which incorporates 20 years of sea surface height data derived from satellite altimetry (Mason et al., 2014), key spatial differences in eddy characteristics between the MC, neighbouring tropical regions and the extratropics were noted. Lower-latitude eddies tend to be fewer in number, are of weaker amplitude and have shorter lifetimes, but are larger and faster-propagating, compared to those at higher-latitudes. These results are consistent with more global analyses of eddy characteristics (e.g. Chelton et al., 2011)

Focusing on several identified eddy hotspots within the MC, and collocating

tracked eddies with reanalysis data, these eddies modify surface heat fluxes between the ocean and atmosphere, influencing near-surface wind convergence. The effect of these eddies on column water vapour, cloud and rainfall was found to be less impactful. Compared to the Kuroshio Extension, a well-known eddy hotspot in the extratropics, SST and surface heat flux anomalies away from the Tropics associated with mesoscale ocean eddies are shown to be much more intense, with correspondingly more distinct and statistically significant influences on cloud and rainfall.

An instantaneous response of the atmosphere to mesoscale ocean eddies therefore may be diminished in the MC, compared to the extratropics. This reduction in response is through the weaker SST anomalies associated with tropical eddies, coupled with faster propagation of these mesoscale features, as well as intraseasonal variability in convection, which is known to feedback onto the surface ocean and modify the eddy-induced air-sea interactions.

5.1.3 Improved understanding of multi-scale mechanisms influencing squall line dynamics

Lastly, this thesis explored the dynamical evolution, such as in the initiation, propagation and dissipation, of squall lines, which are a type of MCS. MCS characteristics are well-studied across the globe, and in the Tropics are known to account for a significant proportion of observed rainfall, including in the MC (e.g. Roca et al., 2014; Crook et al., 2024). One type of MCS which is impactful in the MC is a Sumatra squall, which propagates roughly eastward from Sumatra towards Singapore and Peninsular Malaysia, primarily during the intermonsoon and southwest monsoon periods (Lo and Orton, 2016; Nguyen et al., 2025).

Previous studies have highlighted that Sumatra squalls have characteristics similar to squall lines observed elsewhere, such as in their convective and vertical wind structure (Chan et al., 2019). Hypotheses have linked their initiation to diurnal land-sea breeze circulations over the Barisan mountains of Sumatra, and the Malacca Strait. Propagation is mediated by the low-to-mid-tropospheric wind field, in addition to the presence of density currents. Both theories for initiation and propagation hold similarity to knowledge of convection propagation across the MC (e.g. Hassim et al., 2016; Peatman et al., 2023). However, specific analysis of the dynamics of Sumatra squalls at the storm-scale has so far not been covered extensively enough in the literature.

In Chapter 4, high-resolution convective-permitting model simulations were used to analyse the life cycles of two Sumatra squall case studies which occurred in April 2019. Both Sumatra squalls were shown to initiate primarily through diurnal forcing over the Barisan mountains. These systems had characteristic squall line structure such as having distinct ascending front-to-rear flows and rear inflow jets. Large-scale environmental shear influenced the vertical structure, and supported the resultant development, of the Sumatra squalls. Low-to-mid-tropospheric southwesterlies interacted with density currents and low-level northeasterlies - the latter of which induced shear ahead of the squall line leading edge - leading to squall line propagation and intensification. These features enhanced the moisture flux convergence (MFC) which strengthened convection. Reductions in this MFC, driven by weakening of the aforementioned processes, led to Sumatra squall dissipation.

Equatorial waves were highly active during this period, for which both Sumatra squalls were embedded within the convergent phase of a Kelvin wave. This wave may contribute to convergence in setting up the environment for development of the first

Sumatra squall. The second Sumatra squall occurred in the presence of intensified southwesterlies in the low-to-mid-troposphere, which advected convection onshore towards Sumatra from the Indian Ocean, enhancing the development of convection over the mountains prior to squall line formation. The intensified southwesterlies may also be modulated by the Kelvin wave which then enhanced the propagation of the second Sumatra squall.

Interactions from the storm-scale to planetary-scale therefore both influence the evolution of Sumatra squalls. Additionally, the importance of the diurnal cycle in convective initiation, coupled with the equatorial waves in modulating further development and propagation, highlight event predictability, as past research indicates that the phasing between these two processes can increase the likelihood of extreme rainfall and intensification of convection.

5.2 Contribution of research to the field

Each of the results chapters have given unique insight into processes which have not been covered extensively in meteorological research across the MC. Research into large-scale processes such as the MJO, ENSO and IOD provide us with key knowledge on influences on rainfall over intraseasonal to interannual timescales, and have greater predictive skill. However, synoptic-to-mesoscale and transient processes are more difficult to predict. These processes will also have more direct impacts on communities within the region due to the spatial and temporal scales at which they operate over. Improved knowledge of these processes and interactions at the finer-scales will benefit regional weather forecasters in better understanding and predicting

this higher-order variability in convection and rainfall characteristics.

5.2.1 Individual research themes

The work in Chapter 2 provided further insight into the importance of processes from the extratropics in influencing MC convection. DAIs are chronically understudied in the region, especially compared to cold surges from the Northern Hemisphere, and this work has highlighted how crucial these intrusions are in modulating environmental conditions on synoptic scales. Knowledge of these transients are important particularly for regional modelling practices, where lateral boundary conditions, driven by global models or reanalysis datasets, are prescribed, which may not necessarily represent these processes effectively enough.

Previous studies have primarily shown that DAIs suppress convection due to capping of the atmospheric boundary layer. However, the enhancement of convection and associated rainfall to the east of these intrusions was an important finding in Chapter 2, exhibiting similarity to monsoon bursts over Australia (Allen et al., 2009; Berry and Reeder, 2016). Knowledge of these enhancements of extreme rainfall are a necessity, particularly for the MC where convection initiation and eventual intensification can be spontaneous. The precursor mechanisms identified in this work could provide additional insight into forecasting these changes to the convective environment a few days in advance, as indicated by the lagged response to upper-level disturbances in the Southern Hemisphere.

Furthermore, these intrusions provide one route in interpreting the so-called tropical oceanic moist margin (Mapes et al., 2018). This margin, portrayed as an almost linear boundary between regions of high and low column moisture on seasonal

timescales, exhibits significant non-uniformity in its latitudinal positioning between the Tropics and extratropics on daily-to-subseasonal timescales. Highlighted further in work by Robinson et al. (2024, 2025), variability along this margin can be modulated by a host of weather systems and regimes, such as through synoptic-scale perturbations in mid-tropospheric humidity driven by extratropical DAIs, as just one source.

Analysis of the air-sea interactions associated with mesoscale ocean eddies in the MC, and resultant atmospheric responses in Chapter 3 provided a bridging route within the TerraMaris project between the dominantly atmospheric research, and any ocean-focused studies. The study of Azaneu et al. (2024), as part of the aforementioned project, noted mesoscale variability in SST anomalies driven by surface heat fluxes near Java during an MJO event using observational data. This variability was modulated by an ocean eddy, highlighting processes at these scales as being crucial for modelling the MJO itself.

Chapter 3 therefore sought to answer whether these eddies can significantly modify atmospheric and convective properties. While mesoscale ocean eddies were shown not to lead to a significant atmospheric response in the MC, beyond affecting the surface heat flux and wind convergence fields, this work remains novel and the first of its kind for the region, filling a gap in the literature related to the MC. For example, statistically-informed links between the SST anomalies associated with mesoscale ocean eddies, and various atmospheric characteristics, were identified. The work also emphasised the statement made by Azaneu et al. (2024), where spatiotemporal scales of air-sea interactions across the region are key considerations for ocean-atmosphere coupled modelling at higher horizontal resolutions, raising questions as to how in-

traseasonal variability could influence the associated feedbacks (e.g. Roman-Stork et al., 2021; Souza et al., 2021).

Additionally, and beneficial specifically to the oceanographic community, this work improved the quantification of the number and the characteristics of eddies across the region using extensive satellite observations, which were previously limited to specific basins using more local observations, or for limited time periods (e.g. Purba et al., 2020; Hao et al., 2021). While common eddy tracking approaches tend to negate the near-equatorial regions due to questions as to whether, for example, satellites can necessarily detect these faster moving eddies (Fu et al., 2010), extending analysis further towards the Equator still highlights hotspots of mesoscale ocean variability.

Previous research into Sumatra squalls had not performed as extensive analysis into key initiation, propagation and dissipation mechanisms of these squall lines (Chan et al., 2019). While Nguyen et al. (2025) addressed interactions with large-scale modes of variability over hundreds of subjectively identified squall lines from the Singaporean radar database, in Chapter 4 the more specific roles of equatorial waves dynamics on Sumatra squall characteristics, in environmental pre-conditioning and mediating the propagation of these systems, were highlighted.

Sumatra squall research is an actively growing field. Chapter 4 provided both greater knowledge of these weather systems, while also highlighting their predictability through links with the diurnal cycle of solar heating, and equatorial wave activity. Past studies highlight the importance of the phase locking of these processes in enhancing potential for extreme weather (e.g. Baranowski et al., 2016). These results therefore will give insights for the forecasting community on key diagnostic variables and processes to focus on with regards to predicting, and even improved modelling,

of these squall lines.

However, it is crucial to note that while Sumatra squalls have similar fundamental building blocks to their dynamical structure and life cycle as for those of other squall lines elsewhere across the world, and to those originating from other islands of the MC, these systems were shown to not be wholly generalisable. Differences in the wind and moisture fields, modulated by differences in the role of equatorial waves and synoptic-scale processes, affect the timing of the key convective processes. Therefore, while composite analysis may benefit in producing more general conclusions to squall line characteristics (Nguyen et al., 2025), case study analysis is a much more useful tool for deeper analysis into the variability in dynamics and thermodynamics of convective systems for the region (e.g. Chan et al., 2019; Peatman et al., 2023, 2025).

5.2.2 Synthesis

On top of their standalone contributions to process knowledge, it is important to determine how the different research themes intersect with one another. Direct links between the themes are inherently difficult to hypothesise due to differences in where the key processes explored are most relevant, both geographically and relative to the vertical extent of the atmosphere. Considering the broader field this thesis contributes to, focus can be placed on key drivers of (mesoscale) convection and precipitation variability while synthesising the knowledge gained from each chapter.

Chapter 2 built on past studies which have emphasised the role of DAIs (and other extratropical transients operating over synoptic timescales) in perturbing the wind and moisture fields which then modify regional meteorological patterns (e.g. Tompkins, 2001; Allen et al., 2009). Specific to convection propagation over the western MC as

covered in Chapter 4, Murata et al. (2006) and Seto et al. (2006) both noted convective suppression tied with intensification of westerly winds and reductions in mid-level humidity behind eastward-propagating squall lines over Sumatra. These anomalies originated from the Indian Ocean, but could potentially be traced back to the extratropics as indicated in Feng et al. (2021). Similar enhancements primarily in the mid-to-lower-level wind field are observed trailing MCSs across the MC (e.g. Satomura, 2000; Yanase et al., 2017; Natoli and Maloney, 2023).

The role of synoptic variability in the local wind field, building from the knowledge gained in Chapter 2, could therefore be assessed further in its relationship to the propagation and development of MCSs. In addition, the results in Chapter 4, which indicated the importance of intensified winds potentially associated with local tropical cyclone activity as well as equatorial waves in the evolution of Sumatra squalls, as deduced for MCSs more generally across the region (e.g. Ridout and Flatau, 2011; Peatman et al., 2021), can be factored in. Direct attribution of other synoptic features such as cold surges (e.g. Koseki et al., 2013; Tan et al., 2024) and Borneo vortices (e.g. Crook et al., 2025) to variability in the vertical structures of, and rainfall intensity associated with, MCSs across the MC is an active area of research.

Variability in convection is also inherently sensitive to coupling of atmospheric and oceanic processes given the geographical nature of the MC. Processes occurring across subseasonal timescales will however hold more importance compared to the instantaneous and synoptic timescales analysed in Chapter 3. While transient ocean eddies are insufficient in modifying the boundary layer structure across the MC due to their associated weak SST and surface heat flux anomalies, lower-frequency variability in SST characteristics may enable more sustained and detectable destabilisation of

the lower-troposphere. The MJO is a prime example of where changes to the SSTs can influence environmental preconditioning (such as through enhanced moisture flux convergence) for tropical convection on these timescales (Woolnough et al., 2000).

Subseasonal changes to SST and ocean boundary layer conditions, contributing a large component towards the environmental mean, have indeed been noted to influence variability in the characteristics of more locally-generated convection in the MC. In model studies, prominent mean state biases in SST, in regions such as to the west of Sumatra, feedback onto local land-sea breeze circulations, thereby influencing the diurnal cycle of convection (Dipankar et al., 2019; Li et al., 2020) to which MCS activity over land is strongly constrained by (e.g. Peatman et al., 2023). Similar studies note the sensitivity of land breeze convergence and resultant storm development over regional seas to temperature contrasts between the ocean and the land (e.g. Fujita et al., 2010). These studies, coupled with the discussion in Chapter 3, provide impetus for further studies into the importance of air-sea coupling and general representation of the surface ocean in modulating MC convective variability, which remains overlooked in the literature.

More broadly, however, the research conducted within this thesis has provided better understanding of the rainfall variability and associated dynamics across the MC. Though these processes inherently have poorer predictive skill, due to the scales over which they operate, interactions were identified with known modulators of rainfall characteristics such as the MJO, equatorial waves, and the diurnal cycle, which are easier to predict. Therefore, the dynamical and thermodynamical processes which form the foundations of the regional meteorology could give preexisting means for better forecasting changes to the environmental state on the more transient and synoptic

scales. Provided these interactions are known prior, the processes researched here will be more easily integrated into our knowledge of, and represent crucial components to explaining variability in, convection across the MC.

5.3 Future work

5.3.1 Broader impacts of extratropical transients on the Tropics

A key limitation of the mid-level DAI analysis is the spatial scale employed. While broader dynamical precursors can be observed deep into the extratropics, the work in Chapter 2 only focuses on a domain located south-to-southwest of the MC, which is small relative to the longitudinal extent of the region. Therefore, future work should consider perturbations to mid-level humidity across the entire tropical-extratropical boundary north and south of the MC. This approach would tackle a further issue of the small number of events analysed per season (around 50, over 42 years), and increase the number available for calculating composites around the regions of the driest anomalies. This increase in event number will improve the reliability of statistical tests conducted as part of this thesis, although characteristics may vary across the domain.

Methodologies for this analysis could apply machine learning techniques which have been used to identify the origins of DAIs (e.g. Silverman et al., 2021). These techniques can be modified for detection of the extremes in mid-tropospheric drying at the boundaries, and then work backwards in space and time. The dry perturbation definitions outlined in Robinson et al. (2024) may be a useful metric to utilise. Simi-

lar methodologies could be applied for better determining the Rossby wave breaking structure that is likely to be associated with the development of the DAIs. Disentangling the role of the intensity of the DAIs, in terms of the actual anomaly, areal coverage, and degree of penetration into the moister mid-to-low-troposphere, will also be useful for characterising differences in dry event influences on the convective environment.

Links between the events covered in studies such as Feng et al. (2021) did not consider the direct implications of DAIs on convection and rainfall. Impacts on convective-scale characteristics, primarily driven by the capping of the moist boundary layer, which may too exhibit finer-scale temporal variability, need to be better quantified. Field campaigns such as TOGA COARE provided abundant knowledge on processes within and near to convective clouds during periods with DAIs (e.g. Mapes and Zuidema, 1996). Therefore, case study analysis of DAI activity needs to be conducted. Similar intensive analyses, using high-resolutions CPMs, could also give deeper insights into the dynamical and thermodynamical processes which influence rainfall and convective characteristics both beneath and at the eastern margins of the intrusions.

Improved knowledge of the roles of the MJO on DAI activity may also be gained. The existing hypothesis of the interaction between the MJO and the dry anomalies, provided in Chapter 2 and inferred from observational findings in Kerns and Chen (2014), is unexplored and needs further grounding. Kerns and Chen (2014) noted an interaction between DAIs and equatorial Rossby waves embedded within the active envelope of the MJO as part of the DYNAMO field campaign. Dry air was entrained in the low-level circulations induced by these waves, leading to synoptic-scale breaks in

rainfall. Future research could determine whether these environmental conditions are necessary for enhanced DAI activity, or if they act as a bolster for their propagation into the Tropics.

The representation of DAIs and similar synoptic-scale processes needs to be evaluated using both global nudged and regional (e.g. limited-area) model simulations, to assess the potential for transients to be captured within imposed lateral boundary conditions, driven by global model physics. Sensitivity tests could be employed to modify these boundary conditions and either diminish or enhance the role of extratropical forcing on the Tropics, to evaluate the role of DAIs on the regional environment.

5.3.2 Mesoscale air-sea interactions across the Maritime Continent

In Chapter 3, it was highlighted that ERA5 is largely consistent with ORAS5, and therefore provides a good representation of SST variability, with horizontal grid spacing of $0.25^\circ \times 0.25^\circ$ that may still capture interactions at the mesoscale. Ideally, to better represent the associated signatures of mesoscale ocean eddies on the atmosphere, spatial data resolution would need to be much finer to reduce the requirement for interpolation of data. This fining of spatial resolution would more effectively highlight the variability and magnitude in anomalies such as in the surface heat fluxes and modifications of the wind field.

The vertical resolution of the datasets used in the analysis needs to also be much finer, to extend this work to the influence of eddies specifically on the boundary layer and lower-troposphere (e.g. Ma et al., 2016), if not directly on broader convection. The BARRA reanalysis (Su et al., 2019) could be one data source employed as it

provides atmospheric data, over Australia and the MC region, at higher horizontal (12 km versus 31 km) and vertical (70 versus 37 pressure levels) resolution than ERA5.

Observational data for both oceanic and atmospheric variables, across a long enough time period (multi-decadal) and a fine enough horizontal grid spacing to represent mesoscale ocean eddies (maximum $0.25\,^\circ \times 0.25\,^\circ$), would also benefit further analysis built from Chapter 3. Gulakaram et al. (2023) used extensive observational data and blended products derived from satellites for their study over the Bay of Bengal. However, the datasets are often coarser, up to $1^\circ \times 1^\circ$, larger than the mean radius of eddies derived in Chapter 3. Therefore, high-resolution (eddy-permitting) atmosphere-ocean coupled model simulations may be the solution for improving on existing research.

An alternative approach to this analysis would be to incorporate idealised simulations where model parameters associated with eddy-like features can be modified. Adjusting the SST anomalies induced by the eddies themselves, as well as their spatial scales and propagation rates, would help to evaluate whether this forcing can significantly lead to an atmospheric response in the deep Tropics. However, the requirements for triggering convection in these environments solely from these enforced anomalies are unlikely to be observed in the real world, as deduced by previous work (Skyllingstad et al., 2019). Additional sensitivity experiments would be required to remove background variability on intraseasonal timescales, hypothesised by previous studies to blur the atmospheric response to these eddies (e.g. Souza et al., 2021), as the interactions between the atmosphere and the ocean are inherently two-way.

The work carried out within Chapter 3 assumed that the relationship between SST anomalies in the surface ocean and atmospheric variables is near-instantaneous.

Other studies, including Gulakaram et al. (2018), suggest the response to ocean eddies may in fact be lagged. However, even in research focused on extratropical hotspots of eddy activity, the imprint of an eddy on the atmosphere remains small relative to the mean state (e.g. Frenger et al., 2013). A more viable theory is that impacts on the atmosphere may be more substantial when considering the combined effects of eddies across a region. Studies often quantify high eddy activity using metrics such as eddy kinetic energy and induced mixing (e.g. Pang et al., 2022).

Past research into MJO related air-sea interactions in the SETIO, identified in Chapter 3 and previous studies as a regional eddy hotspot, highlighted SST patterns observed in MJO events that cross the MC are not wholly explained by surface heat flux patterns (Zhang and Ling, 2017). Mesoscale ocean eddies could be contributing to these MJO-related SST patterns, in turn affecting surface heat flux signatures which feedback onto the MJO, as in Azaneu et al. (2024). Deriving a correlation between eddy activity, and SST variability and induced surface heat fluxes, for example through machine learning and statistical methods, may help to better understand the air-sea interactions associated with mesoscale ocean eddies. The cumulative effect of the upward surface heat fluxes generated by greater mesoscale activity, driven by warm eddies in the surface ocean, on the atmospheric boundary layer and convection in the MC is one potential research direction.

5.3.3 Continued analysis of Sumatra squalls

Further research into Sumatra squalls includes the development of methods for objective identification of these weather systems, given existing radar-based datasets are subjective (Nguyen et al., 2025). This analysis could use regional high-resolution

climate model outputs, and derive the leading edge from horizontal gradients in virtual potential temperature, a useful indicator of the density currents which assist in modifying convergence and lift associated with the squall lines (Peatman et al., 2023). Machine learning could also be applied to track the evolution of these squall lines, providing estimators of their primary regions and timings of genesis, intensification and dissipation. This direction of research may help in generalising and compositing over squall line cases, as it would account for the variability in the morphology and locations of the systems themselves.

Additional simulations had been run to complement those used in Chapter 4, with case studies taken from the squall line dataset used in Nguyen et al. (2025). The analytical methods used in this thesis for the two Sumatra squall events can easily be applied for these new case studies. However, case study analysis needs to be run at higher spatial (sub-km) and temporal (sub-hourly) resolution to capture finer-scale convective processes, such as individual cellular generation and structure. Analysis also needs to be broadened to include squall lines which occurred in seasons beyond the boreal spring, and for other years than just 2019. As highlighted in Chapter 4, Pratiwi (2023) and Nguyen et al. (2025) both emphasise a shift in direction of squall line propagation, orientation, and attributed moisture transport between seasons, primarily due to changes in the low-level monsoonal circulation and the ITCZ location.

Various sensitivity experiments may better our mechanistic understanding of Sumatra squall dynamics and thermodynamics. Orographic and island removal experiments have previously been conducted to evaluate the effects of the diurnal land-sea breeze circulations and induced MFC (e.g. Qian, 2008; Tan et al., 2021). These experiments would prove beneficial for understanding how important these processes over

the Barisan mountains are for Sumatra squall initiation beyond the two analysed case studies. These diurnally-varying circulations and thermodynamical processes are important to examine further with relation to nocturnal convergence over the Malacca Strait, which is noted to also assist in convective generation and eventual organisation of these squall lines (e.g. Yi and Lim, 2007; Nguyen et al., 2025).

Further experiments could involve modification of generated density currents, which assist in lift associated with the squall lines, originating from downslope katabatic winds, land breezes, and cold pools. The specific role of cold pools, for example, has been highlighted in the past using tracers in idealised simulations of tropical oceanic convection (Grant et al., 2018), and suggested for future work related to case studies of convection propagation from Sumatra towards the Indian Ocean (Peatman et al., 2023, 2025).

Similar sensitivity experiments can be used to implement, enhance or even diminish the activity of equatorial waves, which in Chapter 4 were determined to potentially influence the environmental pre-conditioning and propagation of the squall lines. This work would follow on from past research highlighting the importance of equatorial waves for the region (e.g. Ferrett et al., 2020; Senior et al., 2023). Work conducted by a Masters student at the University of Leeds over the past year had found for case studies of Sumatra squalls in early May 2019 that equatorial wave activity was minimal, yet squall line generation and propagation was maintained. Equatorial waves could therefore provide a bolster and more favourable environment for these squall lines to generate, but may not be a core necessity.

5.3.4 From field campaigns to modelling studies

Fundamentally, our ability to model and forecast weather within the MC, as addressed throughout this thesis, is limited by the observational network, both over land and within the neighbouring seas. Observational data provides us with the ground-truth of, and therefore foundations to understanding, key processes associated with the regional meteorology, while also being important in data assimilation for reanalysis and models.

This PhD project was involved within the TerraMaris research community, which was initially meant to operate as a field campaign during the boreal winter between Java and Christmas Island, to provide greater insight into regional convective characteristics. The benefit of field campaigns, such as flights through convective systems and neighbouring environments, radiosonde deployments, usage of unmanned aerial vehicles including drones, research cruises, and ocean buoy placements, are well-known. These techniques have been used widely across southeast Asia, in projects such as the Years of the Maritime Continent (YMC, Yoneyama and Zhang, 2020).

As part of this proposed fieldwork, there was potential to understand the effects of changes to mid-level humidity on the convective profile - initial conceptualisation of the work in Chapter 2 came from observations during TerraMaris forecast dry runs. Observational data would benefit this avenue of research further, providing knowledge of sub-daily and convective-scale processes relevant for DAIs and modulation of the environment. Similarly, potential for ocean-based fieldwork was suggested for studying eddy-induced air-sea interactions, building from the work in Chapter 3. The *Caravela* uncrewed vessel, for example, has been used in research for cloud formation in the western tropical Atlantic, and can both enable deployment of autonomous

sea gliders, and collect both meteorological and oceanographic data (Siddle et al., 2021). This vessel could be used to follow mesoscale ocean eddies and better understand interactions between surface ocean mesoscale variability and the lowermost atmosphere.

Studies for convection propagation from Sumatra towards the Indian Ocean have also incorporated observational data derived from field campaigns (Yokoi et al., 2017; Peatman et al., 2021, 2023). In these cases, various atmospheric datasets from the YMC International programme near Bengkulu, Sumatra (Yoneyama and Zhang, 2020) were obtained through the radiosondes that were deployed from the Research Vessel *Mirai*, located offshore of the southwest coast of Sumatra, as well as an automatic weather station and ship-based radar systems. These datasets provide not just high temporal resolution, but also the necessary ground-truth to validate results using reanalysis and model datasets. Unfortunately, similar field campaign data does not exist for the other side of Sumatra - observational data that could be exploited come primarily through ground-based radar.

To develop a new field campaign to address the remaining research questions, in addition to those raised by the broader meteorological community for the MC, is both a time- and finance-related issue. However, with increases in computational power overtime, weather and climate modelling has improved remarkably, providing alternative approaches for research. As outlined in the introduction to this thesis, increasing horizontal grid spacing within models (e.g. Qian, 2008), resolving convection explicitly (e.g. Birch et al., 2016), and introducing ocean-atmosphere coupling (e.g. Xue et al., 2020) have helped in improving the representation of the island geography, land-sea breeze circulations, interactions with large-scale modes of variability, and resultant

rainfall patterns across the MC. While CPMs depend on observations for model development, they continue to provide us with means of testing hypotheses, as models can be fine-tuned for the needs of the user - these include for specific sensitivity tests such as those outlined in the future work recommendations within this chapter.

Ultimately, approaches exploiting the growing number of high-resolution, and often atmosphere-ocean coupled, CPMs remain the most realistic, even if biases persist in the most state-of-the-art models relative to observations. Atmosphere-ocean coupled convective-permitting regional climate simulations were developed as part of TerraMaris for the entirety of the MC over 10 boreal winters, using the MetUM at 2.2 km horizontal grid spacing (Howard et al., 2024). These models captured phenomena such as the diurnal cycle and equatorial waves well, and provide an abundant data source for future research. Each of the three results chapters within this thesis have either incorporated (Chapter 4), or work has suggested using (Chapters 2-3), CPMs. With the correct model physics set-up, coupling, boundary conditions, and a sufficient available data period length, all processes analysed in this thesis could be examined further in tandem.

5.4 Summary and concluding remarks

In conclusion, the analysis conducted within this thesis has broadened our knowledge of processes which influence rainfall patterns across the MC. Each chapter, from exploring tropical-extratropical interactions, to the atmospheric imprint originating from mesoscale ocean variability, to the dynamics and environmental controls on MCS activity, has given novel insight into understudied phenomena crucial for better

understanding the meteorology of the region.

Mid-level DAIs, as studied in Chapter 2, originating from upper-level disturbances along the subtropical jet stream, were shown to propagate towards the MC, leading to general convective suppression, with enhancement of rainfall towards the east on encountering moist return flow from the Tropics. Mesoscale ocean eddy characteristics were better understood more extensively across the MC, compared to previous studies, in Chapter 3. Analysis of the air-sea interactions associated with these eddies suggested tropical environmental characteristics mean their atmospheric imprint is weak, when compared to the extratropics. Lastly, improved understanding of the associated dynamics and thermodynamics relevant to the initiation, propagation and dissipation of Sumatra squalls was gaiend in Chapter 4. Additional interactions with the diurnal cycle and equatorial waves both influence squall line evolution and emphasise the predictability of these events.

Research into mid-level DAIs highlighted the importance of considering the variability between the tropical and extratropical atmosphere on synoptic spatial and temporal scales on regional rainfall patterns, while the scales of importance for ocean-atmosphere interactions in the MC were discussed in Chapter 3. Sumatra squall research has highlighted multi-scale processes and interactions which will benefit effective forecasting and modelling of these high-impact weather systems.

All three of these processes are crucial to examine, as the spatial and temporal scales they operate over, along with the complexities associated with any related scale interactions, limit their predictive skill, compared to larger-scale modes of variability. However, the identified interactions with these more predictive large-scale modes, as well as the diurnal cycle, could improve skill, while better integrating the studied

processes into the broader picture of MC rainfall variability.

The directions of future research related to these topics are numerous, which would help to expand on the knowledge gained through this thesis, or to answer some of the broader questions that remain. Such ideas include modifying approaches used in analysis to assess the credibility of both the employed datasets and methodologies used here, as well as the development of new tools or sensitivity tests to better quantify the importance of various atmospheric and oceanic processes for particular meteorological phenomena. These topics are generally independent from one another, though there is scope for the associated research outcomes and broad themes to be synthesised as suggestions for new studies, requiring deeper conceptualisation.

While future work would also benefit from an increase in the availability of observational data gained through intensive field campaigns, more realistically the usage of the abundance of new state-of-the-art high-resolution, and coupled, CPMs, along with continually developed machine learning techniques, will enable further investigations into the research questions both addressed and suggested. Deeper process knowledge, particular at the finer-scale, is fundamental to improving the model physics and schemes used in NWP, thereby benefiting the weather forecasting community in the region. These benefits will then, further down the line, contribute to better eventual hazard management and mitigation approaches for stakeholders and communities across the MC.

References

Abhik, S., Zhang, C. and Hendon, H. H. (2023), 'The Indo-Pacific Maritime Continent barrier effect on MJO ensemble prediction', *Geophysical Research Letters* **50**, e2023GL105462.

Abramian, S., Muller, C. and Risi, C. (2023), 'Extreme precipitation in tropical squall lines', *Journal of Advances in Modeling Earth Systems* **15**, e2022MS003477.

Adames, A. F. and Maloney, E. D. (2021), 'Moisture mode theory's contribution to advances in our understanding of the Madden-Julian Oscillation and other tropical disturbances', *Current Climate Change Reports* **7**, 72–85.

Adames, A. F. and Wallace, J. M. (2015), 'Three-dimensional structure and evolution of the moisture field in the MJO', *Journal of the Atmospheric Sciences* **72**, 3733–3754.

Aguedjou, H. M. A., Chaigneau, A., Dadou, I., Morel, Y., Baloïtcha, E. and Da-Allada, C. Y. (2023), 'Imprint of mesoscale eddies on air-sea interaction in the tropical Atlantic Ocean', *Remote Sensing* **15**, 3087.

Ajayamohan, R. S., Khouider, B., Praveen, V. and Majda, A. J. (2021), 'Role of diurnal cycle in the Maritime Continent barrier effect on MJO propagation in an AGCM', *Journal of the Atmospheric Sciences* **78**, 1545–1565.

Alfaro, D. A. (2017), 'Low-tropospheric shear in the structure of squall lines: Impacts on latent heating under layer-lifting ascent', *Journal of the Atmospheric Sciences* **74**, 229–248.

Allen, G., Vaughan, G., Brunner, D., May, P. T., Heyes, W., Minnis, P. and Ayers, J. K. (2009), 'Modulation of tropical convection by breaking Rossby waves', *Quarterly Journal of the Royal Meteorological Society* **135**, 125–137.

Appenzeller, C. and Davies, H. (1992), 'Structure of stratospheric intrusions into the troposphere', *Nature* **358**, 570–572.

Arakawa, A. and Schubert, W. H. (1974), 'Interaction of a cumulus cloud ensemble with the large-scale environment, part I', *Journal of the Atmospheric Sciences* **31**, 674–701.

Argüeso, D., Romero, R. and Homar, V. (2020), 'Precipitation features of the Maritime Continent in parameterized and explicit convection models', *Journal of Climate* **33**, 2449–2466.

As-syakur, A. R., Imaoka, K., Ogawara, K., Yamanaka, M. D., Tanaka, T., Kashino, Y., Nuarsa, I. W. and Osawa, T. (2019), 'Analysis of spatial and seasonal differences in the diurnal rainfall cycle over Sumatera revealed by 17-year TRMM 3B42 dataset', *Scientific Online Letters on the Atmosphere* **15**, 216–221.

As-syakur, A. R., Tanaka, T., Osawa, T. and Mahendra, M. S. (2013), 'Indonesian rainfall variability observation using TRMM multi-satellite data', *International Journal of Remote Sensing* **34**, 7723–7738.

Azaneu, M. V., Matthews, A. J., Heywood, K. J., Hall, R. A. and Baranowski, D. B. (2024), 'Impact of a fresh-core mesoscale eddy in modulating oceanic response to a Madden-Julian Oscillation', *Deep Sea Research Part II: Topical Studies in Oceanography* **216**, 105396.

Bai, H., Deranadyan, G., Schumacher, C., Funk, A., Epifanio, C., Ali, A., Endarwin, Radjab, F., Adriyanto, R., Nurhayati, N., Nugraha, Y. and Fauziah, A. (2021), 'Formation of nocturnal offshore rainfall near the west coast of Sumatra: land breeze or gravity wave?', *Monthly Weather Review* **149**, 715–731.

Baidu, M., Schwendike, J., Marsham, J. H. and Bain, C. (2022), 'Effects of vertical wind shear on intensities of mesoscale convective systems over West and Central Africa', *Atmospheric Science Letters* **23**, e1094.

Banacos, P. C. and Schultz, D. M. (2005), 'The use of moisture flux convergence in forecasting convective initiation: historical and operational perspectives', *Weather and Forecasting* **20**, 351–366.

Baranowski, D. B., Flatau, M. K., Flatau, P. J. and Matthews, A. J. (2016), 'Phase locking between atmospheric convectively coupled equatorial Kelvin waves and the diurnal cycle of precipitation over the Maritime Continent', *Geophysical Research Letters* **43**, 8269–8276.

Bernie, D. J., Guilyardi, E., Madec, G., Slingo, J. M. and Woolnough, S. J. (2007), 'Impact of resolving the diurnal cycle in an ocean-atmosphere GCM. Part 1: a diurnally forced OGCM', *Climate Dynamics* **29**, 575–590.

Bernie, D. J., Guilyardi, E., Madec, G., Slingo, J. M., Woolnough, S. J. and Cole, J. (2008), 'Impact of resolving the diurnal cycle in an ocean-atmosphere GCM. Part 2: a diurnally coupled CGCM', *Climate Dynamics* **31**, 909–925.

Berry, G. J. and Reeder, M. J. (2016), 'The dynamics of Australian monsoon bursts', *Journal of the Atmospheric Sciences* **73**, 55–69.

Bessho, K., Date, K., Hayashi, M., Ikeda, A., Imai, T., Inoue, H., Kumagai, Y., Miyakawa, T., Murata, H., Ohno, T., Okuyama, A., Oyama, R., Sasaki, Y., Shimazu, Y., Shimoji, K., Sumida, Y., Suzuki, M., Taniguchi, H., Tsuchiyama, H., Uesawa, D., Yokota, H. and Yoshida, R. (2016), 'An introduction to Himawari-8/9 — Japan's new-generation geostationary meteorological satellites', *Journal of the Meteorological Society of Japan* **94**, 151–183.

Best, M. J., Pryor, M., Clark, D. B., Rooney, G. G., Essery, R. L. H., Menard, C. B., Edwards, J. M., Hendry, M. A., Porson, A., Gedney, N., Mercado, L. M., Sitch, S., Blyth, E., Boucher, O., Cox, P. M., Grimmond, C. S. B. and Harding, R. J. (2011), 'The Joint UK Land Environment Simulator (JULES), model description – Part 1: Energy and water fluxes', *Geoscientific Model Development* **4**, 677–699.

Bickle, M. E., Marsham, J. H., Ross, A. N., Rowell, D. P., Parker, D. J. and Taylor, C. M. (2021), 'Understanding mechanisms for trends in Sahelian squall lines: Roles of thermodynamics and shear', *Quarterly Journal of the Royal Meteorological Society* **147**, 983–1006.

Birch, C. E., Webster, S., Peatman, S. C., Parker, D. J., Matthews, A. J., Li, Y. and Hassim, M. E. (2016), 'Scale interactions between the MJO and the western Maritime Continent', *Journal of Climate* **29**, 2471–2492.

Bithell, M., Gray, L. J. and Cox, B. D. (1999), 'A three-dimensional view of the evolution of midlatitude stratospheric intrusions', *Journal of the Atmospheric Sciences* **56**, 673–688.

Bluestein, H. B. and Jain, M. H. (1985), 'Formation of mesoscale lines of precipitation: severe squall lines in Oklahoma during the spring', *Journal of the Atmospheric Sciences* **42**, 1711–1732.

Boutle, I. A., Eyre, J. E. J. and Lock, A. P. (2014), 'Seamless Stratocumulus Simulation across the Turbulent Gray Zone', *Monthly Weather Review* **142**, 1655–1668.

Brown, R. G. and Zhang, C. (1997), 'Variability of midtropospheric moisture and its effect on cloud-top height distribution during TOGA COARE', *Journal of the Atmospheric Sciences* **54**, 2760–2774.

Browning, K. A. (1997), 'The dry intrusion perspective of extra-tropical cyclone development', *Meteorological Applications* **4**, 317–324.

Bush, M., Boutle, I., Edwards, J., Finnenkoetter, A., Franklin, C., Hanley, K., Jayakumar, A., Lewis, H., Lock, A., Mittermaier, M., Mohandas, S., North, R., Porson, A., Roux, B., Webster, S. and Weeks, M. (2023), 'The second Met Office unified model-JULES regional atmosphere and land configuration, RAL2', *Geoscientific Model Development* **16**, 1713–1734.

Bôas, A. B. V., Sato, O. T., Chaigneau, A. and Castelão, G. P. (2015), 'The signature of mesoscale eddies on the air-sea turbulent heat fluxes in the South Atlantic Ocean', *Geophysical Research Letters* **42**, 1856–1862.

Casey, S. P. F., Dessler, A. E. and Schumacher, C. (2009), 'Five-year climatology of midtroposphere dry air layers in warm tropical ocean regions as viewed by AIRS/Aqua', *Journal of Applied Meteorology and Climatology* **48**, 1831–1842.

Cau, P., Methven, J. and Hoskins, B. (2005), 'Representation of dry tropical layers and their origins in ERA-40 data', *Journal of Geophysical Research: Atmospheres* **110**.

Cau, P., Methven, J. and Hoskins, B. (2007), 'Origins of dry air in the tropics and subtropics', *Journal of Climate* **20**, 2745–2759.

Chan, M. Y., Lo, J. C. F. and Orton, T. (2019), 'The structure of tropical Sumatra squalls', *Weather* **74**, 176–181.

Chelton, D. B., Schlax, M. G., Freilich, M. H. and Milliff, R. F. (2004), 'Satellite measurements reveal persistent small-scale features in ocean winds', *Science* **303**, 978–983.

Chelton, D. B., Schlax, M. G. and Samelson, R. M. (2011), 'Global observations of nonlinear mesoscale eddies', *Progress in Oceanography* **91**, 167–216.

Chelton, D. B., Schlax, M. G., Samelson, R. M. and de Szoeke, R. A. (2007), 'Global observations of large oceanic eddies', *Geophysical Research Letters* **34**.

Chen, B., Xie, L., Zheng, Q., Zhou, L., Wang, L., Feng, B. and Yu, Z. (2020), 'Seasonal variability of mesoscale eddies in the Banda Sea inferred from altimeter data', *Acta Oceanologica Sinica* **39**, 11–20.

Chen, C., Sahany, S., Moise, A. F., Chua, X. R., Hassim, M. E., Lim, G. and Prasanna, V. (2023), 'ENSO–rainfall teleconnection over the Maritime Continent enhances and shifts eastward under warming', *Journal of Climate* **36**, 4635–4663.

Chen, G., Chen, X. and Cao, C. (2022), 'Divergence and dispersion of global eddy propagation from satellite altimetry', *Journal of Physical Oceanography* **52**, 705–722.

Chen, G. and Wang, B. (2019), 'Dynamic moisture mode versus moisture mode in MJO dynamics: importance of the wave feedback and boundary layer convergence feedback', *Climate Dynamics* **52**, 5127–5143.

Chen, S. S., Kerns, B. W., Guy, N., Jorgensen, D. P., Delanoë, J., Viltard, N., Zappa, C. J., Judt, F., Lee, C. Y. and Savarin, A. (2016), 'Aircraft observations of dry air, the ITCZ, convective cloud systems, and cold pools in MJO during DYNAMO', *Bulletin of the American Meteorological Society* **97**, 405–423.

Cheng, Y. H., Ho, C. R., Zheng, Q. and Kuo, N. J. (2014), 'Statistical characteristics of mesoscale eddies in the North Pacific derived from satellite altimetry', *Remote Sensing* **6**, 5164–5183.

Crook, J., Hardy, S., Methven, J., Schwendike, J., Yik, D. J. and Yang, G.-Y. (2025), 'The structure of Borneo vortices and their relationship with cold surges, the Madden–Julian Oscillation and equatorial waves', *Quarterly Journal of the Royal Meteorological Society* **151**, e4905.

Crook, J., Morris, F., Fitzpatrick, R. G. J., Peatman, S. C., Schwendike, J., Stein, T. H., Birch, C. E., Hardy, S. and Yang, G. Y. (2024), 'Impact of the Madden–Julian Oscillation and equatorial waves on tracked mesoscale convective systems over southeast Asia', *Quarterly Journal of the Royal Meteorological Society* **150**, 1724–1751.

Crook, N. A. and Moncrieff, M. E. (1988), 'The effect of large-scale convergence on the generation and maintenance of deep moist convection', *Journal of the Atmospheric Sciences* **45**, 3606–3624.

Danielsen, E. F. (1968), 'Stratospheric-tropospheric exchange based on radioactivity, ozone and potential vorticity', *Journal of the Atmospheric Sciences* **25**, 502–518.

de Vries, A. J., Feldstein, S. B., Riemer, M., Tyrlis, E., Sprenger, M., Baumgart, M., Fnais, M. and Lelieveld, J. (2016), 'Dynamics of tropical-extratropical interactions and extreme precipitation events in Saudi Arabia in autumn, winter and spring', *Quarterly Journal of the Royal Meteorological Society* **142**, 1862–1880.

de Vries, A. J., Ouwersloot, H. G., Feldstein, S. B., Riemer, M., Kenawy, A. M. E., McCabe, M. F. and Lelieveld, J. (2018), 'Identification of tropical-extratropical interactions and extreme precipitation events in the Middle East based on potential

vorticity and moisture transport', *Journal of Geophysical Research: Atmospheres* **123**, 861–881.

Delcroix, T., Chaigneau, A., Soviadan, D., Boutin, J. and Pegliasco, C. (2019), 'Eddy-induced salinity changes in the Tropical Pacific', *Journal of Geophysical Research: Oceans* **124**, 374–389.

DeMott, C. A., Klingaman, N. P., Tseng, W. L., Burt, M. A., Gao, Y. and Randall, D. A. (2019), 'The convection connection: how ocean feedbacks affect tropical mean moisture and MJO propagation', *Journal of Geophysical Research: Atmospheres* **124**, 11910–11931.

Dhame, S., Olonscheck, D. and Rugenstein, M. (2025), 'Higher-resolution climate nodels do not consistently reproduce the observed tropical Pacific warming pattern', *Journal of Climate* **38**, 3131–3149.

Dipankar, A., Webster, S., Huang, X.-Y. and Doan, V. Q. (2019), 'Understanding biases in simulating the diurnal cycle of convection over the western coast of Sumatra: comparison with pre-YMC observation campaign', *Monthly Weather Review* **147**, 1615–1631.

Dipankar, A., Webster, S., Sun, X., Sanchez, C., North, R., Furtado, K., Wilkinson, J., Lock, A., Vosper, S., Huang, X. Y. and Barker, D. (2020), 'SINGV: A convective-scale weather forecast model for Singapore', *Quarterly Journal of the Royal Meteorological Society* **146**, 4131–4146.

Draxler, R. R., Spring, S., Maryland, U. S. A. and Hess, G. D. (1998), 'An overview of the HYSPLIT_4 modelling system for trajectories, dispersion, and deposition', *Australian Meteorological Magazine* **47**, 295–308.

Edwards, J. M. and Slingo, A. (1996), 'Studies with a flexible new radiation code. I: Choosing a configuration for a large-scale model', *Quarterly Journal of the Royal Meteorological Society* **122**, 689–719.

Emam, A. R., Mishra, B. K., Kumar, P., Masago, Y. and Fukushi, K. (2016), 'Impact assessment of climate and land-use changes on flooding behavior in the Upper Ciliwung River, Jakarta, Indonesia', *Water (Switzerland)* **8**, 559.

Fakaruddin, F. J., Nawai, N. A., Abllah, M., Tangang, F. and Juneng, L. (2022), 'Climatological features of squall line at the Borneo coastline during southwest monsoon', *Atmosphere* **13**, 116.

Feng, L., Zhang, T., Koh, T. Y. and Hill, E. M. (2021), 'Selected years of monsoon variations and extratropical dry-air intrusions compared with the Sumatran GPS array observations in Indonesia', *Journal of the Meteorological Society of Japan* **99**, 505–536.

Ferrett, S., Frame, T. H., Methven, J., Holloway, C. E., Webster, S., Stein, T. H. and Cafaro, C. (2021), 'Evaluating convection-permitting ensemble forecasts of precipitation over southeast Asia', *Weather and Forecasting* **36**, 1199–1217.

Ferrett, S., Methven, J., Woolnough, S. J., Yang, G. Y., Holloway, C. E. and Wolf, G. (2023), 'Hybrid dynamical-statistical forecasts of the risk of rainfall in southeast Asia dependent on equatorial waves', *Monthly Weather Review* **151**, 2139–2152.

Ferrett, S., Yang, G. Y., Woolnough, S. J., Methven, J., Hodges, K. and Holloway, C. E. (2020), 'Linking extreme precipitation in southeast Asia to equatorial waves', *Quarterly Journal of the Royal Meteorological Society* **146**, 665–684.

Ffield, A. and Gordon, A. L. (1996), 'Tidal mixing signatures in the Indonesian seas', *Journal of Physical Oceanography* **26**, 1924–1937.

Fink, A. H. and Reiner, A. (2003), 'Spatiotemporal variability of the relation between African Easterly Waves and West African Squall Lines in 1998 and 1999', *Journal of Geophysical Research: Atmospheres* **108**, 4332.

Fletcher, J. K., Parker, D. J., Hunt, K. M., Vishwanathan, G. and Govindankutty, M. (2018), 'The interaction of Indian monsoon depressions with northwesterly midlevel dry intrusions', *Monthly Weather Review* **146**, 679–693.

Fletcher, J. K., Parker, D. J., Turner, A. G., Menon, A., Martin, G. M., Birch, C. E., Mitra, A. K., Mrudula, G., Hunt, K. M., Taylor, C. M., Houze, R. A., Brodzik, S. R. and Bhat, G. S. (2020), 'The dynamic and thermodynamic structure of the monsoon over southern India: new observations from the INCOMPASS IOP', *Quarterly Journal of the Royal Meteorological Society* **146**, 2867–2890.

Frenger, I., Gruber, N., Knutti, R. and Münnich, M. (2013), 'Imprint of Southern Ocean eddies on winds, clouds and rainfall', *Nature Geoscience* **6**, 608–612.

Fu, L. L., Chelton, D. B., Traon, P. Y. L. and Morrow, R. (2010), 'Eddy dynamics from satellite altimetry', *Oceanography* **23**, 15–25.

Fujita, M., Kimura, F. and Yoshizaki, M. (2010), 'Morning precipitation peak over the strait of Malacca under a calm condition', *Monthly Weather Review* **138**, 1474–1486.

Funatsu, B. M. and Waugh, D. W. (2008), 'Connections between potential vorticity intrusions and convection in the eastern tropical Pacific', *Journal of the Atmospheric Sciences* **65**, 987–1002.

Galvin, J. F. (2009), 'The weather and climate of the tropics: Part 8 - Mesoscale weather systems', *Weather* **64**, 32–38.

Geng, B., Katsumata, M. and Taniguchi, K. (2020), 'Modulation of the diurnal cycle of precipitation near the southwestern coast of Sumatra by mixed Rossby-gravity waves', *Journal of the Meteorological Society of Japan* **98**, 463–480.

Ghosh, R. and Shepherd, T. G. (2023), 'Storylines of Maritime Continent dry period precipitation changes under global warming', *Environmental Research Letters* **18**, 034017.

Gill, A. (1980), 'Some simple solutions for heat-induced tropical circulation', *Quart. J. R. Met. Soc* **106**, 447–462.

Godfrey, J. S. (1996), 'The effect of the Indonesian throughflow on ocean circulation and heat exchange with the atmosphere: A review', *Journal of Geophysical Research: Oceans* **101**, 12217–12237.

Golding, B., Mittermaier, M., Ross, C., Ebert, B., Panchuk, S., Scolobig, A. and Johnston, D. (2019), 'A value chain approach to optimising early warning systems', *Global Assessment Report on Disaster Risk Reduction* .

Gonzalez, P. L., Howard, E., Ferrett, S., Frame, T. H., Martínez-Alvarado, O., Methven, J. and Woolnough, S. J. (2023), 'Weather patterns in southeast Asia: enhancing high-impact weather subseasonal forecast skill', *Quarterly Journal of the Royal Meteorological Society* **149**, 19–39.

Gordon, A. L. (2005), 'Oceanography of the Indonesian seas and their throughflow', *Oceanography* **18**, 14–27.

Grant, L. D., Lane, T. P. and van den Heever, S. C. (2018), 'The role of cold pools in tropical oceanic convective systems', *Journal of the Atmospheric Sciences* **75**, 2615–2634.

Gray, W. M. and Jacobson, R. W. (1977), 'Diurnal variation of deep cumulus convection', *Monthly Weather Review* **105**, 1171–1188.

Gulakaram, V. S., Vissa, N. K. and Bhaskaran, P. K. (2018), 'Role of mesoscale eddies on atmospheric convection during summer monsoon season over the Bay of Bengal: a case study', *Journal of Ocean Engineering and Science* **3**, 343–354.

Gulakaram, V. S., Vissa, N. K. and Bhaskaran, P. K. (2023), 'Mesoscale eddies with anomalous sea surface temperature and its relation with atmospheric convection over the North Indian Ocean', *International Journal of Climatology* **43**, 3094–3113.

Hai, O. S., Samah, A. A., Chenoli, S. N., Subramaniam, K. and Mazuki, M. Y. A. (2017), 'Extreme rainstorms that caused devastating flooding across the east coast of Peninsular Malaysia during November and December 2014', *Weather and Forecasting* **32**, 849–872.

Halo, I., Penven, P., Backeberg, B., Ansorge, I., Shillington, F. and Roman, R. (2014), 'Mesoscale eddy variability in the southern extension of the East Madagascar Current: Seasonal cycle, energy conversion terms, and eddy mean properties', *Journal of Geophysical Research: Oceans* **119**, 7324–7356.

Hamel, P. and Tan, L. (2022), 'Blue–green infrastructure for flood and water quality management in southeast Asia: evidence and knowledge gaps', *Environmental Management* **69**, 699–718.

Hao, Z., Xu, Z., Feng, M., Li, Q. and Yin, B. (2021), 'Spatiotemporal variability of mesoscale eddies in the Indonesian seas', *Remote Sensing* **13**, 1017.

Hao, Z., Xu, Z., Feng, M., Zhang, P. and Yin, B. (2022), 'Dynamics of interannual eddy kinetic energy variability in the Sulawesi Sea revealed by OFAM3', *Journal of Geophysical Research: Oceans* **127**, e2022JC018815.

Hardy, S., Methven, J., Schwendike, J., Harvey, B. and Cullen, M. (2023), 'Examining the dynamics of a Borneo vortex using a balance approximation tool', *Weather and Climate Dynamics* **4**, 1019–1043.

Hashim, J. H. and Hashim, Z. (2014), 'Climate change, extreme weather events, and human health implications in the Asia Pacific region', *Asia-Pacific Journal of Public Health* **28**, 8S–14S.

Hassim, M. E., Lane, T. P. and Grabowski, W. W. (2016), 'The diurnal cycle of rainfall over New Guinea in convection-permitting WRF simulations', *Atmospheric Chemistry and Physics* **16**, 161–175.

Hastings, D. A. and Dunbar, P. K. (1999), 'Global land one-kilometer base elevation (GLOBE). Key to geophysical records documentation, No. 34'.
URL: *https://repository.library.noaa.gov/view/noaa/13424*

Hausmann, U. and Czaja, A. (2012), 'The observed signature of mesoscale eddies in sea surface temperature and the associated heat transport', *Deep-Sea Research Part I: Oceanographic Research Papers* **70**, 60–72.

Haylock, M. and McBride, J. (2001), 'Spatial coherence and predictability of Indonesian wet season rainfall', *Journal of Climate* **14**, 3882–3887.

He, Q., Zhan, H., Cai, S., He, Y., Huang, G. and Zhan, W. (2018), 'A new assessment of mesoscale eddies in the South China Sea: Surface features, three-dimensional structures, and thermohaline transports', *Journal of Geophysical Research: Oceans* **123**, 4906–4929.

Hendon, H. H. (2003), 'Indonesian rainfall variability: impacts of ENSO and local air-sea interaction', *Journal of Climate* **16**, 1775–1790.

Hendon, H. H. and Glick, J. (1997), 'Intraseasonal air-sea interaction in the tropical Indian and Pacific oceans', *Journal of Climate* **10**, 647–661.

Hendon, H. H. and Salby, M. L. (1994), 'The life cycle of the Madden–Julian Oscillation', *American Meteorological Society* **51**, 2225–2237.

Hersbach, H., Bell, B., Berrisford, P., Hirahara, S., Horányi, A., Muñoz-Sabater, J., Nicolas, J., Peubey, C., Radu, R., Schepers, D., Simmons, A., Soci, C., Abdalla, S., Abellan, X., Balsamo, G., Bechtold, P., Biavati, G., Bidlot, J., Bonavita, M., Chiara, G. D., Dahlgren, P., Dee, D., Diamantakis, M., Dragani, R., Flemming, J., Forbes, R., Fuentes, M., Geer, A., Haimberger, L., Healy, S., Hogan, R. J., Hólm, E., Janisková, M., Keeley, S., Laloyaux, P., Lopez, P., Lupu, C., Radnoti, G., de Rosnay, P., Rozum, I., Vamborg, F., Villaume, S. and Thépaut, J. N. (2020), 'The ERA5 global reanalysis', *Quarterly Journal of the Royal Meteorological Society* **146**, 1999–2049.

Holloway, C. E., Wing, A. A., Bony, S., Muller, C., Masunaga, H., L'Ecuyer, T. S., Turner, D. D. and Zuidema, P. (2017), 'Observing convective aggregation', *Surveys in Geophysics* **38**, 1199–1236.

Holloway, C. E., Woolnough, S. J. and Lister, G. M. (2012), 'Precipitation distributions for explicit versus parametrized convection in a large-domain high-resolution tropical case study', *Quarterly Journal of the Royal Meteorological Society* **138**, 1692–1708.

Holloway, C. E., Woolnough, S. J. and Lister, G. M. S. (2013), 'The effects of explicit versus parameterized convection on the MJO in a large-domain high-resolution tropical case study. Part I: characterization of large-scale organization and propagation', *Journal of the Atmospheric Sciences* **70**, 1342–1369.

Homeyer, C. R. and Bowman, K. P. (2013), 'Rossby wave breaking and transport between the tropics and extratropics above the subtropical jet', *Journal of the Atmospheric Sciences* **70**, 607–626.

Houze, R. A. (2004), 'Mesoscale convective systems', *Reviews of Geophysics* **42**, 1–43.

Houze, R. A. (2018), '100 years of research on mesoscale convective systems', *Meteorological Monographs* **59**, 17.1–17.54.

Howard, E., Woolnough, S., Klingaman, N., Shipley, D., Sanchez, C., Peatman, S. C., Birch, C. E. and Matthews, A. J. (2024), 'Evaluation of multi-season convection-permitting atmosphere - mixed-layer ocean simulations of the Maritime Continent', *Geoscientific Model Development* **17**(9), 3815–3837.

Hsu, J., Chen, C. A., Lan, C. W., Chiang, C. L., Li, C. H. and Lo, M. H. (2025), 'Impact of land use changes and global warming on extreme precipitation patterns in the Maritime Continent', *npj Climate and Atmospheric Science* **8**, 5.

Huang, X.-Y., Barker, D., Webster, S., Dipankar, A., Lock, A., Mittermaier, M., Sun, X., North, R., Darvell, R., Boyd, D., Lo, J., Liu, J., Macpherson, B., Heng, P., Maycock, A., Pitcher, L., Tubbs, R., McMillan, M., Zhang, S., Hagelin, S., Porson, A., Song, G., Beckett, B., Cheong, W. K., Semple, A. and Gordon, C. (2019), 'SINGV – the convective-scale numerical weather prediction system for Singapore', *ASEAN Journal on Science and Technology for Development* **36**, 81–90.

Huffman, G. J., Bolvin, D. T., Braithwaite, D., Hsu, K., Joyce, R., Kidd, C., Nelkin, E. J., Sorooshian, S., Tan, J. and Xie, P. (2020), 'NASA Global Precipitation Measurement (GPM) Integrated Multi-satellitE Retrievals for GPM (IMERG): Algorithm Theoretical Basis Document (ATBD) Version 06'.
URL: *https://gpm.nasa.gov/sites/default/files/document_files/IMERG_ATBD_V06.pdf*

Ichikawa, H. and Yasunari, T. (2006), 'Time-space characteristics of diurnal rainfall over Borneo and surrounding oceans as observed by TRMM-PR', *Journal of Climate* **19**, 1238–1260.

Ismail, M. F. A., Ribbe, J., Arifin, T., Taofiqurohman, A. and Anggoro, D. (2021), 'A census of eddies in the tropical eastern boundary of the Indian Ocean', *Journal of Geophysical Research: Oceans* **126**, e2021JC017204.

Jang, S., Ekyalongo, Y. and Kim, H. (2021), 'Systematic review of displacement and health impact from natural disasters in southeast Asia', *Disaster Medicine and Public Health Preparedness* **15**, 105–114.

Jia, X. J., Ge, J. W. and Wang, S. (2016), 'Diverse impacts of ENSO on wintertime rainfall over the Maritime Continent', *International Journal of Climatology* **36**, 3384–3397.

Jiang, Y., Zhang, S., ping Xie, S., Chen, Y. and Liu, H. (2019), 'Effects of a cold ocean eddy on local atmospheric boundary layer near the Kuroshio Extension: in situ observations and model experiments', *Journal of Geophysical Research: Atmospheres* **124**, 5779–5790.

Jin, F. and Hoskins, B. J. (1995), 'The direct response to tropical heating in a baroclinic atmosphere', *Journal of the Atmospheric Sciences* **52**, 307–319.

Jochum, M. and Potemra, J. (2008), 'Sensitivity of tropical rainfall to Banda Sea diffusivity in the Community Climate System Model', *Journal of Climate* **21**, 6445–6454.

Johnson, R. H., Ciesielski, P. E. and Cotturone, J. A. (2001), 'Multiscale variability of the atmospheric mixed layer over the western Pacific warm pool', *Journal of the Atmospheric Sciences* **58**, 2729–2750.

Johnson, R. H., Rickenbach, T. M., Rutledge, S. A., Ciesielski, P. E. and Schubert, W. H. (1999), 'Trimodal characteristics of tropical convection', *Journal of Climate* **12**, 2397–2418.

Kang, S., Im, E. S. and Eltahir, E. A. (2019), 'Future climate change enhances rainfall seasonality in a regional model of western Maritime Continent', *Climate Dynamics* **52**, 747–764.

Karlowska, E., Matthews, A. J., Webber, B. G., Graham, T. and Xavier, P. (2024), 'Two-way feedback between the Madden–Julian Oscillation and diurnal warm layers in a coupled ocean–atmosphere model', *Quarterly Journal of the Royal Meteorological Society* **150**, 4113–4132.

Kerns, B. W. and Chen, S. S. (2014), 'Equatorial dry air intrusion and related synoptic variability in MJO initiation during DYNAMO', *Monthly Weather Review* **142**, 1326–1343.

Kiladis, G. N., Wheeler, M. C., Haertel, P. T., Straub, K. H. and Roundy, P. E. (2009), 'Convectively coupled equatorial waves', *Reviews of Geophysics* **47**.

Klingaman, N. P. and DeMott, C. A. (2020), 'Mean state biases and interannual variability affect perceived sensitivities of the Madden-Julian Oscillation to air-sea coupling', *Journal of Advances in Modeling Earth Systems* **12**, e2019MS001799.

Klingaman, N. P. and Woolnough, S. J. (2014), 'The role of air-sea coupling in the simulation of the Madden-Julian Oscillation in the Hadley Centre model', *Quarterly Journal of the Royal Meteorological Society* **140**, 2272–2286.

Knippertz, P. (2007), 'Tropical-extratropical interactions related to upper-level troughs at low latitudes', *Dynamics of Atmospheres and Oceans* **43**, 36–62.

Koch-Larrouy, A., Lengaigne, M., Terray, P., Madec, G. and Masson, S. (2010), 'Tidal mixing in the Indonesian seas and its effect on the tropical climate system', *Climate Dynamics* **34**, 891–904.

Koh, T.-Y. and Teo, C.-K. (2009), 'Toward a mesoscale observation network in south-east Asia', *Bulletin of the American Meteorological Society* **90**, 481–488.

Koseki, S., Koh, T. Y. and Teo, C. K. (2013), 'Effects of the cold tongue in the South China Sea on the monsoon, diurnal cycle and rainfall in the Maritime Continent', *Quarterly Journal of the Royal Meteorological Society* **139**, 1566–1582.

Kumar, K. N., Phanikumar, D. V., Sharma, S., Basha, G., Naja, M., Ouarda, T. B., Ratnam, M. V. and kumar, K. K. (2019), 'Influence of tropical-extratropical interactions on the dynamics of extreme rainfall event: A case study from Indian region', *Dynamics of Atmospheres and Oceans* **85**, 28–40.

Kurian, J., Colas, F., Capet, X., McWilliams, J. C. and Chelton, D. B. (2011), 'Eddy properties in the California current system', *Journal of Geophysical Research: Oceans* **116**.

Kuznetsova, D., Dauhut, T. and Chaboureau, J. P. (2019), 'The three atmospheric circulations over the Indian Ocean and the Maritime Continent and their modulation by the passage of the MJO', *Journal of the Atmospheric Sciences* **76**, 517–531.

Latos, B., Lefort, T., Flatau, M. K., Flatau, P. J., Permana, D. S., Baranowski, D. B., Paski, J. A. I., Makmur, E., Sulystyo, E., Peyrillé, P., Feng, Z., Matthews, A. J. and Schmidt, J. M. (2021), 'Equatorial waves triggering extreme rainfall and floods in southwest Sulawesi, Indonesia', *Monthly Weather Review* **149**, 1381–1401.

Latos, B., Peyrillé, P., Lefort, T., Baranowski, D. B., Flatau, M. K., Flatau, P. J., Riama, N. F., Permana, D. S., Rydbeck, A. V. and Matthews, A. J. (2023), 'The role of tropical waves in the genesis of Tropical Cyclone Seroja in the Maritime Continent', *Nature Communications* **14**, 856.

Lee, T., Fournier, S., Gordon, A. L. and Sprintall, J. (2019), 'Maritime Continent water cycle regulates low-latitude chokepoint of global ocean circulation', *Nature Communications* **10**.

Li, D., Chen, Y., Messmer, M., Zhu, Y., Feng, J., Yin, B. and Bevacqua, E. (2022), 'Compound wind and precipitation extremes across the Indo-Pacific: climatology, variability, and drivers', *Geophysical Research Letters* **49**, e2022GL098594.

Li, X., Lu, R., Chen, G. and Chen, R. (2024), 'Western North Pacific tropical cyclones suppress Maritime Continent rainfall', *npj Climate and Atmospheric Science* **7**, 251.

Li, X., Wang, X. and Babovic, V. (2018), 'Analysis of variability and trends of precipitation extremes in Singapore during 1980–2013', *International Journal of Climatology* **38**, 125–141.

Li, Y., Gupta, A. S., Taschetto, A. S., Jourdain, N. C., Luca, A. D., Done, J. M. and Luo, J. J. (2020), 'Assessing the role of the ocean–atmosphere coupling frequency in the western Maritime Continent rainfall', *Climate Dynamics* **54**, 4935–4952.

Li, Y., Jourdain, N. C., Taschetto, A. S., Gupta, A. S., Argüeso, D., Masson, S. and Cai, W. (2017), 'Resolution dependence of the simulated precipitation and diurnal cycle over the Maritime Continent', *Climate Dynamics* **48**, 4009–4028.

Liang, S., Wang, D., Ziegler, A. D., Li, L. Z. and Zeng, Z. (2022), 'Madden–Julian Oscillation-induced extreme rainfalls constrained by global warming mitigation', *npj Climate and Atmospheric Science* **5**, 67.

Lilly, D. K. (1962), 'On the numerical simulation of buoyant convection', *Tellus* **14**, 148–172.

Lindzen, R. S. and Nigam, S. (1987), 'On the role of sea surface temperature gradients in forcing low-level winds and convergence in the Tropics', *Journal of the Atmospheric Sciences* **44**, 2418–2436.

Liu, H., Li, W., Chen, S., Fang, R. and Li, Z. (2018), 'Atmospheric response to mesoscale ocean eddies over the South China Sea', *Advances in Atmospheric Sciences* **35**, 1189–1204.

Liu, J., Chen, G., Han, G. and Zhang, B. (2021), 'An eddy perspective of global air-sea covariation', *Journal of Meteorological Research* **35**, 882–895.

Liu, X., Chang, P., Kurian, J., Saravanan, R. and Lin, X. (2018), 'Satellite-observed precipitation response to ocean mesoscale eddies', *Journal of Climate* **31**, 6879–6895.

Liu, Y., Yu, L. and Chen, G. (2020), 'Characterization of sea surface temperature and air-sea heat flux anomalies associated with mesoscale eddies in the South China Sea', *Journal of Geophysical Research: Oceans* **125**.

Lo, J. C. F. and Orton, T. (2016), 'The general features of tropical Sumatra squalls', *Weather* **71**, 175–178.

Lock, A. P., Brown, A. R., Bush, M. R., Martin, G. M. and Smith, R. N. B. (2000), 'A New Boundary Layer Mixing Scheme. Part I: Scheme Description and Single-Column Model Tests', *Monthly Weather Review* **128**, 3187–3199.

Love, B. S., Matthews, A. J. and Lister, G. M. (2011), 'The diurnal cycle of precipitation over the Maritime Continent in a high-resolution atmospheric model', *Quarterly Journal of the Royal Meteorological Society* **137**, 934–947.

Lu, J., Li, T. and Shen, X. (2023), 'Precipitation diurnal cycle over the Maritime Continent modulated by ENSO', *Climate Dynamics* **61**, 2547–2564.

Lucas, C. and Zipser, E. J. (2000), 'Environmental variability during TOGA COARE', *Journal of the Atmospheric Sciences* **57**, 2333–2350.

Lucas, C., Zipser, E. J. and Ferrier, B. S. (2000), 'Sensitivity of tropical West Pacific oceanic squall lines to tropospheric wind and moisture profiles', *Journal of the Atmospheric Sciences* **57**, 2351–2373.

Ma, J., Xu, H. and Dong, C. (2016), 'Seasonal variations in atmospheric responses to oceanic eddies in the Kuroshio Extension', *Tellus, Series A: Dynamic Meteorology and Oceanography* **68**.

Ma, J., Xu, H., Dong, C., Lin, P. and Liu, Y. (2015), 'Atmospheric responses to oceanic eddies in the Kuroshio Extension region', *Journal of Geophysical Research: Atmospheres* **120**, 6313–6330.

Ma, L. and Jiang, Z. (2021), 'Reevaluating the impacts of oceanic vertical resolution on the simulation of Madden–Julian Oscillation eastward propagation in a climate system model', *Climate Dynamics* **56**, 2259–2278.

Madden, R. A. and Julian, P. R. (1971), 'Detection of a 40–50 day oscillation in the zonal wind in the tropical Pacific', *Journal of the Atmospheric Sciences* **28**, 702–708.

Madden, R. A. and Julian, P. R. (1972), 'Description of global-scale circulation cells in the Tropics with a 40–50 day period', *Journal of the Atmospheric Sciences* **29**, 1109–1123.

Madden, R. A. and Julian, P. R. (1994), 'Observations of the 40–50-day tropical oscillation - a review', *Monthly Weather Review* **122**, 814–837.

Maddox, R. A. (1983), 'Large-scale meteorological conditions associated with midlatitude, mesoscale convective complexes', *Monthly Weather Review* **111**, 1475–1493.

Majda, A. J. and Stechmann, S. N. (2009), 'A simple dynamical model with features of convective momentum transport', *Journal of the Atmospheric Sciences* **66**, 373–392.

Makarim, S., Sprintall, J., Liu, Z., Yu, W., Santoso, A., Yan, X. H. and Susanto, R. D. (2019), 'Previously unidentified Indonesian Throughflow pathways and freshening in the Indian Ocean during recent decades', *Scientific Reports* **9**.

Maloney, E. D. and Hartmann, D. L. (1998), 'Frictional moisture convergence in a composite life cycle of the Madden-Julian Oscillation', *Journal of Climate* **11**, 2387–2403.

Mapes, B. E., Chung, E. S., M., W. M. H., Masunaga, H., Wimmers, A. J. and Velden, C. S. (2018), 'The meandering margin of the meteorological moist tropics', *Geophysical Research Letters* **45**, 1177–1184.

Mapes, B. E., Warner, T. T. and Xu, M. (2003), 'Diurnal patterns of rainfall in northwestern South America. Part III: Diurnal gravity waves and nocturnal convection offshore', *Monthly Weather Review* **131**, 830–844.

Mapes, B. E. and Zuidema, P. (1996), 'Radiative-dynamical consequences of dry tongues in the tropical troposphere', *Journal of the Atmospheric Sciences* **53**, 620–638.

Marzuki, M., Suryanti, K., Yusnaini, H., Tangang, F., Muharsyah, R., Vonnisa, M. and Devianto, D. (2021), 'Diurnal variation of precipitation from the perspectives of precipitation amount, intensity and duration over Sumatra from rain gauge observations', *International Journal of Climatology* **41**, 4386–4397.

Mason, E., Pascual, A., Gaube, P., Ruiz, S., Pelegrí, J. L. and Delepoulle, A. (2017), 'Subregional characterization of mesoscale eddies across the Brazil-Malvinas Confluence', *Journal of Geophysical Research: Oceans* **122**, 3329–3357.

Mason, E., Pascual, A. and McWilliams, J. C. (2014), 'A new sea surface height-based code for oceanic mesoscale eddy tracking', *Journal of Atmospheric and Oceanic Technology* **31**, 1181–1188.

Matsuno, T. (1966), 'Quasi-geostrophic motions in the equatorial area', *Journal of the Meteorological Society of Japan* **44**, 25–43.

Matthews, A. J. (2000), 'Propagation mechanisms for the Madden-Julian Oscillation', *Q. J. R. Meteorol. Soc.* **126**, 2637–2651.

McGillicuddy, D. J. (2016), 'Mechanisms of physical-biological-biogeochemical interaction at the oceanic mesoscale', *Annual Review of Marine Science* **8**, 125–159.

McPhaden, M. J., Zebiak, S. E. and Glantz, M. H. (2006), 'ENSO as an integrating concept in Earth science', *Science* **314**, 1740–1745.

Melnichenko, O., Amores, A., Maximenko, N., Hacker, P. and Potemra, J. (2017), 'Signature of mesoscale eddies in satellite sea surface salinity data', *Journal of Geophysical Research: Oceans* **122**, 1416–1424.

Mori, S., Jun-Ichi, H., Yamanaka, M. D., Okamoto, N., Murata, F., Sakurai, N. and Hashiguchi, H. (2004), 'Diurnal land-sea rainfall peak migration over Sumatera island, Indonesian Maritime Continent, observed by TRMM satellite and intensive rawinsonde soundings', *Monthly Weather Review* **132**, 2021–2039.

MSS (2019), 'Warmer days expected in the coming fortnight'.
URL: *https://www.nea.gov.sg/media/news/advisories/index/warmer-days-expected-in-the-coming-fortnight*

Mulholland, J. P., Peters, J. M. and Morrison, H. (2021), 'How does vertical wind shear influence entrainment in squall lines?', *Journal of the Atmospheric Sciences* **78**, 1931–1946.

Murata, F., Yamanaka, M. D., Mori, S., Kudsy, M., Sribimawati, T. and Suhardi, B. (2006), 'Dry intrusions following eastward-propagating synoptic-scale cloud systems over Sumatera island', *Journal of the Meteorological Society of Japan* **84**, 277–294.

Mustafa, J. M., Matthews, A. J., Hall, R. A., Heywood, K. J. and Azaneu, M. V. (2024), 'Characterisation of the observed diurnal cycle of precipitation over the Maritime Continent', *Quarterly Journal of the Royal Meteorological Society* **150**, 2602–2624.

Nagai, T., Hibiya, T. and Syamsudin, F. (2021), 'Direct estimates of turbulent mixing in the Indonesian archipelago and its role in the transformation of the indonesian throughflow waters', *Geophysical Research Letters* **48**.

Nakamura, Y. and Takayabu, Y. N. (2022*a*), 'Convective couplings with equatorial Rossby waves and equatorial Kelvin waves. Part I: Coupled wave structures', *Journal of the Atmospheric Sciences* **79**, 247–262.

Nakamura, Y. and Takayabu, Y. N. (2022*b*), 'Convective couplings with equatorial Rossby waves and equatorial Kelvin waves. Part II: Coupled precipitation characteristics', *Journal of the Atmospheric Sciences* **79**, 2919–2933.

Napitu, A. M., Gordon, A. L. and Pujiana, K. (2015), 'Intraseasonal sea surface temperature variability across the Indonesian seas', *Journal of Climate* **28**, 8710–8727.

Narulita, I. and Ningrum, W. (2018), 'Extreme flood event analysis in Indonesia based on rainfall intensity and recharge capacity', *IOP Conference Series: Earth and Environmental Science* **118**, 012045.

Natoli, M. B. and Maloney, E. D. (2023), 'The tropical diurnal cycle under varying states of the monsoonal background wind', *Journal of the Atmospheric Sciences* **80**, 235–258.

Ndarana, T. and Waugh, D. W. (2011), 'A climatology of Rossby wave breaking on the Southern Hemisphere tropopause', *Journal of the Atmospheric Sciences* **68**, 798–811.

Neale, R. and Slingo, J. (2003), 'The Maritime Continent and its role in the global climate: a GCM study', *Journal of Climate* **16**, 834–848.

Nencioli, F., Dong, C., Dickey, T., Washburn, L. and Mcwilliams, J. C. (2010), 'A vector geometry-based eddy detection algorithm and its application to a high-resolution numerical model product and high-frequency radar surface velocities in the Southern California bight', *Journal of Atmospheric and Oceanic Technology* **27**, 564–579.

Nesbitt, S. W., Cifelli, R. and Rutledge, S. A. (2006), 'Storm morphology and rainfall characteristics of TRMM precipitation features', *Monthly Weather Review* **134**, 2702–2721.

Nesbitt, S. W. and Zipser, E. J. (2003), 'The diurnal cycle of rainfall and convective intensity according to three years of TRMM measurements', *Journal of Climate* **16**, 1456–1475.

Ngai, S. T., Juneng, L., Tangang, F., Chung, J. X., Supari, S., Salimun, E., Cruz, F., Ngo-Duc, T., Phan-Van, T., Santisirisomboon, J. and Gunawan, D. (2022), 'Projected mean and extreme precipitation based on bias-corrected simulation outputs of CORDEX southeast Asia', *Weather and Climate Extremes* **37**, 100484.

Nguyen, H., Hassim, M. E., Huan, J. Y., Chua, X. R., Chen, C., Wheeler, M. C., Murphy, B. F., Sahany, S., Moise, A. F. and Peatman, S. C. (2025), 'Large-scale to local factors influencing Sumatra squalls affecting Singapore', *Climate Dynamics* **63**, 286.

Ni, Q., Zhai, X., Wang, G. and Marshall, D. P. (2020), 'Random movement of mesoscale eddies in the global ocean', *Journal of Physical Oceanography* **50**, 2341–2357.

NOAA (2019), 'El Niño regions'.
URL: *https://www.cpc.ncep.noaa.gov/products/analysis_monitoring/ensostuff/nino_regions.shtml*

Nor, M. F. F. M., Holloway, C. E. and Inness, P. M. (2020), 'The role of local orography on the development of a severe rainfall event over Western Peninsular Malaysia: A case study', *Monthly Weather Review* **148**, 2191–2209.

Numaguti, A. (1995), 'Characteristics of 4-to-20-day-period disturbances observed in the equatorial Pacific during the TOGA COARE IOP', *Journal of the Meteorological Society of Japan* **73**, 353–377.

Oh, J. H., Kim, K. Y. and Lim, G. H. (2012), 'Impact of MJO on the diurnal cycle of rainfall over the western Maritime Continent in the austral summer', *Climate Dynamics* **38**, 1167–1180.

Okugawa, R., Yasunaga, K., Hamada, A. and Yokoi, S. (2024), 'Numerical study on the precipitation concentration over the western coast of Sumatra island', *Monthly Weather Review* **152**, 689–704.

Pang, C., Nikurashin, M., Pena-Molino, B. and Sloyan, B. M. (2022), 'Remote energy sources for mixing in the Indonesian Seas', *Nature Communications* **13**, 6535.

Park, K. A., Cornillon, P. and Codiga, D. L. (2006), 'Modification of surface winds near ocean fronts: Effects of Gulf Stream rings on scatterometer (QuikSCAT, NSCAT) wind observations', *Journal of Geophysical Research: Oceans* **111**.

Parker, D. J., Willetts, P., Birch, C., Turner, A. G., Marsham, J. H., Taylor, C. M., Kolusu, S. and Martin, G. M. (2016), 'The interaction of moist convection and mid-level dry air in the advance of the onset of the Indian monsoon', *Quarterly Journal of the Royal Meteorological Society* **142**, 2256–2272.

Parsons, D. B., Yoneyama, K. and Redelsperger, J.-L. (2000), 'The evolution of the tropical western Pacific atmosphere-ocean system following the arrival of a dry intrusion', *Q. J. R. Meteorol. Soc* **126**, 517–548.

Paski, J. A. I., Permana, D. S., Alfuadi, N., Handoyo, M. F., Nurrahmat, M. H. and Makmur, E. E. (2021), 'A Multiscale analysis of the extreme rainfall triggering flood and landslide events over bengkulu on 27th April 2019', *AIP Conference Proceedings* **2320**, 040019.

Pearson, K. J., Lister, G. M., Birch, C. E., Allan, R. P., Hogan, R. J. and Woolnough, S. J. (2014), 'Modelling the diurnal cycle of tropical convection across the 'grey zone", *Quarterly Journal of the Royal Meteorological Society* **140**, 491–499.

Peatman, S. C., Birch, C. E., Schwendike, J., Marsham, J. H., Dearden, C., Webster, S., Neely, R. R. and Matthews, A. J. (2023), 'The role of density currents and gravity waves in the offshore propagation of convection over Sumatra', *Monthly Weather Review* **151**, 1757–1777.

Peatman, S. C., Birch, C. E., Schwendike, J., Marsham, J. H., Howard, E., Woolnough, S. J., Mustafa, J. M. and Matthews, A. J. (2025), 'Physical controls on the variability of offshore propagation of convection from Sumatra', *Journal of Geophysical Research: Atmospheres* **130**, e2024JD042458.

Peatman, S. C., Matthews, A. J. and Stevens, D. P. (2014), 'Propagation of the Madden-Julian Oscillation through the Maritime Continent and scale interaction with the diurnal cycle of precipitation', *Quarterly Journal of the Royal Meteorological Society* **140**, 814–825.

Peatman, S. C., Schwendike, J., Birch, C. E., Marsham, J. H., Matthews, A. J. and Yang, G.-Y. (2021), 'A local-to-large scale view of Maritime Continent rainfall: control by ENSO, MJO and equatorial waves', *Journal of Climate* **34**, 8933–8953.

Pegion, K. and Kirtman, B. P. (2008), 'The impact of air-sea interactions on the simulation of tropical intraseasonal variability', *Journal of Climate* **21**, 6616–6635.

Pegliasco, C., Chaigneau, A., Morrow, R. and Dumas, F. (2021), 'Detection and tracking of mesoscale eddies in the Mediterranean Sea: A comparison between the Sea Level Anomaly and the Absolute Dynamic Topography fields', *Advances in Space Research* **68**, 401–419.

Pegliasco, C., Delepoulle, A., Mason, E., Morrow, R., Faugère, Y. and Dibarboure, G. (2022), 'META3.1exp: a new global mesoscale eddy trajectory atlas derived from altimetry', *Earth System Science Data* **14**, 1087–1107.

Penven, P., Echevin, V., Pasapera, J., Colas, F. and Tam, J. (2005), 'Average circulation, seasonal cycle, and mesoscale dynamics of the Peru Current System: A modeling approach', *Journal of Geophysical Research: Oceans* **110**, 1–21.

Pohl, B., Fauchereau, N., Richard, Y., Rouault, M. and Reason, C. J. (2009), 'Interactions between synoptic, intraseasonal and interannual convective variability over Southern Africa', *Climate Dynamics* **33**, 1033–1050.

Pratiwi, A. (2023), 'Identifying precursor of Sumatra squall line', *E3S Web of Conferences* **464**, 19002.

Purba, N. P., Faizal, I., Damanik, F. S., Rachim, F. R. and Mulyani, P. G. (2020), 'Overview of oceanic eddies in Indonesia seas based on the sea surface temperature and sea surface height', *World Scientific News* **147**, 166–178.

Qian, J. H. (2008), 'Why precipitation is mostly concentrated over islands in the Maritime Continent', *Journal of the Atmospheric Sciences* **65**, 1428–1441.

Ramage, C. S. (1968), 'Role of a tropical 'Maritime Continent' in the atmospheric circulation', *Monthly Weather Review* **96**, 365–370.

Rashid, H. A. and Hirst, A. C. (2017), 'Mechanisms of improved rainfall simulation over the Maritime Continent due to increased horizontal resolution in an AGCM', *Climate Dynamics* **49**, 1747–1764.

Rauniyar, S. P. and Walsh, K. J. (2013), 'Influence of ENSO on the diurnal cycle of rainfall over the Maritime Continent and Australia', *Journal of Climate* **26**, 1304–1321.

Raveh-Rubin, S. (2017), 'Dry intrusions: Lagrangian climatology and dynamical impact on the planetary boundary layer', *Journal of Climate* **30**, 6661–6682.

Raymond, D. J. (1984), 'A wave-CISK model of squall lines', *Journal of the Atmospheric Sciences* **41**, 1946–1958.

Raymond, D. J. and Fuchs, Z. (2009), 'Moisture modes and the Madden-Julian Oscillation', *Journal of Climate* **22**, 3031–3046.

Redelsperger, J.-L. and Lafore, J.-P. (1988), 'A three-dimensional simulation of a tropical squall line: Convective organization and thermodynamic vertical transport', *Journal of the Atmospheric Sciences* **45**, 1334–1356.

Redelsperger, J.-L., Parsons, D. B. and Guichard, F. (2002), 'Recovery processes and factors limiting cloud-top height following the arrival of a dry intrusion observed during TOGA COARE', *Journal of the Atmospheric Sciences* **59**, 2438–2457.

Ridout, J. A. and Flatau, M. K. (2011), 'Convectively coupled Kelvin wave propagation past Sumatra: a June case and corresponding composite analysis', *Journal of Geophysical Research Atmospheres* **116**, D07106.

Riehl, H. (1977), 'Vertical distribution of energy transfer and radar echo tops in the equatorial trough zone', *Monthly Weather Review* **105**, 230–231.

Riehl, H. (1979), 'Climate and weather in the tropics', *London: Academic Press* .

Riehl, H. and Malkus, J. (1958), 'On the heat balance in the equatorial trough zone', *Geophysica* **6**, 503–508.

Robinson, C. M., Narsey, S. and Jakob, C. (2024), 'Synoptic variability in the tropical oceanic moist margin', *Journal of Geophysical Research: Atmospheres* **129**, e2024JD040814.

Robinson, C. M., Narsey, S., Jakob, C. and Nguyen, H. (2025), 'Weather systems associated with synoptic variability in the moist margin', *Weather and Climate Dynamics* **6**, 369–385.

Roca, R., Aublanc, J., Chambon, P., Fiolleau, T. and Viltard, N. (2014), 'Robust observational quantification of the contribution of mesoscale convective systems to rainfall in the tropics', *Journal of Climate* **27**, 4952–4958.

Roca, R. and Fiolleau, T. (2020), 'Extreme precipitation in the tropics is closely associated with long-lived convective systems', *Communications Earth and Environment* **1**, 18.

Rodwell, M. J. (1997), 'reaks in the Asian monsoon: the influence of Southern Hemisphere weather systems', *Journal of the Atmospheric Sciences* **54**, 2597–2611.

Roman-Stork, H. L., Subrahmanyam, B. and Trott, C. B. (2021), 'Mesoscale eddy variability and its linkage to deep convection over the Bay of Bengal using satellite altimetric observations', *Advances in Space Research* **68**, 378–400.

Rotunno, R., Klemp, J. R. and Weisman, M. L. (1988), 'A theory for strong, long-lived squall lines', *Journal of the Atmospheric Sciences* **45**, 463–485.

Rowell, D. P. and Milford, J. R. (1993), 'On the generation of African squall lines', *Journal of Climate* **6**, 1181–1193.

Ryoo, J.-M., Waugh, D. W. and Gettelman, A. (2008), 'Variability of subtropical upper tropospheric humidity', *Atmos. Chem. Phys* **8**, 2643–2655.

Saji, N., Goswami, B., Vinayachandran, P. and Yamagata, T. (1999), 'A dipole mode in the tropical Indian Ocean', *Nature* **401**, 360–363.

Saji, N. and Yamagata, T. (2003), 'Possible impacts of Indian Ocean Dipole mode events on global climate', *Climate Research* **25**, 151–169.

Sakaeda, N., Kiladis, G. and Dias, J. (2020), 'The diurnal cycle of rainfall and the convectively coupled equatorial waves over the Maritime Continent', *Journal of Climate* **33**, 3307–3331.

Sakurai, N., Yamanaka, M. D., Mori, S., Hamada, J.-I., Hashiguchi, H., TAUHID, Y. I., Sribimawati, T. and Suhardi, B. (2005), 'Diurnal cycle of cloud system migration over Sumatera island', *Journal of the Meteorological Society of Japan* **83**, 835–850.

Salio, P., Nicolini, M. and Zipser, E. J. (2007), 'Mesoscale convective systems over southeastern South America and their relationship with the South American low-level jet', *Monthly Weather Review* **135**, 1290–1309.

Satomura, T. (2000), 'Diurnal variation of precipitation over the Indo-China Peninsula: two-dimensional numerical simulation', *Journal of the Meteorological Society of Japan* **78**, 461–475.

Schiemann, R., Demory, M. E., Mizielinski, M. S., Roberts, M. J., Shaffrey, L. C., Strachan, J. and Vidale, P. L. (2014), 'The sensitivity of the tropical circulation and Maritime Continent precipitation to climate model resolution', *Climate Dynamics* **42**, 2455–2468.

Schumacher, C. and Houze, R. A. (2003), 'Stratiform rain in the Tropics as seen by the TRMM precipitation radar *', *Journal of Climate* **16**, 1739–1756.

Scoccimarro, E., Gualdi, S., Bellucci, A., Peano, D., Cherchi, A., Vecchi, G. A. and Navarra, A. (2020), 'The typhoon-induced drying of the Maritime Continent', *PNAS* **117**, 3983–3988.

Senior, N. V., Matthews, A. J., Webber, B. G., Webster, S., Jones, R. W., Permana, D. S., Paski, J. A. and Fadila, R. (2023), 'Extreme precipitation at Padang, Sumatra triggered by convectively coupled Kelvin waves', *Quarterly Journal of the Royal Meteorological Society* **149**, 2281–2300.

Seo, H., O'Neill, L. W., Bourassa, M. A., Czaja, A., Drushka, K., Edson, J. B., Fox-Kemper, B., Frenger, I., Gille, S. T., Kirtman, B. P., Minobe, S., Pendergrass, A. G., Renault, L., Roberts, M. J., Schneider, N., Small, R. J., Stoffelen,

A. and Wang, Q. (2023), 'Ocean mesoscale and frontal-scale ocean–atmosphere interactions and influence on large-scale climate: a review', *Journal of Climate* **36**, 1981–2013.

Seto, T. H., Yamamoto, M. K., Hashiguchi, H., Fukao, S., Abo, M., Kozu, T. and Kudsy, M. (2006), 'Observational study on westerly wind burst over Sumatra, Indonesia by the equatorial atmosphere radar - a case study during the first CPEA campaign', *Journal of the Meteorological Society of Japan* **84A**, 95–112.

Sharma, K., Lee, J. C. K., Porson, A., Chandramouli, K., Roberts, N., Boyd, D., Zhang, H. and Barker, D. M. (2023), 'Adaptive selection of members for convective-permitting regional ensemble prediction over the western Maritime Continent', *Frontiers in Environmental Science* **11**, 1281265.

Siddle, E., Heywood, K. J., Webber, B. G. M. and Bromley, P. (2021), 'First measurements of ocean and atmosphere in the tropical North Atlantic using Caravela, a novel uncrewed surface vessel', *Weather* **76**, 200–204.

Silverman, V., Nahum, S. and Raveh-Rubin, S. (2021), 'Predicting origins of coherent air mass trajectories using a neural network—the case of dry intrusions', *Meteorological Applications* **28**, e1986.

Skyllingstad, E. D., de Szoeke, S. P. and O'Neill, L. W. (2019), 'Modeling the transient response of tropical convection to mesoscale SST variations', *Journal of the Atmospheric Sciences* **76**, 1227–1244.

Small, R. J., deSzoeke, S. P., Xie, S. P., O'Neill, L., Seo, H., Song, Q., Cornillon, P., Spall, M. and Minobe, S. (2008), 'Air-sea interaction over ocean fronts and eddies', *Dynamics of Atmospheres and Oceans* **45**, 274–319.

Smith, J., Birch, C., Marsham, J., Peatman, S., Bollasina, M. and Pankiewicz, G. (2024), 'Evaluating pySTEPS optical flow algorithms for convection nowcasting over the Maritime Continent using satellite data', *Natural Hazards and Earth System Sciences* **24**, 567–582.

Smith, R. K. (1997), 'On the theory of CISK', *Quarterly Journal of the Royal Meteorological Society* **123**, 407–418.

Sobel, A. and Maloney, E. (2013), 'Moisture modes and the eastward propagation of the MJO', *Journal of the Atmospheric Sciences* **70**, 187–192.

Souza, R., Pezzi, L., Swart, S., Oliveira, F. and Santini, M. (2021), 'Air-sea interactions over eddies in the Brazil-Malvinas Confluence', *Remote Sensing* **13**, 1335.

Sprintall, J., Gordon, A. L., Koch-Larrouy, A., Lee, T., Potemra, J. T., Pujiana, K. and Wijffels, S. E. (2014), 'The Indonesian seas and their role in the coupled ocean-climate system', *Nature Geoscience* **7**, 487–492.

Stohl, A. (2001), 'A 1-year Lagrangian "climatology" of airstreams in the Northern Hemisphere troposphere and lowermost stratosphere', *Journal of Geophysical Research Atmospheres* **106**, 7263–7279.

Storer, B. A., Buzzicotti, M., Khatri, H., Griffies, S. M. and Aluie, H. (2022), 'Global energy spectrum of the general oceanic circulation', *Nature Communications* **13**.

Su, C.-H., Eizenberg, N., Steinle, P., Jakob, D., Fox-Hughes, P., White, C. J., Rennie, S., Franklin, C., Dharssi, I. and Zhu, H. (2019), 'BARRA v1.0: the Bureau of Meteorology Atmospheric high-resolution regional reanalysis for Australia', *Geoscientific Model Development* **12**, 2049–2068.

Su, C. Y., Wu, C. M., Chen, W. T. and Chen, J. H. (2022), 'The effects of the unified parameterization in the CWBGFS: the diurnal cycle of precipitation over land in the Maritime Continent', *Climate Dynamics* **58**, 223–233.

Sun, B., Li, B., Yan, J., Zhou, Y. and Zhou, S. (2022), 'Seasonal variation of atmospheric coupling with oceanic mesoscale eddies in the North Pacific Subtropical Countercurrent', *Acta Oceanologica Sinica* **41**, 109–118.

Sun, W., An, M., Liu, J., Liu, J., Yang, J., Tan, W., Dong, C. and Liu, Y. (2022), 'Comparative analysis of four types of mesoscale eddies in the Kuroshio-Oyashio extension region', *Frontiers in Marine Science* **9**.

Sun, X., Huang, X. Y., Gordon, C., Mittermaier, M., Beckett, R., Cheong, W. K., Barker, D., North, R. and Semple, A. (2020), 'A subjective and objective evaluation of model forecasts of sumatra squall events', *Weather and Forecasting* **35**, 489–506.

Supari, Tangang, F., Juneng, L., Cruz, F., Chung, J. X., Ngai, S. T., Salimun, E., Mohd, M. S. F., Santisirisomboon, J., Singhruck, P., PhanVan, T., Ngo-Duc, T., Narisma, G., Aldrian, E., Gunawan, D. and Sopaheluwakan, A. (2020), 'Multi-model projections of precipitation extremes in southeast Asia based on CORDEX-southeast Asia simulations', *Environmental Research* **184**, 109350.

Susanto, R. D. and Ray, R. D. (2022), 'Seasonal and interannual variability of tidal mixing signatures in Indonesian seas from high-resolution sea surface temperature', *Remote Sensing* **14**.

Taburet, G., Sanchez-Roman, A., Ballarotta, M., Pujol, M. I., Legeais, J. F., Fournier, F., Faugere, Y. and Dibarboure, G. (2019), 'DUACS DT2018: 25 years of reprocessed sea level altimetry products', *Ocean Science* **15**, 1207–1224.

Takahashi, H. G. (2011), 'Long-term changes in rainfall and tropical cyclone activity over South and southeast Asia', *Advances in Geosciences* **30**, 17–22.

Tan, H., Ray, P., Barrett, B., Dudhia, J. and Moncrieff, M. W. (2021), 'Systematic patterns in land precipitation due to convection in neighboring islands in the Maritime Continent during MJO propagation', *Journal of Geophysical Research: Atmospheres* **126**, e2020JD033465.

Tan, I., Reeder, M. J., Birch, C. E., Peatman, S. C. and Webster, S. (2024), 'Synoptic and mesoscale dynamics of cold surges over the South China Sea and their control on extreme rainfall', *Journal of Geophysical Research: Atmospheres* **129**, e2024JD040822.

Tangang, F., Chung, J. X., Juneng, L., Supari, Salimun, E., Ngai, S. T., Jamaluddin, A. F., Mohd, M. S. F., Cruz, F., Narisma, G., Santisirisomboon, J., Ngo-Duc, T., Tan, P. V., Singhruck, P., Gunawan, D., Aldrian, E., Sopaheluwakan, A., Grigory, N., Remedio, A. R. C., Sein, D. V., Hein-Griggs, D., McGregor, J. L., Yang, H., Sasaki, H. and Kumar, P. (2020), 'Projected future changes in rainfall in southeast Asia based on CORDEX–SEA multi-model simulations', *Climate Dynamics* **55**, 1247–1267.

Tao, W.-K., Lang, S., Simpson, J., Sui, C.-H., Ferrier, B. and Chou, M.-D. (1996), 'Mechanisms of cloud-radiation interaction in the tropics and midlatitudes', *Journal of the Atmospheric Sciences* **53**, 2624–2651.

Tompkins, A. M. (2001), 'Organization of tropical convection in low vertical wind shears: The role of water vapor', *Journal of the Atmospheric Sciences* **58**, 529–545.

Torti, J. M. (2012), 'Floods in southeast Asia: a health priority', *Journal of Global Health* **2**, 020304.

Tulich, S. N. and Kiladis, G. N. (2012), 'Squall lines and convectively coupled gravity waves in the tropics: Why do most cloud systems propagate westward?', *Journal of the Atmospheric Sciences* **69**, 2995–3012.

van der Wiel, K., Matthews, A. J., Stevens, D. P. and Joshi, M. M. (2015), 'A dynamical framework for the origin of the diagonal South Pacific and South Atlantic Convergence Zones', *Quarterly Journal of the Royal Meteorological Society* **141**, 1997–2010.

Vaughan, G., Antonescu, B., Schultz, D. M. and Dearden, C. (2017), 'Invigoration and capping of a convective rainband ahead of a potential vorticity anomaly', *Monthly Weather Review* **145**, 2093–2117.

Vincent, C. L. and Lane, T. P. (2016), 'Evolution of the diurnal precipitation cycle with the passage of a Madden-Julian Oscillation event through the Maritime Continent', *Monthly Weather Review* **144**, 1983–2005.

Volonté, A., Turner, A. G. and Menon, A. (2020), 'Airmass analysis of the processes driving the progression of the Indian summer monsoon', *Quarterly Journal of the Royal Meteorological Society* **146**, 2949–2980.

Wallace, J. M., Mitchell, T. P. and Deser, C. (1989), 'The influence of sea-surface temperature on surface wind in the Eastern Equatorial Pacific: Seasonal and interannual variability', *Journal of Climate* **2**, 1492–1499.

Wang, B., Liu, F. and Chen, G. (2016), 'A trio-interaction theory for Madden–Julian Oscillation', *Geoscience Letters* **3**, 34.

Wang, L. and Li, T. (2020), 'Reexamining the MJO moisture mode theories with normalized phase evolutions', *Journal of Climate* **33**, 8523–8536.

Wang, S., Sobel, A. H., Tippett, M. K. and Vitart, F. (2019), 'Prediction and predictability of tropical intraseasonal convection: seasonal dependence and the Maritime Continent prediction barrier', *Climate Dynamics* **52**, 6015–6031.

Wang, S., Sobel, A. H., Zhang, F., Sun, Y. Q., Yue, Y. and Zhou, L. (2015), 'Regional simulation of the October and November MJO events observed during the CINDY/DYNAMO field campaign at gray zone resolution', *Journal of Climate* **28**, 2097–2119.

Wang, X., Cheng, X., Liu, X. and Chen, D. (2021), 'Dynamics of eddy generation in the southeast tropical Indian Ocean', *Journal of Geophysical Research: Oceans* **126**, e2020JC016858.

Wang, Y., Ren, H. L., Zhou, F., Fu, J. X., Chen, Q. L., Wu, J., Jie, W. H. and Zhang, P. Q. (2020), 'Multi-model ensemble sub-seasonal forecasting of precipitation over the Maritime Continent in boreal summer', *Atmosphere* **11**, 515.

Ward, N., Fink, A. H., Keane, R. J., Guichard, F., Marsham, J. H., Parker, D. J. and Taylor, C. M. (2021), 'Synoptic timescale linkage between midlatitude winter troughs Sahara temperature patterns and northern Congo rainfall: a building block of regional climate variability', *International Journal of Climatology* **41**, 3153–3173.

Warner, T. T., Mapes, B. E. and Xu, M. (2003), 'Diurnal patterns of rainfall in northwestern South America. Part II: model simulations', *Monthly Weather Review* **131**, 813–829.

Waugh, D. W. and Polvani, L. M. (2000), 'Climatology of intrusions into the tropical upper troposphere', *Geophysical Research Letters* **27**, 3857–3860.

Weisman, M. L., Klemp, J. B. and Rotunno, R. (1988), 'Structure and evolution of numerically simulated squall lines', *Journal of the Atmospheric Sciences* **45**, 1990–2013.

Wernli, H. and Davies, H. C. (1997), 'A Lagrangian-based analysis of extratropical cyclones. I: The method and some applications', *Quarterly Journal of the Royal Meteorological Society* **123**, 467–489.

Wheeler, M. C. and Hendon, H. H. (2004), 'An all-season real-time multivariate MJO index: development of an index for monitoring and prediction', *Monthly Weather Review* **132**, 1917–1932.

Wheeler, M. and Kiladis, G. N. (1999), 'Convectively coupled equatorial waves: analysis of clouds and temperature in the wavenumber-frequency domain', *Journal of the Atmospheric Sciences* **56**, 374–399.

Wijayanti, P., Zhu, X., Hellegers, P., Budiyono, Y. and van Ierland, E. C. (2017), 'Estimation of river flood damages in Jakarta, Indonesia', *Natural Hazards* **86**, 1059–1079.

Wilson, D. R. and Ballard, S. P. (1999), 'A microphysically based precipitation scheme for the UK meteorological office unified model', *Quarterly Journal of the Royal Meteorological Society* **125**, 1607–1636.

Wilson, D. R., Bushell, A. C., Kerr-Munslow, A. M., Price, J. D. and Morcrette, C. J. (2008), 'PC2: A prognostic cloud fraction and condensation scheme. I: Scheme description', *Quarterly Journal of the Royal Meteorological Society* **134**, 2093–2107.

Wirasatriya, A., Susanto, R. D., Kunarso, K., Jalil, A. R., Ramdani, F. and Puryajati, A. D. (2021), 'Northwest monsoon upwelling within the Indonesian seas', *International Journal of Remote Sensing* **42**, 5437–5458.

Wolf, G., Ferrett, S., Methven, J., Frame, T. H., Holloway, C. E., Martinez-Alvarado, O. and Woolnough, S. J. (2024), 'Comparison of probabilistic forecasts of extreme precipitation for a global and convection-permitting ensemble and hybrid statistical–dynamical method based on equatorial wave information', *Quarterly Journal of the Royal Meteorological Society* **150**, 877–896.

Woolnough, S. J., Slingo, J. M. and Hoskins, B. J. (2000), 'The relationship between convection and sea surface temperature on intraseasonal timescales', *Journal of Climate* **13**, 2086–2104.

Woolnough, S. J., Slingo, J. M. and Hoskins, B. J. (2001), 'The organization of tropical convection by intraseasonal sea surface temperature anomalies', *Quarterly Journal of the Royal Meteorological Society* **127**, 887–907.

Xiao, H. M., Lo, M. H. and Yu, J. Y. (2022), 'The increased frequency of combined El Niño and positive IOD events since 1965s and its impacts on Maritime Continent hydroclimates', *Scientific Reports* **12**, 7532.

Xue, P., Malanotte-Rizzoli, P., Wei, J. and Eltahir, E. A. (2020), 'Coupled ocean-atmosphere modeling over the Maritime Continent: a review', *Journal of Geophysical Research: Oceans* **125**, e2019JC014978.

Yamanaka, M. D. (2016), 'Physical climatology of Indonesian Maritime Continent: an outline to comprehend observational studies', *Atmospheric Research* **178-179**, 231–259.

Yamanaka, M. D., Ogino, S. Y., Wu, P. M., Jun-Ichi, H., Mori, S., Matsumoto, J. and Syamsudin, F. (2018), 'Maritime Continent coastlines controlling Earth's climate', *Progress in Earth and Planetary Science* **5**, 21.

Yanase, A., Yasunaga, K. and Masunaga, H. (2017), 'Relationship between the direction of diurnal rainfall migration and the ambient wind over the Southern Sumatra Island', *Earth and Space Science* **4**, 117–127.

Yang, D. and Ingersoll, A. P. (2013), 'Triggered convection, gravity waves, and the MJO: a shallow-water model', *Journal of the Atmospheric Sciences* **70**, 2476–2486.

Yang, G. Y., Feng, X. and Hodges, K. (2023), 'Seasonal and interannual variation of equatorial waves in ERA5 and GloSea5', *Quarterly Journal of the Royal Meteorological Society* **149**, 1109–1134.

Yang, G.-Y., Hoskins, B. and Slingo, J. (2003), 'Convectively coupled equatorial waves: a new methodology for identifying wave structures in observational data', *Journal of the Atmospheric Sciences* **60**, 1637–1654.

Yang, G.-Y. and Slingo, J. (2001), 'The diurnal cycle in the tropics', *Monthly Weather Review* **129**, 784–801.

Yang, G., Yu, W., Yuan, Y., Zhao, X., Wang, F., Chen, G., Liu, L. and Duan, Y. (2015), 'Characteristics, vertical structures, and heat/salt transports of mesoscale eddies in the southeastern tropical Indian Ocean', *Journal of Geophysical Research: Oceans* **120**, 6733–6750.

Yang, S., Cui, X. and Ran, L. (2009), 'Analyses of dry Intrusion and instability during a heavy rainfall event that occurred in northern China', *Atmospheric and Oceanic Science Letters* **2**, 108–112.

Yano, J.-I. and Plant, R. S. (2012), 'Convective quasi-equilibrium', *Reviews of Geophysics* **50**, RG4004.

Yi, L. and Lim, H. (2007), 'Semi-idealized COAMPS® simulations of Sumatra squall lines: the role of boundary forcing', *Advances in Geosciences* **9**, 111–124.

Yokoi, S., Mori, S., Katsumata, M., Geng, B., Yasunaga, K., Syamsudin, F., Nurhayati and Yoneyama, K. (2017), 'Diurnal cycle of precipitation observed in the western coastal area of Sumatra island: offshore preconditioning by gravity waves', *Monthly Weather Review* **145**, 3745–3761.

Yoneyama, K. and Fujitani, T. (1995), 'The behavior of dry westerly air associated with convection observed during the TOGA-COARE R/V Natsushima Cruise', *Journal of the Meteorological Society of Japan* **73**, 291–304.

Yoneyama, K. and Parsons, D. B. (1999), 'A proposed mechanism for the intrusion of dry air into the tropical western Pacific region', *Journal of the Atmospheric Sciences* **56**, 1524–1546.

Yoneyama, K. and Zhang, C. (2020), 'Years of the Maritime Continent', *Geophysical Research Letters* **47**, e2020GL087182.

Yuan, J. and Houze, R. A. (2013), 'Deep convective systems observed by A-Train in the tropical Indo-Pacific region affected by the MJO', *Journal of the Atmospheric Sciences* **70**, 465–486.

Yulihastin, E., Fathrio, I., Trismidianto, Nauval, F., Saufina, E., Harjupa, W., Satiadi, D. and Nuryanto, D. E. (2021), 'Convective cold pool associated with offshore propagation of convection system over the east coast of southern Sumatra, Indonesia', *Advances in Meteorology* **2021**, 2047609.

Zhang, C. (2005), 'Madden-Julian Oscillation', *Reviews of Geophysics* **43**, RG2003.

Zhang, C., Adames, F., Khouider, B., Wang, B. and Yang, D. (2020), 'Four theories of the Madden-Julian Oscillation', *Reviews of Geophysics* **58**, e2019RG000685.

Zhang, C. and Chou, M.-D. (1999), 'Variability of water vapor, infrared radiative cooling, and atmospheric instability for deep convection in the equatorial western Pacific', *Journal of the Atmospheric Sciences* **56**, 711–723.

Zhang, C. and Ling, J. (2017), 'Barrier effect of the Indo-Pacific Maritime Continent on the MJO: perspectives from tracking MJO precipitation', *Journal of Climate* **30**, 3439–3459.

Zhang, T., Yang, S., Jiang, X. and Huang, B. (2016), 'Roles of remote and local forcings in the variation and prediction of regional Maritime Continent rainfall in wet and dry seasons', *Journal of Climate* **29**, 8871–8879.

Zu, Y., Fang, Y., Sun, S., Yang, G., Gao, L. and Duan, Y. (2022), 'The seasonality of mesoscale eddy intensity in the Southeastern Tropical Indian Ocean', *Frontiers in Marine Science* **9**.

Zuo, H., Balmaseda, M. A., Mogensen, K. and Tietsche, S. (2018), OCEAN5: the ECMWF ocean reanalysis system and its real-time analysis component, Technical report, Technical Report 823, ECMWF, Reading, UK.